

EFFECTS OF TYPE 2 DIABETES ON BONE QUALITY

Praveer Sihota



Department of Mechanical Engineering
INDIAN INSTITUTE OF TECHNOLOGY ROPAR

EFFECTS OF TYPE 2 DIABETES ON BONE QUALITY

By

Praveer Sihota

(2015MEZ0003)

Department of Mechanical Engineering

Submitted

In fulfilment of the requirements of the degree

of

Doctor of Philosophy

to the



INDIAN INSTITUTE OF TECHNOLOGY ROPAR

March, 2021

© Indian Institute of Technology Ropar - 2021

All rights reserved

This thesis is dedicated to

Almighty who gave me knowledge, wisdom, perseverance and showed path during my
doctoral research and indeed, throughout my life

"सर्व शक्तिमते परमात्मने श्री रामाय नमः"

I bow before Shri Ram, who is vested with all powers, I bow before the source and reservoir
of all powers, I bow and seek shelter with the supreme soul, Shri Ram



INDIAN INSTITUTE OF TECHNOLOGY ROPAR

CANDIDATE'S DECLARATION

I, **Praveer Sihota**, hereby declare that the thesis entitled “**Effects of Type 2 Diabetes on Bone Quality**” in partial fulfillment of the requirements for the award of the Degree of **Doctor of Philosophy** and submitted to **Department of Mechanical Engineering**, at **Indian Institute of Technology Ropar**, is an original work which has been carried out between **July 2015** to **March 2021** under the joint supervision of **Dr. Navin Kumar** and **Dr. Vishwajeet Mehandia**. The thesis has been documented by me in its entirety. The content of the thesis has not been submitted for the award of any other degree to this or any other University/Institute.

Praveer Sihota

Signature of the Candidate

Date: 18.03.2021

This is to certify that the above declaration made by the **Praveer Sihota** is correct to the best of our knowledge.

Dr. Navin Kumar

Associate Professor

Department of Mechanical Engineering
Indian Institute of Technology Ropar

Dr. Vishwajeet Mehandia

Assistant Professor

Department of Chemical Engineering
Indian Institute of Technology Ropar

ACKNOWLEDGEMENTS

Though only my name appears on the cover of this thesis, many people have contributed to this thesis. I owe my gratitude to all those who have made this thesis possible and made it an experience I will never forget.

It transcends all the written word barriers to owe a deep sense of gratitude and express my profound indebtedness to my guide Dr. Navin Kumar, Associate Professor, Department of Mechanical Engineering, Indian Institute of Technology (IIT) Ropar, for selecting me to work with him. He gave me enormous freedom to explore on my own, allowing me to become an independent researcher and at the same time guided me to recover when my steps faltered. Without his timely monitoring of the progress of research work and efforts to arrange comprehensive research facilities, it would have been impossible to complete this thesis in the present form. His meticulous and concise comments and thoughtful criticism immensely helped me make my endeavor materialized.

I have been amazingly fortunate to have my second guide, Dr. Vishwajeet Mehandia, Department of Chemical Engineering, IIT Ropar. His guidance, insurmountable help, valuable criticism, and continuous and inspiring suggestions in this work production are significant. Every time he corrected my work, he gave me full freedom to grow and explore new and innovative research ideas.

I convey my heartfelt gratitude and my profound sense of regard to my external advisor Dr. Sanjay Kumar Bhadada, Professor and Head, Department of Endocrinology, Post Graduate Institute for Medical Education and Research (PGIMER), Chandigarh. He played multiple roles, from being a guide to a mentor to a Doctor who always there whenever I was stuck with work or other aspects of life. His amicable guidance, expert supervision, and innovative ideas made this work a reality.

I have been receiving generous support from respected Doctoral Committee members, Dr. Anupam Agrawal and Dr. Rakesh Maurya, Department of Mechanical Engineering, IIT Ropar and, Dr. Ravibabu Mulaveesala, Department of Electrical Engineering, IIT Ropar. I stand obliged before their affection and kindness towards me.

A deep sense of gratitude is acknowledged to Professor S. K. Das, Director, IIT Ropar, for providing access to different academic and non-academic facilities, equipment for experimentation, and making life healthy and enjoyable in the IIT Ropar campus. Special thanks for providing six months extended assistantship in COVID 19 pandemic.

I am incredibly thankful to Dr. Prabhat K. Agnihotri, Department of Mechanical Engineering, IIT Ropar, and Dr. Yashveer Singh, Department of Chemistry and Biomedical Engineering, IIT Ropar, for sharing their expertise through the courses taught by them.

I am also thankful to Prof. Vijay Goni, Prof. Sameer Agrawal, Dr. Siddharth Sharma, Dr. Deepak Neradi, Dr. Shailesh Karn, Department of Orthopaedics, PGIMER Chandigarh who helped me in the collection of bone/fingernail samples, clinical data and also helped me to understand the various practical concepts of bone pathology and fragility fracture.

I gratefully acknowledge Prof. Kulbhushan Tikoo, Mrs. Sumathi Poleboina from Department of Pharmacology and Toxicology, and Dr. K. Srinivasan, Scientist, Central Animal Facility, National Institute of Pharmaceutical Education and Research, SAS Nagar Mohali, for sharing their knowledge and experience on the development of the diabetic Sprague-Dawley female rat model.

I sincerely thank Dr. Rajendra Srivastva and Dr. Tarak Mondal for allowing me to use FTIR spectroscopy and TGA. I sincerely thank Dr. Srivatsava Naidu and Dr. Yashveer Singh for allowing me to use Spectrophotometer and Freeze drier, respectively. I would like to express my sincere thanks to Mr. Amit Kaushal, Mr. Harsimran Singh, and Mr. Ajay Jha for their help in performing experiments using XRD, AFM, and nanoindentation, respectively.

I am also thankful to Prof. Sudhakar Rao, Department of Bone and Mineral Metabolism, Henry Ford Hospital, Detroit, USA, Prof. Deepak Vashishth, Department of Biomedical Engineering, Center for Biotechnology and Interdisciplinary Studies, Rensselaer Polytechnic Institute, NY, USA, Dr. Ruban Dhaliwal, Metabolic Bone Disease Center, Upstate Medical University, Syracuse, NY, USA, Dr. Ansu Louis, Department of Humanities and Social Science, IIT Ropar, Dr. Atharva Poundarik, Department of Biomedical Engineering, IIT Ropar, who helped me in the editing, and reviewing my manuscripts.

Special mention is for Dr. Vandana Dhiman, Dr. Ashutosh Arya, Dr. Priyanka Singh, Dr. Gurjeet, Dr. Rimesh Pal, Dr. Darshan Badal, and Dr. JC Bose, Department of Endocrinology, my seniors, friends, who took me through my first experience with bone research and helped me in my baby steps from protocol to data collection to teaching me all concepts as a true friend. I would acknowledge them for not getting annoyed with my simple doubts about the clinical part of this thesis and helping me at any time. Without them, this thesis would never be a reality.

I am thankful to Dr. Anil Pradhan, Dr. Poonam Nehra, Dr. Bharat Ugale, Dr. Sandeep Singh, Dr. Neelam Chauhan, Dr. Subrajyoti, Dr. Rekha Dhiman, Vijay, Suman, Moumita, Anurag, Subhashini, and Gaje for conducting various experiments and fruitful discussions on the

fundamentals of the different theories that were directly or indirectly associated with the research work. I take this opportunity to thank other faculty members, staff, and students of IIT Ropar for their cooperation at all times during the Ph.D. work.

I am thankful to summer interns Rohan, Karthik, Rashmi, and Jonson for assisting me in developing various experimental protocols and fruitful discussions on the fundamentals of the different bone characterization techniques.

I can't thank enough all the lab mates, which were like a family away from my home, who helped in all possible ways to get this work completed. The encouragement and constant stimulation of the entire unit, especially Dr. Rakesh Das, Abhimanyu Kiran, Ram Naresh Yadav, Deonath Kumar, Piyush Lakhani, Piyush Uniyal, Anshul Sharma, Amit Kumar, Krashn K. Dwivedi, Amit Jha, Aakash Soni, Deepak, Saroj Kumar, Shivani and Mr. Rupinder Singh are gratefully acknowledged. They were with me during all ups and downs throughout my thesis work and made my tenure enjoyable, and provided crucial technical support and suggestions.

My friends Mr. Abhimanyu Kiran and Mr. Deonath Kumar deserve a special mention, who ensured that I should take regular breaks from the monotony of hectic life. I could share and talk to them for hours without a pause. They stood by me through the thick and thin and helped me maintain normality.

I dedicate this effort to the prayers and good wishes of my grandmother, parents, my sister, my wife, my little princess Mugdha, parents in law and all other family members who have made me what I am today in every possible way. They have sacrificed their comforts to stand solidly by me during this period. They have inspired me and taught me to go for excellence in everything I do. It is their love and affection that keep me going each and every day of my life.

Finally, I kneel in front of the almighty to give the wisdom and perseverance bestowed upon me during my doctoral research, and indeed, throughout my life.



Praveer Sihota

Place: IIT Ropar, Rupnagar

Date: 18/03.2021

ABSTRACT

EFFECTS OF TYPE 2 DIABETES ON BONE QUALITY

Individuals with type 2 diabetes mellitus (T2D) have a three-fold greater hip fracture risk than those without diabetes, independent of dual-energy x-ray absorptiometry (DXA) determined bone mineral density (BMD) [1]. Previous large studies explain the BMD T-score inability, a quantitative measure, to accurately predict fracture risk in T2D [2,3]. Mechanisms underlying the inferior bone quality and skeletal fragility in diabetes are not fully understood, making the clinical identification of individuals at risk for fractures difficult [4]. Therefore, we aimed to investigate the comprehensive multiscale bone quality parameters such as biomechanical, microstructural, material, and compositional bone properties in a rodent model and clinical populations with and without T2D.

In a rodent study, we have used a combination of a high-fat diet (4 weeks, 58% kcal as fat) and low dose streptozotocin (one time, 35 mg/kg) treatment to develop T2D in female Sprague Dawley rats. In contrast, the control animal received a normal pellet diet (4 weeks, 12% kcal as fat) and an equivalent volume of vehicle (one time, 0.9% saline solution). After eight weeks of establishing the T2D model, the femoral bones were excised, and multiscale bone quality parameters were investigated. We found that the non-enzymatic crosslink ratio (NE-xLR) is elevated in the T2D group. NE-xLR is strongly and negatively correlated with post-yield-displacement, which directly relates to bone fragility. Along with that, the decreased mineral-to-matrix ratio (Fourier transform infrared spectroscopy), decreased nanoindentation determined modulus, increased indentation distance (cyclic reference point indentation), and wider mineral crystal size (x-ray diffraction) in the T2D group compared to non-diabetic, evidenced that the diabetic bone compositional and material properties have changed (diminished), and diabetic bone became weaker and tends to fracture easily. Altogether, our rodent model simulates the disease characteristics of late-stage (insulin resistance and later hypoinsulinemia) for non-obese young T2D and provides potential evidence of diabetic bone fragility at various organization levels [5].

In another study, the femoral head bone tissue specimens were collected from patients with diabetes and known fragility fracture status. Trabecular bone quality parameters were compared in samples of two groups: non-diabetic (n=40) and diabetic (n=30) with a mean duration of disease 7.5 ± 2.8 years. As a result, no significant difference was observed in DXA determined BMD. Bone volume fraction was lower for the diabetic group. Apparent-level

(strength) and tissue-level (nanoindentation determined) modulus and hardness were lower in those with diabetes. Compositional differences between the non-diabetic and diabetic groups included lower mineral-to-matrix ratio (gravimetric), wider mineral crystals, and bone collagen modifications assessed as higher total fluorescent advanced glycation end-products (fAGEs) and non-enzymatic crosslink ratio (NE-xLR). Our findings provide evidence of hyperglycemia's and AGEs detrimental effects on trabecular bone quality at multiple length scales leading to lower energy absorption and toughness, indicative of an increased propensity to bone fragility [6].

After understanding the negative impact of T2D on bone quality, we aim to explore further possibilities of identifying a non-invasive, low-cost diagnostic technique that can help clinicians to predict bone quality beyond bone mineral density accurately. Therefore, first, the multiscale fingernail plate quality is investigated for healthy ($HbA1c \leq 5.9\%$), diabetic controlled ($HbA1c < 7.5\%$), and uncontrolled diabetic ($HbA1c \geq 7.5\%$) groups. It was found that T2D had an adverse effect on the human fingernail plate quality too. The parameters of fingernail plate quality were degraded in a pattern among all the three groups, where the degradation was highest in the case of severity of T2D (uncontrolled) as compared to the healthy group (healthy < diabetic controlled < uncontrolled) [7]. Secondly, the material and compositional properties of bone/fingernail were investigated using nanoindentation studies, and Fourier transform infrared spectroscopy, respectively, and a link in degradation pattern of both compositional/material properties of bone and fingernail plate quality was established. Both bone/fingernails in T2D had lower reduced modulus (E_r), hardness (H), lower Amide I and Amide II area ratio (protein content), higher sugar-to-matrix ratio, and relatively high carboxymethyl-lysine (CML) content compared with non-diabetic patients. Sugar-to-matrix ratio and relative carboxymethyl-lysine (CML) content were strongly and positively correlated with HbA1c for both bone/fingernail. There was a positive correlation between bone and fingernail glycation content. Our findings provide evidence that the degradation pattern of bone and fingernail properties go hand-in-hand in individuals with T2D. Thus, with these two studies, we concluded that the small-scale properties of the fingernail have the potential to serve as a non-invasive surrogate marker of bone quality in T2D [8].

Altogether, this thesis presents the multiscale characterization of bone as a material, the role of bone quality in diabetic fractures, and elucidates the importance of assessment of bone quality to clinicians in understanding and assessing type 2 diabetic fragility fractures. This thesis concluded that diabetes is detrimental to bone quality. The accumulation of AGEs is one of the processes that favor deterioration of bone quality in diabetes leading to material,

structural, compositional, and biomechanical dysfunctionality. Thus, highlight the need for more specific measures to understand and diagnose the bone quality and bone fragility in T2D.

References

1. Karim L, Rezaee T, Vaidya R. The Effect of Type 2 Diabetes on Bone Biomechanics. *Curr. Osteoporos. Rep.* 2019.
2. Petit MA, Paudel ML, Taylor BC, Hughes JM, Strotmeyer ES, Schwartz A V., Cauley JA, Zmuda JM, Hoffman AR, Ensrud KE. Bone mass and strength in older men with type 2 diabetes: The osteoporotic fractures in men study. *J. Bone Miner. Res.* 2010
3. Schwartz A V., Vittinghoff E, Bauer DC, Hillier TA, Strotmeyer ES, Ensrud KE, Donaldson MG, Cauley JA, Harris TB, Koster A, Womack CR, Palermo L, Black DM. Association of BMD and FRAX score with risk of fracture in older adults with type 2 diabetes. *JAMA - J. Am. Med. Assoc.* 2011
4. Shanbhogue V V., Mitchell DM, Rosen CJ, Bouxsein ML. Type 2 diabetes and the skeleton: New insights into sweet bones. *Lancet Diabetes Endocrinol.* 2016.
5. **Sihota P**, Yadav RN, Poleboina S, Mehandia V, Bhadada SK, Tikoo K, Kumar N. Development of HFD -fed/low dose STZ treated female Sprague Dawley rat model to investigate diabetic bone fragility at different organization levels. *JBMR Plus* 2020.
6. **Sihota P**, Yadav RN, Dhaliwal R, Bose JC, Dhiman V, Neradi D, Karn S, Sharma S, Aggarwal S, Goni VG, Mehandia V, Vashishth D, Bhadada SK, Kumar N. Investigation of mechanical, material and compositional determinants of human trabecular bone quality in type 2 diabetes. *J. Clin. Endocrinol. Metab.* 2021.
7. **Sihota P**, Yadav RN, Dhiman V, Bhadada SK, Mehandia V, Kumar N. Investigation of diabetic patient's fingernail quality to monitor type 2 diabetes induced tissue damage. *Sci. Rep.* 2019.
8. **Sihota P**, Pal R, Yadav RN, Neradi D, Karn S, Goni VG, Sharma S, Mehandia V, Bhadada SK, Kumar N, Rao SD, Can Fingernail quality predict the bone damage in type 2 diabetes mellitus: A pilot study, *PLOS ONE*, 2021. (PONE-D-21-04313, Under Review)
9. **Sihota P**, Bhadada SK, Numar N, Assessment of bone fragility in type 2 diabetes beyond bone mineral density, Review article (Under preparation)

List of Abbreviations

Abbreviations	Description
aBMD	Areal Bone Mineral Density
AGEs	Advanced Glycation End-Products
ANCOVA	Analysis of Covariance
ANOVA	Analysis of Variance
ATR	Attenuated Total Reflectance
BMD	Bone Mineral Density
BMI	Body Mass Index
BMSi/BMS	Bone Material Strength Index/ Bone Material Strength
BV/TV	Bone Volume/Tissue Volume, or Bone Volume Fraction
CML	Carboxymethyl-Lysine
cRPI	Cyclic Reference Point Indentation
DC	Diabetic Controlled
DXA	Dual-Energy X-Ray Absorptiometry
EDTA	Ethylene-Diamine-Tetra-Acetic Acid
Er	Reduced Modulus
ER	Endoplasmic Reticulum
E-xLR	Enzymatic Crosslink Ratio
fAGEs	Fluorescent Advanced Glycation End-Products
FEA	Finite Element Analysis
FN	Femoral Neck
FRAX	Fracture Risk Algorithm/Assessment
H	Hardness
HA	Hydroxyapatite
HbA1c	Glycated Hemoglobin
HFD	High-Fat Diet
IDF	International Diabetes Federation
IDI	Indentation Distance Increase
m	Mass of substance
NE-xL	Non-Enzymatic Crosslinks
NE-xLR	Non-Enzymatic Crosslink Ratio
NI	Nanoindentation
NIH	National Institute of Health
NPD	Normal Palate Diet
PBS	Phosphate Buffered Saline
PMMA	Polymethyl Methacrylate
PYD	Post Yield Displacement
SD Rat	Sprague–Dawley Rats
S-S Bond	Disulfide Bond
STZ	Streptozotocin
T2D	Type 2 Diabetes Mellitus
UC	Uncontrolled Diabetic
vBMD	Volumetric Bone Mineral Density
wt	Weight
yrs	Years

List of Tables

- Table 1.1** Various type 2 diabetic rodent models (based on spontaneous, monogenic abnormal leptin/leptin receptor signalling and diet-induced obesity) and results of femora in three-point bending test
- Table 1.2** Human studies conducted on the effect of type 2 diabetes on bone quality parameters
- Table 2.1** Literature review on techniques used to assess diabetic bone quality parameters
- Table 2.2** Definition and description of trabecular bone microstructural parameters
- Table 2.3** Definition and description of cortical bone microstructural parameters
- Table 3.1** Bodyweight and blood glucose of control and diabetic (T2D) groups (at the end of the study), and also the findings of microstructural parameters of control and diabetic (T2D) rat femoral bone
- Table 4.1** Baseline demographic, radiographic, and biochemical parameters of diabetic and non-diabetic groups
- Table 4.2** Findings on Structural and Compositional determinants of Bone quality
- Table 4.3** Correlation analysis of selected significant variables of the diabetic group which has at least one or more significant relationship with at least one other variable
- Table 4.4** Correlation analysis of selected significant variables of the non-diabetic group which has at least one or more significant relationship with at least one other variable
- Table 5.1** Clinical details of fingernail specimens
- Table 5.2** Nail quality parameters of the human fingernail
- Table 5.3** Hardness and Modulus values of each layer of the nail plate for healthy, diabetic controlled (DC), and uncontrolled diabetic (UC) group obtained through nanoindentation experiment
- Table 6.1** Baseline demographic and radiographic parameters of diabetic and non-diabetic women suffered from fragility fracture of the hip

List of Figures

- Figure 1.1** Schematic representations of the different levels of the hierarchical structure of bone and its basic constituent organic and inorganic material
- Figure 1.2** Schematic representation of the relationship between bone quality, bone mineral density, and bone strength, and how inadequate bone strength leads to fragility hip fractures
- Figure 1.3** Determinants of bone quality
- Figure 1.4** Graphical abstract showing the major objectives of the thesis
- Figure 2.1** The key bone quality assessment techniques and their primary outcome along with their utility to study particular bone hierarchy scale
- Figure 2.2** Typical load-displacement curve of three-point bending test, and description of various structural parameters derived from load-displacement curve
- Figure 2.3** Typical stress-strain curve of compression test, and description of various material properties derived from stress-strain curve
- Figure 2.4** Typical load-displacement curve of cyclic reference point indentation (cRPI) test, and description of various parameters derived from cRPI load-displacement curve
- Figure 2.5** Typical load-displacement curve of nanoindentation test, and description of reduced modulus and hardness derived from nanoindentation load-displacement curve
- Figure 2.6** Representative TGA curve which monitor mass loss of a substance as a function of temperature, also their respective first derivatives for femur trabecular bone. The TGA first derivative plots represent the more accurate temperature values associated with the percentage of mass lost, here it can be observed that superficial water completely evaporates before 200 °C, and between 200-600 °C, the degradation and combustion of the bone matrix occurs
- Figure 2.7** Representative XRD pattern ($20^\circ < 2\theta < 45^\circ$) of human cortical femoral bone. The peak at 26° and 40° is used to determine the average crystal length and width in the c-axis direction [002] plane and ab-plane [310] respectively
- Figure 2.8** Representative FTIR Spectrum of undecalcified and decalcified human trabecular bone with the appropriate label of mineral collagen and sugar bands
- Figure 2.9** Scanning electron microscopy image of human cortical bone and a single osteon
- Figure 2.10** Atomic force microscopy image of collagen fibers of demineralized thin bone sections obtained with cryotom
- Figure 3.1** (A) Bodyweight changes in HFD-fed/low dose STZ treated female SD rats compared to normal pellet diet-fed rats of every week, right from the beginning to the end of the study. (B) Schematic of materials and methods and allocation of tissue for each characterization technique.

Left femora were used for microstructural (μ CT), mechanical (3-point bending), and fracture pattern analysis, and right femora were utilized to determine properties at the material level (cRPI), bone composition with FTIR, mean crystallite size with powder XRD and fAGEs content.

Figure 3.2 (A) Representative FTIR spectra with the appropriate label of various bands to analyze the diabetic (T2D) and control femoral cortical bone, (B) represents peak fitting of Amide I band, collagen properties were obtained by peak fitting of Amide I band with subbands (Gaussian curves) at 1610, 1630, 1645, 1660, 1678 and 1692 cm^{-1} , (C) represents the non-enzymatic crosslink (NE-xL) formation schematically in bone collagen

Figure 3.3 (A) Experimental setup of three-point bending test, (B) Representative load-displacement curve resulting from a rat bone loaded to fracture in three-point bending, (C) Representative image of fracture pattern obtained during three-point bending, showing diabetic bone suffer from transverse fracture, whereas control bones suffer from oblique fracture, (D-G) Maximum force (Fmax), stiffness, work-to-failure and post-yield deflection (PYD) graphs respectively, showing a smaller value in the diabetic group

Figure 3.4 (A) Experimental setup of cyclic reference point indentation (cRPI) test, (B-D) Indentation distance increase (IDI), average energy dissipated (Avg-ED) and unloading slope first cycle (US-1st) respectively, showing the increased value of IDI, Ave-ED, ID-1st and TID, and smaller value of US-1st in the diabetic (T2D) group, (E-F) nanoindentation results showing the smaller value of reduced modulus (E_r) and hardness respectively in the diabetic (T2D) group

Figure 3.5 (A) Representative XRD pattern ($20^\circ < 2\theta < 45^\circ$) of SD rat cortical femoral bone. The peak at 26° and 40° is used to determine the average crystal length and width in the c-axis direction [002] plane and ab-plane [310] respectively, (B) Showing mean crystallite length and (C) Showing increased width of mean crystallite in the diabetic (T2D) group

Figure 3.6 (A-D) measures of mineral properties and collagen maturity, showing lower mineral-to-matrix ratio in diabetic (T2D) bone, whereas all other mineral parameters could not reach the level of significance, (E) represents collagen maturity (area ratio of the 1660/1692 cm^{-1} subbands), (F) represents non-enzymatic crosslink ratio [NE-xLR, (the area ratio of the 1678/1692 cm^{-1} subbands, total crosslinking AGEs)], (G) The graph is showing that the fAGEs content is higher in the diabetic group

Figure 3.7 Mechanical property versus a measure of glycation. Graphical data for the mechanical parameter (post-yield-displacement, PYD) versus NE-xLR

Figure 4.1 (A) Determinants of bone quality, (B) The extraction of cylindrical

trabecular bone cores, each 5 mm in diameter and 8-9 mm in length, from femoral heads along the direction of the principal trabeculae using the drilling machine attached with diamond core bit, (C) Characterization techniques used to determine the human trabecular bone quality for diabetes patients; SB: subchondral bone

Figure 4.2 (A) Calculated typical stress-strain plot of compression test for diabetic and non-diabetic groups, (B) Amide I and Amide II bond positions in principal structural unit of collagen in human trabecular bone

Figure 4.3 Representative 3D reconstructed μ CT image: (A) represents the non-diabetic group and (B) represents the diabetic group. The colour map in (C) and (D) represents the variation in trabecular thickness for the non-diabetic and diabetic group, respectively, (E-L) Elastic modulus, yield stress, ultimate stress, yield strain, ultimate strain, post-yield strain, post-yield energy, and toughness respectively, for diabetic and non-diabetic group

Figure 4.4 (A-B) Reduced modulus (E_r) and hardness respectively obtained from nanoindentation, showing smaller value in the diabetic (T2D) group, (C) Representative TGA curves with their respective first derivatives for diabetic and non-diabetic femur trabecular bone heated to 1000 °C. The TGA first derivative plots represent the more accurate temperature values associated with the percentage of mass lost, here it can be observed that superficial water completely evaporates before 200 °C, and between 200-600 °C, the degradation and combustion of the bone matrix occurs (D) Mineral to matrix ratio graph, showing a smaller ratio in the diabetic group

Figure 4.5 (A) Representative XRD pattern ($20^\circ < 2\theta < 45^\circ$) of human femoral trabecular bone. The peak at 26° and 40° is used to determine the average crystal length and width in the c-axis direction and ab-plane respectively, according to Scherrer equation $B(2\theta) = \lambda/L\cos\theta$. Where B is the mean crystal size, λ is the x-ray wavelength (1.5406 \AA), L is the peak width at half maximum and θ is the Bragg angle where the peak is located, (B-C) Mean crystal size graph, showing the insignificant difference in average crystal length but wider width of mean crystal in the diabetic group

Figure 4.6 (A) Representative FTIR spectra with the appropriate label of various bands to analyze the diabetic and non-diabetic femoral trabecular bone, (B) represents peak fitting of Amide I band, collagen properties were obtained by peak fitting of Amide I band with subbands (Gaussian curves) at 1610, 1630, 1645, 1660, 1678 and 1692 cm^{-1} , (C) represents schematically the enzymatic (E-xL) and non-enzymatic crosslink (NE-xL) formation in bone collagen, (D-F) measures of mineral properties, showing all mineral parameters could not reach to the level of significance, (G) represents non-enzymatic crosslink ratio [NE-xLR,

(the area ratio of the 1678/1692 cm^{-1} subbands within the Amide I peak, total crosslinking AGEs), **(H)** represents enzymatic crosslink ratio [E-xLR, the area ratio of the 1660/1678 cm^{-1} subbands within the Amide I peak], **(I)** represents collagen maturity (area ratio of the 1660/1692 cm^{-1} subbands within the Amide I peak), **(J)** showing lower mineral:matrix ratio in the diabetic group

Figure 4.7 **(A)** The graph is showing that the fAGEs content is higher in the diabetic group. **(B-C)**: Mechanical properties versus a measure of glycation (fAGE and NE-xLR). Graphical data for several mechanical parameters versus total fluorescent AGEs **(B-C)** and NE-xLR **(D)** are shown

Figure 4.8 The relationships between bone volume fraction and **A)** modulus, **B)** yield stress, **C)** ultimate stress, **D)** post-yield energy, and **E)** toughness between diabetic and non-diabetics are shown. Data are presented along with best-fit lines (solid lines)

Figure 5.1 Graphical abstract showing increased degradation in fingernail quality with the severity of type 2 diabetes

Figure 5.2 Determinants of nail quality

Figure 5.3 **(A)** Schematic view of the free edge and clipped fingernail plate, **(B)** Pictorial representation of nanoindentation study describing indentation locations on the cross-section of fingernail plate

Figure 5.4 **(A)** Position of Amide I, Amide II, and disulfide bond in the principal keratin structural unit of fingernail plate, **(B)** Showing Raman and FTIR spectra of a CML reference standard

Figure 5.5 Micro CT images of fingernail plate samples describing porosity and density distribution in healthy, diabetic controlled (DC), and uncontrolled diabetic (UC) groups (**A** and **D**- healthy, **B** and **E** -DC, **C**, and **F**- UC)

Figure 5.6 Percentage change in the nail plate quality parameters for diabetic controlled (DC) group (Healthy-DC) and uncontrolled diabetic (UC) group (Healthy-UC) with respect to healthy group **(A)** The percentage increase in porosity and roughness (structural properties), **(B)** Percentage decrease in modulus and hardness (material properties), **(C)** The percentage decrease in Amide I, Amide II, Disulfide bond and Calcium content (Biochemical properties) (the bold values are representing a significant change from the healthy group)

Figure 5.7 SEM images showing the morphology of fingernail plate for healthy, diabetic controlled (DC), and uncontrolled diabetic (UC) groups **(A)** Dorsal phase (healthy), **(B)** Ventral phase (healthy), **(C)** Dorsal phase (DC), **(D)** Ventral phase (DC), **(E)** Dorsal phase (UC), **(F)** Ventral phase (UC)

Figure 5.8 The surface roughness of Dorsal phase of fingernail plate obtained through AFM experiments **(A)** Healthy group, **(B)** diabetic controlled

- (DC) group, (C) uncontrolled diabetic (UC) group
- Figure 5.9** Nanoindentation results, (A) Representative load-displacement curves of healthy, diabetic controlled (DC) and uncontrolled diabetic (UC) group, (B) The percentage decrease in hardness for DC group (Healthy-DC) and UC group (Healthy-UC) with respect to healthy for dorsal, intermediate and ventral layer, (C) The percentage decrease in modulus for DC group (Healthy-DC) and UC group (Healthy-UC) with respect to healthy for the dorsal, intermediate and ventral layer (In the figure the bold values are representing the significant change with respect to the healthy group)
- Figure 5.10** Representative FTIR spectrum of human fingernail plate showing the position of Amide I, Amide II and Disulfide (S-S) bond, CML and methylene (CH₂) deformation band vibrations for healthy, diabetic controlled (DC), and uncontrolled diabetic (UC) groups
- Figure 5.11** AGE measurement in the human fingernail plate through FTIR spectroscopy showed a higher level of relative carboxymethyl-lysine (CML) content in diabetic controlled (DC) and uncontrolled diabetic (UC) groups
- Figure 6.1** Representative FTIR spectra of the human fingernail and trabecular bone (demineralized) showing the position of Amide I, Amide II, sugar, and methylene (CH₂) deformation band vibrations for the non-diabetic and diabetic groups
- Figure 6.2** Measures of bone microstructural parameters for diabetic and non-diabetic trabecular bone, showing lower BV/TV (%) (A), Tb.Th (mm) (B) and Tb.N (1/mm) (C) in diabetic group
- Figure 6.3** Sugar-to-matrix ratio obtained from FTIR, showing higher mean values in the diabetic group for both bone (A) and fingernail (B), respectively
- Figure 6.4** Normalized Amide, I, and Amide II area, obtained from FTIR, showing lower mean values in the diabetic group for both bone (A) and fingernail (B), respectively
- Figure 6.5** Reduced modulus and hardness obtained from nanoindentation, showing lower mean values in the diabetic group for both bone (A) and fingernail (B), respectively
- Figure 6.6** Correlation between HbA1c and the sugar-to-matrix ratio for both bone and fingernail is shown in 6(A) and 6(B), respectively, for diabetic and non-diabetics groups
- Figure 6.7** Correlation between fingernail and bone for diabetic patients and non-diabetics (A) for sugar-to-matrix ratio, (B) for nanoindentation determined reduced modulus, (C) BV/TV of trabecular bone and fingernail reduced modulus

TABLE OF CONTENTS

	Acknowledgments	i
	Abstract	iv
	List of abbreviations	vii
	List of tables	viii
	List of figures	ix
1	Introduction	1
1.1	Type 2 diabetes, its secondary complications, and prevalence	1
1.2	Type 2 diabetes and bone fracture risk	1
1.3	Mechanism behind T2D bone fragility	1
1.4	Hierarchical structure of bone	2
1.5	Bone composition	4
1.6	Bone modeling and remodeling	5
1.7	Bone quality, bone strength, and fragility fractures	5
1.8	Key determinants of bone quality	6
1.9	Current status of research	7
1.10	Research objectives	16
1.11	Dissertation overview and organization	18
2	Assessment of bone fragility in type 2 diabetes beyond bone mineral density	19
2.1	Structural characterization	20
2.1.1	Quantitative computed tomography (QCT)	23
2.1.2	Peripheral quantitative computed tomography (pQCT)	24
2.1.3	High resolution peripheral quantitative computed tomography (HR-pQCT)	25
2.1.4	Dual-energy X-ray absorptiometry (DXA)	27
2.1.5	Trabecular bone score (TBS)	28
2.1.6	Micro-computed tomography (μ -CT)	28
2.1.7	Bone histomorphometry	30
2.2	Mechanical characterization	31
2.2.1	Whole bone test (Three-point bending test)	32
2.2.2	Apparent-level test (Uniaxial compression)	33
2.2.3	Cyclic reference point indentation (cRPI)	35
2.2.4	Osteoprobe	36
2.2.5	Nanoindentation (NI)	37
2.3	Compositional analysis	38
2.3.1	Thermogravimetric analysis (TGA)	39
2.3.2	X-ray diffraction (XRD)	40
2.3.3	Small-angle X-ray scattering (SAXS)	41

2.3.4	Fourier transform infrared spectroscopy (FTIR)	42
2.3.5	Scanning electron microscopy (SEM)	44
2.3.6	Quantitative backscattered electron imaging (qBEI)	44
2.3.7	Energy-dispersive X-ray spectroscopy (EDX)	45
2.3.8	Atomic force microscopy (AFM)	45
2.3.9	Fluorescent spectroscopy	46
2.3.10	Solid-state nuclear magnetic resonance (SSNMR)	47
2.3.11	High-performance liquid chromatography (HPLC)	48
2.4	Summary and discussion	48

3 Development of HFD-fed/low dose STZ treated female Sprague Dawley rat model to investigate diabetic bone fragility at different organization levels 51

3.1	Introduction	52
3.2	Material and methods	53
3.2.1	Animals	53
3.2.2	Experimental design	53
3.3	Measurement of Bone quality parameters	55
3.3.1	Structural parameters (μ -CT)	55
3.3.2	Mechanical and material properties	56
3.3.2.1	Whole bone three-point bending test	56
3.3.2.2	Cyclic reference point indentation (cRPI)	57
3.3.2.3	Nanoindentation (NI)	57
3.3.3	Biochemical analysis	58
3.3.3.1	FTIR	58
3.3.3.2	Mean crystal size (XRD)	59
3.3.3.3	fAGE assay	59
3.3.4	Statistical analysis	60
3.4	Results	61
3.4.1	Structural parameters (μ -CT)	62
3.4.2	Mechanical and material properties	62
3.4.2.1	Whole bone three-point bending test	62
3.4.2.2	Cyclic reference point indentation (cRPI)	63
3.4.2.3	Nanoindentation (NI)	64
3.4.3	Mean mineral crystal size (XRD)	64
3.4.4	Compositional analysis (FTIR) and fAGE assay	65
3.4.5	Interrelationship between variables	66
3.5	Discussion	67

4 Investigation of mechanical, material, and compositional determinants of human trabecular bone quality in type 2 diabetes 73

4.1	Introduction	74
-----	--------------	----

4.2	Material and methods	75
	Study participants	75
	Sample procurement and storage	75
4.3	Assessment of bone quality parameters	77
4.3.1	Microstructural parameters	77
4.3.2	Bulk mechanical properties	78
4.3.3	Bone material properties	78
4.3.4	Thermogravimetric analyses	79
4.3.5	Mean crystal size	79
4.3.6	Mineral and collagen properties	79
4.3.7	Fluorescent advanced glycation end-products (fAGEs) assay	81
4.4	Statistical analysis	81
4.5	Results	82
4.5.1	Patient characteristics	82
4.5.2	Microstructural parameters	83
4.5.3	Mechanical properties	83
4.5.4	Material properties	85
4.5.5	Composition	85
4.5.6	Mean mineral crystal size	86
4.5.7	Mineral and collagen properties	87
4.5.8	Florescent advanced glycation end-products (fAGEs)	90
4.5.9	Interrelationships between variables	90
4.6	Discussion	92
5	Investigation of diabetic patient's fingernail quality to monitor type 2 diabetes-induced tissue damage	99
5.1	Introduction	100
5.2	Material and methods	101
	Sample collection	101
	Sample grouping	102
5.3	Determinants of nail quality	103
5.3.1	Measurement of density	103
5.3.2	Measurement of porosity	103
5.3.3	Surface morphology and calcium content	103
5.3.4	Surface roughness	104
5.3.5	Material properties	104
5.3.6	CML, protein, and disulfide bond content	105
5.3.7	Statistical Analysis	106
5.4	Results	106
5.4.1	Patient's characteristics	106
5.4.2	Porosity	106
5.4.3	Surface morphology and roughness	108

5.4.4	Material properties	110
5.4.5	Calcium content	111
5.4.6	CML, protein, and disulfide bond content, and protein structure	112
5.5	Discussion	113
6	Can fingernails predict bone damage in type 2 diabetes? A pilot study	117
6.1	Introduction	117
6.2	Research design and methods	118
	Study participants	118
	Sample procurement and storage	119
6.2.1	Microstructural parameters by μ -CT	119
6.2.2	Fingernail and Bone material properties by nanoindentation	119
6.2.3	Collagen and Keratin properties by Fourier Transform Infrared Spectroscopy (FTIR)	120
6.2.4	Statistical analysis	120
6.3	Results	121
6.3.1	Patient's characteristics	121
6.3.2	Structural parameters (μ -CT)	122
6.3.3	Collagen and keratin properties and measurement of glycation	123
6.3.4	Material properties	125
6.3.5	Interrelationships between variables	126
6.4	Discussion	127
7	Summary, contributions, and future scope	131
7.1	Summary of key results	131
7.2	Contribution of thesis	132
7.3	Limitations of this thesis	133
7.4	Future scope of this study	134
7.5	Conclusive remarks	135
	References	136
	Complete list of publications	156
	Curriculum vitae (CV)	158

CHAPTER 1

INTRODUCTION

1.1 Type 2 diabetes, its secondary complications, and prevalence

Type 2 Diabetes (T2D) is characterized by high blood glucose levels resulting from Insulin resistance and/or relative insulin deficiency [1], which causes a substantial socioeconomic burden globally [2]. Diabetes potentially affects almost every organ in the human body and causes head-to-toe damage, i.e., heart, kidney, nerves, eye, skin, blood vessels, and bone [3]. According to International Diabetes Federation (IDF) 2019, 463 million adults (age range 20-79) have diabetes (including both type 1 and type 2 diabetes) worldwide. Among them, approximately 60% of the world's diabetics live in Asia. Moreover, India is home to the second-largest number of diabetic cases (77 million in 2019) [4] and being with the fastest population growth rate; this data is expected to increase further in the coming years [5]. The above information shows that the prevalence of diabetes is substantially high, which should not be overlooked.

1.2 Type 2 diabetes and bone fracture risk

Nearly three times increased hip fracture risk observed in people with diabetes attracted the attention of researchers [6]–[10]. The 10-year hip fracture risk for both men and women is high for patients with T2D compared to non-diabetes, regardless of BMD T-score [11]. At present, the Dual-energy X-ray Absorptiometry (DXA) is the gold standard to diagnose osteoporosis and accordingly identify low BMD and T-score for individuals at risk for fracture. However, the clinical utility of DXA in T2D is limited due to normal to high areal bone mineral density (BMD) in individuals with diabetes [12]. Furthermore, the fracture risk assessment tool (FRAX) is available, which provides a relatively comprehensive diagnosis of fracture risk by incorporating aBMD, T-score along with age, gender, BMI, previous fracture history, and smoking status, in its algorithm to generate FRAX score which gives the probability of a hip fracture within the next ten years. However, FRAX does not incorporate diabetes (presence, duration, or severity) as a risk factor. Therefore, both the DXA and FRAX underestimate the fracture risk in patients with T2D [13], and thus, clinicians have difficulty taking appropriate preventative measures for these patients [7], [12], [14]–[18].

1.3 Mechanism behind T2D bone fragility

The mechanisms underlying high fracture risk in T2D are not well understood. Prolonged

hyperglycemia increases the non-enzymatic reactions (Maillard reactions) and forms advanced glycation end-products (AGEs) through post-translation modification [19]. AGEs then accumulate in the bone tissue and react irreversibly with amino acid residues of peptides or proteins to form protein crosslinks [20]. This phenomenon, widely recognized as non-enzymatic crosslinks (NE-xL), is the underlying mechanism for multiple complications of diabetes, as it alters normal cellular functioning, disruption, and suppression of bone remodeling processes via osteoblasts and osteoclasts [21], [22]. AGEs accumulation may also change the bone mineralization and bone strength at macroscale [23].

The prolonged hyperglycemia and AGEs accumulation are believed to manifest first at the molecular level in bone [24], [25]. These molecular changes subsequently affect the properties of the bone's hierarchical organization and lead to an overall loss in bone strength at macroscale [24], [25]. Thus, the study of the hierarchical structure of bone is essential to get a comprehensive diagnosis of altered bone quality and fracture risk assessment.

1.4 Hierarchical structure of bone

The primary function of bone is to provide mechanical support (via bone tissue mechanical properties, for example, stiffness and toughness) and protection to vital organs. From a material point of view, the bone has a hierarchical structure with cascaded building blocks' arrangements at defined length scales. The different levels of the hierarchical structure of bone are shown in **Figure 1.1**.

The intact structure of bone is called whole bone, which represents the macrostructure of bone. Whole bones fulfill the responsibilities of bearing different types of loads in various combinations, including compression, tension, bending, and torsion [14]. The macrostructure may range between several cm to 10 mm.

The mesostructure consists of two types of bone tissue depending on porosity: trabecular and cortical. Trabecular bone has more porosity and an intricate random network of trabeculae, involved in metabolic activity and mostly found in areas that need effective load distribution, such as joint regions and vertebral bodies. In comparison, cortical bone is a denser bone located at the outer shaft of long bones and provides strong structural support [14]. Further, the trabecular bone is generally more sensitive to pathologic changes than cortical bone. Thus trabecular sites are highly clinically significant for diseased or aging populations. Mesostructure ranges between 10 mm to 500 μm [26].

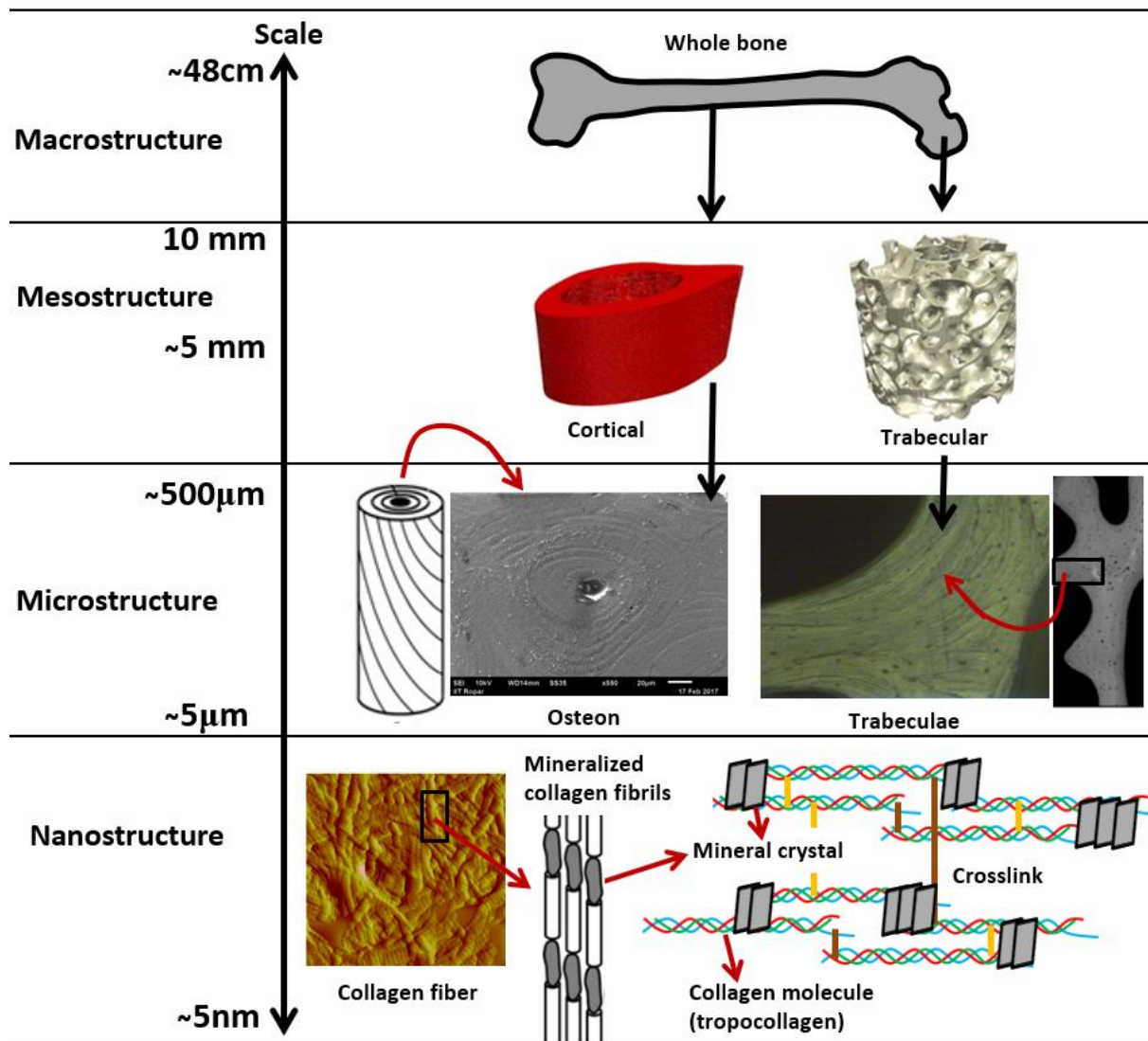


Figure 1.1 Schematic representations of the different levels of the hierarchical structure of bone and its primary constituent organic and inorganic material

At the microstructure level, the basic structural unit of cortical bone is the osteon or Haversian system, which includes concentric rings of calcified matrix called lamellae (singular = lamella) and a Haversian canal (contains blood vessels and nerves). On the other hand, trabecular bone's basic structural unit is trabeculae (singular = trabecula) arranged in a lattice-like network. The microstructure of bone ranges between 500 µm to ~5 µm [26].

The nanostructure hierarchy of bone consists of collagen fiber (~5–10 µm diameter) made up of an array of mineralized collagen fibrils. It is known as the basic structural unit of bone matrix (100 nm in diameter and ~5–10 µm in length). The fibrils are composed of self-assemble type 1 collagen molecules (tropocollagen) (~1.5 nm diameter and ~300 nm length) which are secreted by the osteoblast cells (bone-forming cells) into the extracellular space.

Later, small mineral crystals of hydroxyapatite (HA) which is actually not stoichiometric lattice and more like a carbonated apatite with substitutions, are deposited in the gap between collagen fibrils, due to this the collagen fibrils become mineralized as the bone tissue grows and matures. These mineral crystals are oriented parallel to each other in the long axis direction of the collagen fibril. The nanostructure of bone ranges between $\sim 5\mu\text{m}$ to $\sim 5\text{nm}$ [26].

At the lowest scale, the tropocollagen molecule consists of different amino acids ($\sim 1/3$ is glycine, $\sim 1/6$ are either proline or hydroxyproline, and the remaining residues are lysine and arginine). The glycine allows the individual collagen chains to align compactly, and numerous hydrogen bonds stabilize this helix. Hydroxyproline facilitates hydrogen bonding with water and other amino acids in collagen, while the lysine and arginine play a vital role in post-translational processes to assemble higher-level structures [27].

The study of the hierarchical structure of bone is significant because a small change at the molecular level, either due to age or disease, can have drastic effects on bone macroscale mechanical properties.

1.5 Bone composition

The bone is a composite structure and primary composition of bone material comprised of a mineral phase (imperfect hydroxyapatite (HA) $\text{Ca}_{10}(\text{PO}_4)_6(\text{OH})_2$) approximately (50-70 wt %), an organic matrix (90% type I collagen (20-40 wt %), and water content (5-10 wt %) [28]. The amount of mineral content is the primary determinant of bone mechanical stiffness and strength [29]. The organic phase provides tensile strength, ductility, and toughness to the bone [14]. Whereas the water in bone mainly presents in two categories: bound and unbound. Bound water exists in Ca^{2+} coordination sites on the mineral and is associated with collagen fibrils. Unbound water, or bulk water, is mainly present in the pores of the Haversian and lacuna-canalicular systems. The water in bone plays roles in physiological signaling, transport ions and nutrients, and a key role in bone mineralization whereby collagen-bound water is gradually replaced by calcium apatite-like mineral [30]. It is also reported that water provides stability in various bone mineral and organic interfaces [31], both bound and unbound water influenced mechanical properties [32], [33] and provide viscoelastic or time-dependent behavior to bone [34], [35]. Further, any alterations in the organic matrix can manifest differently to overall mechanical properties than modifications in the mineral content. Despite that knowledge, collagen assessment is severely neglected in clinical

examinations to predict mechanical behavior and skeletal integrity [36]. Therefore, assessing the individual constituent (mineral, matrix, and water content) of bone is important to get more insight into the bone quality and predict overall mechanical properties at the macroscale.

1.6 Bone modeling and remodeling

Bone metabolism is mainly two types: modeling and remodeling. Both processes are carried out by the same bone cells (osteoblast, osteoclast, and osteocytes), but the end-result differs fundamentally. Modeling is responsible for the bone shape and mass changes during growth, whereas remodeling is known to renew existing bone. Bone remodeling occurs in two distinct phases: resorption of the old or damaged bone tissue by osteoclasts followed by new bone formation by osteoblasts, whereas osteocytes are actively involved in the routine turnover of the bone matrix through various mechanosensory mechanisms [37]. Bone remodeling is a constant process, and any mismatch in bone resorption and bone formation rates within the remodeling process can lead to bone loss. Over time, bone loss can change the structure of trabecular bone from plate-like to rod-like and also results in loss of connectivity, which has impact on mechanical properties of the bone tissue [38].

1.7 Bone quality, bone strength, and fragility fractures

A bone fracture is inherently a biomechanical event; therefore, the main focus of bone quality assessment is to explain the macroscale mechanical performance of bone. With this point of view, the National Institute of Health (NIH) defined bone quality as the total characteristics of bone that influence the bone's resistance to fracture or the totality of features/characteristics that influence a bone's ability to resist fracture [39].

In another study, bone quality is defined as the geometric and material factors that contribute to fracture resistance independently of DXA BMD [35]. On the other hand, we hypothesized that either if bone strength (which is directly correlated with BMD) or bone quality is not adequate, then minor trauma or even side-fall can lead to bone fractures. This type of low-impact fracture is known as fragility fractures, as shown in **Figure 1.2**.

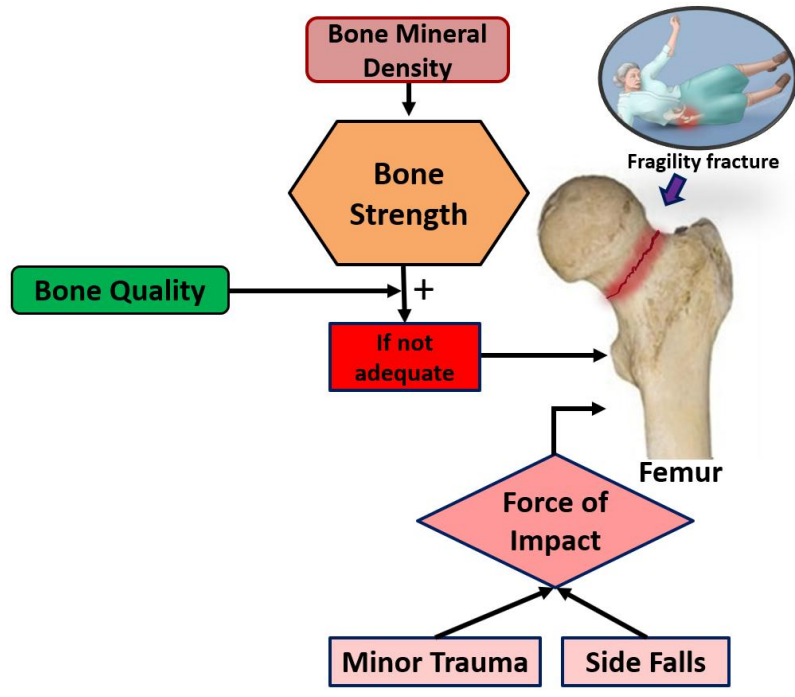


Figure 1.2: Schematic representation of the relationship between bone quality, bone mineral density, and bone strength, and how inadequate bone quality/strength leads to fragility hip fractures

1.8 Key determinants of bone quality

The bone quality is derived from various physical characteristics of the bone tissue at multiple length scales. The key contributing factors to bone quality are bone macro- (whole bone geometry) and micro- structure, bone mechanical-material properties, bone mineral content, mean crystal size, collagen content, and its secondary structure, accumulated AGEs content in the bone matrix, accumulation of microdamage (damage %), and the bone cell activity-dynamics as shown in **Figure 1.3** [38].

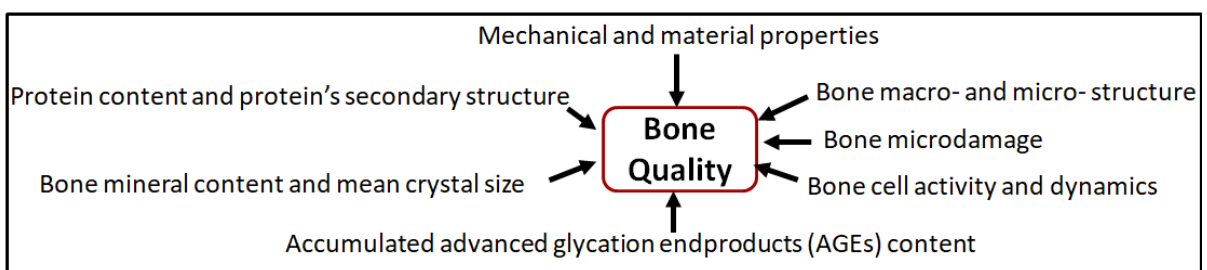


Figure 1.3 Determinants of bone quality [38]

There are various techniques available for the *ex vivo* assessment of bone quality parameters.

A specific method's choice depends on our objective, type of bone (cortical/trabecular), shape/size of the bone, and the amount of bone available. For example, the measurement of traditional biomechanical properties at mesoscale- tension, compression, and bending depends on the bone sample's shape and size. The bone quality assessment techniques at different organization levels of bone are discussed in detail in Chapter 2.

1.9 Current status of research

The effects of T2D on bone quality have been examined individually in rodent models [23], [40]–[43], *in vitro* studies of human and bovine bone tissue [44]–[47], human studies *in vivo* [48]–[50], and recently *ex vivo* studies in a clinical population of patients with osteoarthritis undergoing total hip replacement surgery [51]–[53].

At present, to simulate the human T2D and to investigate the effect of T2D on bone quality, both obese and non-obese rodent diabetic models are available based on spontaneous, monogenic abnormal leptin/leptin receptor signaling and diet-induced obesity, and reported weaker diabetic bones [54], [55], [64]–[66], [56]–[63]. The above described rodent models of T2D has its own advantages and disadvantages, thus selection of model is done based on the requirement. For example: in spontaneous diabetic rat model (animals with one or several genetic mutations), the development of diabetes is highly genetically determined, unlike heterogeneity seen in humans. Also humans T2D is multi-factorial, strongly associated with lifestyle and dietary factor. Further, the mortality due to ketosis problem is high in animals with spontaneous diabetic rat model and requires insulin treatment in later stage for survival. However the advantage of spontaneous diabetic rat model is that the animals develop characteristic features resembling human T2D and require small sample size of animals because small variability is observed in results. Furthermore, in diet-induced obesity models, the feeding of a high-fat diet (HFD) alone requires a long time, as well as no hyperglycemia develops upon simple dietary treatment in genetically normal animals. However, the advantage of diet induced T2D model is that here over nutrition is thought to cause T2D, as well as adverse effect of toxicity of chemicals on other body vital organs can be avoided [67].

The non-obese rodent model of T2D published by Saito et al. [62] demonstrated deteriorated structural, mechanical properties of stiffness, modulus, ultimate load, and energy absorption in the femur of spontaneously diabetic (onset of diabetes at 12–13 months of age) non-obese male WBN/Kob rats vs. Wistar (non-diabetic) controls (kept on the same diet). Zhang et al. [54] showed a decrease in the maximum load by 21% and energy absorption by 29.7% in the

femur of age- and sex-matched 6-month-old spontaneous diabetic (onset early after birth) non-obese male Goto-Kakizaki (GK) rats vs. male Wistar rats (kept on the same diet). Whereas no-significant difference is reported in elastic modulus among both the groups, it might be because different rat strain is used for comparison. Other than non-obese T2D rat models, many obese diabetic rat models showed a decline in mechanical properties in the three-point bending test. Kimura et al. [68] demonstrated deteriorations in the maximum load (44%), stiffness (28%), and energy absorption (77%) in the femur of Spontaneously Diabetic Torii (SDT-fa/fa) rats (obese T2D, onset at eight weeks of age) compared to Sprague–Dawley rats (control animals) at the 40 weeks of age (kept on the same diet). Prisby et al. [55] observed a significant reduction in the ultimate load (NS, by 18.8%) and stiffness (17.5% and 23%) in the femur of diabetic male ZDFfa/fa (onset at 10-12 weeks) vs. ZDF+/? (control) rats at 13 and 20 weeks of age, respectively (kept on the same diet). Reinwald et al. [58] demonstrated decreased ultimate load by 30%, stiffness by 39%, and work-to-fracture by 36% in the femur of 33 weeks old male diabetic ZDFfa/fa (fatty) vs. ZDFfa/+ (lean control) rats. They also observed a significant reduction in the ultimate load by 19% and stiffness by 15.6% in the femur of age-matched ZDSD compared to CDSD rats (disease onset 15-21 weeks of age). Gallant et al. [40] demonstrated decreased ultimate stress by 14.9%, modulus by 10.4%, and toughness by 50%, and post-yield toughness by 67% in the femur of T2D ZDSD male rats compared to control CD male rats, at the 32 weeks of age (HFD given for 12 weeks, since 20 weeks of age). Reddy et al. [69] demonstrated reduced maximum load by 37%, bending stiffness by 38%, and energy absorption to yield and toughness by 27% and 34%, respectively, in the femur of 10-week-old Sprague-Dawley rats treated with STZ (65 mg/kg body weight) for seven weeks. It indicates, all studies published so far using various T2D rat models showed lower femoral bone strength in the diabetic group with a three-point bending test, as summarized in **Table 1.1** below. These studies showed that the elevated accumulation of AGEs [42], [59], [70], [71] and altered collagen crosslinks [57], [62], [70], [72]–[74] can reduce mechanical properties. Few studies also reported the altered material properties with nanoindentation [56], [73], [75], and micro-indentation [23], [40], [59], [76] test.

Table 1.1: Various type 2 diabetic rodent models (based on spontaneous, monogenic abnormal leptin/leptin receptor signaling and diet-induced obesity) and results of femora in three-point bending test

Authors	Year	Material	Model category	Parameters investigated	Limitation
Reddy et al. [69]	2001	10-week-old Sprague-Dawley rats	Chemically induced diabetic rats, Treated with STZ (65 mg/kg body weight)	Reduced maximum load by 37%, bending stiffness by 38%, and energy absorption to yield and toughness by 27% and 34%, respectively	Relatively high dose of STZ causes direct insulin deficiency rather than the consequence of insulin resistance, It causes a drastic reduction in the bodyweight
Saito et al. [62]	2006	Male WBN/Kob rats vs. Wistar (non-diabetic) controls, Kept on the same diet	Spontaneous, Non-obese model, The onset of diabetes at 12–13 months of age	Deteriorations in the structural, mechanical properties of stiffness, modulus, ultimate load, and energy absorption	The development of diabetes is highly genetically determined, whereas in humans, the T2D is multi-factorial, strongly
Zhang et al. [54]	2009	Age- and sex-matched 6-month-old male Goto-Kakizaki (GK) rats vs. Male Wistar rats, Kept on the same diet	Spontaneous, Non-obese model, The onset of diabetes early after birth	Decrease in the maximum load by 21% and energy absorption by 29.7% in the femur	associated with lifestyle and dietary factor, Control rats belong to a different strain in [54] and [62]
Kimura et al. [68]	2012	Spontaneously Diabetic Torii (SDT-	Spontaneously diabetic from the Sprague-	Reduced maximum load by (44%), stiffness (28%), and	

		fa/fa) rats, obese, T2D onset at eight weeks of age, control animals SD rats, Age 40 weeks, Kept on the same diet	Dawley rat strain, Obese model	energy absorption (77%)	
Prisby et al. [55]	2008	Diabetic male ZDFfa/fa vs. ZDF+/? (control) rats at 13 and 20 weeks of age, Kept on the same diet	Severe obesity developed due to hyperphagia caused by abnormal leptin/leptin receptor signaling, The onset of disease at 10-12 weeks	Significant reduction in the ultimate load (NS, by 18.8%) and stiffness (17.5% and 23%) in the femur	Leptin or leptin receptor deficiency is not an important contributor to develop diabetes in humans (or very rare <1%), Only male rats are prone to become diabetic, Expensive model
Reinwald et al. [58]	2009	33 weeks old male diabetic ZDFfa/fa (fatty) vs ZDFfa/+ (lean control) rats.	Abnormal leptin/leptin receptor signaling, Obese model	Decreased ultimate load by 30%, stiffness by 39%, and work-to-fracture by 36% *significant reduction in the ultimate load by 19% and stiffness by	

		*age-matched ZDSD compared to CDS D rats (disease onset 15- 21 weeks of age)		15.6% in the ZDSD model	
Gallant et al. [40]	2013	Type 2 diabetic ZDSD male rats compared to control CD male rats, at the 32 weeks of age (HFD gave for 12 weeks, in the past 20 weeks of age)	Develop diabetes over time due to polygenetic and environmental factors – dietary manipulation	Decreased ultimate stress by 14.9%, modulus 10.4%, toughness 50%, and post-yield toughness by 67%	Only male rats are prone to become diabetic, Accessibility of animals and/or expense also tend to limit its utility
Barriere et al. [43]	2018	Male Wistar rats Control group- regular chow, Diabetic group- high-fat/high-	High-fat/high-fructose diet with low dose STZ, Genetically normal animals	Not available	

		fructose diet			
Zhang et al. [77]	2008	Wistar male rats Diabetic group- (HFD once or twice by i.p.), Control group- regular chow	HFD with multiple low dose STZ, Genetically normal animals	Not available	
Srinivasan et al. [65]	2005	Male SD rats, Diabetic group-HFD, Control group-NPD	HFD with four weeks, end of 4 th week -low dose STZ, obese model, genetically normal animals	Not available	

Numerous studies reported the bone turnover markers: C-terminal telopeptide of type I collagen (CTX), osteocalcin (OC), and procollagen type 1 N-terminal propeptide (P1NP) known as bone formation markers, and RANKL, TRAP5b are bone resorption markers are found lower in T2D. It indicates overall lower bone turnover in diabetic bone [78]–[81].

In vitro studies have also been conducted by incubating human and bovine tissue in highly concentrated ribose and glucose solutions (at least 100x greater than physiologic conditions) to study the effect of aging and T2D on bone mechanical properties [44]–[47]. The *in vitro* studies primarily provide evidence that in hyperglycemic conditions, the AGEs accumulate in the trabecular and cortical bone matrix and results in diminished energy absorption capacity at mesoscale [44]–[47]. Additionally, *in vitro* studies report the decreased osteoblast proliferation and differentiation [82], [83] and reduced osteoclast differentiation [84] in glycosylated collagen, which results in reduced bone turnover.

In vivo imaging studies have been conducted on T2D patients by using pQCT [85], and HRpQCT [15], [16], [48]–[50], [86]–[88]. Very first evidence of impaired cortical strength in T2D originally came from a pQCT study in a cohort of older men [85]. Later HR-pQCT study reported that higher cortical porosity (in elderly female patients with and without T2D) alone was found correlated with impaired bone strength determined by micro-finite element analysis, and provided a potential explanation for the inability of BMD to explain the elevated fracture risk in patients with T2D [16]. Some more *in vivo* imaging studies reported a similar bone microstructure and BMD in T2D patients than controls; with higher radial cortical porosity in the T2D patients. Whereas, one study reported no difference in vBMD, microstructure, and cortical porosity between T2D and controls [50]. There is contradictory evidence about the cortical porosity in patients with T2D, but majority of studies reported increased cortical porosity in T2D patients.

To date, only three *in vivo* studies have been conducted in people with and without T2D using an impact-based reference point indentation technique (OsteoProbe) [48]–[50]. Here the bone material strength index (BMSi) of tibial (cortical) bone is calculated with respect to plastic (PMMA) block and reported that patients with T2D had greater BMSi compared to those without T2D. Also, the BMSi is inversely correlated with glycated hemoglobin (HbA1c) [48], [50]. Human studies conducted on type 2 diabetes to evaluate bone quality parameters are summarized in **Table 1.2**.

Few recent *ex vivo* studies have directly assessed bone tissues' biomechanical properties from people with and without T2D undergoing total hip arthroplasty [51]–[53]. One of the studies [51] shows the deteriorated material properties in cortical bone (femoral neck) assessed by cyclic reference point indentation, but no significant difference is observed in trabecular bone mechanical properties, microstructural parameters, and fluorescent AGEs in T2D patients compared to non-diabetics. Another study shows that increased mineral content in T2D is associated with better trabecular microstructure, but T2D negatively affects the collagen matrix [53]. Also, the high concentrations of AGEs can increase fragility by reducing bone ability to absorb energy before fracture, especially for the subset of T2D patients with low BV/TV. In the third study, [52] data show that the accumulation of AGEs is associated with impaired bone microstructure. However, the mechanical properties did not differ between diabetic and non-diabetic groups. Pritchard et al. [89] reported that a combination of elevated mean calcium concentration in bone and lower mineralization heterogeneity in adults with T2D might have adverse effects on bone biomechanical properties. One more study

conducted by Wolfel et al. [90] using femoral bone obtained from T2D organ donors during the autopsy and show that higher carboxymethyl-lysine (CML) accumulation in the diabetic group, also high porosity T2D subgroup presents with changed mineralization pattern and lower mineral maturity. It can be concluded from above studies that the trabecular microstructure and mechanical properties did not differ between diabetic and non-diabetic groups. However few studies reported that the bone glycation is associated with impaired bone mineralization, collagen quality and increased fragility by reducing bone ability to absorb energy before fracture.

Table 1.2: Human studies conducted on the effect of type 2 diabetes on bone quality parameters

Authors	Year	Material	Method	Parameters	Remark
Farr et al. [48]	2014	<i>In vivo</i> , T2D (N=30), and 30 age-matched non-diabetic, T2D for >10 yrs and 30 age-matched, non-diabetic controls, Distal radius and tibia	DXA, HR-pQCT, Osteoprobe	aBMD ×, BMSi ↓, Ct.Po (radial) ↑, Serum markers of bone turnover ↓,	
Furst et al. [50]	2016	<i>In vivo</i> T2D (N=16), postmenopausal women and 19 matched controls participants,	Osteoprobe, skin autofluorescence (SAF), serum bone turnover markers	BMSi ↓ (9.2% in T2D), SAF ↑, bone formation marker procollagen type 1 amino-terminal propeptide in T2D ↓,	
Nilsson et al. [49]	2017	<i>In vivo</i> Women aged 75 to 80 years in Tibia and Radius	DXA, HR-pQCT, Osteoprobe	aBMD ×, Ct.Po (radius), BMSi (tibia)↓, BV/TV ↓, Tb.N (tibia) ↓	Relatively fit T2D patients
Chen et al. [91]	2017	<i>Ex vivo</i> Tibial plateaus	μ-CT, Micro-FE	BV/TV ↓, Tb.N ↓,	Comorbidity with knee OA,

		(TKA), Non-diabetic (n=70) and diabetes (n=51), controls cadaver donors (n=20)	analysis,	SMI ↑, Tb.Sp ↑ Conn.D ↓ E ↓	Only T2D cases not studied, Duration of disease not mentioned
Karim et al. [51]	2018	<i>Ex vivo</i> T2D (n = 20) and non- diabetic (n = 33) subjects undergoing THR surgery	μ-CT, compression tests, cRPI (cortical bone)	Ct.TMD ×, Ct.Po × CID ↑, IDI ↑ Yield Stress ↓ fAGEs × Serum -pentosidine ×	Diabetes for short duration is studied, DXA aBMD not reported, Comorbidity of osteoarthritis present
Hunt et al. [53]	2019	<i>Ex vivo</i> Trabecular bone from Femoral neck, Men n=31 T2DM, n=34 non-DM	μ-CT, and compression tests	AGE -pentosidine ↑ Sugar:matrix ↑ Mineral:matrix ↑ Compression - strength ↑	Presence of osteoarthritis, Participants' glycemic control was only on the order of months
Wolfel et al. [90]	2020	<i>Ex vivo</i> Organ donors during autopsy, Femoral cross-sections (Cortical bone) of approximately 1.5 cm thickness, N=16 T2D N=11 age-matched healthy	μ-CT, SEM- backscattered mode, NI, FTIR, fAGEs, CML-ELISA	Ct.Po ↑, Mineral:matrix ↑ CML ↑, fAGEs ×, NI ×, Osteon density ↓	Duration of diabetes and/or comorbidities were not evaluated, HbA1c not reported, DXA aBMD not reported, Autopsy samples were used

Piccoli et al. [52]	2020	<i>Ex vivo</i> Postmenopausal women affected by osteoarthritis undergoing elective hip replacement, n=19 T2D, n=73 non-diabetic	Gene expression RT-PCR, DXA, μ -CT, compression tests, fAGEs	fAGEs \uparrow vBMD \downarrow BV/TV \downarrow Tb.Sp \uparrow SOST gene expression \uparrow RUNX2 and osteocalcin \downarrow	Postmenopausal women affected by osteoarthritis, AGEs were measured only for five subjects
---------------------	------	---	--	--	--

In summary, rodent studies and a few recent human studies helped to understand the effects of T2D on bone as whole but dissimilar methods set hurdles to compare each study's results. A limitation of the previous human studies is that bone tissue was collected at the time of arthroplasty and may have confounding effects associated with arthritis (including increased trabecular bone density). Moreover, no direct link between alterations in bone quality and reduced mechanical performance has been formed. Furthermore, no prior studies of bone tissue material properties in humans have been conducted with diabetes (specifically uncontrolled diabetes and longer diabetes duration) and known fragility fracture status.

1.10 Research Objectives

While summarizing the contributions of previous studies, we also identify the critical hypothesis and concerns that form the basis of our proposed objectives. The main idea derived is as - the hyperglycemia, accumulation of AGEs, and non-enzymatic cross-linking are the underlying mechanism for multiple complications of diabetes, including altered bone quality and diminished mechanical performance of bone at the macroscale. The following research objectives have been proposed and also presented graphically in **Figure 1.4**:

1. To simulate human T2D and to investigate diabetic bone fragility, many rodent diabetic models have been developed. Still, the outbred genetically normal non-obese diabetic rat model is not available that can better simulate the metabolic characteristics of non-obese T2D, those have a high prevalence in Asia. Therefore, in first objective, a combination of high-fat diet and low dose streptozotocin treatment is used to develop late-stage of T2D in female Sprague Dawley (SD) rats and compared the effects of T2D on multiscale bone quality parameters.

2. Second objective addresses the issue of decreased bone quality in patients with T2D. To date only animal studies and few recent studies of human tissue have attempted to address decreased bone quality in T2D. A limitation of the previous human studies is that bone tissue was collected at the time of arthroplasty and may therefore have confounding effects associated with arthritis (including increased trabecular bone density). Furthermore, no prior studies of bone tissue material properties in humans have been conducted with diabetes and known fragility fracture status. The current study is novel in examining human bone tissue following the first hip fragility fracture. Also the increased bone fragility and reduced energy absorption to fracture associated with T2D cannot be explained by bone mineral density alone, therefore investigation of multiscale bone quality parameters were needed. Thus, here the role of T2D in altering biomechanical, microstructural, and compositional properties of bone in individuals with fragility fractures is investigated.

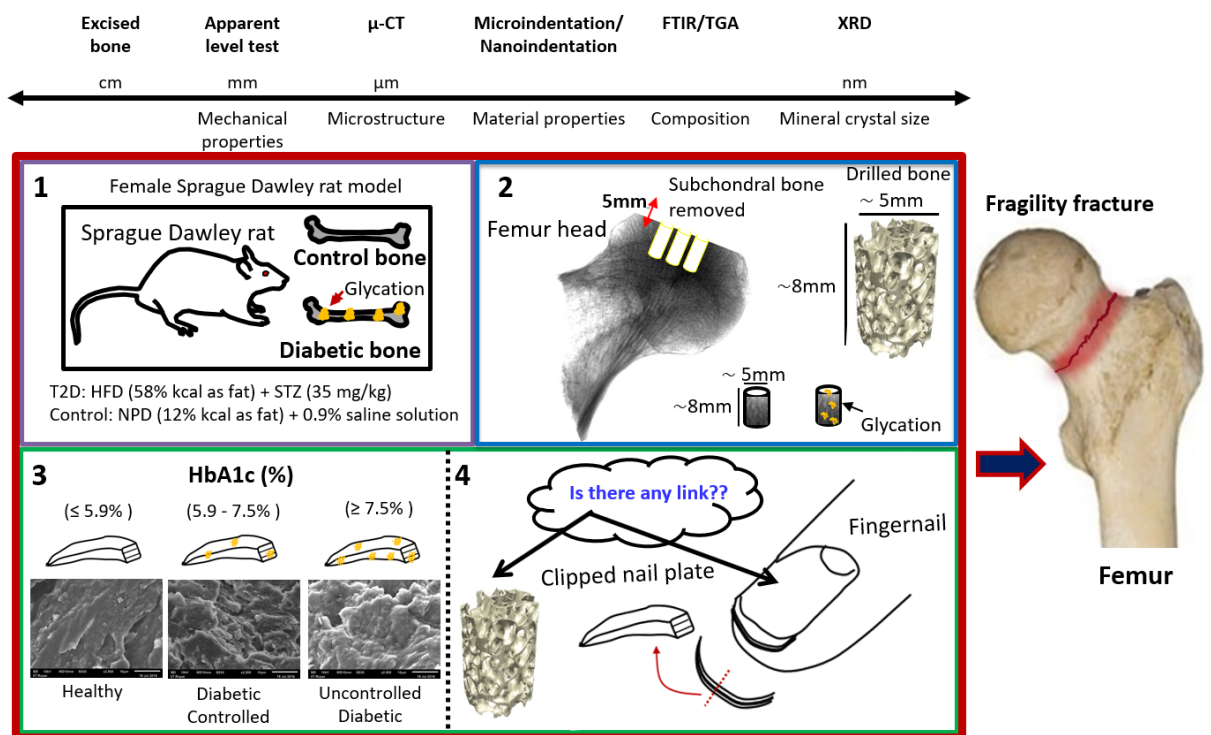


Figure 1.4 Graphical abstract showing the major objectives of the thesis

3. Clinically no such technique is available which can assess the altered tissue quality associated with T2D noninvasively. To explore possibilities of identifying a non-invasive, low-cost diagnostic technique that can help clinicians to predict bone quality beyond bone mineral density accurately, the multiscale fingernail plate quality is investigated with severity of T2D. Third objective aimed to explore the possibility

that the small-scale properties of the fingernail have the potential to serve as a non-invasive surrogate marker of bone quality in T2D.

4. The fourth objective was to study the material and compositional properties of bone/fingernail, in patients (recruited in objective 2) with diabetes and known fragility fracture status. Here we aim to establish a link in degradation pattern of both compositional/material properties of bone and fingernail plate quality.

1.11 Dissertation Overview and Organization

The thesis consists of seven Chapters and is organized as follows:

Chapter 1, Introduction, provides details about increased fracture risk in patients with T2D compared to those without T2D, motivated to work in this area. The limitations of conventional diagnostic tools which underestimate the individuals with T2D having increased fracture risk are discussed. The proposed mechanisms for how T2D can change bone quality are briefly described. The hierarchical structure of bone is discussed in detail, and how bone quality is associated with bone strength is also reported. A summary of the current state of relevant literature is provided, followed by a statement of research objectives for this work.

Chapter 2 covers techniques available to study bone quality at multiple length scales: microstructural, mechanical, material, and compositional properties. Many of the methods described are utilized in subsequent chapters.

The next four chapters are dedicated to the proposed research work.

Chapter 3 explain the development of HFD-fed low dose STZ treated T2D female Sprague Dawley rat model and the investigation of cortical bone (femora) quality parameters at multiple length scales.

Chapters 4 present the comparison in microstructural, material, and compositional properties of trabecular bone, in individuals with and without T2D and known fragility fracture status.

To investigate an alternative approach to predict bone fragility, Chapters 5 will incorporate the detailed investigation of the adverse effect of severity of T2D on human fingernail plate quality. Extension to this study, Chapter 6 presents the material and compositional properties of fingernails and bone in individuals with and without type 2 diabetes.

Chapter 7 Summarizes and discusses the key results of Chapters 3-6, discusses limitations of our work, and proposes directions for future research.

CHAPTER 2

ASSESSMENT OF BONE FRAGILITY IN TYPE 2 DIABETES BEYOND BONE MINERAL DENSITY

The previous chapter summarizes that bone quality deficits in type 2 diabetes (T2D) underlie the compromised bone strength in diabetes and leads to fragility fractures. Previously large studies reported the inability of bone mineral density (BMD) T-score, a quantitative measure, to predict fracture risk accurately in T2D. Various other *in vivo* and *ex vivo* techniques have been used to investigate bone quality and bone strength. However, each method presents its own challenges for utilization in routine clinical practice. This review presents the multiscale bone quality assessment, each technique's primary outcome, and limitations (**Figure 2.1**). Also, it summarizes the utility of different methods to study the *in vivo* and *ex vivo* bone quality and strength parameters in a previous rodent model and clinical population with and without diabetes **Table 2.1**. The purpose of this review is to highlight the multiscale characterization of bone as a material, the role of material properties plays in diabetic fractures, and to elucidate the importance of assessment of bone quality to clinicians in understanding and to assess type 2 diabetic fragility fractures.

Scale		Assessment techniques	Main Outcome
Macroscale	~48cm ↑	Whole bone testing QCT, pQCT	Strength, Toughness Morphology (shape, size)
		DXA	BMD
Mesoscale	10 mm	Mechanical testing	Strength, Modulus, Toughness
	~5 mm	QCT TBS	vBMD TBS score (fracture risk of vertebral bodies)
Microscale	~500μm	HRpQCT, cRPI, Osteoprobe MicroCT SEM qBEI Histology/ Histomorphometry	Microstructure, Porosity IDI, BMSi/BMS BV/TV, Ct.Po, Tb.N Microcracks BMDD Cellular activity and dynamics
	~5μm		
Nanoscale		NI FTIR and Raman	Er and H Mineral: matrix and Collagen structure
	~5nm ↓	AFM XRD,SAXS TGA EDX HPLC/UPLC	Collagen alignment Crystal size, Orientation Composition Elemental details Collagen cross-links

Figure 2.1 The key bone quality assessment techniques and their primary outcome along with their utility to study particular bone hierarchy scale

2.1 Structural Characterization

Structural parameters include macroscale features such as the shape, size, and cross-sectional properties of the whole bone (i.e., length, cortical diameters, and thickness) to microscale parameters such as the bone volume fraction, trabecular microstructure, cortical porosity, microdamage accumulation, and quantification of the vascular network. In the last few decades, many powerful *in vivo* (QCT, pQCT, HRpQCT, MD-CT, MRI, DXA) and *ex vivo*

(high-resolution μ -CT) imaging techniques have been developed to characterize the structural properties of diabetic bone; a few of them are discussed below:

Table 2.1: A literature review on techniques used to assess diabetic bone quality parameters

Scale		Animal study (Rodent model)	Clinical populations
Imaging techniques	QCT	Kimura (2012) [68]	Napoli (2018) [92], Melton (2008) [93]
	pQCT	Silva (2009) [72], Hamann (2013) [94], Reinwald (2009) [58], Prisby (2008) [55]	Melton (2008) [93], Petit (2010) [85]
	HRpQCT (<i>in vivo</i>)		Burghardt (2010) [16], Shu (2012) [86], Patsch (2013) [15], Farr (2014) [48], Paccou (2016) [87], Furst (2016) [50], Nilsson (2017) [49], Samelson (2018) [88]
	DXA (<i>in vivo</i>)	Saito (2006) [62], Zhang (2009) [54], Reinwald (2009) [58], Erdal (2010) [66], Ionova-Martin (2010, 2011) [95][71], Ealey (2006) [96], Devlin (2014) [59]	Vestergaard (2007) [7], Melton (2008) [93], Farr (2014) [48], Nilsson (2017) [49], Piccoli (2020) [52], Shanbhogue (2015) [97], Shu (2012) [86], Patsch (2013) [15], Yamamoto (2008) [98], Napoli (2018) [92], Schwartz (2001, 2009) [99] [100], Petit (2010) [85], Dhaliwal (2014) [12], Furst (2016) [50]
	μ -CT	Silva (2009) [72], Reinwald (2009) [58], Kimura (2012) [68], Gallant (2013) [40], Acevedo (2018) [42], Marin (2018) [41], Nyman (2011) [56], Creecy (2017, 2018) [57], [70], Xu (2013) [101], Ionova-Martin (2010) [95], Kerckhofs (2016) [102], Mansur (2015) [75], Devlin (2014) [59], Huang (2016) [103]	Chen (2017) [91], Karim (2018) [51], Hunt (2019) [53], Piccoli (2020) [52], Wolfel (2020) [90]

Mechanical test	3-point bending	Reddy (2001) [69], Saito (2006) [62], Prisby (2008) [55], Zhang (2009) [54], Reinwald (2009) [58], Kimura (2012) [68], Gallant (2013) [40], Acevedo (2018) [42], Silva (2009) [72], Marin (2018) [41], Rubin (2016) [23], Nyman (2011) [56], Creecy (2016, 2018) [70] [57], Hamann (2013) [94], Xu (2013) [101], Ionova-Martin (2010, 2011) [71], [95], Ealey (2006) [96], Mansur (2015) [75], Devlin (2014) [59], Huang (2016) [103]	
	Compression	Creecy (2018) [70], Ealey (2006) [96]	Karim (2018) [51], Hunt (2019) [53], Piccoli (2020) [52]
	Tensile	Erdal (2010) [66],	
	Fracture toughness	Creecy (2017) [57], Ionova-Martin (2011) [71]	
Material properties	Micro-indentation	Farlay (2016) [73]	
	Nano-indentation	Farlay (2016) [73], Nyman (2011) [56], Mansur (2015) [75]	Wolfel (2020) [90]
	cRPI	Gallant (2013) [40], Rubin (2016) [23], Hammond (2014) [76], Devlin (2014) [59]	Karim (2018) [51],
	Osteoprobe (<i>in vivo</i>)	NA	Farr (2014) [48], Nilsson (2017) [49], Furst (2016) [50]
Composition properties	TGA		Sekar (2011) [104]
	Raman	Marin (2018) [41], Rubin (2016) [23], Hammond (2014) [76], Creecy (2017, 2018) [57], [70]	
	FTIR	Bozkurt (2016) [105], Hunt (2018) [74], Boyar (2003) [106], Mansur (2015) [75],	Hunt (2019) [53], Sekar (2011) [104], Wolfel

		Mieczkowska (2015) [107]	(2020) [90]
	SAXS	Acevedo (2018) [42]	
	XRD		Sekar (2011) [104]
	qBEI, qXRI	Mansur (2015) [75], Mieczkowska (2015) [107]	Pritchard (2013) [89], Wolfel (2020) [90]
	SEM EDX	Ionova-Martin (2010, 2011) [71], [95]	Sekar (2011) [104], Pritchard (2013) [89]
	AFM	Hammond (2014) [76]	
	HPLC/UPLC	Silva (2009) [72], Saito (2006) [62], Farlay (2016) [73], Hunt (2018) [74], Creecy (2017, 2018) [57], [70],	Hunt (2019) [53], Oren (2011) [108]
	fAGE assay	Acevedo (2018) [42], Creecy (2018) [70], Ionova-Martin (2011) [71], Devlin (2014) [59]	Karim (2018) [51], Hunt (2019) [53], Piccoli (2020) [52], Wolfel (2020) [90]
Histology/ Histomorphometry		Silva (2009) [72], Zhang (2009) [54], Hamann (2013) [94], Devlin (2014) [59]	Chen (2017) [91], Wolfel (2020) [90], Jesse (1995) [109],
Serum biochemistry: CML, PEN		Creecy (2018) [70], Hamann (2013) [94], Xu (2013) [101], Ionova-Martin (2011) [71]	Shu (2012) [86], Yamamoto (2008) [98], [92], Schwartz (2009) [100], Furst (2016) [50], Wolfel (2020) [90]

2.1.1 Quantitative Computed Tomography (QCT)

Medical 3D QCT primarily measures the volumetric bone mineral density (vBMD, mg/cm³) *in vivo* for central and peripheral skeletal sites (at the lumbar spine and hip). When x-rays pass at an object of interest, they get attenuated after interacting with the matter. These attenuated x-rays are recorded by a detector placed opposite the radiation source. The x-ray source and detector rotate around the object and collect multiple 2D radiographic images, which are processed further with tomographic algorithms to create 3D image reconstruction. Digital image processing is used to produce 3D bone microstructure. The dedicated bone-equivalent calibration phantom (calcium hydroxyapatite) is imaged simultaneously with the

patient to convert the x-ray attenuation to bone density [110].

The central QCT (in-plane resolution: ~500 μm) is particularly useful to measure cortical thickness and volume of clinically relevant sites - hip or lumbar spine. In the lumbar spine, two or three vertebrae are usually imaged, L1–L2 or L1–L3, to reduce dose, whereas, in the hip, the femoral neck, trochanter, and intertrochanteric region are analyzed. Notably, the QCT can measure BMD values and bone geometry of trabecular and cortical bone independently but inefficient to quantify trabecular microstructure because the resolution of QCT is not sufficient to depict the thickness of individual trabeculae (50 to 300 μm). Some notable disadvantages of QCT include the higher radiation dose (0.06– 2.9 mSv) per 3D scan for bone structure evaluation [110], [111]. Some other disadvantages of QCT include high instrumentation expense and high per use costs, the inability to measure thin vertebral cortices, low device availability and higher precision error than that of DXA [35]. In general, the coefficient of variance (CV) is less than 3% in QCT analysis. [112]. However, the advanced 3D volumetric QCT (vQCT) technique has improved precision for measuring spine or hip from approximately 2-3% for single-slice to approximately 1-2% for volumetric measurements [112].

In one of the animal studies, QCT findings revealed decreased BMD of the whole tibia and shortening of tibia and femur in diabetic rats, compared to control rats [68]. In human studies, Napoli et al. [92] measured lumbar spine vBMD using QCT and reported similar vBMD for T2D and non-diabetic men and concluded that T2D was not associated with higher prevalence/incidence of vertebral fractures in older men. In another study, QCT and pQCT reported similar cortical vBMD, bone cross-sectional area, cortical thickness, and load-to-strength ratio in the diabetic and control groups [93]. In summary, QCT reported decreased BMD, shortening of tibia and femur in diabetic rats, whereas similar vBMD and bone geometry in diabetic patients.

2.1.2 Peripheral quantitative computed tomography (pQCT)

Peripheral QCT (pQCT) imaging is a subset of QCT that permits *in vivo* assessment of BMD, bone geometry, and evaluation of cortical as well as trabecular bone microstructure at appendicular bones such as the distal radius and tibia with more satisfactory resolution (in-plane resolution: ~200 to 500 μm) than QCT. The effective radiation dose per pQCT scan is lower than 0.01 mSv. The pQCT system can assess compartmental bone density as well as indices of apparent trabecular and cortical microstructure with the precision of <4% [113].

The first evidence of impaired cortical strength in T2D originally came from a pQCT study in a cohort of older men [85]. In animal studies, the *ex vivo* pQCT analysis revealed significantly lower total and trabecular vBMD at the lumbar vertebra (L4) and distal femur [94]. Also, vertebral trabecular morphology was found compromised in diabetic rodent strains compared to non-diabetic rats [55], [58], [94].

2.1.3 High resolution peripheral quantitative computed tomography (HR-pQCT)

The second generation HRpQCT (Xtreme CT II, Scanco 128 Medical AG, Switzerland) can provide separate vBMD measurements and microstructural parameters of cortical and trabecular bone with higher resolution 61 μm isotropic voxel size. It can also assess proximal tibia/radius and knee, along with distal radius/tibia, hand, fingers. The effective radiation dose per HRpQCT scan is around 0.003 mSv which is substantially lower than QCT. The Xtreme CT II offers substantial improvements in reproducibility compared to its previous version; first generation Xtreme CT I (XCTI, 82 μm isotropic voxel dimension) for all trabecular parameters (XCT II: 0.8–2.4%; XCT: 4.1–4.9%) as well as Ct.Th (XCT II: 1.1–1.2%; XCT: 1.6–3.6%) but not density-based measures (XCT II: 0.6–1.5%; XCT: 0.8–2.0%) or Ct.Po (XCT II: 11.0–13.3%; XCT: 6.2–12.5%) [114].

HRpQCT enables micro- finite element analysis with microstructural detail: cortical thickness and porosity, trabecular number, trabecular thickness and porosity, and trabecular separation. However, the HR-pQCT is not approved for clinical use at this time. It is limited to peripheral skeletal sites and cannot provide direct insight into fragility fractures' at clinically relevant areas: lumbar spine or proximal femur. The motion artifacts are another issue that sometimes limits morphological analysis of bone microstructure with HR-pQCT [110].

Despite these limitations, various techniques (pQCT, HRpQCT) have been used in research to investigate *in vivo* assessment of cortical and trabecular vBMD, bone geometry, microstructural parameters, and mechanical strength estimation through finite-element analysis of distal radius and tibia of diabetic patients [15], [16], [48]–[50], [86]–[88], [97]. In MrOS [85], pQCT was used to assess bone strength at peripheral sites in T2D, and lower bone bending strength was observed at midshaft regions of radius and tibia in those with T2D, despite no differences in cortical vBMD. Though pQCT is a clinically available tool, the imaging resolution remains a limitation.

Consequently, various approaches have been proposed to include bone quality changes and explain poor bone mechanical properties. For example, the first HRpQCT study reported high

cortical porosity in the diabetic group despite higher trabecular vBMD, trabecular thickness, and modulus in elderly female patients with T2D than in those without T2D [16]. Here, the cortical porosity differences alone were correlated with impaired bone strength determined by micro-finite element analysis (μ FEA). This investigation provides a potential explanation for the inability of BMD to explain the elevated fracture risk in patients with T2D [16]. One more study reported no differences in peripheral bone microstructure between postmenopausal women with and without T2D (without a history of fragility fractures) [86]. Another study recruited postmenopausal diabetic women with and without fragility fractures and comparing them with non-diabetic controls with and without fractures showed that reduction in stiffness, failure load, and cortical load fraction (with μ FEA) possibly associated with high cortical porosity [15]. Simultaneously, they reported that the cortical porosity is not a general characteristic of diabetes but is only exhibited by T2D patients with fragility fracture. Also, lower total and cortical BMD with relatively maintained trabecular microstructure are reported [15]. Some more studies reported a similar bone microstructure and BMD in T2D patients than controls; however, radial cortical porosity tended to be higher in the T2D patients [48], [87], [88]. A different study showed higher vBMD, failure load, and more favorable bone microstructure in the diabetic group than the non-diabetic group [49]. In that line, one more study reported higher trabecular BV/TV (%) and bone stiffness (with μ FEA) at the radius but not at the tibia and more increased trabecular thickness at both sites in T2D patients. Whereas no difference is reported in vBMD, microstructure, and cortical porosity between T2D and controls [50]. In summary, majority of studies reported that no differences in peripheral bone microstructure, and vBMD, whereas cortical porosity tended to be higher in the T2D patients and possibly associated with reduced failure load. However, it should be noted that these data are restricted to peripheral sites only and do not provide measurements in axial regions such as the hip and spine, which both are common fracture sites for fragility fractures in T2D patients.

Though, one *ex vivo* study conducted on human cadaveric bone determined the relationship between biomechanical strength of the hip/spine, and vBMD and FE estimated strength at the radius/tibia measured by HR-pQCT. This study reported a strong correlations between properties of the distal tibia (total vBMD and simulated strength) and the biomechanical strength of proximal femora from the same donor [115]. Another study reported that large cortical bone pores (diameter > 100 μ m) in the tibia was associated with decreased (simulated) hip strength [116]. In summary, a strong association is observed between

tibia/femur data.

2.1.4 Dual-energy X-ray absorptiometry (DXA)

DXA is the most widely used non-invasive technique for measuring areal bone mineral density (aBMD, g/cm^2) of the lumbar spine (L1–L4), proximal femur (femoral neck and total hip), and forearm (distal), with short acquisition time. In DXA, two different energy levels of x-ray beams pass through the bone. When soft tissue absorption is subtracted out, each beam's energy absorbed by bone is evaluated based on differential transmitted beam intensities analyzer (with an algorithm), then calibrated with a standard known radiographic density, which gives the calculated value of BMD. Finally, the resulting bone density data are compared with known populations from which assessments are made regarding overall density and fracture risk. However, it should be noted that the QCT-derived BMD measurement technique allows the determination of true volumetric BMD (vBMD, g/cm^3) while DXA BMD is the mass of bone mineral within the 2D scan area (aBMD, g/cm^2) [35], [111].

According to WHO standards, the DXA outcome is used to identify those at risk of osteoporotic fracture. Osteoporosis can be diagnosed if the value of aBMD is 2.5 or more standard deviations (SD) below the mean value of a young reference population (T score at or below -2.5). At present, the DXA is the gold standard to diagnose osteoporosis and accordingly identify low aBMD and T-score for individuals at risk for fracture. One study reported that DXA measurements have a low precision error (short-term precision spine 1.3%, total hip 1.2%, and femoral neck 1.4%) [117]. However, the clinical utility of DXA in T2D is limited due to either normal or elevated aBMD in T2D, which suggests that their increased fracture risk might be due to other factors that are not captured by aBMD measurements [7], [12], [48], [50], [93].

The previously reported large studies explained the BMD T-score's inability to accurately predict fracture risk in T2D [11], [85]. In the Study of Osteoporotic Fractures [11], for a given age and T-score, the risk of hip or non-spine fracture was higher in women with T2D than those without diabetes after 25 years follow-up. While T-score is useful in fracture risk assessment in women with and without diabetes, T-score underestimates fracture risk in T2D [11], [118]. Meanwhile, the International Osteoporosis Foundation (IOF) recommends adjusting BMD T-score for diabetes to avoid underestimation of risk in clinical practice [118].

2.1.5 Trabecular bone score (TBS)

The trabecular bone score (TBS) is developed to overcome the limitations of BMD measurements and to provides additional volumetric information - bone architecture at low cost by using DXA images of the lumbar spine. This method utilizes an experimental variogram of 2D projection DXA images at the same site to calculate the trabecular bone score. Higher TBS value reflects denser trabecular bone structure, whereas low TBS is associated with more porous or osteoporotic trabecular bone [12], [110], [119]. One study reported that TBS of >1.31 indicate denser/normal bone, TBS 1.23 to 1.31 revealed partially degraded, and TBS < 1.23 show porous/degraded bone [120]. The precision error of TBS vary from 1.12-2.1% depending on the design of the study and machine involved [121].

TBS predicts fracture risk, independent of BMD. However, TBS is a surrogate measurement of trabecular architecture and not a tool for assessing bone strength. Also, there are clear recommendations not to use TBS alone for treatment recommendation [110].

2.1.6 Micro-computed tomography (μ -CT)

Micro-computed tomography is an *ex vivo* imaging technique used to study cortical and trabecular bone microstructure. Usually, bone biopsies, excised bone tissues, or key skeletal sites of small animals can be scanned with a resolution of ~ 0.5 to $100 \mu\text{m}$. Similar to QCT and HRpQCT, tomographic algorithms generate μ -CT 3D images, but the attenuation data is collected in a slightly different manner: desktop μ -CT scanners designed for *ex vivo* specimens often have a rotational specimen stage and a stationary x-ray source and detector, while scanners intended for *in vivo* small animal scans have a fixed stage and a rotational source-detector gantry. This technique's primary advantages include the ability to characterize the details of trabecular microstructure, cortical porosity and pore size, microdamage, and even the osteocyte network or vascular network. However, more satisfactory resolutions come at the cost of longer scan durations and greater radiation exposure. Besides, the specimen sizes that can be scanned *ex vivo* at the highest resolutions are limited (~ 100 mm diameter, 140 mm length). The dedicated bone-equivalent standard phantom (calcium hydroxyapatite, QRM GmbH, Mohrendorf, Germany) is imaged with the same parameters as the bone samples for bone density calibration. Later the mean gray value was calibrated based on the linear relationship between gray matter and density [122].

The following microstructural parameters can be calculated with μ -CT: trabecular volume

fraction (BV/TV, %), trabecular number (Tb.N, 1/mm), trabecular thickness (Tb.Th, mm), trabecular separation (Tb.Sp, mm), structure model index (SMI), degree of anisotropy (DA), connectivity density (Conn.D), cortical bone area (Ct.Ar, mm²), average cortical thickness (Ct.Th, mm), tissue mineral density (TMD, g/cm³) and cortical porosity (Ct.Po, %). Remarkably, the TMD has the same units as vBMD, but the volume of interest for TMD excludes voids and soft tissue. Therefore, TMD represents the bone material's density, whereas vBMD may include porosity, and adequate scan resolution should be carefully considered to achieve accurate cortical porosity measurements [123]. A brief description of trabecular and cortical microstructural parameters obtained through μ -CT is provided in **Table 2.2** and **Table 2.3**, respectively. In general, the reproducibility of μ -CT examination after rescanned and reanalyzed 20 human biopsy specimens was 2–6% for trabecular structural parameters. In high resolution μ -CT reproducibility was further high, with precision errors of 1.57–4.69% for lacuna parameters, and of 1.01–9.45% for vascular canal parameters [124].

A recent *ex vivo* study on human specimens using μ -CT on the proximal femoral head showed no change in microstructural parameters [51], [52], including cortical porosity between T2D patients compared to non-diabetic controls [51]. Another *ex vivo* study on human trabecular bone specimens reported a slightly elevated but not statistically significant trabecular BV/TV ($p=0.125$) in men with T2D compared to non-diabetics. However, this study reported nearly similar trabecular bone microstructural parameters other than Tb.SP [53]. One study identified a high porosity phenotype within the T2D group illustrated by an approximately 4-fold higher cortical porosity in the T2D group than the controls [90]. Another study on human bone tissue following the first hip fragility fracture reported lower BV/TV (%) in people with diabetes when compared to non-diabetics [38]. In summary, there is contradictory evidence about the association between T2D and BV/TV.

Table 2.2 Definition and description of trabecular bone microstructural parameters

Abbreviation	Variable	Description	Units
TV	Total volume	Volume of the entire region of interest	mm ³
BV	Bone volume	Volume of the region segmented as bone	mm ³
BV/TV	Bone volume fraction	Ratio of the segmented bone volume to the	%

		total volume of the region of interest	
Tb.N	Trabecular number	Measure of the average number of trabeculae per unit length	1/mm
Tb.Th	Trabecular thickness	Mean thickness of trabeculae, assessed using direct 3D methods	mm
Tb.Sp	Trabecular separation	Mean distance between trabeculae, assessed using direct 3D methods	mm
Conn.D	Connectivity density	A measure of the degree of connectivity of trabeculae normalized by TV	1/mm ³
SMI	Structure model index	An indicator of the structure of trabeculae; SMI will be 0 for parallel plates and 3 for cylindrical rods	
DA	Degree of anisotropy	1= isotropic, >1=anisotropic by definition; DA=length of longest divided by shortest mean intercept length vector	dimensionless

Table 2.3 Definition and description of cortical bone microstructural parameters

Tt.Ar	Total cross-sectional area inside the periosteal envelope	mm ²
Ct.Ar	Cortical bone area = cortical volume (Ct.V)/ (number of slices * slice thickness)	mm ²
Ct.Ar/Tt.Ar	Cortical area fraction	%
Ct.Th	Average cortical thickness	mm
Ps.Pm	Periosteal perimeter	mm
Ec.Pm	Endocortical perimeter	mm
Ct.Po	Cortical porosity: In a given cortical region, the volume of pores (Po.V, mm ³)/ total volume of cortical bone compartment (Ct.V, mm ³)	%
Ct.Po.Dm	Mean pore diameter, calculated based on a porosity thickness map generated via 3D sphere-filling	mm

2.1.7 Bone histomorphometry

Bone histomorphometry is a quantitative histological assessment of a calcified bone biopsy performed to obtain quantitative information of bone microstructure, cellular activity, and particularly bone remodeling that is not available by any other investigative approach. It is

considered a valuable and well-established clinical and research tool in bone metabolism for studying the pathogenesis of bone diseases and defining mechanisms by which drugs affect the bone. The iliac crest is the preferred site for bone biopsy, and the ideal biopsy should contain inner and outer cortical plates with intervening trabecular bone [37].

Bone histomorphometric parameters are divided into structural and remodeling parameters. The structural parameters provide information about bone mass and structure, such as trabecular bone volume (BV/TV, %), trabecular thickness (Tb.Th), trabecular separation (Tb.Sp), and cortical width (Ct.Wi). The remodeling parameters are further divided into static and dynamic categories. The static parameters provide information about the amount of un-mineralized bone (osteoid) and extent of resorption cavities such as osteoid volume, osteoid surface, osteoid thickness, eroded surface, osteoblast surface, and osteoclast surface. In contrast, the dynamic remodeling parameters provide information about bone formation rate and can only be measured when patients have been tetracycline-labeled before the biopsy. As a result, labeling agent deposits at sites of new bone formation by binding irreversibly to hydroxyapatite at the mineralization front and allow these regions to be visualized and quantitatively analyzed. The dynamic remodeling parameters include mineralizing surface, mineral apposition rate, bone formation rate, adjusted apposition rate, mineralization lag time, and activation frequency [37], [125].

The main limitation with this technique is its invasive nature of a bone biopsy which also required expertise. Additionally, a bone biopsy is painful, requires operation theatre, and involves the risk of infection or delayed healing immensely in individuals with diabetes. Few dynamic histomorphometry studies on diabetic bone reported lower bone formation in trans iliac crest biopsies [109], [126]. One of those studies reported lower bone formation in T2D, but the numbers were very small (n=6 T2D patients; 2 female) [109]. In another study, reduced histomorphometric indices of bone formation were observed in T2D subjects, including mineralizing surface, bone formation rate, and osteoblast surface [126]. One recent study reported static bone histomorphometry parameters of femur's cortical bone from diabetic donors and found deficient cellular activity in the cortical bone tissue in aged human cohorts [90]. In summary, the T2D is associated with reduced bone formation.

2.2 Mechanical characterization

Mechanical properties can be assessed at different organization levels of bone hierarchy, such as testing whole-bone at the macroscale, bone tissue testing at mesoscale, and

investigation of bone material properties at microscale or nanoscale. In general, mechanical testing of bone involves stabilizing the bone of interest in testing grip, applying a load (or displacement), and measuring the resulting deformation. The key properties quantified in mechanical testing to define bone's resistance to fracture are stiffness, strength, toughness, and fracture toughness. 1) stiffness, the ability to resist elastic/reversible deformation; 2) strength, the ability to resist plastic/permanent deformation; 3) toughness, the ability to absorb energy during deformation; and 4) fracture toughness, the ability to prevent cracks initiation and progression. Here in this section, the detail is provided about key mechanical testing, their outcome variables, and the length scale assessed by each test, along with a brief description of bone tissue handling and storage conditions.

2.2.1 Whole bone test (Three-point bending test)

Macroscale mechanical testing of whole bones is a destructive method and is therefore only possible in *ex vivo* studies of animal and cadaveric bone. Long bones and vertebrae are generally used for whole-bone testing, and typical loading modes include bending and compression, respectively.

In three-point bending, the femoral bone is often chosen because the diaphyseal cross-section is approximately elliptical, which simplifies subsequent mechanical analyses. The bones were placed in such a way that the posterior side down on the bottom support and the central loading roller apply force at mid-diaphysis. The specimens are preloaded with a suitable load, it also ensure proper contact between the test specimen and the loading roller. To test samples till failure, a single-cycle ramp function at a constant displacement rate is applied with no displacement end limit [127], [128]. The bending tests are performed at room temperature while keeping the specimen hydrated through Phosphate-buffered saline (PBS) spray. The load-displacement data is captured at a suitable time interval which is further used to plot the load-displacement curve (**Figure 2.2**) and calculate the maximum load (F_{max} , N), stiffness (N/mm), work-to-failure (N.mm), and post-yield displacement (PYD, mm). Here, F_{max} is the greatest load achieved before fracture, stiffness is measured as the slope of the linear portion of the load-displacement curve, work-to-failure represented as the area under the load-displacement curve (whole bone toughness), and PYD refers to displacement (D) that occurs between fracture (D_{fx}) and yielding (D_{yield}) [$PYD = D_{fx} - D_{yield}$]. The yield point is calculated with a 0.2% offset method [129], [130].

However, the whole bone testing conditions do not satisfy some of the engineering theory's assumptions, which include uniform cross-sections along the long axis of the bone and homogeneous material properties. This could be a reason that the estimated material properties from whole-bone testing are poorly correlated with material properties assessed directly at a smaller scale [131]. Therefore, the direct assessment of smaller-scale material properties is essential.

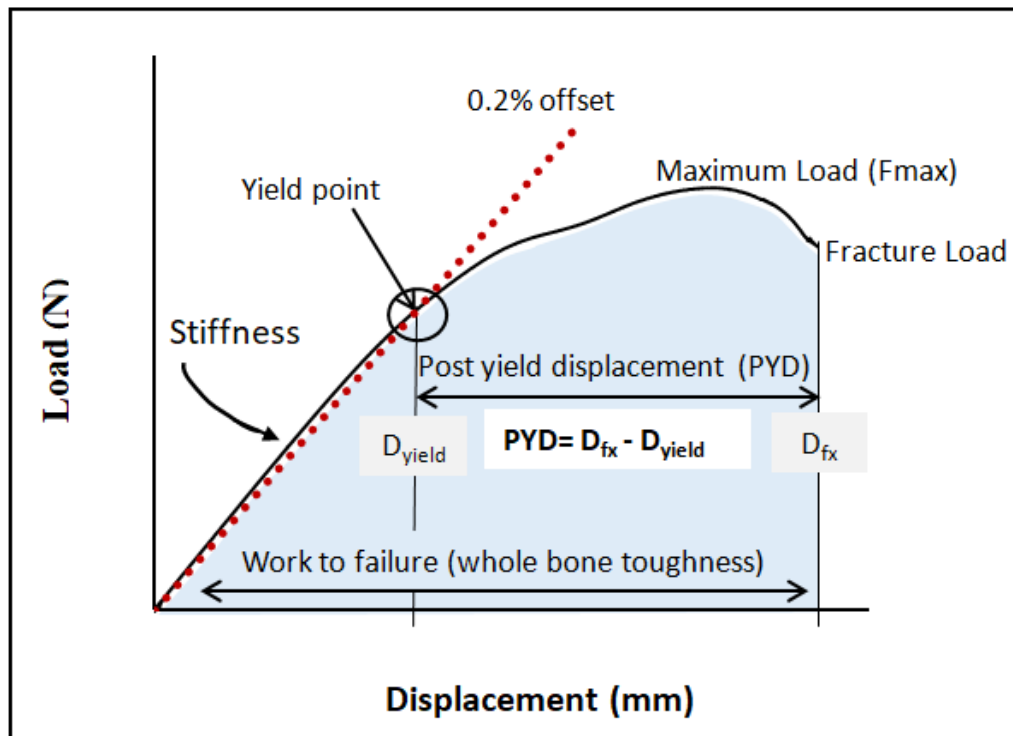


Figure 2.2 Typical load-displacement curve of three-point bending test, and description of various structural parameters derived from load-displacement curve

2.2.2 Apparent-level test (Uniaxial compression)

The compression test is performed on uniformly machined specimens of cortical and trabecular tissue (width: mm to cm, length: mm to cm) to determine the material properties such as apparent-level modulus, strength, and toughness. At this level of mechanical testing, the effect of bone microstructure, bone volume fraction, and bone composition is included in measured properties. Thus, the outcome at this structural hierarchy is called apparent-level properties. In general, the drilled trabecular bone core is utilized for the compression test. The bone core's top and bottom surfaces are ground to make it parallel to each other, and the length-to-diameter ratio should be kept approximately 1.5:1 for testing. The bone core is fitted in customized mild steel cylindrical end caps to eliminate movement during mechanical

testing [132]. The specimen is preloaded with a load of ~5 to 10N to ensure proper contact between the test specimen and compression plate. Then, preconditioning cycles are applied to increase the reproducibility of mechanical testing and minimize the toe region, afterward, the final testing is conducted. The load-displacement data is captured and converted into stress-strain data by normalizing with the sample's geometry determined by μ -CT or other means to estimate tissue-level material properties. The typical stress-strain plot of bone is shown in **Figure 2.3**, with the description of various material properties derived from the stress-strain curve. Later, several mechanical parameters can be determined, including elastic modulus, yield point (using the 0.2% offset method), ultimate point (defined as the point of maximum load), post-yield strain (determined as the difference between an ultimate strain and yield strain), post-yield strain energy, and toughness [127], [132], [133].

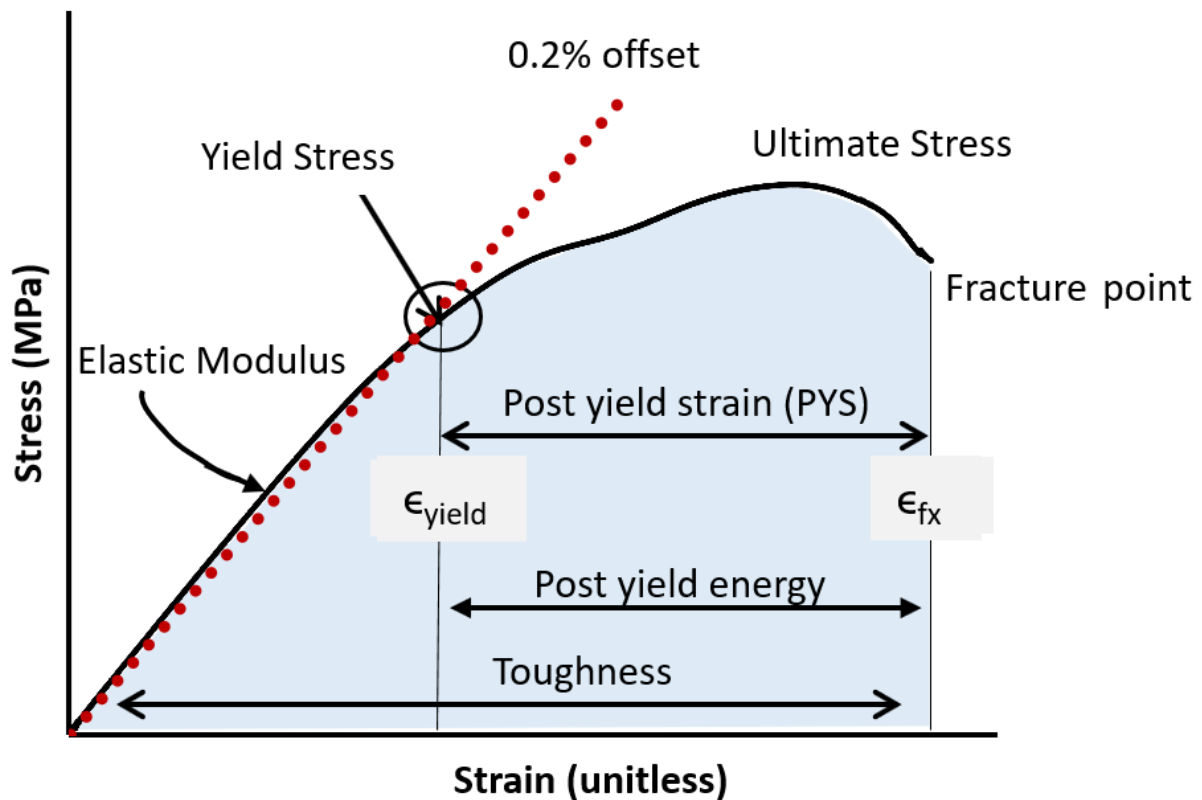


Figure 2.3 Typical stress-strain curve of bone compression test, and description of various material properties derived from the stress-strain curve

Few recent *ex vivo* studies have directly assessed the biomechanical compression properties of bone tissues from people with and without T2D undergoing total hip arthroplasty [51]–[53]. Two studies reported that the mechanical properties did not differ between diabetic and non-diabetic groups [51], [52]. Another study [53] indicates that the high mineral content in

T2D is associated with increased trabecular bone strength. In contrast, increased AGEs are related to deteriorated post-yield strain and toughness in trabecular bone of T2D compared to non-diabetics [38]. In summary, the pre-yield properties are not significantly different among both the groups - with and without diabetes.

2.2.3 Cyclic reference point indentation (cRPI)

In bone, indentation testing can be performed at several length scales, and it gives information regarding the resistance of bone tissue to plastic/permanent deformation. The cyclic reference point indentation (cRPI) is a technique that provides a measure of bone mechanical properties, particularly Biodent's cyclic loading profile, which illustrates creep or fatigue associated with crack growth in the bone tissue. The essential advantage of this technique is its ability to measure bone material properties directly and removes the influence of a larger length scale. For example, suppose diabetic tibia is tested with reference point indentation. In that case, the tibial length and cortical cross-sectional geometry do not influence the measured outcome, whereas material properties of tibial mid-shaft remain the important outcome variable [134].

The cRPI can be used to measure bone material properties either *ex vivo* or *in vivo* (in animal studies). This cRPI device is known as BioDent[®] (Active Life Scientific, Santa Barbara, CA), which can operate with customizable parameters, including preconditioning, maximum indentation force, and cycle number. Indentations were made using a probe assembly consisting of a reference probe with the blunted end (~5 mm cannula length) and test probe with spherical tip (2.5 μm radius point) that tapers from a 90° cone shape to cylindrical shaft (BP2 probe, Active Life Scientific, Santa Barbara, CA). The output measurement is a load-indentation distance curve with each cycle presented on the same plot. Before actual measurement, the probe is indented on a PMMA block according to the manufacturer's indication to ensure proper function. Later, for fixed load, the distance by which the probe inserted into the bone was recorded as shown in **Figure 2.4**, which further used to calculate indentation distance (ID, indentation distance measured in the first cycle [μm]), total indentation distance (TID, total indentation distance across all cycles [μm]), indentation distance increase (IDI, increase in the indentation distance in the last cycle relative to that in the first cycle [μm]), average energy dissipation (avg ED, area enclosed by the test's hysteresis loop from the third to last cycle [μJ]), unloading slope (US, unloading slope of the first cycle [$\text{N}/\mu\text{m}$]), and average unloading slope (avg US, average unloading slope from third to last cycle [$\text{N}/\mu\text{m}$]) [134], [135]. The IDI to a fixed force is an essential parameter of

cRPI testing to distinguish the fragile bone from less easily fractured bone [136]. Also, it is inversely correlated to bone toughness [40]. Other outcomes are US-1st, an indicator of bone material stiffness, and Avg-ED to measure unrecovered bone deformation (plasticity) [130]. However the inter-animal variability is 16% (US-1st) to 25% (ED-1st and IDI) on skeletally mature rats [137], and Inter-individual variability of *in vivo* measures on human patients is reported between 15-24% for IDI and 10–17% for TID [138].

One human study reported higher creep indentation distance and indentation distance increase in cortical bone from T2D than in non-diabetics [51]. In rodent studies, some altered indentation properties are reported to be mainly larger indentation distances in cortical bone, suggesting impaired cortical bone tissue properties. [23], [40], [76]. These studies evident that increased IDI is observed for both animal and human studies.

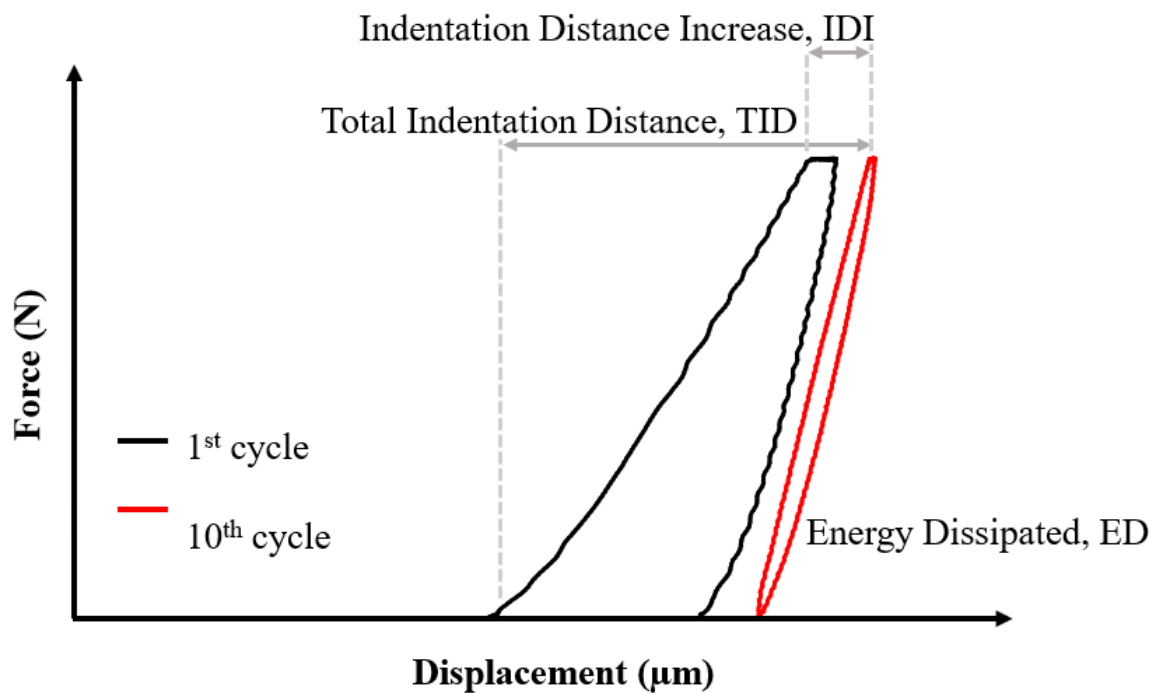


Figure 2.4 Typical load-displacement curve of cyclic reference point indentation (cRPI) test, and description of various parameters derived from cRPI load-displacement curve

2.2.4 Osteoprobe

Osteoprobe[®] (Active Life Scientific, Santa Barbara, CA) is an impact-based microindentation instrument. Its loading profile reflects energy dissipation of bone material due to a major crack created by a single high-velocity, high-energy load. The *in vivo* indentation is performed in three phases: 1) a linear preload of 10N, which passes through soft tissue; 2) a single impact load of 30N to create a force to drive the probe into bone, and the displacement

transducer measures indentation distance increase (IDI, μm) during impact and 3) unloading of the probe. With Osteoprobe, few separate indentations are made >2 mm apart. The indents are made on the anteromedial surface of the tibia. The outcome parameter, bone material strength index (BMSi)/bone material strength (BMS), is calculated as the average indentation distance into the bone normalized to the indentation distance into the polymethyl methacrylate (PMMA) reference phantom $\times 100$ [134]. BMSi is a direct measure of fracture resistance, and higher IDI indicates the lower BMSi; in other words, bone is weak and tends to be more easily fractured [139]. One study reported that Osteoprobe provides reproducible measurements of the material strength of bone in laboratory samples as well as in clinical trials on humans and horses [140]. Another study reported intraobserver coefficient of variance (CV) is 3.2%, observed from duplicate measurements performed on 30 elderly women [141].

In previous *in vivo* studies, the micro-indentation (Osteoprobe) of the tibial cortex has been performed to demonstrate that the estimated bone material strength index (BMSi) is decreased in T2D compared to controls [48]–[50]. The BMSi is inversely correlated with prolonged hyperglycemia [48], [50] and explains the increased fracture risk in T2D [49]. However, the indentation distance of Osteoprobe has not been validated with standard mechanical testing outcomes; thus, it is unknown how BMSi is associated with mesoscale stiffness, strength, and toughness [142]. The Osteoprobe technique's limitations are that here hardness value cannot be determined because this technique does not facilitate measuring the deformation geometry. Also, the measurement of Osteoprobe is limited to the mid-diaphysis of tibial bone, and it does not represent the BMS value at clinically relevant fracture sites such as the femoral neck and spine [50].

2.2.5 Nanoindentation (NI)

Nanoindentation tests provide more information about the material properties through the use of depth-sensing transducers. The bone sample's desired size is prepared with a low-speed diamond blade saw (IsoMet, Buehler, Lake Bluff, IL, USA). Later, the bone specimen is embedded in epoxy, the cured sample is ground and polished because surface polishing artifact can lead to variability in outcome measures [143]. Nanoindentation test is performed using Berkovich pyramidal tip. The instrument's calibration is performed with the help of standard fused quartz and aluminum samples following the standard procedure [144], [145]. Locations for indents are identified, and several indents with a fixed peak load (in μN) and a

suitable load function are performed on the samples' surface. During indentation, the tip displacement is continuously measured to produce a load-displacement curve, further used to determine the reduced modulus (E_r) and hardness (H) using Oliver and Pharr method [146], [147]. Here, hardness represents the average pressure under load. It is calculated as the maximum load divided by the indentation contact area. The reduced modulus represents its resistance to elastic/reversible deformation, calculated from the slope of the unloading portion of the load-displacement curve [146]. The typical load-displacement curve of the nanoindentation test and a description of reduced modulus and hardness derived from this curve are shown in **Figure 2.5**. One study reported that the CV for hardness and modulus were (29% and 23%), and (22% and 17%) respectively, whereas the CV is observed significantly lower (CV=1–9%) for the reference materials (LDPE, PC and PMMA) tested in same condition. This variation is found high due to the nanoscale heterogeneity in bone samples [148].

A drawback of the nanoindentation technique is the requirement of careful sample preparation (e.g., surface polishing); specifically, the surface irregularities must be smaller compared to the indentation size [149].

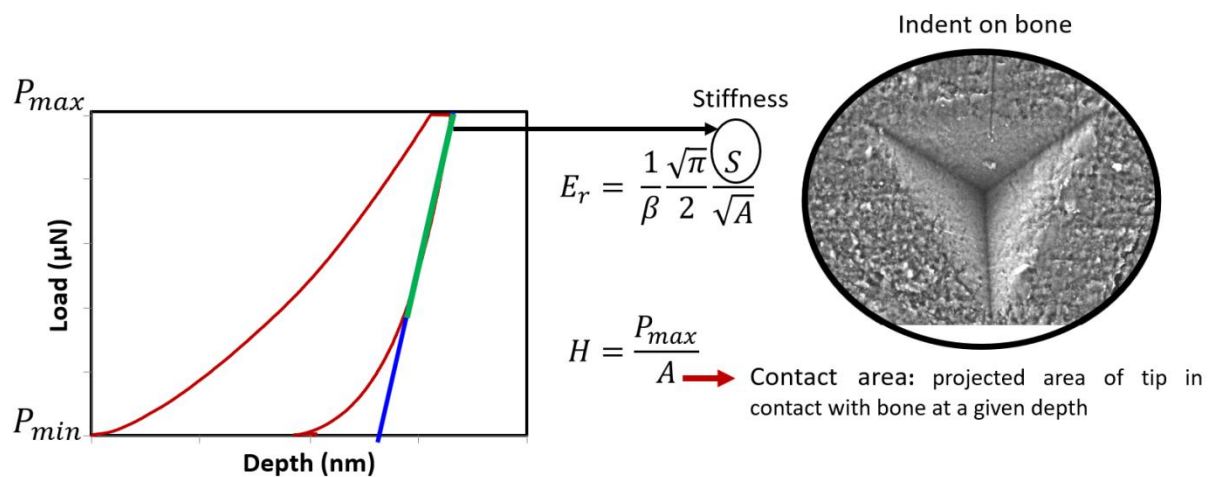


Figure 2.5 Typical load-displacement curve of nanoindentation test, and description of reduced modulus and hardness derived from nanoindentation load-displacement curve

2.3 Compositional analysis

As described in the previous chapter, the bone composition consists of the organic matrix (composed mainly of type 1 collagen), a hydroxyapatite-like mineral phase, and water content. Any alterations in bone composition due to age or disease can have drastic effects on

bone macroscale mechanical properties. Therefore, assessing the individual constituent of bone is essential to get more insight into the bone quality and predict whole bones' structural integrity. The compositional analysis includes the gravimetric analysis, investigation of mean crystal size, mineral-to-matrix ratio, enzymatic and non-enzymatic collagen crosslinks, and quantification of bone glycation as described below.

2.3.1 Thermogravimetric analysis (TGA)

TGA is used to quantify the composition of individual constituents of bone. It monitors bone mass loss with temperature and measures total mineral, organic, and water contents, including carbonated minerals, providing additional insight into the bulk composition. This method complements Raman or Fourier Transform Infrared (FTIR) spectroscopy analyses which measure specific components of the mineral (phosphate) and collagen (Amide I).

Nearly 8 to 12 mg of bone is kept in an alumina crucible, and the TGA experiment is performed at a constant heating rate of 10 °C/min in a controlled air atmosphere. The bone sample is heated to 1000 °C. The change in mass is monitored by TGA, as shown in **Figure 2.6**. The decrease in percentage mass up to 200 °C is considered to be the result of the loss of water; from 200 °C to 600 °C is organic content and loss of carbonate content to 800 °C. The percentage mass at 600 °C represents the mineral content, but it depends on the amount of mass lost due to water. Thus, mineral content is translated to dry weight percentage with equation (1) to avoid the influence of water content.

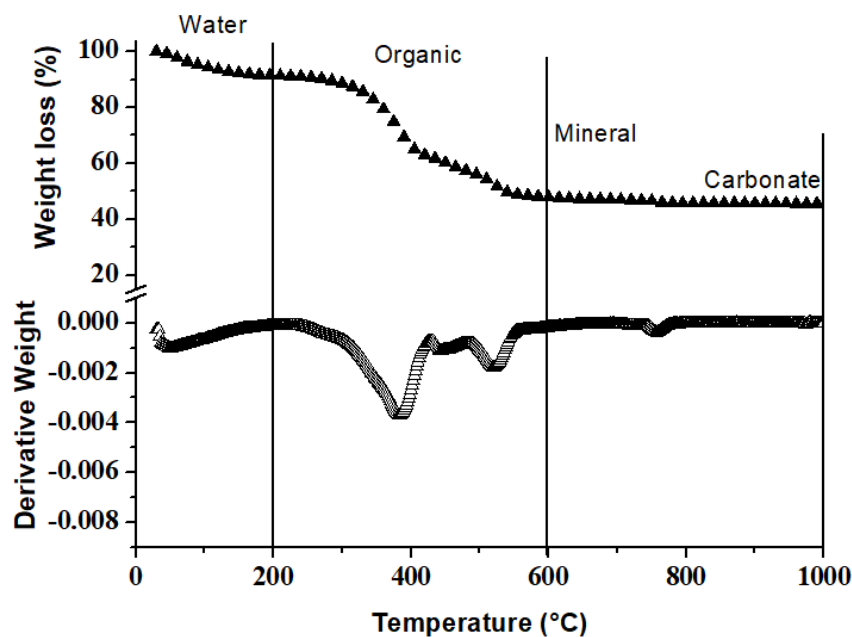


Figure 2.6 The representative TGA curve monitors mass loss of a substance as a function of

temperature and their respective first derivatives for femur trabecular bone. The TGA first derivative plots represent the more accurate temperature values associated with the percentage of mass lost, here it can be observed that superficial water completely evaporates before 200 °C, and between 200-600 °C, the degradation and combustion of the bone matrix occurs

$$\text{mass 600 °C (\%dry weight)} = \frac{\text{mass 600 °C (\% initial weight)}}{\text{mass 200 °C (\% initial weight)}} \times 100 \quad (1)$$

The mineral-to-matrix ratio is calculated as the ratio between the percentages of mass (% dry weight) remaining after heating to 600 °C and the organic mass loss between 200 °C and 600 °C [150], [151]. Also, the TGA results are highly reproducible where CV is nearly 2.8%.

2.3.2 X-ray diffraction (XRD)

In the XRD technique, the bone mineral diffraction pattern is analyzed to quantify mean crystal size (length and width). For this, x-rays are irradiated on the matter; due to this high energy absorption, the electrons in the atom oscillate about their mean positions. When an electron decelerates (loses energy), it emits electromagnetic radiation is known as scattering. And a large number of superimposed scattered waves are known as the diffracted beam. In XRD analysis, the constructive interference of scattered waves (diffraction pattern) is measured and analyzed [152]. Before the experiment, the bone sample is defatted and dehydrated in increasing ethanol concentrations (70% to 100%) for 10 minutes each. The specimen is wet ground in acetone using mortar and pestle until a uniform and homogeneous powder is obtained. Later the XRD pattern is obtained using a suitable diffractometer.

The typical XRD spectrum of trabecular bone is shown in **Figure 2.7**. Diffraction peaks at $2\theta = 26^\circ$ and 40° correspond to the 002 plane (c-axis direction) and 310 planes (perpendicular to the c-axis direction, also known as ab-plane), respectively. The data of 002 and 310 planes are utilized to calculate the average length and width of mineral crystal, respectively [153]–[155]. Cu-tube by $\text{CuK}\alpha$ radiation wavelength of 1.5406 \AA is used. The average crystal size of bone mineral is obtained by using the Scherrer equation, $B(2\theta) = \lambda/L\text{Cos}\theta$, where B is the mean crystal size, λ is the x-ray wavelength, θ is the Bragg angle, and L is the peak width at half-maximum [150], [151], [153]. One study reported that the

average crystallite size in the c-direction varied considerably between subjects, and variation ranges between 5.7-6.3% [156].

Previous rodents and the human study reported a wider mean mineral crystal size in the diabetic group than the non-diabetic group; in contrast, no difference is observed in mean crystal length [38], [130]. The wider crystal size without a change in length decreases the aspect ratio (surface area/volume) of apatite crystals and explains the reduced elastic modulus of bone material [157]. Furthermore, altered crystal shape can also affect crystal connectivity, orientation, and arrangement [157].

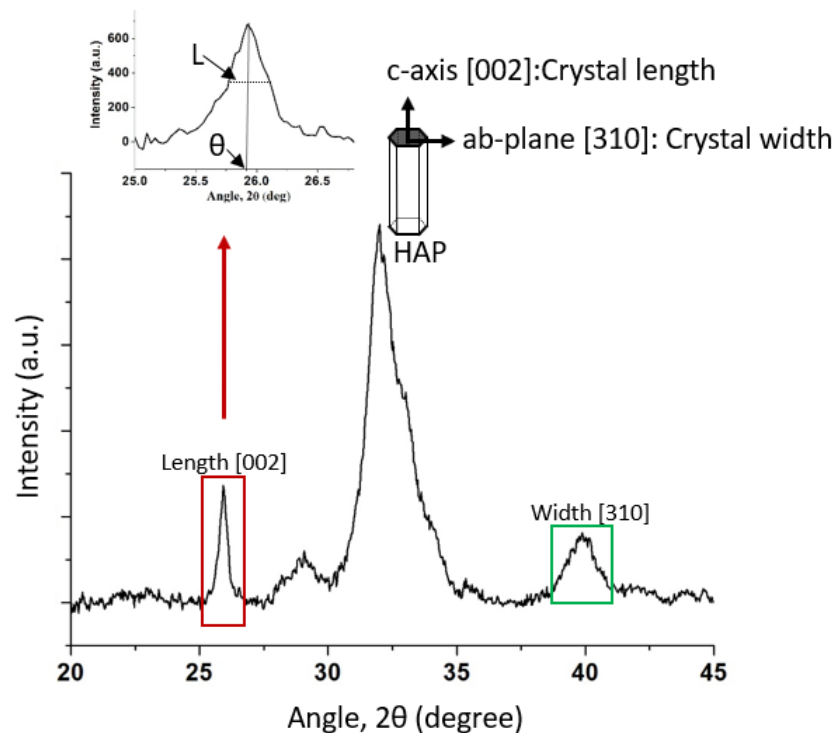


Figure 2.7 Representative XRD pattern ($20^\circ < 2\theta < 45^\circ$) of human cortical femoral bone. The peak at 26° and 40° is used to determine the average crystal length and width in the c-axis direction [002] plane and ab-plane [310], respectively

2.3.3 Small-angle X-ray Scattering (SAXS)

SAXS is a scattering technique for the investigation of materials in the nanometer range. Scattering is when the incident radiation is absorbed and then reemitted in different directions as described above. Here, the scattered rays from an incident x-ray beam are measured to examine the average crystal thickness, shape, and predominant orientation [154], [158]. Structural investigations by X-ray scattering are mainly based on elastic scattering, without any change of energy/wavelength between the incoming and measured

radiation. The limitation of SAXS involved its lower signal-to-noise ratio than XRD. Thus, a synchrotron source is required to produce high energy and monochromatic x-ray beam [159]. Also, in SAXS analysis, thin sections of calcified bone are utilized in transmission mode.

One study reported that bone proteins osteocalcin and osteopontin regulate bone mineral crystal size and organization in a codependent manner, where osteocalcin governs the physical properties of bone minerals. In contrast, osteopontin deals with the regulation of the mineral composition [160]. Another study reported the mean mineral crystal thickness of different animal bones [158], and trabecular bones obtained from human iliac crest biopsies [161], [162]. One study concluded that both collagen and mineral crystals are predominantly aligned parallel to the principal stress direction [162]. The mean crystal thickness is varying at different skeletal sites inside the trabecular and cortical structure. One study reported that mechanical properties of mineralized collagen fibril are more sensitive to crystal thickness than its width, which can be explained as the change in sliding area is more for unit increase in thickness than unit increase in width of crystal. Thus despite the same vBMD, thicker crystal results higher degradation in tissue mechanical properties as compared to wider crystals [163]. In summary, the alteration in crystal thickness is associated with altered mechanical properties of bone at macroscale.

2.3.4 Fourier transform infrared spectroscopy (FTIR)

FTIR is primarily used to measure bone composition. The FTIR spectrum is recorded with FTIR spectrophotometer in total reflectance (ATR) mode, under the constant pressure, in the spectral region of 4000 to 400 cm^{-1} . It can also be recorded in either transmission or absorption mode. When characteristic frequencies of an incident infrared beam are absorbed by molecular bonds in the sample, the resulting interferogram is fast Fourier transformed into a spectrum in the frequency domain.

By analyzing the coefficient of variation of the different analysis methods, it was found that not all analysis methods exhibit the same repeatability and sensitivity. Thus one study recommended to work with normalized spectra, to increase the reproducibility of results [164]. Thus normalized bone mineral and collagen related following parameters are calculated: carbonate-to-phosphate ratio [area ratio of the carbonate ν_2 peak (852-890 cm^{-1}) to phosphate ν_1 - ν_3 peak (916-1180 cm^{-1})], mineral crystallinity [intensity ratio of 1030 cm^{-1} to 1020 cm^{-1} , which is related to crystal size and stoichiometric perfection], and the acid phosphate content [intensity ratio of 1127 cm^{-1} to 1096 cm^{-1} , which characterizes acid

phosphate substitution into stoichiometric hydroxyapatite] [165], [166]. The collagen maturity [area ratio of 1660 cm^{-1} to 1690 cm^{-1}] is measured within the Amide I peak [167], [168]. The mineral-to-matrix ratio is calculated with the area ratio of the phosphate ν_1 - ν_3 peak (916-1180 cm^{-1}) to Amide I peak (1596-1712 cm^{-1}) [165], [166].

Furthermore, the demineralized bone section [53] is used to calculate the mean integrated area ratio (relative content) of sugar-to-matrix ratio [area of the sugar peak [(ν CO and ν CC peaks) (900-1100 cm^{-1}) to Amide I peak (1596-1712 cm^{-1})] [165], [166]. The typical FTIR spectra of undecalcified and decalcified human trabecular bone with the appropriate label of mineral collagen and sugar bands are shown in **Figure 2.8**.

Both FTIR and Raman spectroscopy can be used to determine the characteristic fingerprints of molecular bond vibrations of bone material because both techniques have the capability to differentiate the molecular signals arising from either organic matrix components or from constituents of the hydroxyapatite (phosphate, carbonate). The strong molecular bond vibrations in the FTIR spectrum correspond to weak bond vibrations in the Raman spectrum and vice-versa, because typically a change in dipole moment indicates an IR, and a change in polarizability indicates a Raman active-mode. The advantages of FTIR include its high sensitivity and high signal-to-noise ratio (SNR) relative to Raman, allowing faster data collection. FTIR spectroscopy's disadvantage consists of the requirement of sample dehydration because water dominates the absorption spectrum in the infrared. Thus, it is not preferred to analyze the biological tissues *in vivo* in their native hydrated states with FTIR. On the other hand, Raman spectroscopy's advantage includes the finer spatial resolution ($\sim 1 \mu\text{m}$), the ability to scan hydrated specimens, and the capability to analyze biological tissue *in vivo*. However, Raman analysis limitation includes its relatively low SNR and substantially increase scan times relative to FTIR [169]–[171].

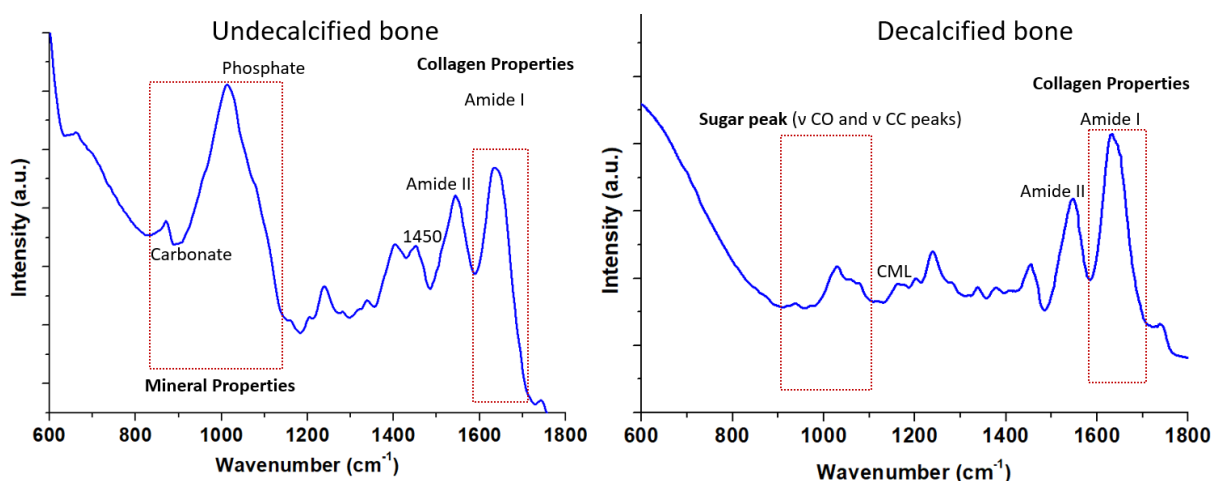


Figure 2.8 Representative FTIR spectrum of undecalcified and decalcified human trabecular bone with the appropriate label of mineral collagen and sugar bands

2.3.5 Scanning electron microscopy (SEM)

The SEM is a versatile surface characterization technique that can analyze bone topographical information at the micrometer and sub-micrometer levels. When high-energy electrons interact with the bone surface, then backscattered and secondary electrons are produced. In SEM imaging, the secondary electrons escape out from the sample with less kinetic energy and are collected by a detector, digitized, and converted into the computerized signal to give the signature of the bone surface's morphology. The bone surface is coated with a thin layer of platinum using an ion sputter coating technique to avoid surface charge creation. Subsequently, the bone samples' surface morphology can be studied through the scanning electron microscope shown in **Figure 2.9**; here, the SEM image of human cortical bone and a single osteon is presented.

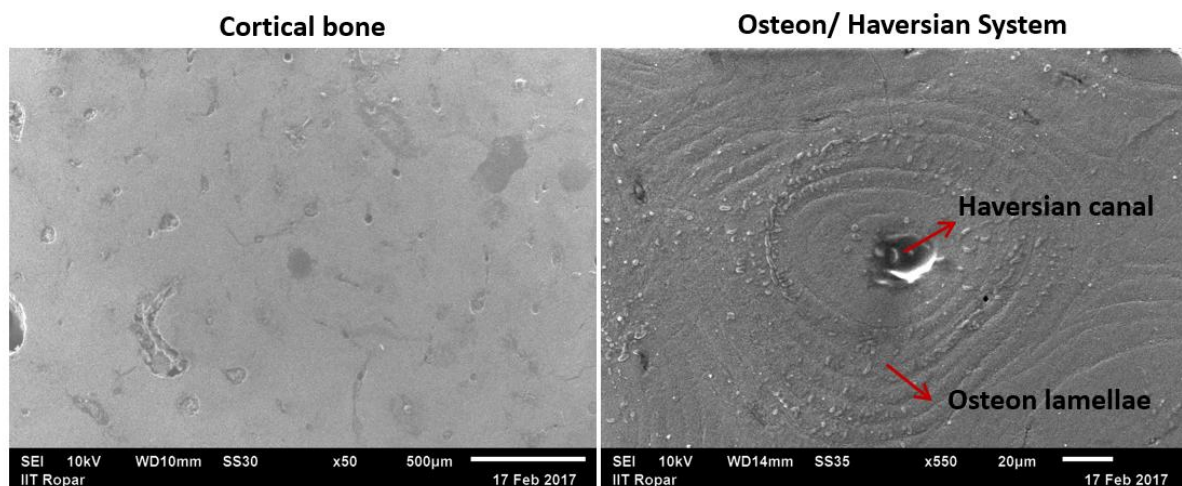


Figure 2.9 Scanning electron microscopy image of human cortical bone and a single osteon

SEM's advantage is that it allows higher resolution than standard histology by optical microscopy, and thin sectioning of the sample is not required. If environmental SEM is utilized to study bone surface morphology, then the coating of a thin conductive layer before imaging can be avoided. SEM imaging can characterize both the organic and mineral components of bone. For example, SEM can demonstrate micro-cracks in the bone surface, the orientation of collagen fiber, bone formation, and resorption regions associated with bone remodeling.

2.3.6 Quantitative backscattered electron imaging (qBEI)

As described above, the SEM technique also produces a backscattered electron signal which

is the beam electrons; after scattering from the sample, they revert by the electrostatic effect, utilized in quantitative backscattered electron imaging (qBEI). When an electron beam interacts with the sample, some of the incident electrons collide with atoms in the sample, causing the electrons to be scattered backward. This backscattering of electron is proportional to the atomic number Z of the atom with which it collides; therefore, higher atomic numbered atoms will generate a higher backscattering signal, also called Z contrast. Among the key constituents of bone mineral (Ca, O, H, P, Mg) and organic matrix (C, O, H, N, P), calcium has the highest Z number ($Z = 20$). Therefore, calcium dominates qBEI image contrast, and it helps to explore different stages of bone tissue mineralization. The primary outcome of the qBEI technique is bone mineral density distribution (BMDD), which describes local variation in mineralization. The BMDD measurement is calibrated against a calcium standard to determine calcium weight in the unknown bone specimen. The key limitation of the qBEI technique is the need for a highly polished surface because surface topography significantly affects backscattering. For proper polishing, the bone sample is embedded in PMMA [172]. In one study, proximal femur specimens from men and women (age 65 years) are studied with qBEI and observed lower mineralization heterogeneity in adults with type 2 diabetes. These microscopic alterations in bone mineralization indicate suppressed bone remodeling, further elucidate deleterious effects on the biomechanical properties of bone and higher fracture risk in adults with type 2 diabetes [89]. Whereas another study reported high cortical porosity in diabetes associated with changed mineralization patterns [90].

2.3.7 Energy-dispersive X-ray spectroscopy (EDX)

EDX is an analytic tool attached with SEM, has the capability to conduct elemental composition of the sample of interest. In EDX, the area of interest is irradiated with high-intensity x-rays; this yields a characteristic peak for the elements present in the sample. Depending upon the peak heights, the concentration of the ingredients can be calculated. Sample preparation for EDX examination requires specimen dehydration and metal coating. EDX is primarily used to analyze the calcium/phosphorus (Ca/P) ratio in bone sample [173], [174].

2.3.8 Atomic Force Microscopy (AFM)

Atomic force microscopy (AFM) is a high-resolution technique used for surface characterization at a nanometer scale. In AFM, a cantilever has a tip in front of it, which feels the sample surface and maps the surface's height. The tip height alters when it passes any

bump or groove, and the feedback reconstructs the surface as an image of the sample. Hence, it gives three-dimensional information of the surface depending upon the force-distance measurement dynamics between the AFM tip and sample surface. In topography analysis, a silicon tip is used in contact mode.

Apart from topography, AFM can determine nanomechanical (elastic and viscous) properties of bone material. AFM has been utilized to quantify the ultrastructure of bone includes determination of mineral crystal size, collagen fibril alignment and structure, and 67 nm band pattern of collagen fibrils and surface of fractured bone [175]–[178]. The AFM image of collagen fibers alignment is shown in **Figure 2.10**. One major advantage of AFM is that it has a similar spatial resolution as transmission electron microscopy without excessive sample dehydration. Thus it is possible to characterize the sample near biological condition. Furthermore, minimal sample preparation is required while maintaining a sub-nanometer resolution. In contrast, AFM disadvantages include a small scan area (scan area: hundreds of μm by hundreds of μm , height amplitude limit: 10 to 20 μm) and image distortion of some topological features such as overhangs and steep edges [35].

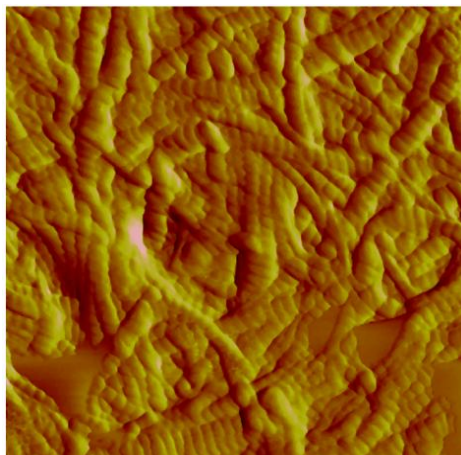


Figure 2.10 Atomic force microscopy image of collagen fibers of demineralized thin bone sections obtained with cryotom

2.3.9 Florescent spectroscopy

Total fluorescent AGEs (fAGEs) accumulated in the bone matrix are measured using fluorescence spectrometry and normalized to collagen concentration [46], [179]. The bone specimen is lyophilized overnight, then hydrolyzed in 6N HCl (100 $\mu\text{l}/\text{mg}$ bone) at 110 $^{\circ}\text{C}$ for 20 h. The fluorescence is measured in a flat-bottom 96-well plate using a multi-mode microplate reader at an excitation of 360 nm and an emission of 460 nm. The fluorescence data of the specimen is normalized with serially diluted quinine standards (stock: 10 μg quinine per 1 mL of 0.1 N H_2SO_4) measured in the same way [46], [179]. Next, the

absorbance assay of hydroxyproline is performed to determine collagen content to normalize the total fluorescence [179], [180]. The absorbance of the specimens and standards is measured at a wavelength of 570 nm using the same microplate reader. Total fAGEs are reported in units of ng quinine fluorescence/mg collagen. The collagen content is derived based on prior knowledge that collagen consists of 14% hydroxyproline [181].

The previous study [182] reported that the accumulation of AGEs is a cause for abnormal collagen synthesis and altered collagen structure in the bone. One recent study found a 1.5-fold increase in fAGEs content in T2D compared with non-diabetic postmenopausal women, having a mean duration of diabetes was nearly 15 years [52]. Whereas in other studies [51], [53], a significant difference in fAGEs was not observed between T2D and non-diabetic groups. One study included samples for a shorter disease duration of nearly two years [51], whereas, in another study duration of diabetes was not reported [53].

2.3.10 Solid-state nuclear magnetic resonance (SSNMR)

SSNMR operates using the principle of nuclear magnetic resonance (NMR), also called magnetic resonance spectroscopy. The working principle includes the alignment (polarization) of nuclear magnetic spins in the direction of a strong constant external magnetic field. Subsequently, an external weak oscillating radio frequency (RF) pulse is applied, which perturbed the alignment of nuclear spins. In the relaxation period, the local electromagnetic waves are emitted by the nuclei of the sample, which are detected and analyzed to get details of the structure of a molecule, its functional groups, and details of the chemical environment of molecules. SSNMR spectroscopy can be carried out in the native or intact form of bone [24], and probes generate compositional details of bone with picometer resolution. The limitation of SSNMR includes the requirement of a dedicated magic angle spinning machine and a strong magnetic field to get well-resolved spectra.

The most common NMR isotopes used to study bone are ^1H (proton), ^{31}P , ^{43}Ca , and ^{13}C , and variation in these isotopes' chemical shifts are recorded as the outcome variable. In previous study [32], proton NMR is used to measure the concentration of bound and mobile (pore) water in bone specimen *ex vivo*. The proton relaxation times differ between the two water compartments, which emit two distinct signals. It is also reported that bound water concentration is positively correlated with bone strength and toughness, and this parameter may become a useful clinical marker of fracture risk. Another study said that both types of waters in bone influenced bone mechanical properties [33].

Along with bone water concentration, SSNMR spectroscopy can be used to study the

organic matrix, inorganic bone mineral phase, and also the interface between these two components. The bone mineral can be observed by ^{43}Ca and ^{31}P NMR since most phosphorus and calcium contents exist in the carbonated hydroxyapatite nanocrystals in the mineral phase. Whereas the organic matrix is investigated using ^{13}C NMR methods since most of the carbon content is present in the organic matrix of bone [183].

2.3.11 High-Performance Liquid Chromatography (HPLC)

HPLC is an analytical chemistry technique that works on a mass transfer process that involves the selective adsorption of components for material analyses. In HPLC, the separation of dissolved *ex vivo* bone sample mixture takes place inside the column between stationary phase (containing sorbent particles of known size 2–50 μm) and a mobile phase (solvent or solvent mixture which is pumped at high pressure through the separation column). Component separation occurs due to the varying degrees of chemical interaction of the sample components with the sorbent particles. Each component elutes from the column at a signature rate, and the concentration of each component is measured precisely with a detector at the eluting end. The advantage of HPLC includes the precise measurement of concentrations of molecular components as low as picomole and the ability to measure many components in one test. However, HPLC is a destructive technique and requires sample homogenization and technical expertise [184].

The HPLC technique's main outcome is quantifying enzymatic (E-xL) and non-enzymatic (NE-xL) collagen cross-links, bone turnover markers, and amino acid composition. E-xL forms through the action of lysyloxidase, and gradually the un-mature divalent crosslink converts into mature and stable trivalent crosslink. Therefore, E-xL measured using the summation of both immature crosslinks of dehydrodihydroxynorleucine (DHLNL) and dehydrohydroxylysinoxorleucine (HLNL) and the mature crosslinks of pyridinoline (Pyr) and deoxypyridinoline (Dpyr). Whereas the NE-xL (pentosidine: one of AGEs) is a pentose-derived fluorescent cross-link formed between arginine and lysine residues in collagen and is thought to accumulate in connective tissues with aging and T2D [62], [185]. The enzymatic cross-links (E-xL, beneficial cross-links) in humans stabilize around 10-15 years of age and provide mechanical strength, whereas non-enzymatic cross-links (NE-xL) are associated with increased bone fragility [27], [186], [187].

2.4 Summary and Discussion

Clinical tools such as DXA and FRAX underestimate the fracture risk in patients with T2D.

It is hypothesized that the presented bone quality parameters can provide complementary information to accurately identify patients at risk of fracture. Here we reviewed techniques at multiple length scales to assess the biomechanical, microstructural, material, and compositional bone properties, along with some of their key outcomes and trends in diabetic bone research.

The techniques we review for structural characterization include imaging techniques, where QCT, pQCT, HRpQCT, and DXA can be utilized *in vivo*. However, QCT is limited to the scan resolution and high radiation dose, and HR-pQCT is not approved for clinical use at this time and is limited in the scanning of peripheral sites, which are expected to resolve as technological advances. In contrast, high-resolution μ -CT and bone histomorphometry techniques analyze bone tissue microstructure *ex vivo*. Among all structural characterization techniques, only bone histomorphometry has the potential to provide information about dynamic bone remodeling parameters but only when if patients have been tetracycline-labeled before the biopsy. Recently one study reported longitudinal *in vivo* μ -CT for assessment of localized bone turnover and mineralization kinetics for monitoring callus remodeling process of individual animals in preclinical fracture healing study (35). Further, all x-ray-based imaging technique omits the input of organic matrix, and solely focus on BMD and bone microstructure, however, it is reported that collagen also provides a significant role in the bone-toughening mechanism.

Also, we review the mechanical testing techniques used to investigate the mechanical properties of bone at multiple length scales of bone hierarchy. Here, destructive mechanical testing such as the whole bone three-point bending/compression test is not feasible for the clinical population for fracture risk evaluation; it is well-suited with animal studies on the excised long bone/vertebra to evaluate overall bone strength. However, the utility of Biodent for *in vivo* biomechanical analysis is useful for animal studies, particularly in longitudinal studies. On the other hand, Osteoprobe is helpful to investigate bone material strength in the clinical population, particularly when multiple-time data is required (longitudinal studies). However, some limitations with Osteoprobe are that this technique does not facilitate measuring the deformation geometry; thus, the hardness value cannot be determined. Osteoprobe results (BMSi values) might be influenced with cortical bone microstructure, so it is not truly a material level test. Also it does not provide bone material strength at the clinically relevant site; usually reported studies provided BMSi at the mid-diaphysis of the tibial bone. Nanoindentation technique can measure the hardness,

but it requires rigorous sample preparation, which is a critically important step to be done; otherwise, the surface polishing artifact can lead to variability in outcome measures.

Finally, we review the techniques used to investigate bone compositional properties. To analyze the mineral-to-matrix ratio- TGA, FTIR, and Raman can be utilized. TGA measures the ratio of the total mineral content (including carbonated hydroxyapatite) to the total organic content, however in FTIR and Raman, the mineral content is represented by the peak area of phosphate band (916-1180 cm^{-1}), and the organic matrix content is limited to the peak area of Amide I band (1596-1712 cm^{-1}) [150]. Approximately every compositional technique requires its specific sample preparation, such as XRD - homogenization of bone needed, SAXS required thin bone sections, FTIR requires freeze-dried thin bone sections, SEM and qBEI required extensive polished surface with a metal coating, and HPLC required bone sample in dissolved form. Despite the potential to assess bone composition alteration and offer powerful mechanistic insights, many compositional characterization techniques are not fit for clinical use because they required bone biopsies and cannot be performed noninvasively. In the reviewed methods, only NMR and Raman have the potential to do *in vivo* assessment of bone quality.

While these techniques have increased our understanding of bone fragility in diabetes, however, each method presents its own challenges for utilization in routine clinical practice. Therefore, further work is needed to assess their application for regular clinical use. Additionally, no single method can completely characterize bone fragility. Thus, a combination of bone assessment techniques is required to generate a more specific and direct assessment of bone quality to aid clinical assessment of fracture risk in diabetes. Useful combinations of bone quality and strength prediction for *in vivo* human clinical studies could be HRpQCT used with FEA modeling, Osteoprobe, and Raman. This combination will allow non-invasive prediction of the vBMD, structural and mechanical properties by HRpQCT. Osteoprobe will provide data about bone material strength, and Raman spectroscopy will allow simultaneous examination of the compositional properties. In contrast, combinations of multiscale bone quality and strength prediction for *ex vivo* studies on rodents and clinical populations are presented in subsequent Chapters 3-4, respectively.

CHAPTER 3

DEVELOPMENT OF HFD-FED/LOW DOSE STZ TREATED FEMALE SPRAGUE DAWLEY RAT MODEL TO INVESTIGATE DIABETIC BONE FRAGILITY AT DIFFERENT ORGANIZATION LEVELS

Type 2 diabetes (T2D) adversely affects the normal functioning, intrinsic material properties, and structural integrity of many tissues, and bone fragility is one of them. To simulate human T2D and to investigate diabetic bone fragility, many rodent diabetic models have been developed. Still, the outbred genetically normal non-obese diabetic rat model is not available that can better simulate the disease characteristics of non-obese T2D patients, those have a high prevalence in Asia. In this study, we have used a combination of high-fat diet (4 weeks, 58% kcal as fat) and low dose streptozotocin (STZ, 35 mg/kg, intraperitoneally, at the end of 4th week) treatment to develop T2D in female Sprague Dawley (SD) rats. After eight weeks of the establishment of the T2D model, the femoral bones were excised after sacrificing rats (animal age ~21-22 weeks); n=10 with T2D, n=10 without diabetes. The bone microstructure (μ -CT), mechanical and material properties (three-point bending, cRPI, nanoindentation), mean mineral crystallite size (XRD), bone composition [mineral-to-matrix ratio, non-enzymatic crosslink ratio (NE-xLR), (FTIR)], and total fluorescent AGE (fAGE) were analyzed.

As a result, we found that diabetic bone has reduced whole bone strength and compromised structural properties (μ -CT). The NE-xLR is elevated in the T2D group and strongly and negatively correlated with post-yield-displacement (PYD), which suggests the possibility of bone fragility due to lack of glycation control. Along with that, the decreased mineral-to-matrix ratio and modulus increased IDI, and wider mineral crystallite size in the T2D group evidenced that the diabetic bone composition and material properties have changed, and bone became weaker and tends to easily fracture. Altogether, this model simulates the natural history and metabolic characteristics of late-stage of type 2 diabetes (insulin resistance and as disease progress develops hypoinsulinemia) for non-obese young (and/or adolescent) T2D patients (Asians) and provides potential evidence of the diabetic bone fragility at various organization levels.

3.1 Introduction

Diabetes potentially affects almost every organ in the human body and causes head-to-toe damage, i.e., heart, kidney, nerves, eye, skin, blood vessels, and bone [3]. Nearly 50-80% increased extremity fracture risk observed in people with diabetes attracted the attention of researchers [17]. Furthermore, approximately 60% of the world's diabetics live in Asia, and being with the fastest population growth rate, this data is expected to increase further in the coming years [5].

In addition to the burden of disease in Asia, the phenotypes of Asian type 2 diabetics are also distinct as compared by non-Asians (particularly Caucasians) because Caucasian diabetics are obese, whereas a large proportion of patients with T2D in Asian countries are non-obese [188]–[192]. At present, to simulate the human T2D and to investigate the issue of T2D and bone, both obese and non-obese rodent diabetic models are available based on spontaneous, monogenic abnormal leptin/leptin receptor signaling and diet-induced obesity, and reported weaker diabetic bones [54], [55], [64]–[66], [56]–[63]. For example, Saito et al. [62] and Zhang et al. [54] used spontaneously non-obese diabetic rat model in their studies, but in their model, the development of diabetes is highly genetically determined, unlike heterogeneity seen in humans, and also in humans, the T2D is multifactorial, strongly associated with lifestyle and dietary factor. In Zucker fatty rats and Zucker diabetic fatty rats, severe obesity is developed due to hyperphagia caused by abnormal leptin/leptin receptor signalling, but leptin or leptin receptor deficiency is not an important contributor to develop diabetes in humans (or vary rare <1%) [58], [63]–[65]. On the other hand, the ZDSD (develop diabetes over time due to polygenetic and environmental factors -dietary manipulation) and UCD-T2D rats better simulate the development and progression of T2D for Westernized societies (Caucasians), where a high rate of T2D is due to dietary-induced obesity [58], [64] [42]. Furthermore, in diet-induced obesity models, the feeding of a high-fat diet (HFD) alone requires a long time, as well as no hyperglycemia, develops upon simple dietary treatment in genetically normal animals [67]. Hence, the particular gap in knowledge is that there is a need to establish the ideal rat model for type 2 diabetes by using outbred genetically normal rats, which can better simulate the natural history and metabolic characteristics of non-obese type 2 diabetic patients (mainly Asians). Also, it can be used to characterize the skeletal fragility in non-obese type 2 diabetics.

Here, we hypothesized that the disease (T2D) pattern could be achieved by combining the feeding of HFD and low dose STZ treatment, which will cause mild- hyperglycemia (a condition similar to prediabetes) due to insulin resistance (because the feeding of HFD for four weeks, hyperinsulinemia) and will further develop hyperglycemia due to low dose STZ treatment on HFD-fed insulin-resistant animals (hypoinsulinemia). Further will utilize this model to characterize the bone composition, material properties, and structural properties of diabetic bone. While working on this hypothesis, we have developed a high-fat diet-fed and low-dose STZ-treated type 2 diabetic rat model by using genetically-normal outbred female SD rats that simulates the natural history and metabolic characteristics of the non-obese young (and/or adolescent) Asian T2D patients. We have further investigated the skeletal fragility parameters: structural and mechanical properties of the femoral bone, bone material properties (cRPI, NI), mean crystallite size (XRD), collagen cross-links [non-enzymatic cross-links NE-xL] and fAGEs content in the diabetic femoral cortical bone as compared to the controls. This study provides detailed insight and extensive evidence on the effect of T2D on cortical bone quality of non-obese genetically normal outbred female SD rats.

3.2 Material and methods

3.2.1 Animals

Approximately seven to eight (7-8) weeks old female Sprague Dawley rats (170-180g) were procured from the central animal facility of the institute at the beginning of the study. They were maintained under the standard environmental condition such as temperature $20\pm 2^{\circ}\text{C}$, humidity $50\pm 10\%$, and 12 hours light and dark cycle with food and water *ad libitum*. All protocols were approved by the Institutional Animal Ethics Committee (IAEC Approval Number 17/74, NIPER) and performed in accordance with the guidelines of the Committee for the Purpose of Control and Supervision of Experiments on Animals (CPCSEA), New Delhi, India.

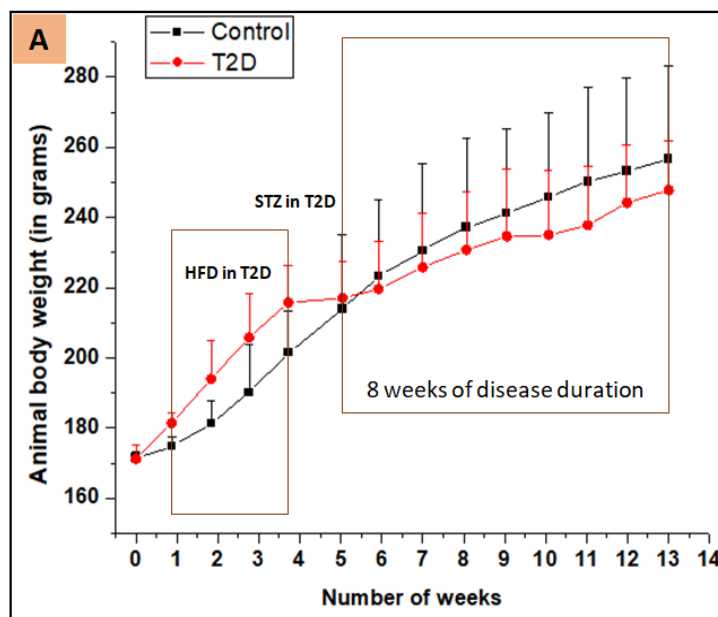
3.2.2 Experimental design

Animals were acclimatized for one week before the initiation of the experiment. Now, the animals were divided into two groups. First, the control group, fed with commercially available normal pellet diet (12% kcal as fat, Pranav Agro Industries, New Delhi, India), and second, the diabetic group received a high-fat diet (HFD) (in-house prepared round balls) (58% kcal of fat) for four weeks that causes insulin resistance in animals. At the end of the 4th week, they were injected with a low dose of streptozotocin [(STZ), Sigma Aldrich, MO, USA], i.e., 35 mg/kg dissolved in ice-cold 0.01M citrate buffer; pH 4.4 via intraperitoneal

route, after fasting of 12 hours, whereas control animals received an equivalent volume of vehicle. After one week from the injection of streptozotocin, plasma glucose levels were measured, and rats showing blood glucose concentration more than 250 mg/dl included in the T2D group. The rats were allowed to continue to feed on their respective diets until the end of the study [65]. Here, the diabetic group rats become insulin resistant due to HFD-feed, and hence, even the slight insult by a low dose of STZ compromises the beta-cell function and leads to hypoinsulinemia.

Body-weight was recorded every week, right from the beginning to the end of the study **Figure 3.1 (A)**. At the end of the study, overnight-fasted rats were anesthetized under light ether, and blood samples were collected from the tip of the tail vein. Blood samples were collected in Ethylene-diamine-tetra-acetic acid (EDTA) for the determination of HbA1C and preparation of plasma. Plasma glucose and blood HbA1c were estimated as per the manufacturer’s guidelines (Accurex Biomedical Pvt. Ltd., Mumbai, India; Tulip Diagnostics Pvt. Ltd., Goa, India).

After sacrifice, the femora of both the groups were dissected, wrapped in PBS soaked gauge, kept into ziplocked plastic bags, labeled, and subsequently stored at -80°C. Before experiments, the bones were equilibrated to room temperature. The left femora were utilized for microstructural (μ -CT), 3-point bending, and fracture pattern analysis and right femora were used to determine properties at the material level (cRPI and NI), bone composition with FTIR and fAGEs content as shown in **Figure 3.1(B)**.



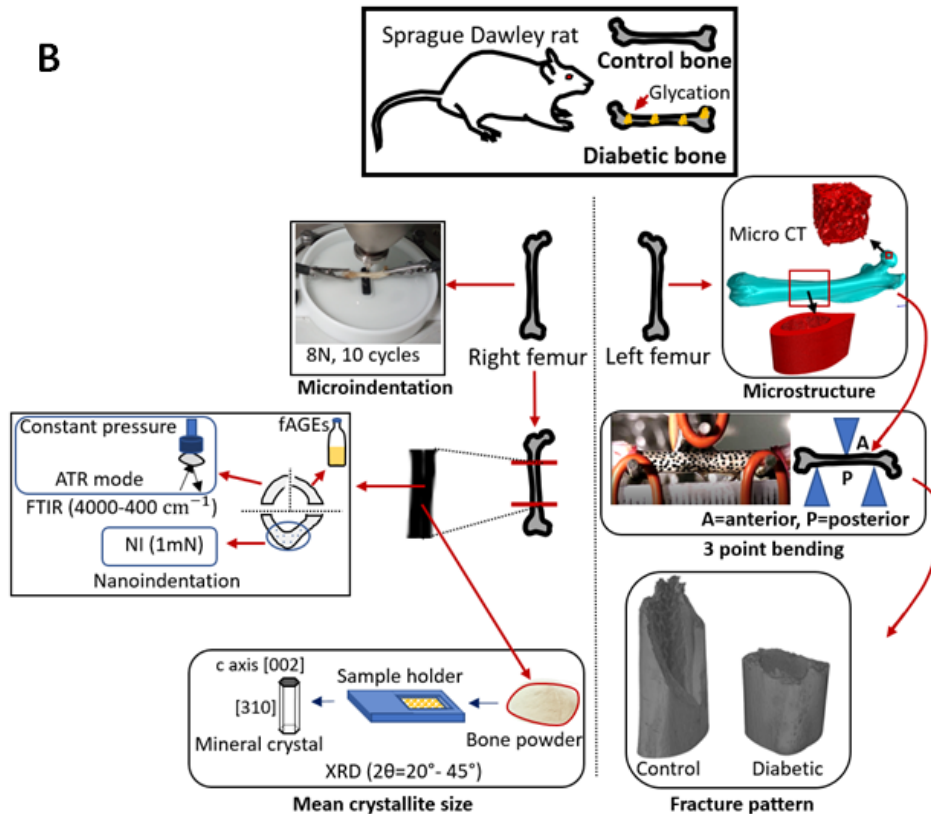


Figure 3.1 (A) Body-weight changes in HFD-fed/low dose STZ treated female SD rats compared to normal pellet diet-fed rats of every week, right from the beginning to the end of the study. (B) Schematic of materials and methods and allocation of tissue for each characterization technique. Left femora were used for microstructural (μ -CT), mechanical (3-point bending), and fracture pattern analysis, and right femora were utilized to determine properties at the material level (cRPI), bone composition with FTIR, mean crystallite size with powder XRD and fAGEs content.

3.3 Measurement of Bone quality parameters

3.3.1 Structural parameters (μ -CT)

To determine the structural parameters of cortical (mid-diaphysis of femoral) and trabecular (femoral head) bone, the left femora were scanned along the cylindrical axis using the nanotom-S high-resolution μ -CT system (Phoenix/x-ray, GE Sensing & Inspection Technologies, Germany). The source was set at 55 kV and 160 μ A, exposure time 500 ms, frame averaging 7, and a voxel size of 20 μ m and 5 μ m to scan the entire femoral bone and femora head, respectively. For bone density calibration, two phantoms with 200 mg/cc and 800 mg/cc of hydroxyapatite (QRM GmbH, Mohrendorf, Germany) were imaged with the

same parameters as the bone samples. Later the mean gray value was calibrated based on the linear relationship between gray value and density [122].

The reconstruction of raw data was performed using Datos.rec (phoenix/x-ray, GE Measurement & Control; Germany). The bone was segmented from the background based on the grayscale value of the image, and for segmentation, manual thresholding is done (with suitable gray values of trabecular and cortical bone separately). The noise removal Gaussian filter ($\sigma = 1$) was applied, and then reconstructed images were imported in Scan-IP (Simpleware Ltd, UK) and ImageJ's plugin BoneJ [193] [software by National Institute of Health (NIH), available at (<https://imagej.nih.gov/ij/>)]. The midpoint between the greater trochanter and the endpoint of the distal femora was calculated to identify mid-diaphysis. Then, the cylindrical volume of 1 mm above and below this mid-diaphysis was selected as the region of interest to obtain a 3D model, which was further utilized to calculate microstructural parameters of cortical bone. Likewise, the cubical volume of $1.5 \times 1.5 \times 1.5 \text{ mm}^3$ was selected as the region of interest from the center of the femoral head to calculate trabecular bone microstructural parameters. The following microstructural parameters were calculated: trabecular volume fraction (BV/TV, %), trabecular number (Tb.N, 1/mm), trabecular thickness (Tb.Th, mm), trabecular separation (Tb.Sp, mm), structure model index (SMI), degree of anisotropy (DA), connectivity density (Conn.D), cortical bone area (Ct.Ar, mm^2), and average cortical thickness (Ct.Th, mm). This study was performed according to previously published protocol [123].

3.3.2 Mechanical and material properties

3.3.2.1 Whole bone three-point bending test

After μ -CT imaging, the left femora were utilized for the three-point bending test. The femora were kept in a saline-soaked gauge until immediately before testing. The bones were placed in such a way that the posterior side down on the bottom support (19 mm span) and the central loading roller apply force at mid-diaphysis, as described in previous published protocol [58]. The radius of curvature of each support was 2 mm. The specimens were preloaded with 10N to ensure proper contact between the test specimen and the loading roller. To test samples till failure, a single-cycle ramp function at a constant displacement rate of 10 mm/min is applied with no displacement end limit [127], [128]. The bending tests were performed using an electromagnetic testing system (Electroforce 3200, Bose, Eden Prairie, MN, USA) at room temperature while keeping the specimen hydrated through PBS spray. To ensure uniform deformation without any movement of the specimen, a digital microscope

(Dino-Lite 5MP, Taiwan) was utilized. The load-displacement data were captured at 0.01 sec time interval which further used to calculate the maximum load (F_{\max} , N), stiffness (N/mm), work-to-failure (N.mm) and post-yield displacement (PYD, mm). Here, F_{\max} is the greatest load achieved before fracture, stiffness is measured as the slope of the linear portion of the load-displacement curve, work-to-failure represented as the area under the load-displacement curve (whole bone toughness), and PYD refers to displacement (D) that occurs between yielding (D_{yield}) and fracture (D_{fx}) [$\text{PYD} = D_{\text{fx}} - D_{\text{yield}}$]. The yield point is calculated with a 0.2% offset method [129].

3.3.2.2 Cyclic reference point indentation (cRPI)

The mid-diaphysis region of the right femora was tested through a cyclic reference point indentation (cRPI) instrument under wet conditions. It provides a measure of bone mechanical properties, in particular, the resistance of the bone to micro-indentation at the tissue level. Six indents were performed on the anterior region of the femora, separated by 1–2 mm, repeatedly for ten indentation cycles at a frequency of 2 Hz, with a maximum force of 8 N. Before actual measurement, the probes were tested on a PMMA block according to manufacturer's indication to ensure proper function. Later, for fixed load, the distance by which the probe was inserted into the bone was recorded, which was further used to calculate indentation distance increase (IDI, μm), average energy dissipation (Avg-ED, μJ), and first cycle unloading slope (US-1st, N/ μm). Measurements were averaged for each sample and used to calculate the mean of each group. Testing was done according to previously published protocol [135].

The IDI with cyclic loading to a fixed force is an important parameter of cRPI to distinguish the fragile bone from less easily fractured bone [136]. It is the absolute penetration depth increase from the 1st cycle to the last cycle of each test, and also it is inversely correlated to the bone toughness [40]. Other outcomes of interest are the US-1st (slope of the unloading portion of the first cycle), an indicator of bone material stiffness, and Avg-ED is a measure of unrecovered bone deformation (plasticity).

3.3.2.3 Nanoindentation (NI)

The cross-section of the mid-diaphysis of the right femora was cut with a low-speed diamond blade saw (IsoMet, Buehler, Lake Bluff, IL, USA) and then embedded in epoxy, which takes nearly two hours to get cured. After curing, the samples were ground (Buehler Eco Met 250 grinder and polisher) with abrasive papers of 1200 and 2000 grit size under the water cooling

condition and polished with diamond solutions of particle sizes of 1, 0.5, and 0.25 μm , and then samples were sonicated for 10 minutes. The nanoindentation experiment was carried out within an hour using a TI-950 Tribo Indenter (Hysitron Inc., Minneapolis, MN) with Berkovich pyramidal tip in the moist state. Eight indents with a peak load of 1000 μN were applied to the cross-section of the bone with a load function consisting of a ten-second loading and unloading segment and a ten-second hold time. The load-displacement curves obtained in these indentation tests were analyzed to determine the reduced modulus (E_r) and hardness (H) by using the method of Oliver and Pharr (OP) [146].

3.3.3 Biochemical analysis

3.3.3.1 FTIR

The 1/4th diaphysis of bone samples was freeze-dried overnight and directly break in the particle size of few microns by using mortar and pestle. Later, the FTIR spectra were recorded with the help of Bruker IFS 66v/S FTIR spectrophotometer in Attenuated Total Reflectance (ATR) mode under the constant pressure in the spectral region of 1800 to 400 cm^{-1} as shown in **Figure 3.2(A)**. After recording the spectra, OriginPro 8 (OriginLab, Northampton, MA) software is used to do baseline correction and calculate peak intensity and area under the curve. Also, the mean values were calculated for each measured parameter for each group.

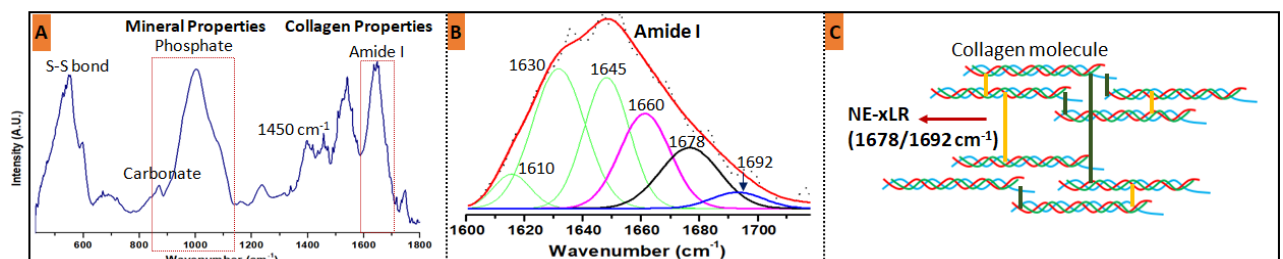


Figure 3.2(A) Representative FTIR spectra with an appropriate label of various bands to analyze the diabetic (T2D) and control femoral cortical bone, **(B)** represents peak fitting of Amide I band, collagen properties were obtained by peak fitting of Amide I band with subbands (Gaussian curves) at 1610, 1630, 1645, 1660, 1678 and 1692 cm^{-1} , **(C)** represents the non-enzymatic crosslink (NE-xL) formation schematically in bone collagen

The bone mineral and collagen-related following parameters were calculated. The mineral parameters include the mineral to matrix ratio [area ratio of the phosphate v1-v3 peak (916-1180 cm^{-1}) to Amide I peak (1596-1712 cm^{-1})], the carbonate to phosphate ratio [area ratio of the carbonate v2 peak (852-890 cm^{-1}) to phosphate v1-v3 peak (916-1180 cm^{-1})], the mineral crystallinity [intensity ratio of 1030 cm^{-1} to 1020 cm^{-1} , which is related to crystal size and

stoichiometric perfection], and the acid phosphate content [intensity ratio of 1127 cm^{-1} to 1096 cm^{-1} , which characterizes acid phosphate substitution into stoichiometric hydroxyapatite] [165], [166].

The collagen parameters were measured through Amide I peak because it possesses structural information about the collagen matrix and is also the location of the strongest peaks for the non-enzymatic cross-link (NE-xL) pentosidine (AGE) [21]. Thus, subbands of the Amide I band were peak fit with Gaussian curves at 1610, 1630, 1645, 1660, 1678, and 1692 cm^{-1} by using peak analyzer tool in OriginPro 8.5 software as shown in **Figure 3.2(B)**. These peaks were chosen based on second derivative spectra. From the analysis of Amide I subbands, the non-enzymatic crosslink-ratio [(NE-xLR), area ratio of 1678 cm^{-1} to 1692 cm^{-1} subbands] and the collagen maturity [area ratio of 1660 cm^{-1} to 1690 cm^{-1} (related to the ratio of pyridinoline to divalent crosslinks)] were measured within the Amide I peak. Where the measurement of NE-xLR enables to measure of the collagen quality associated with NE-xL and is an indirect measure of overall AGEs (which makes cross-links) content in bone tissue itself [21], [167]. The schematic presentation of NE-xL is shown in **Figure 3.2(C)**.

3.3.3.2 Mean crystal size (XRD)

The bone samples of the right femora were powdered directly using mortar and pestle by keeping in acetone. The bone powder is dried in a fume hood and transferred in tightly sealed cryovials. The Panalytical X'Pert Pro multipurpose diffractometer (Netherlands) was used to record XRD patterns with 40 kV and 40 mA with no spinning. Cu-tube by $\text{CuK}\alpha$ radiation wavelength of 1.5406 Å is used. The experiments were conducted with the slow scan at $2\theta = 20^\circ$ to 45° , with a step size of $0.0334^\circ/2\theta$ and count time at each step of 250 seconds. The Xpert Highscore plus software is used for postprocessing, to do background correction and fit the diffraction peaks observed at $2\theta = 26^\circ$ [belongs to the c-axis direction (002 plane) indicate the average length of crystal] and $2\theta=40^\circ$ [belongs to (310 plane) perpendicular to the c-axis direction indicate the average width of crystal] [155]. The average crystallite size of bone mineral is obtained by using the Scherrer equation, $B(2\theta) = \lambda/L\text{Cos}\theta$, where B is the mean crystallite size, λ is the x-ray wavelength, θ is the Bragg angle, and L is the peak width at half-maximum. The protocol is adopted from published studies [150], [155].

3.3.3.3 fAGE assay

Total fAGEs were measured using fluorescence spectrometry and normalized to collagen concentration similarly as in the previous studies [46], [179], [180]. The cortical bone

samples were lyophilized overnight then hydrolyzed in 6N HCl (100 µl/mg bone) at 110 °C for 20 h in hydrolysis vials with screw caps. The hydrolysate was cooled at room temperature, collected in a microcentrifuge tube, and centrifuged at 13000 rpm at 4°C (Eppendorf 5424R microcentrifuge). The supernatant is collected, diluted (ten times with DI water), and fluorescence was measured in a flat-bottom 96-well plate using a multi-mode microplate reader (CLARIOstar Plus, BMG LABTECH) at an excitation of 360 nm and an emission of 460 nm. The fluorescence of bone samples was normalized with serially diluted quinine standards (stock: 10 µg quinine per 1 mL of 0.1 NH₂SO₄) measured in the same way.

Next, to quantify hydroxyproline (absorbance assay), a chloramine-T solution (0.05M chloramine T, 2-methoxy ethanol, and hydroxyproline buffer in 2:3:5 respectively) was added to the hydroxyproline standards (stock sol: 2mg hydroxyproline in 1ml 0.001N HCl) and the bone hydrolysates (as mentioned above) in 1:2 ratio and incubated for 20 min at room temperature in the dark to oxidize hydroxyproline, then 3.15 M perchloric acid was added to the above solution and incubated for 5min to quench chloramine-T. At last, the *p*-dimethylaminobenzaldehyde solution was added, and the mixture was incubated for 20 min at 60°C; the color change is observed in this incubation, then samples were cooled at room temperature for 5 min, and absorbance of the specimens and standards was measured at a wavelength of 570 nm using the same microplate reader. Total fAGEs are reported in units of ng quinine fluorescence/mg collagen. The collagen content is derived based on prior knowledge that collagen consists of 14% hydroxyproline [181]. All experiments were performed in darkness at room temperature.

3.3.4 Statistical analysis

Distributions for all variables were plotted to identify potential outliers, and the points beyond two standard deviations of the mean were removed from the analysis. Statistical analysis was performed using SPSS (v.21, SPSS Inc., Chicago, IL, USA) and Microsoft Office Excel (2007). The distribution of the data was tested for normality by the Kolmogorov-Smirnov test. The homogeneity of variances was analyzed using Levene's test. Between-group differences of calculated parameters were analyzed for statistical significance using Student's t-tests or Mann-Whitney U tests, as appropriate, after testing for normality and homogeneity of variances. The mean values and standard deviation (SD) were calculated for the measured parameters. Pearson correlation tests were used to determine relationships between variables in T2D and control group separately. Forward stepwise regression tests were conducted for

mechanical properties using measures of glycation (fAGE and NE-xLR) as independent variables. A confidence level of $p < 0.05$ implies a statistical significance between the groups, where $p < 0.05$, $p < 0.01$, and $p < 0.001$ denote the level of significance.

3.4 Results

After four weeks of HFD-feed, the plasma insulin value is higher from 1.72 ± 0.058 to 2.61 ± 0.088 mIU/L ($p < 0.001$) in control to the T2D group, respectively, which evidenced the condition of hyperinsulinemia due to insulin resistance. After eight weeks of the establishment of the T2D model (**Table 3.1**), the difference in body weight is nonsignificant. The difference in fasting blood glucose and HbA1c is found statistically higher ($p < 0.001$) in the T2D group as compared to the control group. The plasma insulin value is decreased by 21.4% ($p = 0.038$) in the T2D group as compared to the control group, which evidenced the condition of hypoinsulinemia. Also, the T2D group animals show abnormalities in lipid metabolism as evidenced by significantly increased plasma triglyceride ($p < 0.001$) and plasma total cholesterol levels ($p = 0.001$), which contribute to various cardiovascular complications.

Table 3.1 Body weight and blood glucose of control and diabetic (T2D) groups (at the end of the study), and also the findings of microstructural parameters of control and diabetic (T2D) rat femoral bone

	Control (n=10)	T2D (n=10)	p value
Body Weight (gm)	252.8 ± 30.67	247.8 ± 13.92	0.748
Fasting Glucose (mg/dl)	97.9 ± 10.46	292.5 ± 45.69	<0.001***
HbA1c (%)	6.08 ± 0.39	7.89 ± 0.52	<0.001***
Plasma Insulin (mIU/L)	2.82 ± 0.588	2.216 ± 0.197	0.038*
Plasma Triglyceride (mg/dl)	64.21 ± 8.39	213.66 ± 29.06	<0.001***
Plasma Total Cholesterol (mg/dl)	63.68 ± 7.78	130.64 ± 26.53	0.001**
Microstructural Parameters (μ-CT)			
Trabecular bone parameters			
Trabecular volume fraction (BV/TV) (%)	46.14 ± 2.10	38.54 ± 6.05	0.015*
Trabecular number (Tb.N) (1/mm)	5.048 ± 1.20	4.32 ± 0.44	0.210
Trabecular thickness (Tb.Th) (mm)	0.095 ± 0.017	0.089 ± 0.011	0.539
Trabecular separation (Tb.Sp) (mm)	0.142 ± 0.037	0.166 ± 0.029	0.23
Structure model index (SMI)	1.29 ± 0.68	1.51 ± 0.48	0.547
Degree of anisotropy (DA)	3.39 ± 0.59	3.87 ± 1.56	0.50
Connectivity density (Conn.D)	775 ± 290	458 ± 251	0.43

(1/mm ³)			
Trabecular tissue mineral density (Tb.TMD) (mg/cc)	739.0 ± 343	963.0 ± 105	0.160
Cortical bone parameters			
Cortical tissue mineral density (Ct.TMD) (mg/cc)	1594.7 ± 50	1604.1 ± 114	0.87
Cortical area (Ct.Ar) (mm ²)	6.76 ± 0.28	5.72 ± 0.85	0.019*
Cortical thickness (Ct.Th) (mm)	0.70 ± 0.02	0.61 ± 0.05	0.013*
All data are expressed as mean ± SD; *p<0.05, **p<0.01, ***p<0.001 respectively compared to the control group; HbA1c: glycosylated hemoglobin A1c			

3.4.1 Structural parameters (μ -CT)

The mean values of microstructural parameters are calculated and shown in **Table 3.1** for the T2D and control groups. The difference in cortical and trabecular tissue mineral density (Ct.TMD or Tb.TMD) could not reach the level of significance. The T2D group had significantly lower values of trabecular volume fraction (16.5%, **p=0.015**), Ct.Ar (15.4%, **p=0.019**), Ct.Th (12.9%, **p=0.013**) and J (23.5%, **p=0.035**) compared to control group. The difference between the mean value of Tb.N (p =0.21), Tb. Th (p =0.54), Conn.D (p =0.43), Tb. Sp (p =0.23), SMI (p =0.55), and DA (p=0.50) do not reach the level of significance in the T2D group as compared to the control group. Even though the thinning of trabeculae and the trabecular number is not significantly different in the T2D group, but lower values of these parameters contribute to reduced trabecular bone volume fraction (BV/TV) in the T2D group.

3.4.2 Mechanical and material properties

3.4.2.1 Whole bone three-point bending test

The experimental setup, representative load-displacement curve, and image of fracture pattern are shown in **Figure 3.3(A-C)**, respectively. The image of fracture pattern for diabetic and control group shown that the diabetic bone suffers from transverse fracture (shortest and direct crack path, n=7/10), where control bone suffers from oblique fracture (increased deflection in the crack path, n=9/10). This finding revealed the altered matrix properties of diabetic bone. Further, the mean values of F_{max} , stiffness, work-to-failure, and PYD all are found to be lower by **36.9%**, **p<0.001**, **57%**, **p<0.001**, **41%**, **p=0.004** and **36.8%**, **p=0.039** respectively in the diabetic group as compared to the control group as shown in **Figure 3.3(D-G)**. Thus, diabetic bone consists of compromised load-bearing

capacity (F_{max}), deformation resistance within the elastic region (stiffness), reduced capacity to absorb energy before fracture [work-to-failure (whole bone toughness)], and reduced ductility (PYD, plasticity) compared to control group.

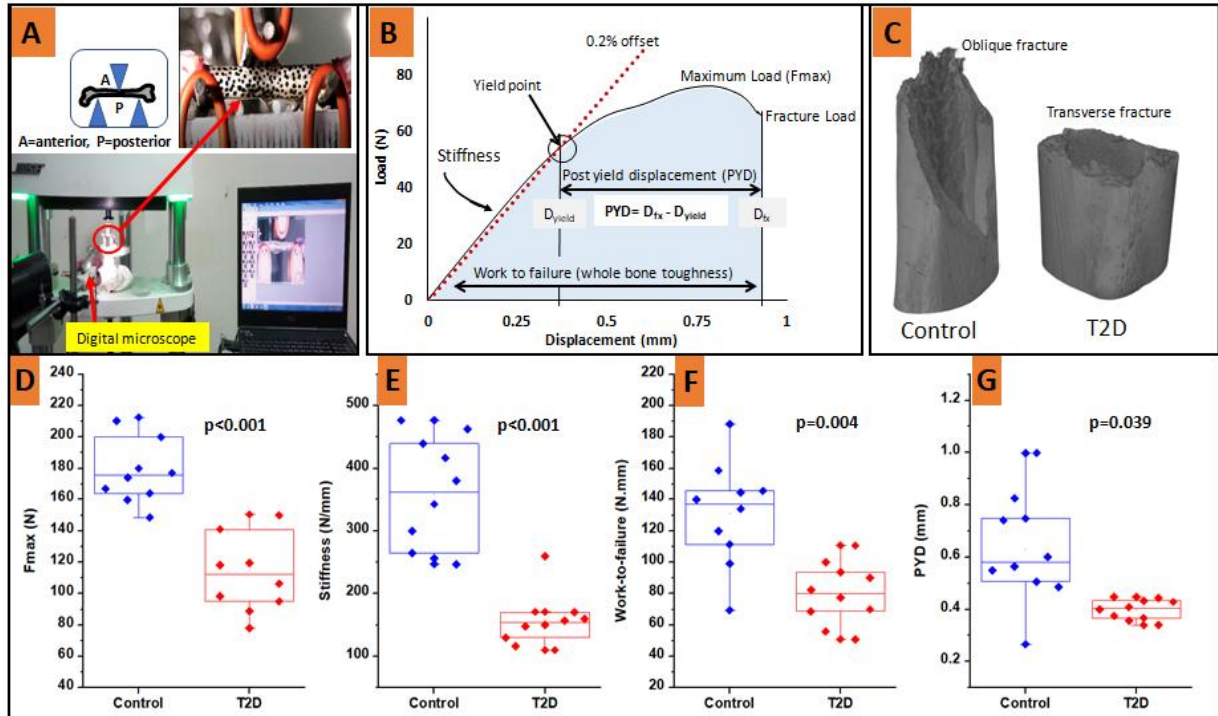


Figure 3.3(A) Experimental setup of three-point bending test, (B) Representative load-displacement curve resulting from a rat bone loaded to fracture in three-point bending, (C) Representative image of fracture pattern obtained during three-point bending, showing diabetic bone suffer from transverse fracture, whereas control bones suffer from oblique fracture, (D-G) Maximum force (F_{max}), stiffness, work-to-failure and post-yield deflection (PYD) graphs respectively, showing a smaller value in the diabetic (T2D) group

3.4.2.2 Cyclic reference point indentation (cRPI)

The experimental setup and mean values of IDI, Avg-ED, US-1st, ID-1st and TID are shown in **Figure 3.4(A-F)** for control and T2D groups. The T2D group had significantly higher values of IDI, Avg-ED, ID-1st, and TID [(by 14.7%, $p=0.027$), (by 11.3%, $p=0.046$), (by 4.1%, $p=0.047$) and (by 4.7%, $p=0.041$) respectively], which indicate that the T2D bone is less resistant to fracture (IDI) and favors larger amount of unrecovered bone deformation (Avg-ED) as compared to controls. Also, the lower value for US-1st (by 9.1%, $p=0.040$) is observed in the T2D group, which indicates T2D bones have lower matrix stiffness.

3.4.2.3 Nanoindentation (NI)

The load-displacement data obtained through nanoindentation tests for both the groups reveal that under the same load of 1000 μN , the T2D group had significantly lower values of modulus (16.22 ± 0.78 GPa to 20.6 ± 1.04 GPa, $p=0.008$) and hardness (0.387 ± 0.039 GPa to 0.577 ± 0.039 GPa, $p=0.007$), because the T2D bone undergoes greater deformation, whereas control bones undergo lesser deformation under the same loading. The modulus and hardness are both found to be lower by **21.4%** and **32.9%**, respectively, in the T2D group as compared to the control group, and the result is shown in **Figure 3.4(G-H)**.

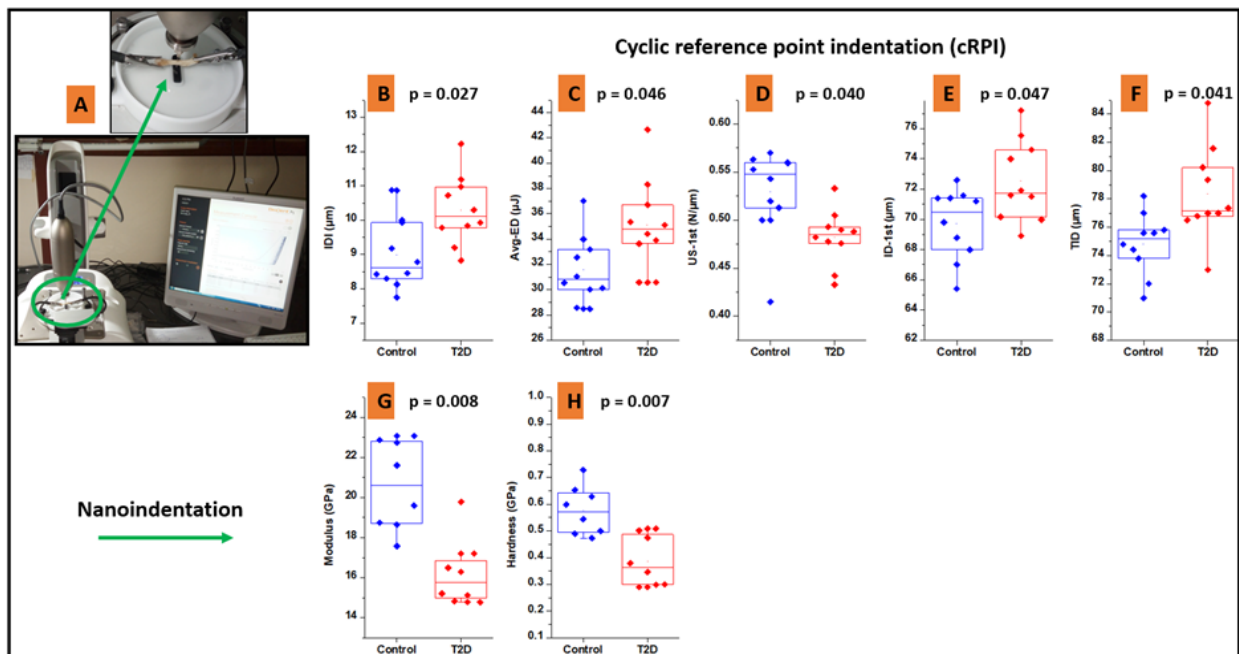


Figure 3.4(A) Experimental setup of cyclic reference point indentation (cRPI) test, **(B-D)** Indentation distance increase (IDI), average energy dissipated (Avg-ED) and unloading slope first cycle (US-1st) respectively, showing the increased value of IDI, Ave-ED, ID-1st and TID, and smaller value of US-1st in the diabetic (T2D) group, **(E-F)** nanoindentation results showing the smaller value of reduced modulus (E_r) and hardness respectively in the diabetic (T2D) group

3.4.3 Mean mineral crystal size (XRD)

The typical XRD pattern of cortical bone is shown in **Figure 3.5(A)**. The average crystallite length was decreased from 18.29 ± 0.73 nm to 16.67 ± 0.85 nm, and the width was increased from 4.64 ± 0.11 nm to 5.18 ± 0.19 nm in control to T2D groups, respectively. The lower value of mean crystallite length is found insignificant (8.9%, $p=0.168$), and crystallite width size

(11.7%, $p=0.037$) is found significant in the T2D group with respect to the control group, as shown in **Figure 3.5(B)**.

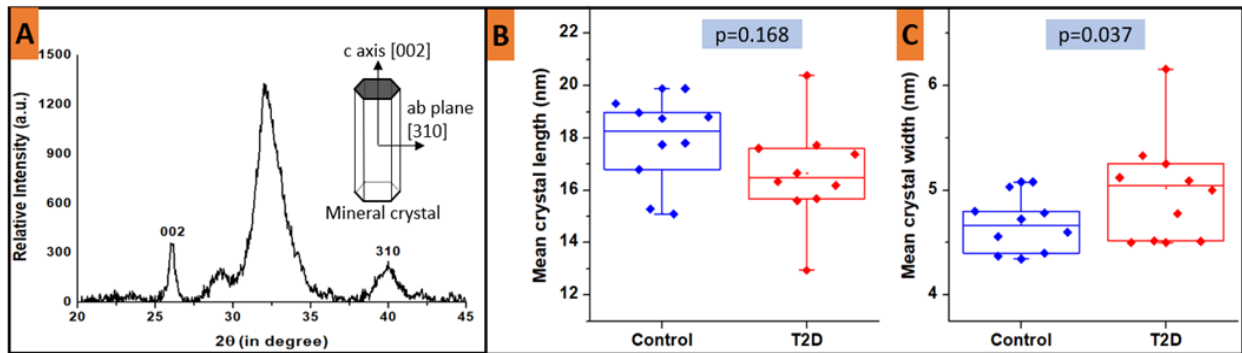


Figure 3.5(A) Representative XRD pattern ($20^\circ < 2\theta < 45^\circ$) of SD rat cortical femoral bone. The peak at 26° and 40° is used to determine the average crystal length and width in the c-axis direction [002] plane and ab-plane [310] respectively, **(B)** Showing mean crystallite length and **(C)** Showing increased width of mean crystallite in the diabetic (T2D) group.

3.4.4 Compositional analysis (FTIR) and fAGE assay

Figure 3.6(A-D) shows the mineral-based parameters, where T2D bone had lower mineral/matrix ratio [by 33.46%, ($p=0.039$)], and nearly similar carbonate/phosphate ratio [by 22.22% ($p=0.099$)], mineral crystallinity [by 9.93%, ($p=0.073$)] and acid phosphate content [by 6.94%, ($p=0.631$)] in both the groups.

The collagen parameters: collagen maturity and collagen crosslinks [NE-xLR (area ratio of the $1678/1692\text{ cm}^{-1}$ subbands)] are calculated and shown in **Figure 3.6(E-F)**. The T2D bone had significantly higher NE-xLR [by 85.65%, $p=0.011$] compared to the control bones. No change is observed in collagen maturity ($p=0.961$).

The average fAGEs concentration is higher from 288.6 ± 33.5 to 412.4 ± 36.6 ng quinine/mg collagen, in control to the T2D group, respectively, as shown in **Figure 3.6(G)**. The fAGEs concentration is found significantly higher (42.9%, $p=0.034$) in the T2D group with respect to the control group, which revealed that the non-enzymatic glycation is higher in the T2D group.

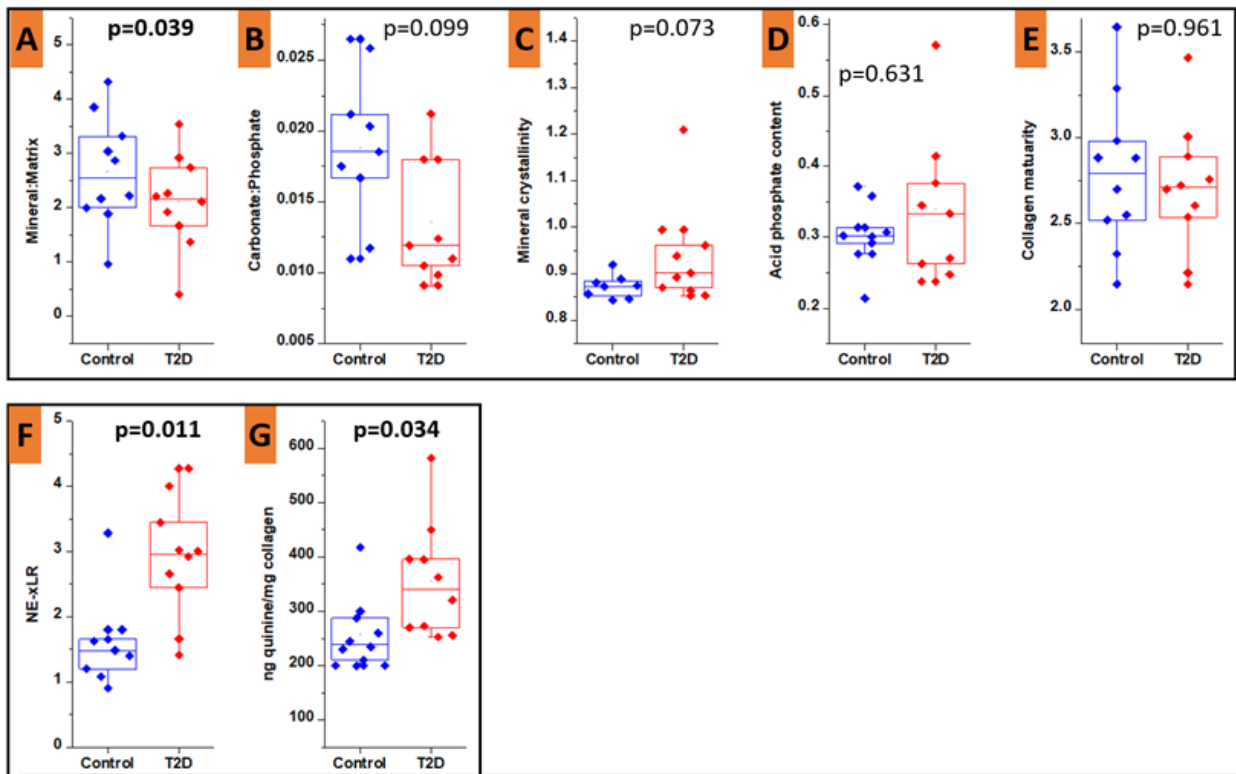


Figure 3.6(A-D) measures of mineral properties and collagen maturity, showing lower mineral-to-matrix ratio in diabetic (T2D) bone, whereas all other mineral parameters could not reach the level of significance, **(E)** represents collagen maturity (area ratio of the 1660/1692 cm^{-1} subbands), **(F)** represents non-enzymatic cross-link ratio [NE-xLR, (the area ratio of the 1678/1692 cm^{-1} subbands, total cross-linking AGEs)], **(G)** The graph is showing that the fAGEs content is higher in the diabetic group

3.4.5 Interrelationship between variables

Within the diabetic group, the HbA1c is found positively correlated with NE-xLR ($r=0.685$, $p=0.029$), whereas the correlation between HbA1c and fAGE is found non-significant. HbA1c is negatively correlated with BV/TV ($r=-0.731$, $p=0.039$), and tended to negatively associated with cortical thickness ($r=-0.722$, $p=0.067$) and cortical area ($r=-0.645$, $p=0.118$) in diabetic group. Correlations between HbA1c and mechanical parameters revealed that within the diabetic group, the HbA1c is strongly and negatively correlated with F_{\max} ($r=-0.708$, $p=0.033$). HbA1c is also found negatively correlated with mean crystallite width ($r=-0.752$, $p=0.032$) in the diabetic group. All other microstructural and compositional parameters are not significantly correlated with HbA1c in both groups. Also, none of the parameters in T2D, as well as the control group, is significantly correlated with plasma insulin value (lower circulating insulin) measured at the end of the study.

Within diabetic group itself, the fAGE and NE-xLR are correlated with mean crystallite width ($r=0.833$, $p=0.010$) and PYD ($r=-0.697$, $p=0.025$) respectively. Whereas in the non-diabetic group, the fAGE and NE-xLR do not correlate significantly with any of the parameters.

Forward stepwise regression tests to predict mechanical properties as a dependent variable using measures of glycation (fAGE and NE-xLR) as independent variables showed that within the diabetic group, the NE-xLR can explain up to 48.6% ($p = 0.025$) of variance in PYD (Figure 3.7).

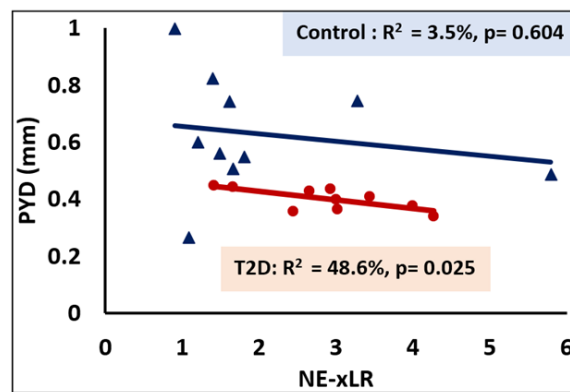


Figure 3.7 Graph represents mechanical parameter (post-yield-displacement, PYD) versus a measure of glycation (NE-xLR)

3.5 Discussion

This study was initiated to develop an animal model of type 2 diabetes with HFD-fed/low dose STZ by using genetically-normal outbred female SD rats that simulates the natural history and metabolic characteristics of the non-obese young (and/or adolescent) T2D patients. This model provides potential evidence that 8-week persistent hyperglycemia degrades the structural, mechanical, material, and compositional properties of the femoral bone while having comparable Ct.TMD (femur) among animals of T2D and control groups. Here we explored the associated changes due to diabetes on bone quality parameters, which involves the wider mean crystallite size, decreased mineral-to-matrix ratio, increased non-enzymatic collagen crosslinks (NE-xLR), and total non-enzymatic glycation content (fAGEs), and their effects on bone mechanical, microstructural and material properties.

Firstly, the assessment of bone microstructure after μ -CT showed lower cortical area (Ct.Ar) and cortical thickness (Ct.Th) in those with T2D when compared to the controls. This compromised cortical microstructure results in a lower value of F_{max} in three-point bending

indicates the lower femoral bone's strength in the diabetic group. Along with lower F_{max} , the lower value of stiffness (represents less load obtained capability to achieve a given displacement during the elastic region) and PYD (which represents the diabetic bone is less ductile) is observed in the diabetic group. In general, the ductile bone accommodates more plastic deformation before fracture, whereas brittle bone favors very little PYD [129]. Likewise, the lower value of toughness is observed in the diabetic group, which represents, the diabetic bone is less tough (more brittle) because the tougher bone stores a larger amount of energy before fracture.

Likewise, at the material level in the cRPI and NI test, the lower value of the first cycle unloading slope [US-1st, (bone matrix stiffness)] and reduced modulus is observed respectively in the diabetic group. Also, the ability of energy storage and fracture resistance is compromised in the diabetic group, which is evidenced by the higher value of Avg-ED and IDI in the diabetic bone as compared to the control group. Our finding is consistent with the literature, where higher IDI (cRPI) was found to have a deeper indentation and more easily fractured bone [51], [136], [194]. The lower values of modulus and hardness (NI) are directly associated with an altered bone composition, which is evidenced by a lower mineral to matrix ratio (FTIR) in the diabetic bone. Whereas a previous study on Zucker diabetic Sprague-Dawley rats by Hammond et al. [76], which showed increased values of mineral-to-matrix ratio relative to controls, might be because they used obese diabetic rat strain. Another possible reason for decreased reduced modulus (NI) is the wider mean crystallite size (XRD) in the T2D group. Indeed, the wider crystallite size being with constant length results in the decreased aspect ratio (surface area/volume) of apatite crystals, absorbs little energy, and results in reduced elastic modulus of bone material [157]. Furthermore, this altered crystal shape also can affect crystal connectivity, orientation, and arrangement [157], results in reduced resistance to load. This result is consistent with the finding of the previous study, which reported that the bones of older animals and osteoporotic patients have larger crystal size, and their bone tends to fracture more easily [195], [196]. Similar to our result, Boyar et al. [106] also identified the increased apatite crystal sizes for the diabetic femur, which indicates the increased crystallinity that is widely seen in osteoporosis [106].

Further, the weaker diabetic bone behavior is evidenced by a transverse (in-plane) fracture pattern, which indicates the relative loss of bone material heterogeneity. In comparison, control bone showing diagonal (oblique/out of plane) fractures, which indicates the quasi-brittle (heterogenous) nature of the bone material. Our finding is consistent with the previous

study; those have reported that the failure of tougher bone specimens is governed by increased deflection and longer crack path, whereas shorter, more direct crack path, as well as less-distributed damage, were evidenced during failure of the weaker bones [197]. This might be because relatively very similar elastic modulus (material level) in the bone of the T2D group could lead to small and straight crack paths compared to the control group.

We hypothesized the main reason for weaker and brittle bone in T2D is prolonged hyperglycemia (increased HbA1c). Here we found that the HbA1c is negatively correlated with Ct.Th and F_{max} and positively correlated with NE-xLR, which revealed that hyperglycemia is responsible for compromised structural and mechanical properties and increased non-enzymatic cross-links in bone material of the diabetic group. We have also observed the elevated fAGEs content and increased NE-xLR in the diabetic group as compared to the control group, as well as the NE-xLR is negatively correlated with PYD. Indeed, the non-enzymatic cross-links favor material rigidity by restricting the deformation (plasticity) of collagen fibers, reduces fibril stretching and sliding, and thereby reduces tissue ductility and toughness, which makes the bone more brittle [22], [29], [198]. This altered matrix property facilitates microcrack generation and cracks growth and thus makes the bone more susceptible to fracture [44], [187]. Similar to our results, Saito et al. [62] demonstrated increased NE-xL (pentosidine) in spontaneously diabetic WBN/Kob rats. Acevedo et al. [42] showed increased AGEs content by 27% in obese UCD-T2D rats vs. lean SD rats. Therefore, these elevated levels of fAGEs and NE-xLR found in our study explain the material incompetence- lower toughness and ductility (PYD) in three-point bending, and reduced ability of energy storage (Avg-ED) and lower fracture resistance (IDI) at the material level (cRPI) for diabetic bone as compared to control group.

Similar to our outbred genetically normal non-obese T2D rat model, other diabetic rodent models (spontaneous, abnormal leptin/leptin receptor signaling, diet-induced obesity) also showed a similar trend of three-point bending test. The non-obese rodent model of T2D published by Saito et al. [62] demonstrated deteriorations in the structural, mechanical properties of stiffness, modulus, ultimate load, and energy absorption in the femur of spontaneously diabetic (onset of diabetes at 12–13 months of age) non-obese male WBN/Kob rats vs. Wistar (nondiabetic) controls (kept on the same diet). Zhang et al. [54] showed a decrease in the maximum load by 21% and energy absorption by 29.7% in the femur of age- and sex-matched 6-month-old spontaneous diabetic (onset early after birth) non-obese male Goto-Kakizaki (GK) rats vs. male Wistar rats (kept on the same diet). Whereas no-significant

difference is reported in elastic modulus among both the groups, it might be because different rat strain is used for comparison.

Other than non-obese T2D rat models, there are many obese diabetic rat models that showed a decline in mechanical properties in the three-point bending test. Kimura et al. [68] demonstrated deteriorations in the maximum load (44%), stiffness (28%), and energy absorption (77%) in the femur of Spontaneously Diabetic Torii (SDT-fa/fa) rats (obese T2D, onset at eight weeks of age) compared to Sprague–Dawley rats (control animals) at the 40 weeks of age (kept on the same diet). Prisby et al. [55] observed a significant reduction in the ultimate load (NS, by 18.8%) and stiffness (17.5% and 23%) in the femur of diabetic male ZDFfa/fa (onset at 10-12 weeks) vs. ZDF+/? (control) rats at 13 and 20 weeks of age, respectively (kept on the same diet). Reinwald et al. [58] demonstrated decreased ultimate load by 30%, stiffness by 39%, and work-to-fracture by 36% in the femur of 33 weeks old male diabetic ZDFfa/fa (fatty) vs. ZDFfa/+ (lean control) rats. They also observed a significant reduction in the ultimate load by 19% and stiffness by 15.6% in the femur of age-matched ZDSD compared to CDSR rats (disease onset 15- 21 weeks of age). Gallant et al. [40] demonstrated decreased ultimate stress by 14.9%, modulus by 10.4%, and toughness by 50%, and post-yield toughness by 67% in the femur of T2D ZDSD male rats compared to control CD male rats at 32 weeks of age (HFD gave for 12 weeks, since 20 weeks of age). Reddy et al. [69] demonstrated reduced maximum load by 37%, bending stiffness by 38%, and energy absorption to yield and toughness by 27% and 34%, respectively, in the femur of 10-week-old Sprague-Dawley rats treated with STZ (65 mg/kg body weight) for seven weeks. It indicates, all studies published so far using various T2D rat models showed lower femoral bone strength in the diabetic group with a three-point bending test, as reported in this study.

The advantage of our HFD-fed/low dose STZ treated model is that it is neither inbred nor genetically determined, easily available, and relatively inexpensive. This model also shows the abnormalities in lipid metabolism (evidenced by increased plasma triglyceride and plasma total cholesterol levels), which contribute to various cardiovascular complications, as in the case of human T2D patients. Secondly, the presented model (HFD-fed/low dose STZ) can develop diabetes in both males and females [65], [77], [199], whereas in ZDF and ZDSD rat models, only male rats are prone to become diabetic [58], [63]–[65] and the accessibility of animals and/or expense also tend to limit its utility [65], [199].

Along with the advantages of the presented model, the main limitation involved here is that the use of (low dose) chemical treatment (STZ), which causes partial loss of pancreatic beta cells by direct cytotoxic action on it (unlike in human). It is unique and different from other combination rat models since the dose of STZ selected causes diabetes only in HFD-fed insulin-resistant rats, whereas it fails to induce the same in normal control rats resembling the situation in humans with risk factors of insulin resistance to be more prone to develop type 2 diabetes than others without them. If only STZ treatment is used to induce diabetes, then the relatively high dose (STZ; $>50 \text{ mg kg}^{-1}$) is needed, which causes direct insulin deficiency rather than the consequence of insulin resistance and exhibits a drastic reduction in the body weight. Hence, it depicts symptoms and characteristics typically more of human type 1 rather than type 2 diabetes [67], [69]. If STZ treatment is not used, then feeding of HFD alone requires a long time, as well as no hyperglycemia, develops upon simple dietary treatment in genetically normal animals [67]. Thus, the combination of HFD-fed/low dose STZ treatment is adopted to develop T2D, which simulates the condition of mild- hyperglycemia (a condition similar to prediabetes) due to insulin resistance (because of the feeding of HFD for a period of 4 weeks, hyperinsulinemia) and further develop hyperglycemia due to low dose STZ treatment on HFD-fed insulin-resistant animals (hypoinsulinemia). This condition closely simulates the phenotype of non-obese Asian type 2 diabetes as they have less insulin resistance (not to the same extent as in obese patients) and disproportionally reduced insulin secretion, as compared with obese patients with T2D (Caucasian). Importantly, non-obese patients with T2D have a similar increased risk of cardiovascular disease as obese T2D patients [189], [200].

In summary, the combination of HFD-fed/low dose STZ treated T2D non-obese rat model is developed by using genetically-normal outbred female SD rats, which simulates the metabolic characteristics of late-stage of type 2 diabetes for non-obese young (and/or adolescent) T2D patients (Asians). This study also showed that the NE-xLR is elevated in the T2D group and strongly and negatively correlated with PYD, which directly explains the bone fragility. Along with that, the reduced modulus (NI) and mineral-to-matrix ratio (FTIR), increased IDI (cRPI) and wider mineral crystallite size (XRD) in the T2D group evidenced that the composition of diabetic bone has changed; it became weaker and tended to easily fracture.

In conclusion, HFD-fed/low dose STZ treated T2D non-obese rat model can simulate the natural history and metabolic characteristics of the non-obese young (and/or adolescent)

Asian T2D patients. This study also showed that 8-week persistent hyperglycemia affects the femoral bone quality at various organization levels. Notably, the increased non-enzymatic cross-links result in compromised mechanical performance and diminished bone strength in T2D. Furthermore, a clear understanding of this model and the impact of diabetes on mineral and collagen quality could be helpful in designing specific treatment strategies for non-obese diabetic patients.

CHAPTER 4

INVESTIGATION OF MECHANICAL, MATERIAL AND COMPOSITIONAL DETERMINANTS OF HUMAN TRABECULAR BONE QUALITY IN TYPE 2 DIABETES

Increased bone fragility and reduced energy absorption to fracture associated with type 2 diabetes (T2D) cannot be explained by bone mineral density alone. This study, for the first time, reports on alterations in bone tissue's material properties obtained from individuals with diabetes and known fragility fracture status. The aim of this study is to investigate the role of T2D in altering biomechanical, microstructural, and compositional properties of bone in individuals with fragility fractures. Therefore, femoral head bone tissue specimens were collected from patients who underwent replacement surgery for fragility hip fracture. Trabecular bone quality parameters were compared in samples of two groups: non-diabetic (n=40) and diabetic (n=30), with a mean duration of disease 7.5 ± 2.8 years. As a result, no significant difference was observed in aBMD between the groups. Bone volume fraction (BV/TV) was lower in the diabetic group due to fewer and thinner trabeculae. The apparent-level toughness and post-yield energy were lower in those with diabetes. Tissue-level (nanoindentation) modulus and hardness were lower in this group. Compositional differences in the diabetic group included lower mineral-to-matrix ratio, wider mineral crystals, and bone collagen modifications - higher total fAGEs, higher non-enzymatic-cross-link-ratio (NE-xLR) and altered secondary structure (Amide bands). There was a strong inverse correlation between NE-xLR and post-yield-strain, fAGEs and post-yield energy, and fAGEs and toughness. Hence, the current study is novel in examining bone tissue in T2D following the first hip fragility fracture. Our findings provide evidence of hyperglycemia's detrimental effects on trabecular bone quality at multiple length scales leading to lower energy absorption and toughness-indicative of increased propensity to bone fragility.

4.1 Introduction

Type 2 diabetes (T2D) affects bone homeostasis leading up to three-fold increased hip fracture risk compared to those without diabetes [8], [14], [201]. This high fragility fracture risk is observed despite adequate areal bone mineral density (aBMD) in T2D [11], [12], [15], [17], [18], [118]. Thus, aBMD underestimates fracture risk in T2D, making the clinical identification of those at risk for fractures difficult. Beyond aBMD, the key factors contributing to bone strength are the parameters of bone quality – microstructure, bone material properties, bone mineral content and mean crystal size, bone protein (Amide I and II) quantity and its secondary structure, and the bone cell activity and dynamics (**Figure 4.1A**). These determinants have been examined individually in few studies, and material properties are often listed as the cause of poor bone quality in diabetes [51]–[53], [202]. Only animal studies [23], [40]–[42], [74], [130] and three recent studies of human tissue have attempted to address this question comprehensively [51]–[53]. A limitation of the previous human studies is that bone tissue was collected at the time of arthroplasty and may therefore have confounding effects associated with arthritis (including increased trabecular bone density) [51]–[53]. Furthermore, no prior studies of bone tissue material properties in humans have been conducted with known diabetic status and known fragility fracture status. The current study is novel in examining human bone tissue following the first hip fragility fracture.

The mechanisms underlying this poor bone quality and high fracture risk in diabetes are not well understood. Prolonged hyperglycemia leads to an increase in the non-enzymatic reactions (Maillard reactions) and the formation of advanced glycation end-products (AGEs) through post-translation modification [19]. AGEs then accumulate in the bone tissue and react irreversibly with amino acid residues of peptides or proteins to form protein adducts or protein crosslinks [20]. This phenomenon, widely recognized as non-enzymatic cross-linking (NE-xL), is the underlying mechanism for multiple complications of diabetes, as it alters normal cellular functioning and tissue quality [21], [22]. AGE accumulation may also alter mineralization through hyperglycemia affecting bone strength [23].

In the present *ex vivo* study, we aimed for multi-scale characterization of bone tissue from individuals with and without diabetes following hip fracture. This study includes - investigation of the structural parameters at voxel size consistent with the use of micro-computed tomography (μ -CT) and corresponding apparent level mechanical properties measured through the uniaxial compression test. We also examine bone material properties

(nanoindentation) as well as bone composition [thermogravimetric analysis (TGA)], mineral crystal size [X-ray diffraction (XRD)], alterations in protein content, enzymatic (E-xLR), non-enzymatic cross-link ratio (NE-xLR) [Fourier transform infrared spectroscopy (FTIR)], and fAGE content in the human diabetic bone tissue.

4.2 Material and methods

Study participants

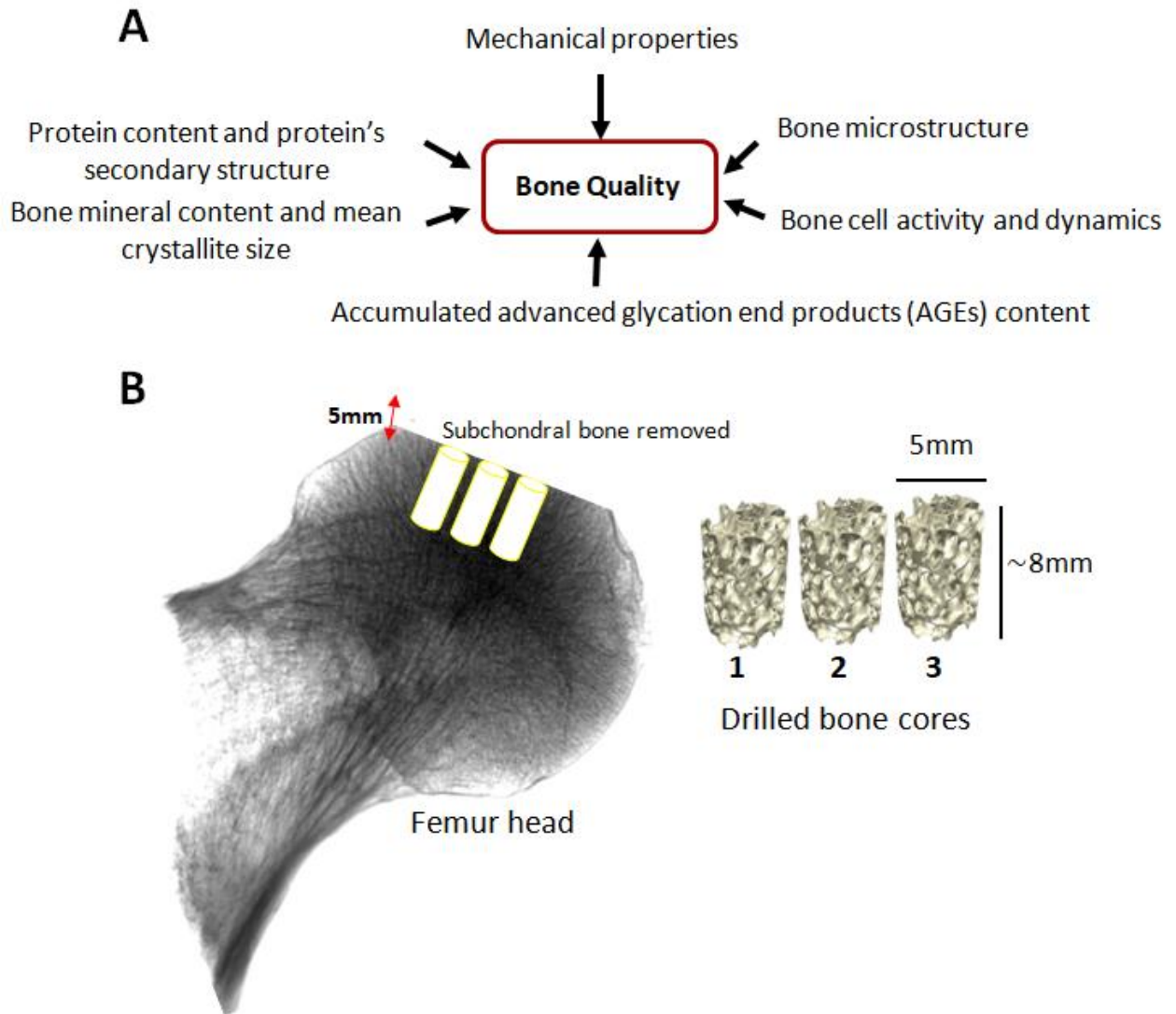
Bone samples were taken from two groups of patients who underwent bipolar hemiarthroplasty or total hip replacement following fragility fracture of hip - patients without diabetes (n=40) and with diabetes (n=30). Replacement surgery was the recommended treatment as these hip fractures were unsuitable for management with a cannulated cancellous screw or proximal femoral nail. Patients' age also favored replacement surgery for a better outcome. Type 2 diabetes was diagnosed according to the American *Diabetes* Association criteria [203]. None of the patients had a history of hip fracture prior to the fracture reported here. Patients with cancer, osteoarthritis, renal dysfunction, primary or secondary hyperparathyroidism, unexplained elevated alkaline phosphatase, and secondary osteoporosis (chronic steroid or antiepileptic use) were excluded from the study.

All patients with diabetes were taking anti-diabetic medications (metformin, sulfonylurea, or insulin). None were on pioglitazone or SGLT2 inhibitors. All participants involved in the study were from Northern India. The study was approved by the Institutional Ethics Committee (Approval Number PGI/IEC/2015/171) of the Postgraduate Institute of Medical Education and Research, Chandigarh. Written informed consent was obtained from each study participant. Demographic, clinical, biochemical, and aBMD (contralateral femoral neck BMD using HOLOGIC Discovery A QDR 4500; Hologic, Inc., Bedford, MA, USA) were recorded for all participants.

Sample procurement and storage

Femoral heads were collected from patients undergoing replacement surgery for hip fractures. From each femoral head, 5-7 cylindrical trabecular bone cores, each 5 mm in diameter and 8-9 mm in length, were extracted from femoral heads along the direction of the principal trabeculae using the drilling machine attached with diamond core bit as shown in (**Figure 4.1B**). The bone cores were cleaned with a water jet, wrapped in saline-soaked gauze (PBS 7.4 pH), transferred into sample bags, labeled, and subsequently stored at -20°C [51]. Bone

cores were then used for different characterization techniques, as shown in (Figure 4.1C). All experiments were conducted within one month after the collection of the femoral head.



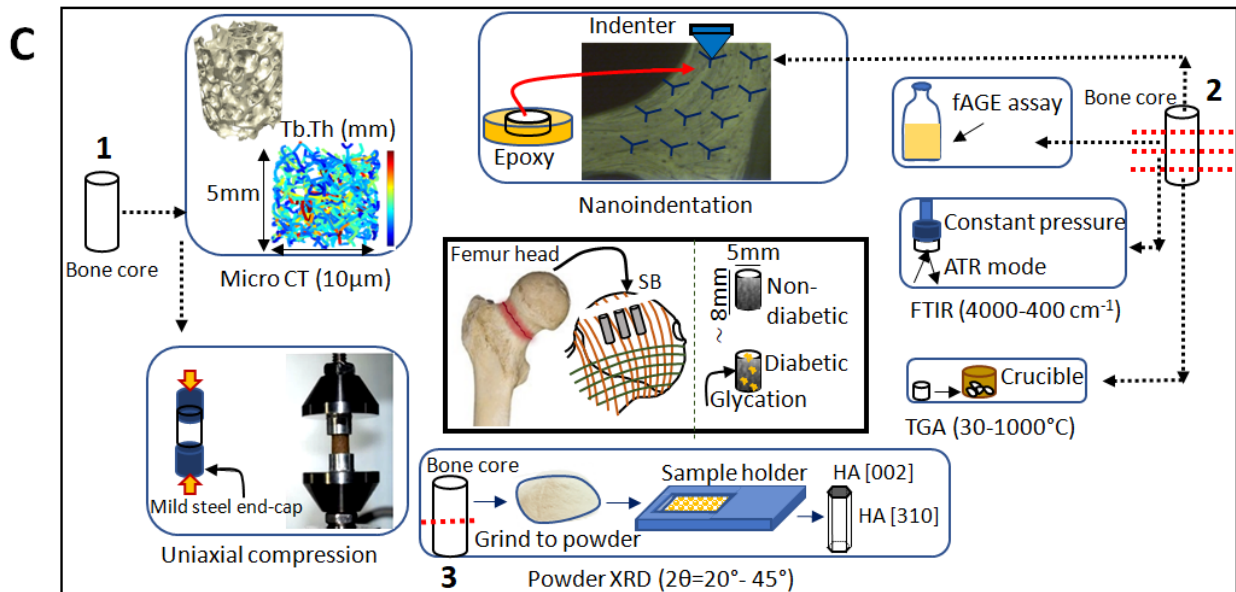


Figure 4.1 (A) Determinants of bone quality, (B) The extraction of cylindrical trabecular bone cores, each 5 mm in diameter and 8-9 mm in length, from femoral heads along the direction of the principal trabeculae using the drilling machine attached with diamond core bit, (C) Characterization techniques used to determine the human trabecular bone quality for diabetes patients; SB: subchondral bone

4.3 Assessment of bone quality parameters

4.3.1 Microstructural parameters

The microstructural parameters were studied by using μ -CT. One bone core of each patient was air-dried and scanned along the cylindrical axis on a μ -CT system (Phoenix/x-ray, GE Sensing & Inspection Technologies, Germany) using 10 μ m voxel size, 45 keV tube voltage, 250 μ A beam current, 250 sec integration time, and 10 frames. Reconstruction of scanned images was collected using Phoenix software (phoenix/x-ray, GE Measurement & Control; Germany), and reconstructed images were imported in Scan-IP (Simpleware Ltd, UK) and Image J's plugin BoneJ [software by National Institute of Health, available at (<https://imagej.nih.gov/ij/>)] [193]. Following structural parameters were obtained: bone volume fraction (BV/TV), trabecular thickness (Tb.Th), trabecular separation (Tb.Sp), trabecular number (Tb.N), structure model index (SMI), and degree of anisotropy (DA) [123].

4.3.2 Bulk mechanical properties

After μ -CT imaging, the bone cores were utilized for compression testing. The samples were rehydrated in saline-soaked gauzes for 2 hours at 4°C. Mean specimen length of 8 mm and length to diameter ratio of nearly 1.5:1 were used for testing. The bone cores were glued in customized mild steel cylindrical end caps to minimize end-effects [132]. Compression test was performed on each core to measure the mechanical properties using an electromagnetic testing system (Electroforce 3200, Bose, Eden Prairie, MN, USA with the specification of load cell: $\pm 450\text{N}$, and LVDT: stroke length $\pm 6.5\text{mm}$ with $0.1\mu\text{m}$ resolution) at room temperature while keeping the specimen hydrated in PBS spray [204]. The specimens were preloaded to 5N to ensure proper contact between the test specimen and the compression plate. Then, preconditioning between 0.05 to 0.2 % strain was done in three cycles to minimize the toe region. Monotonic testing was conducted at a strain rate of 0.01 s^{-1} until 1 mm displacement. The load-displacement data were captured at 100 Hz frequency and converted into stress-strain data shown in **(Figure 4.2A)** to determine several mechanical parameters, including elastic modulus, yield point (using the 0.2% offset method), ultimate point (determined as the point of maximum load), post-yield strain (determined as the difference between an ultimate strain and yield strain), post-yield strain energy, and toughness [127], [132], [133].

4.3.3 Bone material properties

The bone material properties were determined using nanoindentation. A bone core from each patient was embedded in epoxy and used to determine material level properties via nanoindentation. The embedded samples were ground, polished in diamond solutions with particle sizes of 3, 1, 0.25, and $0.05\ \mu\text{m}$ (Buehler Eco Met 250 grinder and polisher), and abrasive papers of 1200, 2000, and 4000 grit sizes, under the water cooling condition. The samples were cleaned ultrasonically with distilled water between each polishing step.

Nanoindentation tests were performed using a TI-950 Tribo Indenter (Hysitron Inc., Minneapolis, MN, USA) with Berkovich pyramidal tip, having an included angle of 142.3° and tip radius of $\sim 150\text{ nm}$. The calibration of the instrument was performed using standard fused quartz and aluminum samples following the standard procedure [144], [145]. Locations for indents were identified using an in-situ scanning probe microscope integrated with the nanoindentation system. All tests were performed at room temperature in moist conditions.

Twenty (20) indents with a peak load of 3000 μN were applied to the longitudinal sections of the core [143]. The load function consisted of a ten-second ramp to peak force segment, followed by a thirty-second hold and an unloading segment of ten seconds. The thirty-second hold time was adopted to eliminate creep effects [205]. The load-displacement curves, obtained from indentation tests, were analyzed to determine the reduced modulus (E_r) and hardness (H) (average of 20 indents) using Oliver and Pharr method in Triboscan (Hysitron) [146], [147].

4.3.4 Thermogravimetric analyses

Thermogravimetric analyses (TGA) were performed to compare the bulk mineral to matrix ratio. Approximately 8 to 12 mg of trabecular bone underwent TGA analysis (TGA/DSC1 instrument, Mettler Toledo, Greifensee, Switzerland) in a controlled air atmosphere from room temperature to 1000 $^{\circ}\text{C}$ with a heating rate of 10 $^{\circ}\text{C}/\text{min}$. The thermal data were analyzed in STARe software (version 12.1). The mineral to matrix ratio was calculated as the ratio between the percentages of mass (% dry weight) remaining after heating to 600 $^{\circ}\text{C}$ and the organic mass loss between 200 $^{\circ}\text{C}$ and 600 $^{\circ}\text{C}$. The protocol was adapted from published studies [150], [151].

4.3.5 Mean crystal size

In order to obtain a powder, the half bone core was defatted and dehydrated in increasing concentrations of ethanol (70% to 100%) for 10 minutes each. The specimen was wet ground in acetone using mortar and pestle until a uniform and homogeneous powder was obtained³¹. X-ray diffraction (XRD) measurements were performed using $\text{CuK}\alpha$ radiation at 40 kV and 40 mA (X'Pert PRO, PANalytical) from 20 to 45 $^{\circ}$ 2θ . The Xpert Highscore plus software was used for background correction and to fit the diffraction peaks at $2\theta = 26^{\circ}$ and 40 $^{\circ}$ corresponding to 002 (c-axis direction) and 310 planes (ab-plane), respectively. The data of 002 and 310 planes were utilized to calculate the average length and width of mineral crystal, respectively, using the Scherrer equation [153]–[155].

4.3.6 Mineral and collagen properties

FTIR spectra were recorded from the freeze-dried bone section of donors using Bruker IFS 66v/S FTIR spectrophotometer in Attenuated Total Reflectance (ATR) mode, under the constant pressure, in the spectral region of 4000 to 400 cm^{-1} and used to calculate the following parameters: carbonate to phosphate ratio [area ratio of the carbonate ν_2 peak (852-

890 cm^{-1}) to phosphate ν_1 - ν_3 peak (916-1180 cm^{-1}), mineral crystallinity [intensity ratio of 1030 cm^{-1} to 1020 cm^{-1} , which is related to crystal size and stoichiometric perfection], and the acid phosphate content [intensity ratio of 1127 cm^{-1} to 1096 cm^{-1} , which characterizes acid phosphate substitution into stoichiometric hydroxyapatite] [165], [166]. The Amide I band (**Figure 4.2B**) possesses structural information about the collagen matrix and is also the location of the strongest peaks for the non-enzymatic cross-link (NE-xL) pentosidine [21]. Thus, sub-bands of the Amide I band were fitted with Gaussian curves at 1610, 1630, 1645, 1660, 1678, and 1692 cm^{-1} by using a peak analyzer tool in OriginPro 8.5 software. These peaks were chosen based on the second derivative approach. From the analysis of Amide I sub-bands, the non-enzymatic collagen crosslink-ratio (NE-xLR) [21] and enzymatic collagen cross-link ratio (E-xLR) [167] were measured through the area ratio of the 1678/1692 cm^{-1} and 1660/1678 cm^{-1} sub-bands, respectively. The measurement of the non-enzymatic cross-link ratio (NE-xLR) enables the estimation of overall AGE content in bone tissue itself [21]. Also, the collagen maturity [area ratio of 1660 cm^{-1} to 1690 cm^{-1}] was measured within the Amide I peak [167], [168]. The integrated area ratio (relative content) of Amide I and Amide II [206]–[208] bands were normalized with respect to methylene (CH_2) deformation band at 1450 cm^{-1} , similar to previous studies [208], [209]. Finally, the mineral to matrix ratio [area ratio of the phosphate ν_1 - ν_3 peak (916-1180 cm^{-1}) to Amide I peak (1596-1712 cm^{-1})] was measured [165], [166].

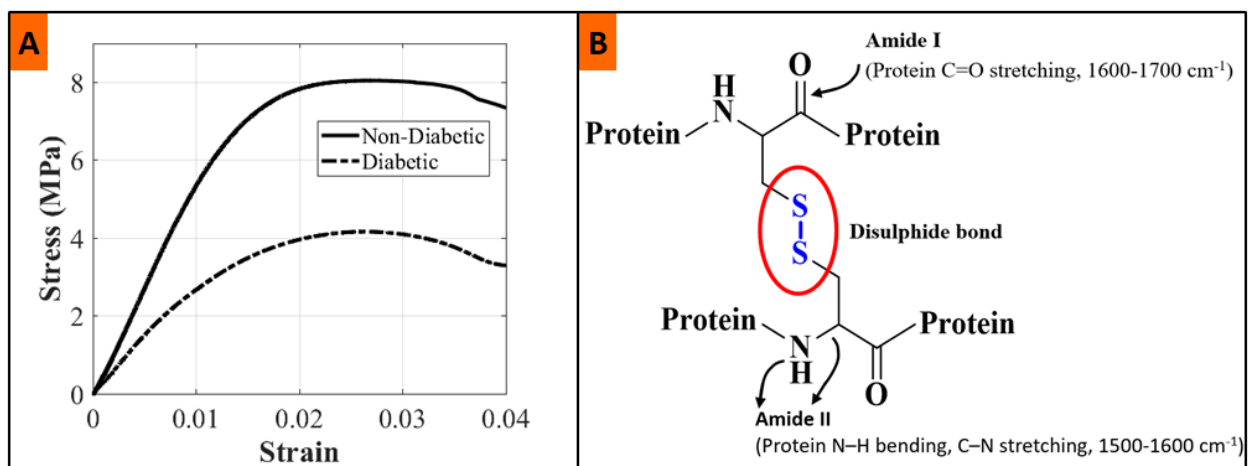


Figure 4.2 (A) Calculated typical stress-strain plot of compression test for diabetic and non-diabetic groups, (B) Amide I and Amide II bond positions in principal structural unit of collagen in human trabecular bone

4.3.7 Fluorescent advanced glycation end-products (fAGEs) assay

Total fluorescent AGEs (fAGEs) were measured using fluorescence spectrometry and normalized to collagen concentration, similar to the previous studies [46], [179]. The 1/4th bone cores of each donor were lyophilized overnight, then 45-55mg dried specimens were hydrolyzed in 6N HCl (100 μ l/mg bone) at 110 °C for 20 h in hydrolysis vials with screw caps. The hydrolysate was cooled at room temperature, collected in a microcentrifuge tube, and centrifuged with 13000 rpm at 4°C (Eppendorf 5424R microcentrifuge). The supernatant is collected, diluted (ten times with DI water), and fluorescence was measured in a flat-bottom 96-well plate using a multi-mode microplate reader (CLARIOstar Plus, BMG LABTECH) at an excitation of 360 nm and an emission of 460 nm. The fluorescence data of specimens were normalized with serially diluted quinine standards (stock: 10 μ g quinine per 1 mL of 0.1 N H₂SO₄) measured in the same way [46], [179]. Next, the absorbance assay of hydroxyproline was performed to determine collagen content to normalize the total fluorescence [179]. Total fAGEs are reported in units of ng quinine fluorescence/mg collagen. The collagen content is derived based on prior knowledge that collagen consists of 14% hydroxyproline [181]. All solutions used were freshly prepared, and experiments were performed in darkness at room temperature.

4.4 Statistical analysis

Distributions of mechanical properties were plotted to identify potential outliers, and the data from five donors (three from the non-diabetic group and two from the diabetic group) with values two standard deviations beyond the mean were removed from all analyses. The distribution of the data was tested for normality by the Kolmogorov-Smirnov test. The homogeneity of variances was analyzed using Levene's test. Between-group differences of calculated parameters were analyzed for statistical significance using Student's t-tests after testing for normality and homogeneity of variances. Mean values and standard deviation were calculated for the measured parameters. Pearson correlation tests were used to determine relationships between variables. Forward stepwise regression tests were conducted for mechanical properties using all significant parameters as independent variables. An analysis of covariance (ANCOVA) was conducted to compare the differences in mechanical properties among groups by using BV/TV as a covariate. The post-hoc power calculation was performed by comparing the mean value of post-yield energy and toughness between diabetic and non-diabetic groups using an ANOVA test. A confidence level of $p < 0.05$ implies a statistical significance between the groups where $p < 0.05$, $p < 0.01$, and $p < 0.001$ denote the

level of significance. Statistical analysis was performed using SPSS (v.21, SPSS Inc., Chicago, IL, USA) and Microsoft Office Excel (2007).

4.5 Results

4.5.1 Patient characteristics

Table 4.1 shows the baseline characteristics of patients with diabetes (n=30) and without diabetes (n=40). The mean age of the diabetic and non-diabetic group was 69.7±10.0 and 69.8±10.2 years, respectively. The sex distribution among groups was also similar. Other than pre-operative glycosylated hemoglobin A1c (HbA1c) levels, no significant differences were observed in other baseline characteristics, including aBMD, T score, and biochemical parameters between diabetic and non-diabetic groups. The duration of diabetes ranges from 4 to 15 (7.5±2.8) years.

Table 4.1 Baseline demographic, radiographic, and biochemical parameters of diabetic and non-diabetic groups

Parameters	Non-diabetic group (n=40)	Diabetic group (n=30)	p-value
Gender (females) n, %	25, 62.5	19, 63.3	0.198
Age (years)	69.8 ± 10.2	69.7 ± 10.0	0.961
<i>Biochemical</i>			
Pre-operative HbA1c (%)	5.4 ± 0.4	7.9 ± 1.8	< 0.001
Diabetes duration (years)	Na	7.5 ± 2.8	na
Serum calcium (mg/dl)	8.4 ± 0.6	8.5 ± 0.6	0.306
Serum phosphorus (mg/dl)	3.4 ± 0.7	3.4 ± 0.6	0.658
PTH (pg/ml)	39.3 ± 21.0	41.4 ± 38.4	0.791
25-hydroxy Vitamin D (ng/ml)	22.3 ± 8.6	22.5 ± 8.5	0.932
ALP (IU/L)	134.2 ± 75.8	131.2 ± 36.9	0.875
<i>Imaging</i>			
FN aBMD (gm/cm ²)	0.600 ± 0.091	0.578 ± 0.106	0.329
FN T score	-2.6 ± 0.87	-2.5 ± 0.78	0.696
<i>Medications</i>			
Metformin use (n, %)	0	15, 50	

Metformin + Sulfonylurea use (n, %)	0	12, 40	
Metformin + Sulfonylurea + Insulin use (n, %)	0	3, 10	
Anti-osteoporotic treatment ¹ (n, %)	2, 5	1, 3.3	
All data are expressed as mean \pm SD, na: not applicable; HbA1c: glycosylated hemoglobin A1c; ALP: alkaline phosphatase; FN: Femoral neck; aBMD: areal bone mineral density ¹ bisphosphonate (alendronate)			

4.5.2 Microstructural parameters

Representative μ -CT images and a map of trabecular thickness in diabetic and non-diabetic bones are shown in **Figure 4.3 A-D**, and the mean values of microstructural parameters are shown in **Table 4.2**. The diabetic group had significantly lower BV/TV (14.21%, **p = 0.03**), Tb.Th (mm) (10.8%, **p = 0.019**), and Tb.N (1/mm) (8.0%, **p = 0.033**), higher Tb.Sp (mm) (12.27%, **p = 0.095**) and structure model index (SMI) (24.48%, **p = 0.037**) compared to the non-diabetic group. We observed similar mean values (**p=0.475**) of the degree of anisotropy (DA) among both groups. The mean value of SMI for the diabetic and non-diabetic groups is 2.39 ± 0.19 and 1.92 ± 0.12 , respectively (**p=0.037**), indicating that the rod-like trabeculae structure is dominant in the diabetic group, compared to non-diabetics.

4.5.3 Mechanical properties

The mean values of modulus, yield stress, ultimate stress, yield strain, ultimate strain, post-yield strain, post-yield energy, and toughness for both groups are shown in **Figure 4.3 E-L**. The modulus, yield stress, ultimate stress, post-yield energy and toughness were found to be lower by 25% (**p=0.03**), 27% (**p=0.01**), 25% (**p=0.02**), 47% (**p=0.007**) and 45% (**p=0.005**), respectively in the diabetic group as compared to the non-diabetic group. These results indicate that the load-bearing and energy absorption capacity is significantly compromised in diabetic bone. However, yield strain, ultimate strain, and post-yield strain did not differ across groups.

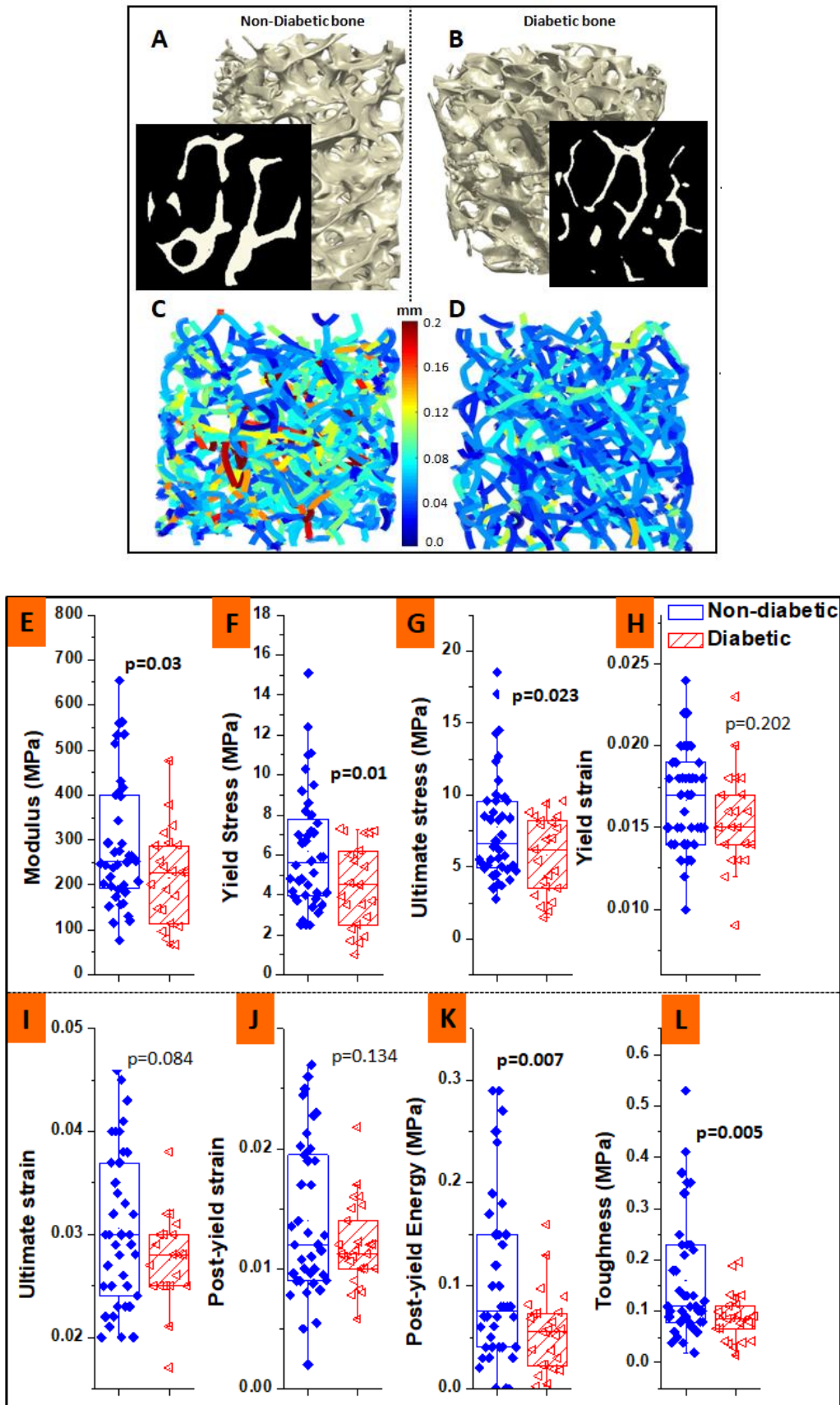


Figure 4.3 Representative 3D reconstructed μ -CT image: (A) represents the non-diabetic group, and (B) represents the diabetic group. The color map in (C) and (D) represents the

variation in trabecular thickness for the non-diabetic and diabetic group, respectively, (**E-L**) Elastic modulus, yield stress, ultimate stress, yield strain, ultimate strain, post-yield strain, post-yield energy, and toughness respectively, for diabetic and non-diabetic group

4.5.4 Material properties

Nanoindentation tests for both the groups reveal that under the same load of 3000 μN , the diabetic group had significantly lower values of modulus (7.37 ± 2.96 GPa to 9.0 ± 2.7 GPa, **p=0.033**) and hardness (0.294 ± 0.150 GPa to 0.444 ± 0.152 GPa, **p=0.014**) than the non-diabetic group. The modulus and hardness were found to be lower by 18.1% and 33.8%, respectively, in the diabetic group as compared to the non-diabetic group (**Figure 4.4 A-B**).

4.5.5 Composition

Representative thermo-gravimetric analysis (TGA) curves of weight (%) vs temperature with their respective first derivatives are plotted in (**Figure 4.4C**). The percentage of weight associated with water content [$m_{24^\circ\text{C}} (\%) - m_{200^\circ\text{C}} (\%)$], organic content [$m_{200^\circ\text{C}} (\%) - m_{600^\circ\text{C}} (\%)$], mineral content [$m_{600^\circ\text{C}} (\%) / m_{200^\circ\text{C}} (\%)$] and carbonate content [$m_{600^\circ\text{C}} (\%) - m_{800^\circ\text{C}} (\%)$] are shown in **Table 4.2**. Diabetic bones exhibited decreased mineral content (**p=0.038**) compared with non-diabetics. No significant differences are found in the organic content ($p=0.087$), water content ($p=0.335$) and carbonate content ($p=0.988$). Mineral/matrix ratio indicate that diabetic bones had lower mineral/matrix ratio compared with non-diabetics (**p = 0.016**) as shown in (**Figure 4.4D**).

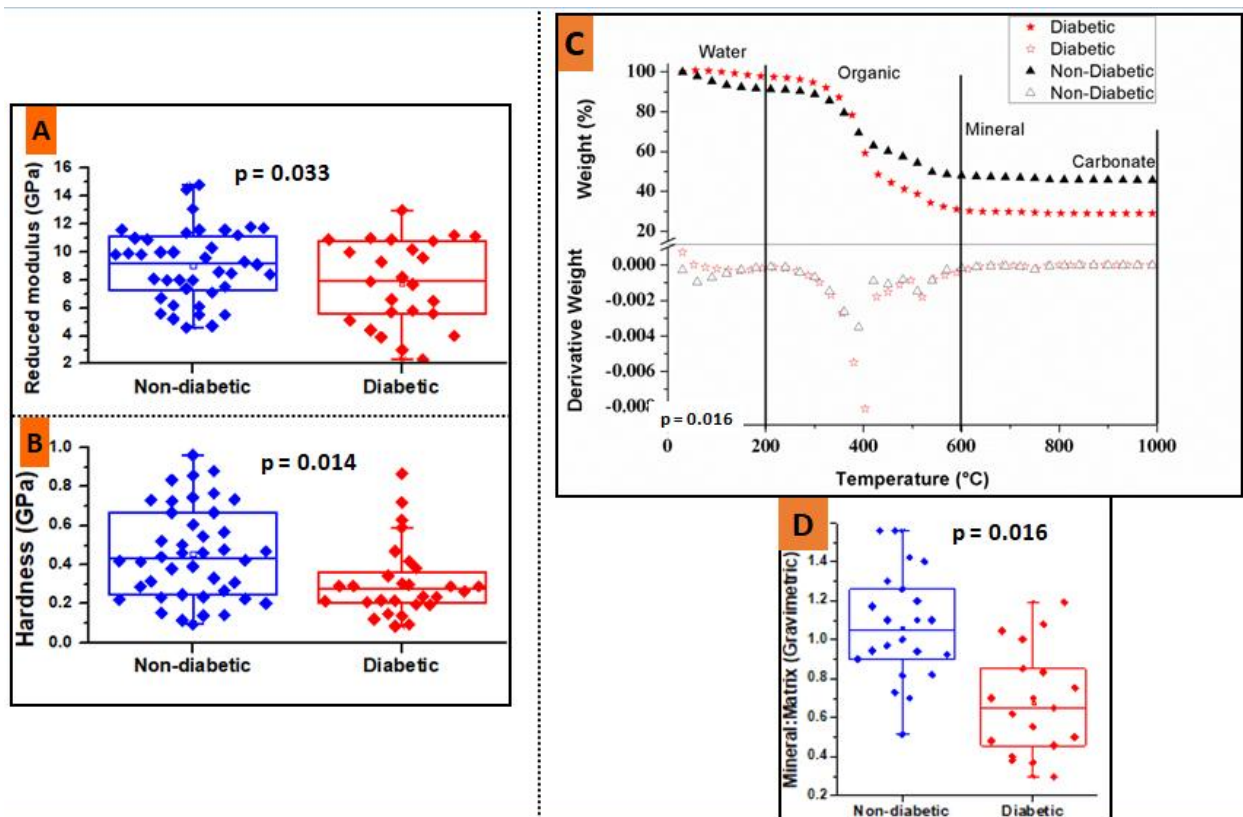


Figure 4.4 (A-B) Reduced modulus (E_r) and hardness respectively obtained from nanoindentation, showing smaller value in the diabetic (T2D) group, **(C)** Representative TGA curves with their respective first derivatives for diabetic and non-diabetic femur trabecular bone heated to 1000 °C. The TGA first derivative plots represent the more accurate temperature values associated with the percentage of mass lost, here it can be observed that superficial water completely evaporates before 200 °C, and between 200-600 °C, the degradation and combustion of the bone matrix occurs **(D)** Mineral to matrix ratio graph, showing a smaller ratio in the diabetic group * $p < 0.05$

4.5.6 Mean mineral crystal size

The representative XRD pattern of trabecular bone is shown in **(Figure 4.5A)**. The mean crystal length was not different between the groups **(Figure 4.5B)**, whereas diabetic bone had a significantly larger crystal width than the non-diabetic bones (8.12 ± 2.07 nm vs. 6.57 ± 1.33 nm, $p = 0.024$) as shown in **(Figure 4.5C)**.

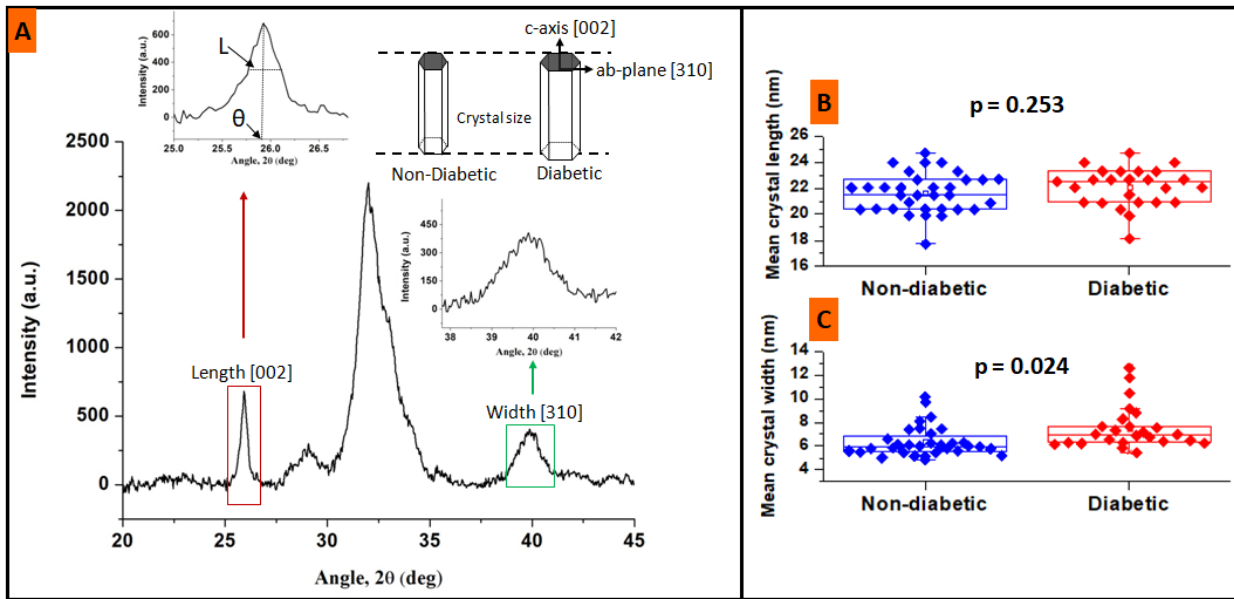


Figure 4.5 (A) Representative XRD pattern ($20^\circ < 2\theta < 45^\circ$) of human femoral trabecular bone. The peak at 26° and 40° is used to determine the average crystal length and width in the c-axis direction and ab-plane respectively, according to Scherrer equation $B(2\theta) = \lambda/L\cos\theta$. Where B is the mean crystal size, λ is the x-ray wavelength (1.5406 \AA), L is the peak width at half maximum and θ is the Bragg angle where the peak is located, **(B-C)** Mean crystal size graph, showing the insignificant difference in average crystal length but wider width of mean crystal in the diabetic group

4.5.7 Mineral and collagen properties

The representative FTIR spectra of bone with the appropriate label of various bands and schematic presentation of enzymatic and non-enzymatic collagen cross-links are shown in **Figure 4.6 (A-C)**. The mineral-based parameters, including mineral crystallinity ($p=0.073$), carbonate/phosphate ratio ($p=0.58$), and acid phosphate content ($p=0.84$), were not significantly different between the groups (**Figure 4.6 D-F**).

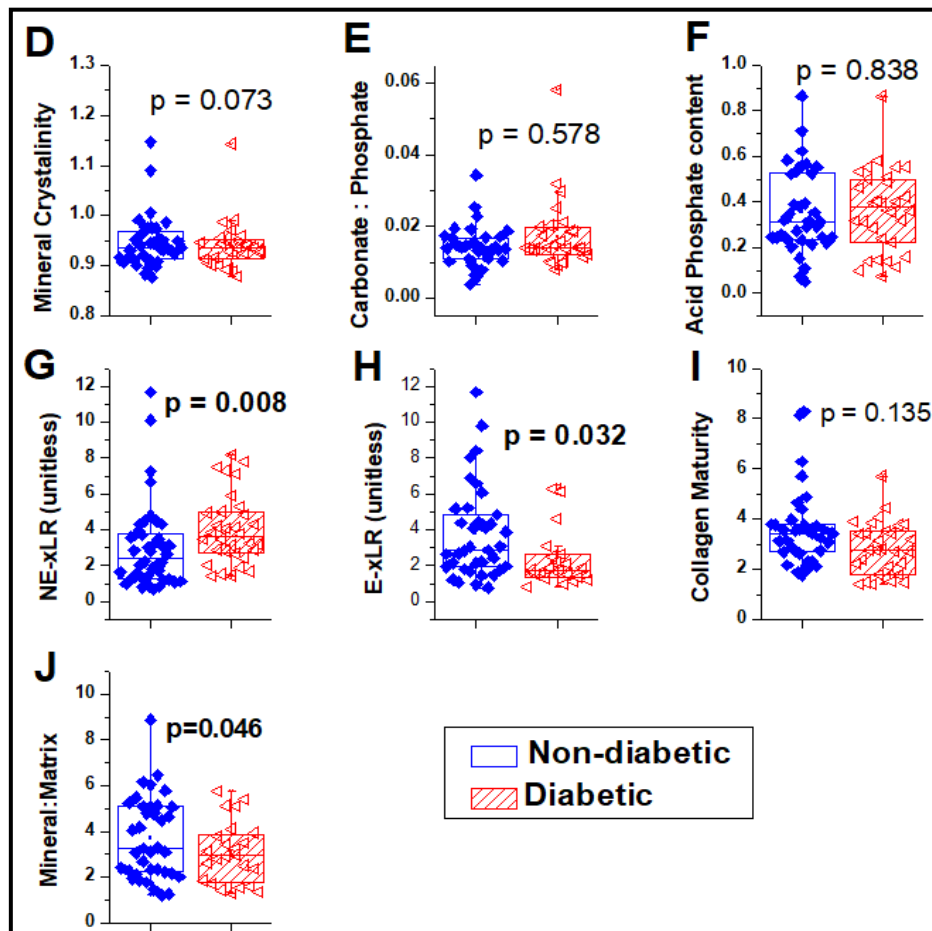
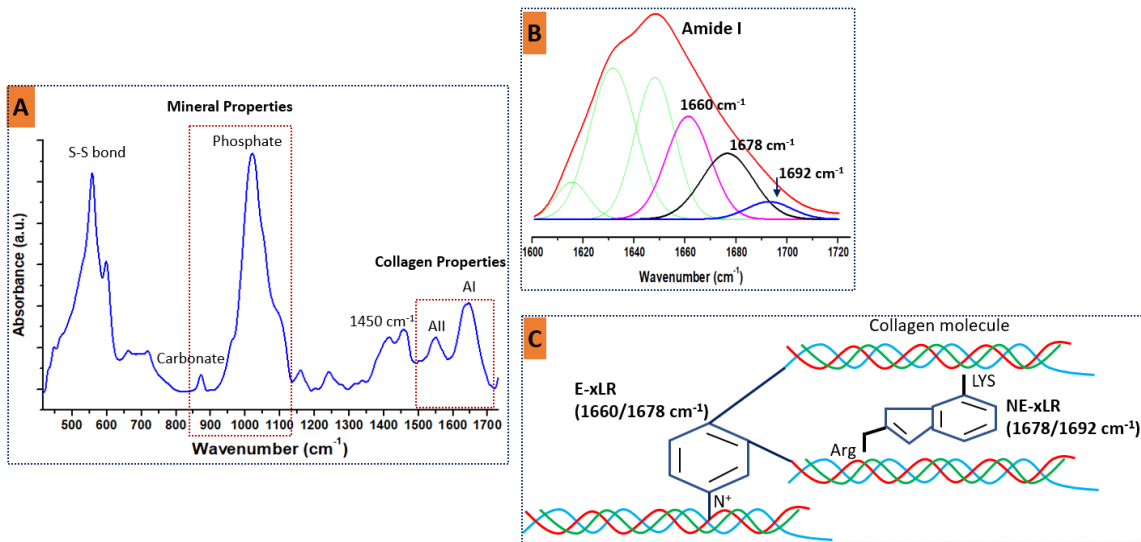


Figure 4.6 (A) Representative FTIR spectra with the appropriate label of various bands to analyze the diabetic and non-diabetic femoral trabecular bone, (B) represents peak fitting of Amide I band, collagen properties were obtained by peak fitting of Amide I band with subbands (Gaussian curves) at 1610, 1630, 1645, 1660, 1678 and 1692 cm^{-1} , (C) represents

schematically the enzymatic (E-xL) and non-enzymatic crosslink (NE-xL) formation in bone collagen, **(D-F)** measures of mineral properties, showing all mineral parameters could not reach to the level of significance, **(G)** represents non-enzymatic cross-link ratio [NE-xLR, (the area ratio of the 1678/1692 cm^{-1} subbands within the Amide I peak, total cross-linking AGEs)], **(H)** represents enzymatic cross-link ratio [E-xLR, the area ratio of the 1660/1678 cm^{-1} subbands within the Amide I peak], **(I)** represents collagen maturity (area ratio of the 1660/1692 cm^{-1} subbands within the Amide I peak), **(J)** showing lower mineral:matrix ratio in the diabetic group

The collagen cross-links [NE-xLR (area ratio of the 1678/1692 cm^{-1} sub-bands), E-xLR (area ratio of the 1660/1678 cm^{-1} sub-bands)] and collagen maturity (area ratio of 1660/1690 cm^{-1}) are shown in **(Figure 4.6 G-I)**. The diabetic bone had significantly higher NE-xLR [by 46.6%, **p=0.008**] and lower E-xLR [by 35%, **p=0.032**] compared to the non-diabetic bone, whereas no significant difference was observed in collagen maturity. Further, the diabetic bone had lower mineral/matrix ratio [by 21.1%, (**p=0.046**)] as shown in **(Figure 4.6J)**.

Table 4.2 shows the shift in the position of Amide I (**p = 0.02**) and Amide II (**p = 0.009**) bands. The diabetic group had a lower value of area under the normalized peaks of Amide I and Amide II bands by 47.36% (**p< 0.001**) and 52.4% (**p<0.001**), respectively, compared to the non-diabetic group. These results indicate that the secondary structure of Amide I and Amide II proteins is altered, and the quantity of these proteins is lower in the diabetic bone.

Table 4.2 Findings on structural and compositional determinants of the bone quality

Characterization techniques	Parameters studied	Study groups		
		Non-Diabetic	Diabetic	p-value
Structural Parameter (μ -CT)	Bone volume fraction (BV/TV) (%)	21.6 \pm 5.50	18.53 \pm 5.37	0.031*
	Trabecular thickness (Tb.Th, mm)	0.167 \pm 0.029	0.149 \pm 0.026	0.019 *
	Trabecular separation (Tb.Sp, mm)	0.603 \pm 0.149	0.677 \pm 0.166	0.095
	Trabecular number (Tb.N, 1/mm)	1.25 \pm 0.176	1.15 \pm 0.136	0.033 *
	Structure model index (SMI)	1.92 \pm 0.12	2.39 \pm 0.19	0.037*
	Degree of anisotropy (DA)	0.612 \pm 0.102	0.579 \pm 0.198	0.475
Composition (TGA)	Water (weight %)	14.8 \pm 9.4	11.6 \pm 6.2	0.335

		Organic (weight %)	43.4 ± 9.5	50.8 ± 10.1	0.087
		Mineral (dry weight %)	49.3 ± 7.5	40.9 ± 10.7	0.038*
		Carbonate (weight %)	1.67 ± 0.3	1.67 ± 0.4	0.988
Macro molecular vibrations (FTIR)	Protein structure	Amide I position (cm ⁻¹)	1643.8 ± 6.3	1647.3 ± 4.4	0.02*
		Amide II position (cm ⁻¹)	1543.1 ± 6.1	1547.8 ± 7.02	0.009
	Protein content	Amide I band area/1450 band area	6.97 ± 3.87	3.67 ± 2.08	<0.001
		Amide II band area/1450 band area	2.56 ± 1.47	1.22 ± 0.91	<0.001
* p<0.05, ** p<0.01 and ***p<0.001 respectively compared to the non-diabetic group, data is expressed as mean ± SD					

4.5.8 Florescent advanced glycation end-products (fAGEs)

The diabetic bone had a 32.1% higher fAGEs concentration than the non-diabetic bone (443 ± 198 vs. 335 ± 155 ng quinine/mg collagen, **p=0.015**) as reported in **Figure 4.7A**.

4.5.9 Interrelationships between variables

Pre-operative HbA1c was positively correlated with fAGEs ($r=0.635$, $p<0.001$) and NE-xLR ($r=0.561$, $p=0.006$). Correlations between HbA1c and mechanical properties revealed that within the diabetic group, HbA1c is significantly and negatively correlated with post-yield energy ($r=-0.402$, $p=0.047$), whereas this relationship was not significant in the non-diabetic group. Other than the reported parameters, none of the parameters were correlated with HbA1c. Furthermore, fAGEs were negatively correlated with mineral/matrix ratio ($r=-0.487$, $p=0.016$), BV/TV ($r=-0.488$, $p=0.021$), Tb.Th ($r=-0.454$, $p=0.044$), and positively correlated with NE-xLR ($r=0.367$, $p=0.045$). fAGEs were also negatively correlated with mechanical properties, including post-yield energy ($r=-0.489$, **p=0.013**) and toughness ($r=-0.441$, **p=0.027**) in the diabetic group, as shown in **Figure 4.7 (B-C)**. Additionally, the NE-xLR was negatively correlated with the post-yield strain ($r=-0.433$, **p=0.031**) in the diabetic but not in the non-diabetic group, as shown in **Figure 4.7D**. The detailed correlation analysis of selected significant variables is reported in **Table 4.3** and **Table 4.4** for diabetic and non-diabetic groups, respectively.

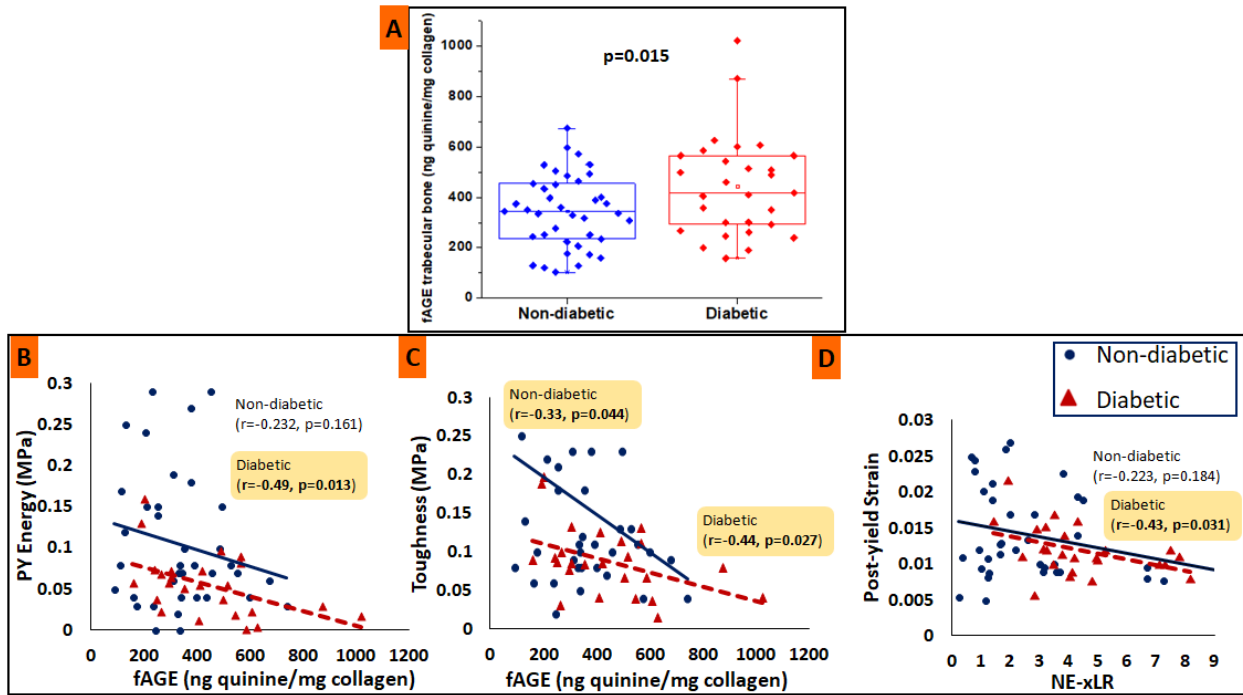


Figure 4.7 (A) The graph is showing that the fAGEs content is higher in the diabetic group. (B-C): Mechanical properties versus a measure of glycation (fAGE and NE-xLR). Graphical data for several mechanical parameters versus total fluorescent AGEs (B-C) and NE-xLR (D) are shown.

ANCOVA analysis comparing the effect of change in BV/TV on the change in mechanical properties between groups demonstrated that both regression slopes and intercept for modulus, yield stress, and ultimate stress were similar between groups, as shown in **Figure 4.8 A-C**, respectively. The regression slopes of post-yield energy ($p=0.792$) and toughness ($p=0.977$) were also similar between groups, whereas the intercept was significantly lower in the diabetic group for these properties ($p=0.028$) and ($p=0.032$) (**Figure 4.8 D-E**). These results reveal that the magnitude of change in BV/TV does not account for the differences in post-yield properties observed between the two groups.

Forward stepwise regression tests to predict mechanical properties as a dependent variable using all significant parameters as independent variables showed that in the diabetic group, the BV/TV, fAGEs, and mineral-to-matrix ratio (FTIR) could explain up to 86.7% ($p < 0.001$) of variance in ultimate strength, whereas in the non-diabetic group, only BV/TV was observed to be a significant predictor explaining up to 39.8% of the variance in ultimate strength. Mineral-to-matrix ratio (FTIR) and Tb.Th were found to predict yield strain up to 77.4% ($p < 0.001$) in the diabetic group.

The power of the study was performed by comparing the mean value of post-yield energy and toughness between diabetic and non-diabetic groups, and this outcome was found to be 88% and 82%, respectively.

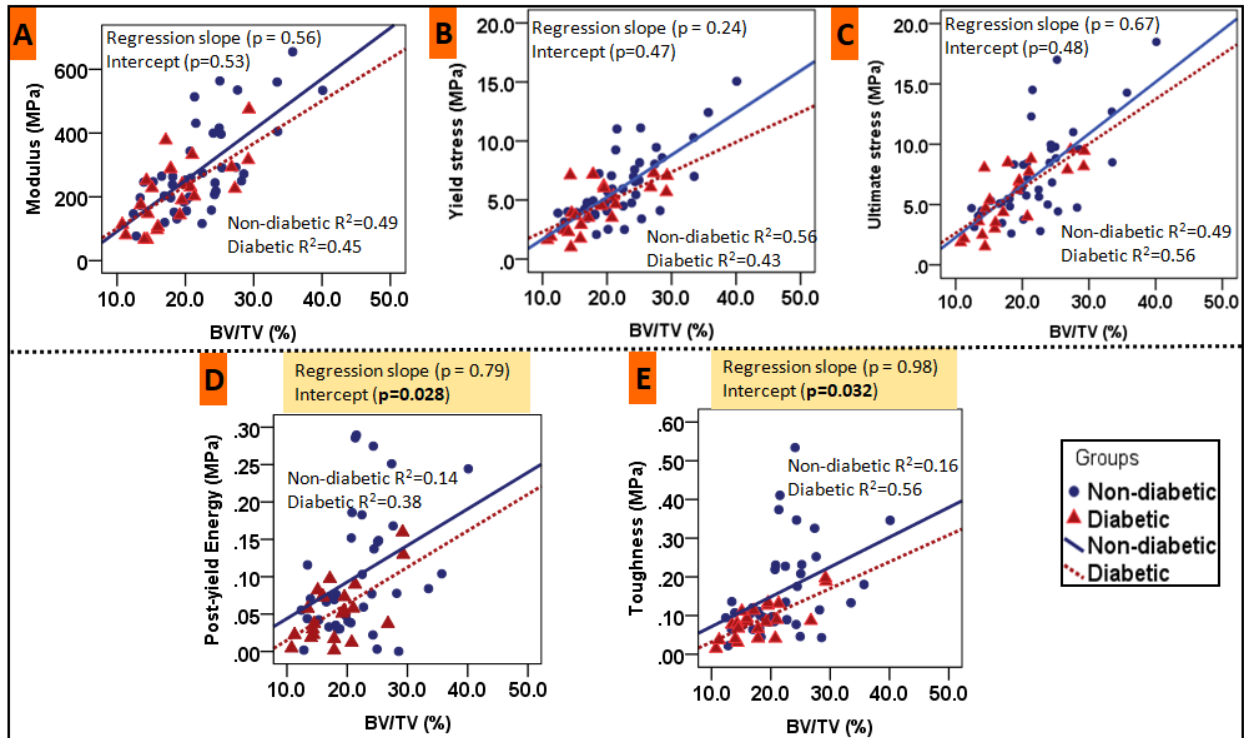


Figure 4.8 The relationships between bone volume fraction and **A)** modulus, **B)** yield stress, **C)** ultimate stress, **D)** post-yield energy, and **E)** toughness between diabetic and non-diabetics are shown. Data are presented along with best-fit lines (solid lines).

4.6 Discussion

This is the first investigation linking biomechanical, microstructural, material, and compositional properties of human bone in individuals with diabetes and known fragility fractures. Our findings provide evidence of the detrimental effects of hyperglycemia on trabecular bone quality at multiple scales leading to lower energy absorption and toughness and result in increased bone fragility in patients with T2D.

The overall loss in bone quality and strength may be governed by a cascade of events happening at different length scales, such as abnormalities in the mineral and collagen quality at the nanoscale, accumulation of unrepaired microdamage or microcracks at the microscale, and changes in the trabecular architecture and a decrease in the trabecular connectivity at the

mesoscale. Furthermore, any alteration in the properties locally, either at micro- or nano-level, affects the properties of the hierarchical organization of bone at higher scales [24], [25]. Thus, our findings of differences at nanoscale and microscale can be linked to each other and to higher scales to get a comprehensive diagnosis of altered bone quality and fracture risk in diabetes. To this end, forward stepwise regression analysis of multiscale data, presented here, shows that the BV/TV, fAGE, and mineral-to-matrix ratio (FTIR) can explain up to 86.7% of the variance in ultimate strength. Also, the mineral-to-matrix ratio (FTIR) and Tb.Th together can explain up to 77.4% of the variance in yield strain. Thus, in addition to bone microstructure (BV/TV, Tb.Th), nanoscale characteristics of bone (mineral to matrix ratio) and collagen quality (fAGEs) are important predictors of the loss in mechanical properties and the associated increase in fracture risk of diabetic bone.

Particularly, the assessment of bone microstructure with μ -CT showed lower BV/TV (%) in diabetics when compared to the non-diabetics. Moreover, the structure was noticeably altered, evidenced by the thinning of trabeculae and, in general, by fewer trabeculae. Indeed, due to this compromised bone microstructure, a lower value of ultimate stress (uniaxial compression) is observed in those with diabetes. The results of uniaxial compression tests found in our study are consistent with previously published studies [196], [210]–[213]. Our results of microstructural parameters are slightly different from those reported in earlier studies [51]–[53]. However, in these studies, bone tissue was obtained from individuals with obesity and/or severe arthritis, which could explain their findings of the same or increased BV/TV in those compared with diabetes. It is also possible that our study finding of lower BV/TV in diabetes is related to the distinct phenotypes of Asians [130], [188]–[192].

At the apparent-level (uniaxial-compression) and tissue level (nanoindentation), the lower value of modulus (deformation resistance), observed with the diabetic bone, are directly associated with decreased mineral to matrix ratio (FTIR). The wider crystal size without a change in length decreases the aspect ratio (surface area/volume) of apatite crystals and explains the reduced elastic modulus of bone material [157]. Furthermore, altered crystal shape also can affect crystal connectivity, orientation, and arrangement [157].

We also observed the increase in protein misfolding (altered secondary structure of proteins) and a decrease in relative protein content (Amide I and Amide II) in the diabetic bone. The altered secondary structure is primarily responsible for the change in the structural integrity of the collagen in bone [214]. This altered collagen structure can change the hydration level of collagen and/or change in shape, size, orientation, and growth of inorganic mineral content

[31] as noted above.

One of the reasons for the degradation of bone quality in diabetes could be prolonged hyperglycemia (HbA1c) which may increase the accumulation of AGEs in the bone matrix. In correlation analysis, we found the HbA1c is positively correlated with fAGEs content and NE-xLR. We also observed the reduced enzymatic collagen cross-link ratio (E-xLR) and increased non-enzymatic collagen cross-link ratio (NE-xLR) in the diabetic group as compared to the non-diabetic group. The enzymatic cross-links (E-xL, beneficial cross-links) are responsible for mechanical strength, whereas NE-xL is associated with bone fragility [27], [186], [187]. Our findings of reduced E-xLR and increased NE-xLR are evidence of AGE accumulation (NE-xL) in the bone, which induces tissue damage through structural modification of proteins and abnormal collagen fibril organization in the diabetic bone. The reduction of E-xLR can be associated with hyperglycemia and oxidative stress (OS) [198], [215]. Further, the NE-xL (AGE accumulation) in diabetic bone favors material rigidity by restricting the uncoiling of the triple helical structure of collagen (flexibility) and confining the natural energy dissipation process during loading to a limited region [29]. Such changes will alter the nature of microdamage formation in bone from diffuse cracking, characteristic of ductile materials, to linear microcracks, making bone more susceptible to fracture [44], [187], [216]. Indeed, in the present study, elevated levels of HbA1c, fAGEs, and NE-xLR correlated negatively with bone biomechanical properties – post-yield energy, toughness, and post-yield strain in diabetes. Also, the lower value of intercept of post-yield energy and toughness in the diabetic group (ANCOVA) revealed that the glycated bone exhibited lesser energy dissipation and reduced toughness. Our results are consistent with previously published studies that reported the accumulation of AGEs as a cause for abnormal collagen synthesis and altered collagen structure [182] in the bone. Thus, changes in collagen, mineral, altered bone composition at the nanoscale, and lower bone volume fraction and trabecular architecture at the microscale in the diabetic group provide detailed insight on skeletal fragility in diabetes and improve the current understanding of the impact of diabetes on bone homeostasis.

In the present study, FN BMD T-scores were similar among those with T2D and without diabetes. The deficits in bone quality in T2D mentioned above underlie the compromised bone strength in diabetes. These findings explain the inability of the BMD T-score, a quantitative measure, to accurately predict fracture risk in T2D as previously reported in large studies [11], [85]. In the Study of Osteoporotic Fractures [11], for a given age and T-score, the risk of hip or non-spine fracture was higher in women with T2D than those without

diabetes after 25 years of follow-up. While T-score is useful in fracture risk assessment in women with and without diabetes, however, T-score underestimates fracture risk in T2D [11], [118].

Various techniques (pQCT, HRpQCT, Osteoprobe) have been used in research to investigate the bone quality and bone strength. However, each technique presents its own challenges for utilization in routine clinical practice. In MrOS [85], pQCT was used to assess bone strength at peripheral sites in T2D, and lower bone bending strength was observed at midshaft regions of radius and tibia in those with T2D, despite no differences in cortical vBMD. Though pQCT is a clinically available tool, the imaging resolution remains a limitation. Consequently, various approaches have been proposed to include changes in bone quality and explain poor bone mechanical properties, such as those reported here. For example, bone strength estimated by micro-finite element analysis (micro-FEA/HR-pQCT) at the distal radius has been shown to be lower in T2D compared to controls [16]. Similarly, micro-indentation of the tibial cortex has been performed to demonstrate that the estimated bone material strength index (BMSi) is decreased in T2D compared to controls [48]–[50]. While these techniques have increased our understanding of bone fragility in diabetes, further work is needed to assess their application for routine clinical use. The only tool currently approved for clinical assessment of bone quality is the trabecular bone score (TBS) [12], [119], which helps to predict fracture risk, independent of BMD. However, TBS is a surrogate measurement of trabecular architecture and not a tool for the assessment of bone strength. Hence, diagnostic tools are needed for specific and direct assessment of bone quality to aid clinical assessment of fracture risk in diabetes. Meanwhile, the International Osteoporosis Foundation (IOF) recommends adjusting BMD T-score for diabetes to avoid underestimation of risk in clinical practice [118].

This study has some limitations. First, this study is limited to *ex vivo* assessments of bone quality in patients who underwent hip fragility fractures. Non-fracture controls with and without diabetes were not studied; however, it is not feasible to obtain a femoral head specimen from healthy controls. Second, the study focuses exclusively on trabecular bone and does not include properties of cortical bone. Other studies have reported the increased cortical porosity [15], [16], [90] and altered cortical bone material properties *in vivo* by demonstrating decreased BMSi (measured through Osteoprobe) in those with diabetes compared to controls [48]–[50]. Also, the study lacks information on the effect of type of diabetes treatment (insulin, metformin, and other anti-diabetic treatment) on bone properties. Sample sizes within each subgroup are small, and a large randomized clinical trial would be

necessary to draw any meaningful conclusion regarding the effect of diabetes treatment on bone properties. Further, we could not assess bone remodeling via dynamic bone labeling. Lastly, we used femoral head specimens instead of the femoral neck (typical fracture site) because, in most cases of fracture, femoral necks are extensively and variably damaged either due to fracture or during surgery. Thus, it was difficult to obtain uniform specimens from all patients. Hence to avoid site-specific differences, we took samples from the femoral head.

Despite the above-mentioned limitations, our study's major strength is that the explants characterized here are from the patients with diabetes with known fragility fractures. Further, this study includes a wide range of duration and severity of the disease, and this is an important and unique aspect of our study because a longer duration of diabetes is typically required for skeletal changes in diabetes to fully manifest. The severity and duration of diabetes are known to greatly affect fracture risk [15], [217], and therefore it may also affect the degree of compositional changes. This aspect could also explain the differences between fAGEs results in our study and those reported in other studies [51], [53], where a significant difference in fAGEs was not observed between groups. One study [51] included samples for a shorter duration of disease of nearly two years, whereas, in another study [53], the information of the duration of diabetes was not reported. The results of our fAGEs content are consistent with one recent study [52] that found a 1.5-fold increase in fAGEs content in women with T2D of the mean duration of nearly 15 years compared with non-diabetic women.

In conclusion, the study findings provide evidence that diabetes affects the trabecular bone quality at multiple organization levels. The accumulation of AGEs is one of the processes that favor deterioration of bone quality in diabetes leading to material, structural, compositional, and biomechanical dysfunctionality. Overall, together with altered structure and material properties, these novel findings of changes in the composition of bone explain the compromised mechanical performance and diminished bone strength in diabetes. Finally, this study demonstrates that whilst osteoporotic bones are fracture prone, diabetes is detrimental to bone quality, thus highlighting the need for more specific measures to understand and diagnose the bone quality and bone fragility in T2D.

Table 4.3 Correlation analysis of selected significant variables of the diabetic group which has at least one or more significant relationship with at least one other variable

Diabetic group	Modulus	Yield strength	Ultimate strength	Yield strain	Ultimate strain	Yield energy	PY-energy	PY-strain	Toughness	BVTV	HbA1c	fAGE	NE-xLR	E-xLR	M:M FTIR	Tb.Th
Modulus	1	.710**	.729**	-0.134	0.019	.548*	.485*	0.125	.620**	.674**	0.048	-0.122	0.187	0.376	0.158	0.41
Yield strength	.710**	1	.950**	0.306	0.247	.924**	0.197	0.023	.499*	.655**	0.314	0.141	0.306	0.098	0.333	.633**
Ultimate strength	.729**	.950**	1	0.239	0.299	.842**	0.368	0.14	.623**	.749**	0.253	-0.292	0.294	0.133	0.37	.670**
Yield strain	-0.134	0.306	0.239	1	.558**	.631**	-0.196	-0.172	0.085	0.117	0.111	0.031	0.017	-0.069	0.331	0.092
Ultimate strain	0.019	0.247	0.299	.558**	1	0.395	0.144	.722**	0.282	0.084	-0.119	0.025	-0.378	-0.082	0.233	0.155
Yield energy	.548*	.924**	.842**	.631**	0.395	1	0.154	-0.057	.533*	.560**	0.181	-0.032	0.207	0.032	0.459	.493*
PY-energy	.485*	0.197	0.368	-0.196	0.144	0.154	1	0.306	.919**	.617**	-.402*	-.489*	0.042	0.156	0.273	.484*
PY-strain	0.125	0.023	0.14	-0.172	.722**	-0.057	0.306	1	0.255	0.003	-0.238	0.028	-.433*	-0.031	-0.033	0.108
Toughness	.620**	.499*	.623**	0.085	0.282	.533*	.919**	0.255	1	.747**	-0.331	-.441*	0.094	0.157	0.38	.613**
BVTV	.674**	.655**	.749**	0.117	0.084	.560**	.617**	0.003	.747**	1	-0.159	-.488*	0.051	.526*	0.341	.804**
HbA1c	0.048	0.314	0.253	0.111	-0.119	0.181	-.402*	-0.238	-0.331	-0.159	1	.635**	.561**	-0.307	0.007	-0.269
fAGE	-0.122	0.141	-0.292	0.031	0.025	-0.032	-.489*	0.028	-.441*	-.488*	.635**	1	.367*	-0.354	-.487*	-.454*
NE-xLR	0.187	0.306	0.294	0.017	-0.378	0.207	0.042	-.433*	0.094	0.051	.561**	.367*	1	-0.37	0.112	-0.001
E-xLR	0.376	0.098	0.133	-0.069	-0.082	0.032	0.156	-0.031	0.157	.526*	-0.307	-0.354	-0.37	1	-0.105	0.145
M:M FTIR	0.158	0.333	0.37	0.331	0.233	0.459	0.273	-0.033	0.38	0.341	0.007	-.487*	0.112	-0.105	1	0.361
Tb.Th	0.41	.633**	.670**	0.092	0.155	.493*	.484*	0.108	.613**	.804**	-0.269	-.454*	-0.001	0.145	0.361	1

** Correlation is significant at the 0.01 level (2-tailed)
* Correlation is significant at the 0.05 level (2-tailed)
PY: post-yield

Table 4.4 Correlation analysis of selected significant variables of the non-diabetic group, which has at least one or more significant relationship with at least one other variable

Non-diabetic group	Modulus	Yield strength	Ultimate strength	Yield strain	Ultimate strain	Yield energy	PY-energy	PY-strain	Toughness	BVTV	HbA1c	fAGE	NE-xLR	E-xLR	M:M FTIR	Tb.Th
Modulus	1	.791**	.767**	0.122	0.164	0.292	.545**	-0.058	.477**	.701**	-.332*	-0.184	-0.028	0.253	0.261	.341*
Yield strength	.791**	1	.974**	0.029	0.077	0.258	.603**	-0.015	.569**	.746**	-0.274	-0.162	-0.033	0.076	0.197	.441**
Ultimate strength	.767**	.974**	1	0.022	0.069	0.247	.601**	-0.017	.576**	.698**	-0.291	-0.143	-0.035	0.069	0.224	.431**
Yield strain	0.122	0.029	0.022	1	.973**	.972**	.545**	-0.03	-0.02	0.029	0.039	-0.231	-0.094	.405*	-0.035	-0.054
Ultimate strain	0.164	0.077	0.069	.973**	1	.958**	.607**	0.087	0.079	0.078	-0.044	-0.283	-0.143	.419*	-0.037	-0.039
Yield energy	0.292	0.258	0.247	.972**	.958**	1	.675**	-0.042	0.124	0.192	-0.05	-0.272	-0.072	.389*	0.008	0.067
PY-energy	.545**	.603**	.601**	.545**	.607**	.675**	1	0.055	.815**	.405*	-0.243	-.328*	-0.02	0.158	0.085	0.186
PY-strain	-0.058	-0.015	-0.017	-0.03	0.087	-0.042	0.055	1	0.113	-0.121	0.105	-0.137	-0.223	0.097	-0.008	-0.1
Toughness	.477**	.569**	.576**	-0.02	0.079	0.124	.815**	0.113	1	.370*	-0.283	-0.232	0.029	-0.147	0.102	0.211
BVTV	.701**	.746**	.698**	0.029	0.078	0.192	.405*	-0.121	.370*	1	-0.266	0.009	-0.108	0.103	0.09	.566**
HbA1c	-.332*	-0.274	-0.291	0.039	-0.044	-0.05	-0.243	0.105	-0.283	-0.266	1	.296*	.396**	-.353*	-0.057	-0.125
fAGE	-0.184	-0.162	-0.143	-0.231	-0.283	-0.272	-.328*	-0.137	-0.232	0.009	.296*	1	0.019	-0.111	-0.205	.315*
NE-xLR	-0.028	-0.033	-0.035	-0.094	-0.143	-0.072	-0.02	-0.223	0.029	-0.108	.396**	0.019	1	-.430**	-0.107	-0.014
E-xLR	0.253	0.076	0.069	.405*	.419*	.389*	0.158	0.097	-0.147	0.103	-.353*	-0.111	-.430**	1	0.128	0.219
M:M FTIR	0.261	0.197	0.224	-0.035	-0.037	0.008	0.085	-0.008	0.102	0.09	-0.057	-0.205	-0.107	0.128	1	-0.185
Tb.Th	.341*	.441**	.431**	-0.054	-0.039	0.067	0.186	-0.1	0.211	.566**	-0.125	.315*	-0.014	0.219	-0.185	1

** Correlation is significant at the 0.01 level (2-tailed)
* Correlation is significant at the 0.05 level (2-tailed),
PY: post-yield

CHAPTER 5

INVESTIGATION OF DIABETIC PATIENT'S FINGERNAIL QUALITY TO MONITOR TYPE 2 DIABETES INDUCED TISSUE DAMAGE

Long-term Type 2 Diabetes (T2D) affects the normal functioning of the heart, kidneys, nerves, arteries, bones, and joints. The T2D gradually alters the intrinsic material properties and structural integrity of the tissues, and prolonged hyperglycemia causes chronic damages to these tissues' quality. Clinically no such technique is available which can assess the altered tissue quality associated with T2D. In the present study, the microstructural characterization (surface morphology, surface roughness, density, and calcium content), material characterization (modulus, hardness), and macromolecular characterization (disulfide bond content, protein content, and its secondary structure) are investigated among healthy, diabetic controlled (DC) and uncontrolled diabetic (UC) group of fingernail plate. It is found that T2D has an adverse effect on human fingernail plate quality. The parameters of nail plate quality are changing in a pattern among all three groups. The properties mentioned above are degrading in the DC group, but the degradation is even worst in the case of severity of T2D (UC group) as compared to the healthy group (Healthy<DC<UC). This study suggests that the fingernail plate quality has the potential to become a new avenue to assess the secondary diabetic complications, i.e., to assess the bone quality.

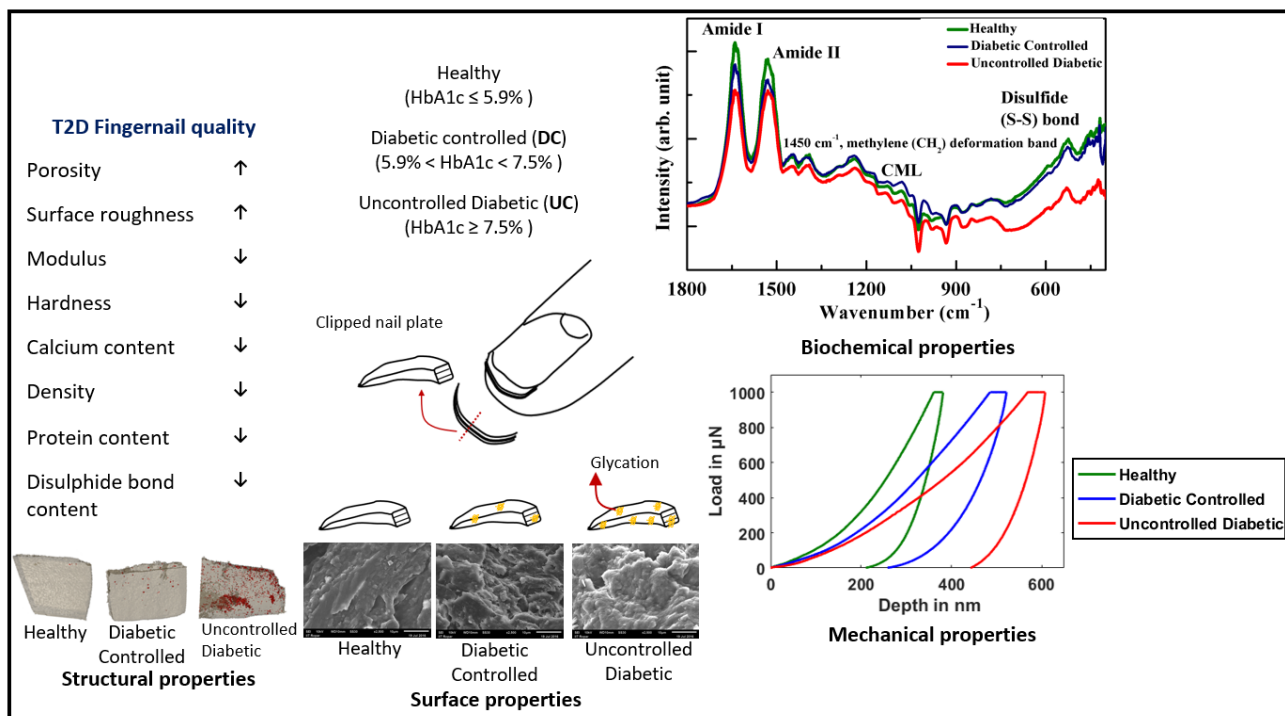


Figure 5.1 Graphical abstract showing increased degradation in fingernail quality with the severity of type 2 diabetes

5.1 Introduction

The T2D is diagnosed based on the elevated blood glucose and the HbA1c (Hemoglobin A1c, glycated hemoglobin) level [1]. The HbA1c is a reliable representation of long-standing uncontrolled blood glucose (hyperglycemia) [1]. The long-standing hyperglycemia is prone to increase the non-enzymatic reactions (Maillard reactions) and form advanced glycation end-products (AGEs) [218]–[221]. Among a diverse group of compounds, one of the best-studied AGE is carboxymethyl-lysine (CML) [23], [41].

Clinically there is a lack of suitable techniques which can assess or monitor the general tissue damage associated with T2D. One of the early diagnoses of tissue damage can be the monitoring of adverse changes in tissue quality. For testing the tissue quality *ex vivo*, the surgeon needs to do a biopsy, which is painful, invasive, and involves the risk of infection or slow healing. Therefore, the keratinized epithelial tissue such as the fingernail plate is a useful site to monitor the general tissue damage because the major constituent of the fingernail plate (Keratins, present in $\pm 85\%$) is also prone to glycation [219], [222], [223]. Interestingly, the growth of the nail plate is slow; hence it is a particularly important material to evaluate the long-term effects of hyperglycemia on the tissue quality [224]. Additionally, this monitoring technique is painless, non-invasive, and it is also economical because it does

not consume expensive reagents. After considering the advantages of studying the fingernail plate quality, we have explored the available literature on fingernail plate, and it is best inferred that comprehensive research is still lacking on the effect of T2D on fingernail plate quality.

The major parameters that contribute to nail plate quality (**Figure 5.2**) are the nail surface morphology and roughness, tissue density, mineral content, material properties, disulfide bond content, and protein composition and structure [225]. In this study, we have investigated the above nail plate quality parameters for healthy, diabetic controlled (DC), and uncontrolled diabetic (UC) groups of fingernail plate.

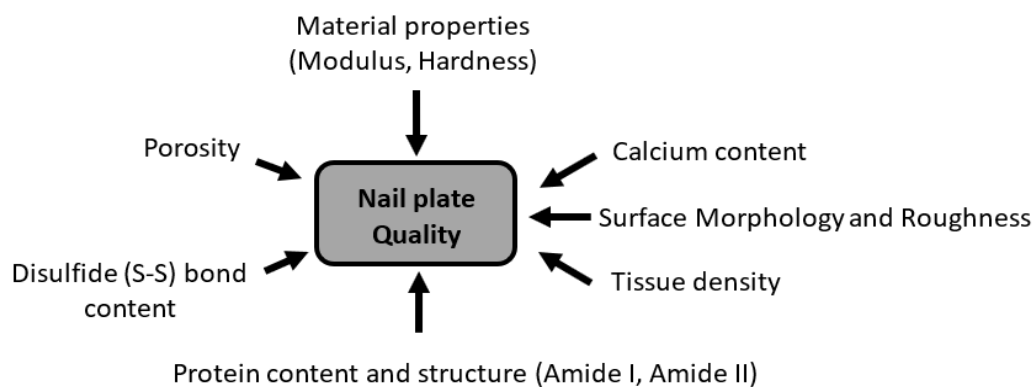


Figure 5.2 Determinants of nail quality

5.2 Material and methods

Sample collection

The clipped fingernail plate samples **Figure 5.3(A)** were collected from forty-five (N=45) patients suffering from T2D for more than five years (based on patient’s clinical records) and randomly selected thirty (N=30), healthy volunteers. The patients suffering from comorbidity diseases such as renal dysfunction, primary and secondary hyperparathyroidism, osteoporosis, unexplained elevated ALP (alkaline phosphatase), and fungal infection in the fingernail were excluded from this study. The age group of the study population was 40 years and above (≥ 40 years). Nail plate samples were collected from a distal part of the right-hand middle finger, 2-4 mm in width, using a nail clipper. Collected nail samples were sectioned into 5-6 small pieces so that they can be utilized for different characterization techniques. Later the samples were transferred into sample bags, labeled, and subsequently stored at -20° C. All experiments were conducted within one months’ time after the collection of nail samples. The clinical data of T2D patients were also recorded, along with the collection of

finger nail samples. All methods were carried out in accordance with relevant guidelines and regulations. The study was approved by the institutional ethics committee (Postgraduate Institute of Medical Education and Research, Chandigarh, India). Written informed consent was obtained from each study participant.

Sample grouping

The fingernail samples were classified into three groups based on the clinical conditions of T2D prescribed by American Diabetes Association (ADA) guidelines [1], [203]. The first group was referred to as uncontrolled diabetic (UC). It includes the T2D patients having HbA1c greater than or equal to 7.5% [226]. The second group was referred to as the diabetic controlled (DC) group, and it contains T2D patients having HbA1c levels less than 7.5% [226]. The third group was healthy volunteers, and their HbA1c level less than or equal to 5.9% [1]. The HbA1c was measured at a single time point at time of enrollment of patients. After grouping, it was found out that 25 samples belonged to the UC group and 20 to the DC group. The mean age and age range of the study population in healthy, DC, and UC groups were 58 (42-77), 55 (40-77), and 60 (42-70) years, respectively. The mean age among all the three groups is found statistically insignificant, as mentioned in **Table 5.1**. The mean length of T2D (7 years) is found comparable among all the patients. All participants involved in the study belonged to North India.

Table 5.1 Clinical details of fingernail specimens

Group no	Group name	Gender Distribution		Age (years)	Average HbA1c (%)
		Male	Female		
1	UC (uncontrolled diabetic)	10	15	60 (42-70)	8.4 (7.7-14) ***
2	DC (diabetic controlled)	8	12	55 (40-77)	6.6 (6.2-7.3) **
3	Healthy	12	18	58 (42-77)	5.4 (5.1-5.9)

** p <0.01 and *** p<0.001 compared to healthy group

5.3 Determinants of nail quality

5.3.1 Measurement of density

The density of all three groups of nail samples was measured with a density kit (MS DNY 54, Mettler Toledo, Greifensee, Switzerland), integrated with an electronic balance (MS105DU, Mettler Toledo, Greifensee, Switzerland).

5.3.2 Measurement of porosity

The structure of the nail plate from each group is studied using high-resolution μ -CT (Phoenix Nanotom S, GE Sensing and Inspection Technologies), equipped with a high power nano focus tube with a Molybdenum target. Projection images on a CCD camera are obtained with a resolution of 2 μm for porosity analysis and 10 μm to study density variation among all three nail groups. The images are stored as TIFF files. Indexed grey values are obtained in a 16-bit format which varies between 12000 to 27000 for nail samples. The ScanIP software is used to evaluate the porosity present in the nail samples. The porosity is calculated using the formula given in equation-1 below [227].

$$\text{Porosity} = (\text{volume of pores}/\text{total volume of nail plate sample}) \times 100\% \quad (1)$$

5.3.3 Surface morphology and calcium content

The surface morphology of the nail plate (dorsal phase and ventral phase) samples were studied through a scanning electron microscope (JEOL JSM-6610LV). To make the samples conducting, an ion sputter coating technique is used to coat a thin layer of platinum. Samples were observed with the secondary electron (SE) mode at a 10 kV accelerating voltage. The cross-sectional image (after tearing the nail plate sample perpendicular to its side of growth) of the nail plate is also captured through SEM and shown in **Figure 5.3(B)**.

The calcium content was studied with Energy Dispersive X-ray Spectroscopy (EDXS) using a Bruker XFlash 6I30 detector integrated with a scanning electron microscope (JEOL JSM-6610LV).

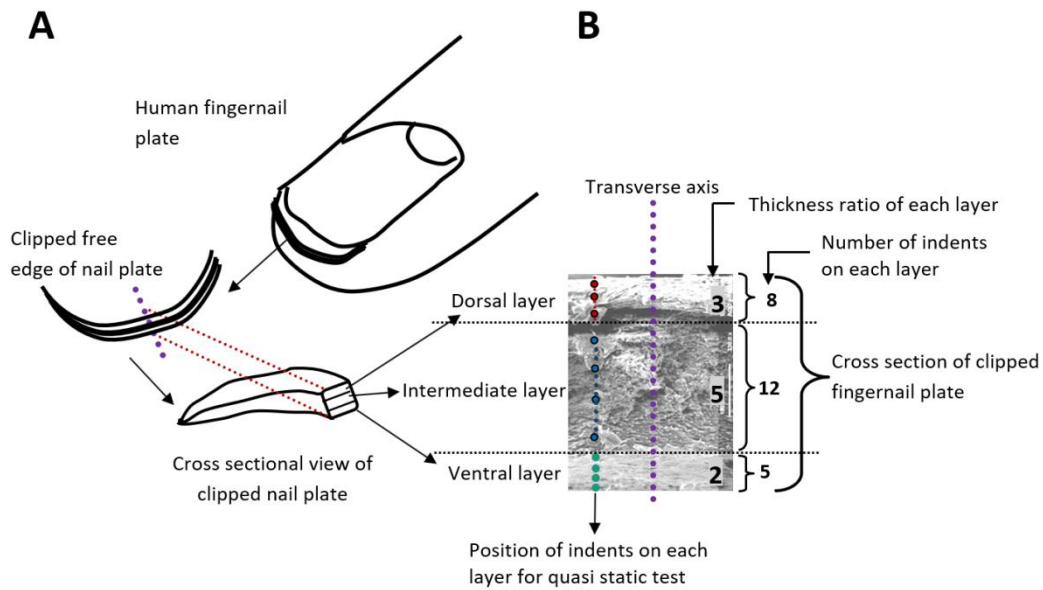


Figure 5.3(A) Schematic view of the free edge and clipped fingernail plate, **(B)** Pictorial representation of nanoindentation study describing indentation locations on the cross-section of fingernail plate

5.3.4 Surface roughness

Bruker multimode-8 Atomic Force Microscope (AFM) equipped with a silicon tip is used in contact mode to quantify the surface roughness for the clipped dorsal phase of the fingernail plate. The samples were fixed from the ventral side on a small disk with the help of low viscosity cyanoacrylate adhesive, and the area of $10\ \mu\text{m} \times 10\ \mu\text{m}$ was scanned for the dorsal phase of each group.

5.3.5 Material properties

The cross-sections of fingernail plates were embedded in epoxy, which takes 2 hours to get cured. After curing, the samples were ground (Buehler Eco Met 250 grinder and polisher) with abrasive papers under the water cooling condition and polished with diamond solutions of particle sizes of 1, 0.5, and $0.25\ \mu\text{m}$. At last, the samples were sonicated for 10 minutes, and then the nanoindentation experiment was carried out.

Nanoindentation tests were performed using a TI-950 Tribo Indenter (Hysitron Inc., Minneapolis, MN) with Berkovich pyramidal tip, having an included angle of 142.3° and tip radius of $\sim 150\ \text{nm}$. Locations for indents were identified using an optical microscope integrated with the nanoindentation system, and the tests were performed at room temperature.

A peak load of 1000 μN was applied on the cross-section of the fingernail plates. A load function consisting of a ten-second loading to peak force segment, followed by a thirty-second hold and a ten-second unloading segment, was used [205]. Twenty-five indents were performed parallel to the transverse axis on nail plate samples. The nail plate is composed of three histological layers; the dorsal is the upper layer, the intermediate is the middle layer, and the lower one is the ventral layer [228]–[232]. Depending on the layer-wise (dorsal: intermediate: ventral) thickness ratio (3: 5: 2) of the fingernail plate [233], [234], we have got eight indents on the dorsal layer, twelve indents on the intermediate layer, and five indents on the ventral layer as shown in **Figure 5.3(B)**. The load-displacement curves obtained in these indentation tests were analyzed to determine the reduced modulus (E_r) and hardness (H) by using the method of Oliver and Pharr (OP) [146], [147].

5.3.6 CML, protein and disulfide bond content

The position of Amide I (protein C=O stretching, $1600\text{--}1700\text{ cm}^{-1}$), Amide II (protein N–H bending, C–N stretching, $1500\text{--}1600\text{ cm}^{-1}$), and disulfide bond (stretching vibrations of S–S bonds, $500\text{--}550\text{ cm}^{-1}$) in the principal keratin structural unit of the nail plate is shown in **Figure 5.4 (A)**. The FTIR spectra were recorded to study the macromolecular vibrations of the above-mentioned parameters with the help of Bruker IFS 66v/S FTIR spectrophotometer in Attenuated Total Reflectance (ATR) mode under the constant pressure in the spectral region of $4000\text{ to }400\text{ cm}^{-1}$. After recording the spectra, the peak position (local maximum method), peak intensity, and area under the curve were calculated with OriginPro 8 (OriginLab, Northampton, MA) software. The mean values for the peak positions, band area of Amide I and Amide II [206], [207], and intensity of disulfide bond were calculated for each group. The intensity of the disulfide bond was measured with respect to the methylene (CH_2) deformation band at 1450 cm^{-1} [209].

The mean integrated area ratio (relative content) of 1150 cm^{-1} (carboxymethyl-lysine, CML)/ 1450 cm^{-1} was also calculated. Relative CML content has previously been validated with Raman spectroscopy [23], [41], where CML is a lysine derivative and lysine reference has a significant Raman band at $\sim 1150\text{ cm}^{-1}$ highlighted in these studies [23], [235]. Here we have validated the presence of CML peak by both Raman and FTIR spectroscopies. For reference, both Raman and FTIR spectra of a CML standard (Cayman chemical company, Michigan, USA) are included in **Figure 5.4(B)**.

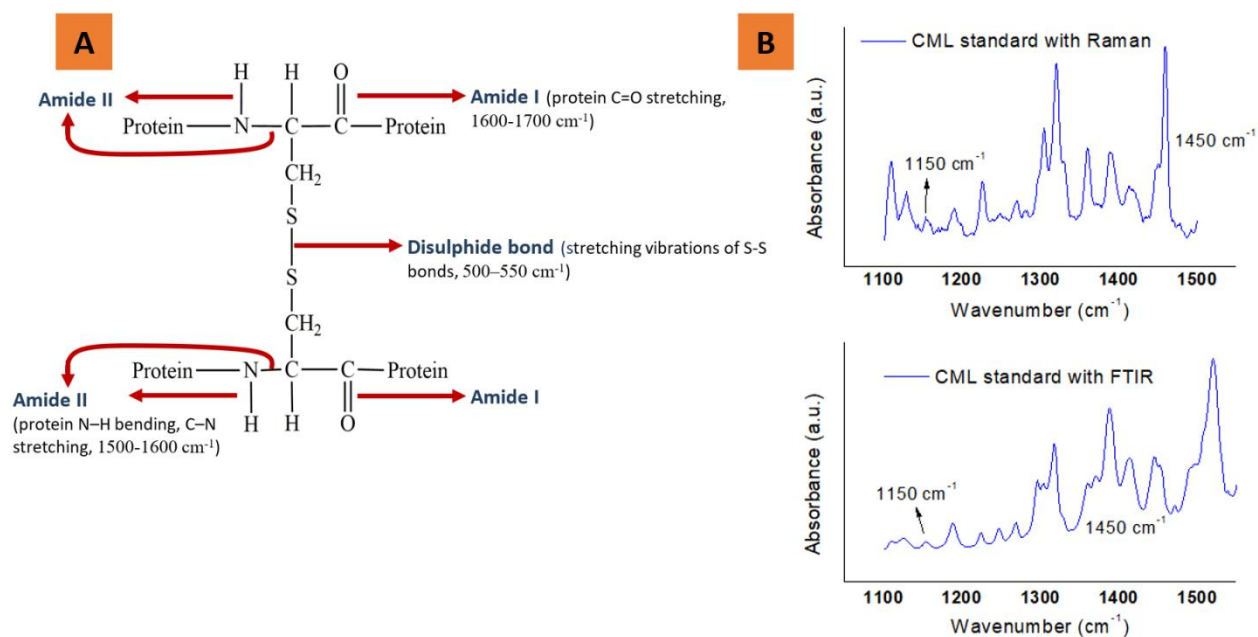


Figure 5.4 (A) Position of Amide I, Amide II, and disulfide bond in the principal keratin structural unit of fingernail plate, (B) showing Raman and FTIR spectra of a CML reference standard

5.3.7 Statistical Analysis

All the analyses were performed using SPSS 21.0 software. The normality of the data distribution was evaluated by Kolmogorov-Smirnov test [219]. A multivariate ANOVA with Tukey HSD post hoc was used to make all comparisons [85], [236]. A confidence level of $p < 0.05$ implies a statistical significance between the groups. Results are reported as the mean \pm SEM with *, ** and *** denoting $p < 0.05$, $p < 0.01$, and $p < 0.001$, respectively.

5.4 Results

5.4.1 Patient's characteristics

The distribution of males and females are found 40% and 60% respectively in all three groups, as mentioned in **Table 5.1**. The mean HbA1c levels are found significantly high for DC and UC groups 6.6 (6.2-7.3)%, and 8.4 (7.7-14)% respectively as compared to healthy 5.4 (5.1-5.9)% as shown in **Table 5.1**.

5.4.2 Porosity

The fingernail plate porosity is shown with red color in **Figure 5.5(A-C)** for healthy, DC, and UC groups, respectively.

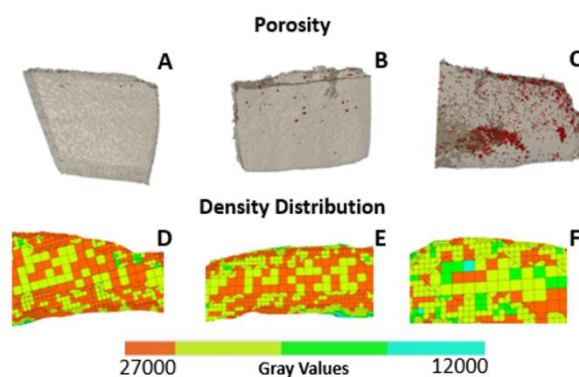


Figure 5.5 μ -CT images of fingernail plate samples describing porosity and density distribution in healthy, diabetic controlled (DC), and uncontrolled diabetic (UC) groups (A and D- healthy, B and E -DC, C, and F- UC)

The porosity is small in the healthy group, moderate in the DC group, and high in the UC group. The mean values of percentage porosity are presented in **Table 5.2**. The percentage increase in porosity is 35.5% in the DC group and 93.3% ($p < 0.001$) in the UC group with respect to the healthy group, as shown in **Figure 5.6(A)**. The density distributions are shown in **Figure 5.5(D-F)** for the healthy, DC, and UC groups, respectively. The higher gray values in these figures (shown with orange color) indicate the presence of denser content (minerals), which is found high in the healthy group, moderate in the DC group, and small in the UC group.

Table 5.2 Nail quality parameters of the human fingernail

Characterization techniques		Parameters studied	Study groups		
			Healthy	Diabetic controlled (DC)	Uncontrolled diabetic (UC)
Calcium content (EDXS)		Ca (weight %)	0.64±0.04	0.60±0.07	0.16±0.04***
Tissue density		Density (g/cc)	1.31-1.35	1.28-1.32	0.99-1.20**
Microstructure (μ -CT)		Porosity (%)	0.020±0.003	0.031±0.007	0.298±0.041***
Surface roughness	AFM	Roughness (Rq) (nm)	48.93±4.12	53.88±3.68	81.03±4.31*
Material properties (Nanoindentation)		Modulus (GPa)	4.66±0.08	4.20±0.12*	3.86±0.12***
		Hardness (GPa)	0.21±0.05	0.18±0.04	0.16±0.05***
Macro molecular vibrations (FTIR)	Protein structure	Amide I position (cm^{-1})	1640.72±3.69	1643.93±2.88	1646.24±3.31**
		Amide II position (cm^{-1})	1534.23±3.21	1536.11±3.77	1537.84±1.30*
	Protein content	Amide I band area (arb. unit)	0.45±0.16	0.35±0.14	0.24±0.08**
		Amide II band area (arb. unit)	0.36±0.12	0.27±0.09	0.18±0.05**

	Disulfide (S-S) bond content	Peak height S-S peak/CH ₂ peak	0.98±0.12	0.68±0.11	0.33±0.11***
* p<0.05, ** p<0.01 and ***p<0.001 respectively compared to healthy group					

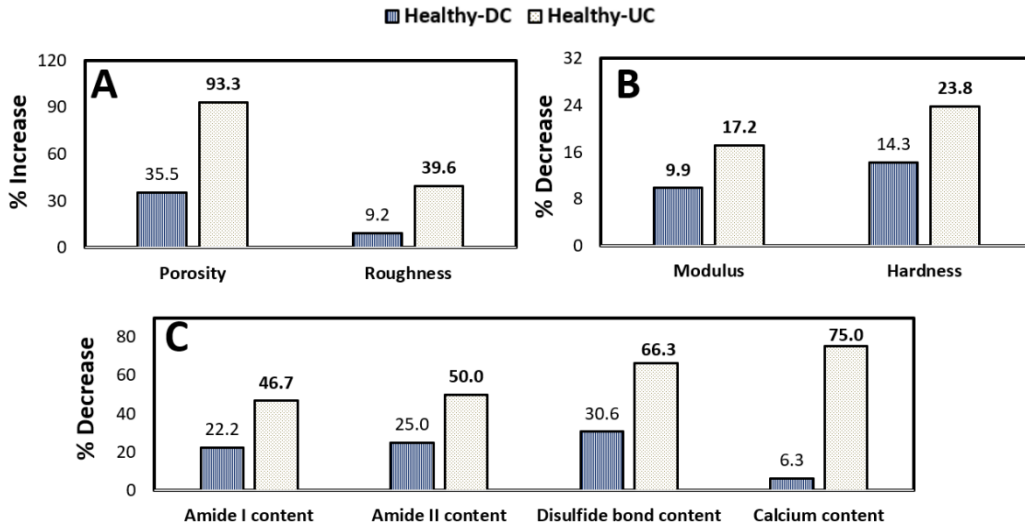


Figure 5.6 Percentage change in the nail plate quality parameters for diabetic controlled (DC) group (Healthy-DC) and uncontrolled diabetic (UC) group (Healthy-UC) with respect to healthy group (A) The percentage increase in porosity and roughness (structural properties), (B) Percentage decrease in modulus and hardness (material properties), (C) The percentage decrease in Amide I, Amide II, Disulfide bond and Calcium content (Biochemical properties) (In the figure, the bold values are representing a significant change from the healthy group)

5.4.3 Surface morphology and roughness

The SEM images of the dorsal and ventral phase (surface morphology) of the clipped nail plate are shown in **Figure 5.7** for healthy, DC, and UC samples. The results revealed that the surface morphology is moderately altered in the DC group and highly altered in the UC group as compared to the healthy group. In T2D groups, the surface morphology of the ventral layer is affected more than the dorsal layer because the bottom layer of the nail plate is more glycated than the upper layer as it remains in close contact with the blood vessels and the interstitial fluid [219].

The surface roughness measured through AFM is shown in **Figure 5.8**, and the root-mean-square value of roughness (Rq) obtained through these experiments is shown in **Table 5.2**. The percentage increase in surface roughness is 9.2% in the DC group and 39.6% (**p=0.04**) in the UC group, as shown in **Figure 5.6(A)**.

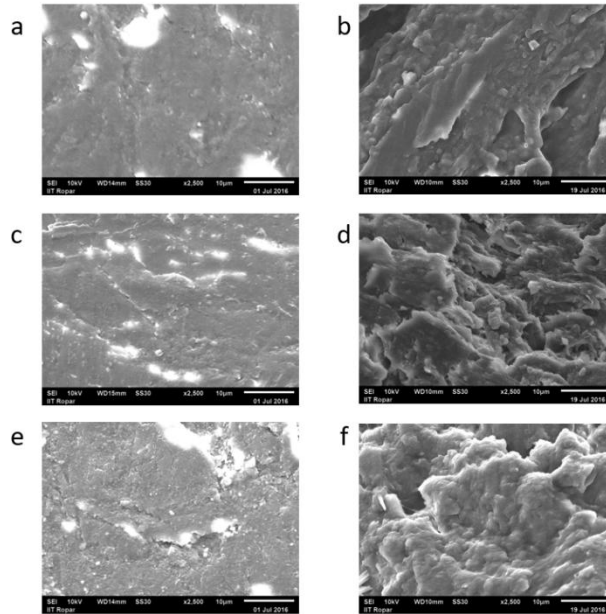


Figure 5.7 SEM images showing the morphology of fingernail plate for healthy, diabetic controlled (DC), and uncontrolled diabetic (UC) groups (a) Dorsal phase (healthy), (b) Ventral phase (healthy), (c) Dorsal phase (DC), (d) Ventral phase (DC), (e) Dorsal phase (UC), (f) Ventral phase (UC)

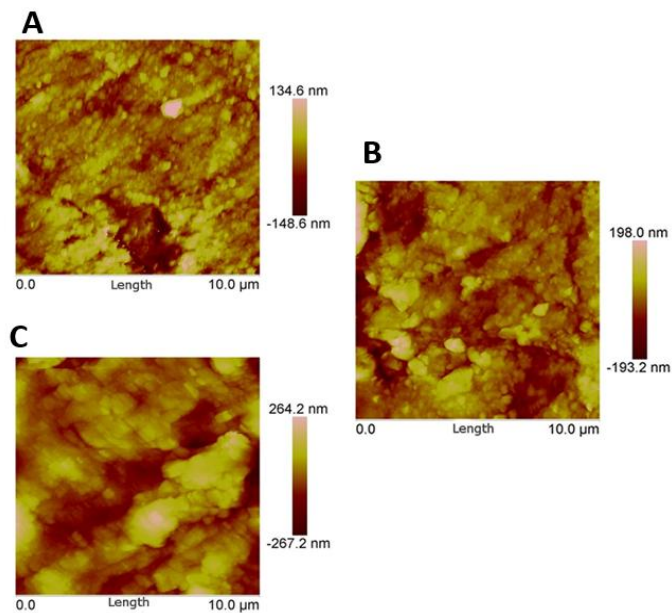


Figure 5.8 Surface roughness of dorsal phase of fingernail plate obtained through AFM experiments (A) Healthy group, (B) diabetic controlled (DC) group, (C) uncontrolled diabetic (UC) group

5.4.4 Material properties

The representative load-displacement curves obtained through nanoindentation tests are shown in **Figure 5.9(A)** for all three groups, which reveal that under the same load of 1000 μN , the healthy group undergoes small deformation, DC group shows moderate deformation, and UC group shows high deformation. The values of hardness and modulus of the dorsal, intermediate, and ventral layers within each group are averaged because no statistically significant difference is found between the layers. Later the mean values of hardness and reduced modulus are calculated for healthy, DC, and UC groups and shown in **Table 5.2**. The percentage decrease in the modulus calculated for DC and UC group with respect to the healthy group is (9.87%, $p=0.01$) and (17.17%, $p<0.001$) respectively, as shown in **Figure 5.6(B)**. The percentage decrease in the value of hardness for the DC and UC group with respect to the healthy group is (14.29%, $p=0.07$) and (23.81%, $p<0.001$) respectively, as shown in **Figure 5.6(B)**.

The layer-wise analysis of hardness and modulus is also conducted for each layer individually among all three groups and presented in **Table 5.3**. The values of the percentage decrease in hardness for healthy and DC group and healthy and UC group for dorsal, intermediate, and ventral layer are shown in **Figure 5.9(B)**. The degradation in values of hardness is significant in each layer of the UC group with respect to the healthy group (dorsal 19.49% ($p=0.02$), intermediate 22.18% ($p=0.01$), and ventral 23.88% ($p=0.03$)), and the degradation is slightly higher in the ventral layer as compared to dorsal layer.

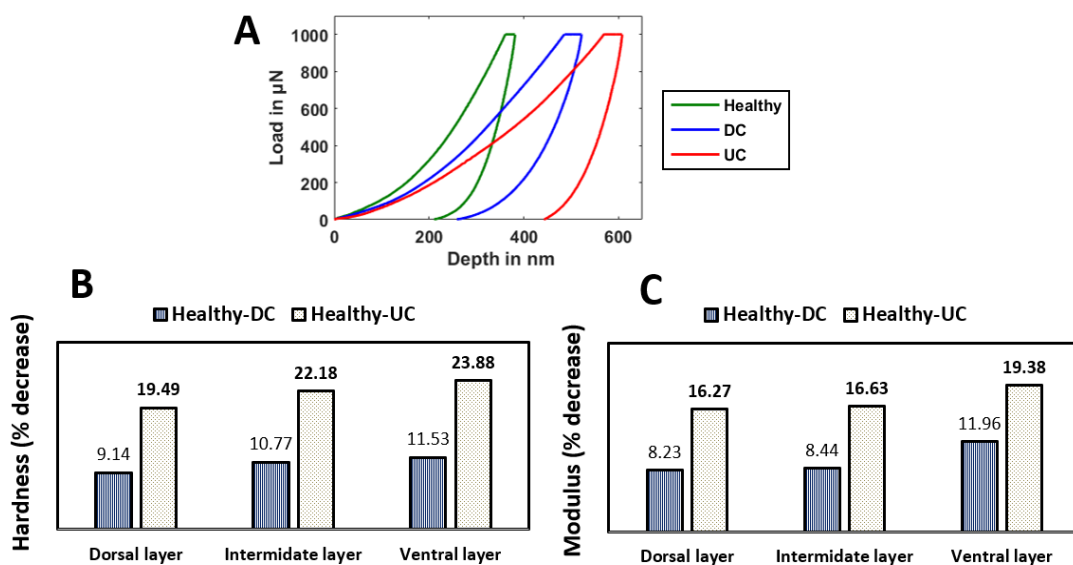


Figure 5.9 Nanoindentation results, **(A)** Representative load-displacement curves of healthy, diabetic controlled (DC) and uncontrolled diabetic (UC) group, **(B)** The percentage decrease in hardness for DC group (Healthy-DC) and UC group (Healthy-UC) with respect to healthy for dorsal, intermediate and ventral layer, **(C)** The percentage decrease in modulus for DC group (Healthy-DC) and UC group (Healthy-UC) with respect to healthy for the dorsal, intermediate and ventral layer (In the figure the bold values are representing the significant change with respect to the healthy group)

Similarly, the comparison is also made for a percentage decrease in modulus values, and this is shown in **Figure 5.9(C)**. The degradation in values of modulus is also significant in each layer of UC group with respect to healthy group (dorsal 16.27% (**p=0.02**), intermediate 16.63% (**p=0.002**) and ventral 19.38% (**p=0.001**)). The results of the layer-wise analysis revealed that the material properties of all three layers are getting degraded almost equally due to T2D, and the degradation is slightly higher in the ventral layer as compared to the dorsal layer.

Table 5.3 Hardness and Modulus values of each layer of the nail plate for healthy, diabetic controlled (DC), and uncontrolled diabetic (UC) group obtained through nanoindentation experiment

	Hardness (GPa)			Modulus (GPa)		
	Healthy	DC	UC	Healthy	DC	UC
Dorsal	0.219 ± 0.05	0.199±0.06	0.176±0.07	4.94± 0.84	4.53±0.67	4.13±0.67
Intermediate	0.200± 0.05	0.179±0.04	0.156±0.06	4.63± 0.61	4.24±0.62	3.86±0.80
Ventral	0.199 ± 0.06	0.176±0.05	0.151±0.09	4.42±0.62	3.89±0.43	3.56±0.74
The bold values are representing the significant change with respect to the healthy group						

5.4.5 Calcium content

The calcium content (weight %) of the fingernail plate for all three groups is shown in **Table 5.2**. The percentage decrease in calcium concentration is approximately 6.3% for the DC group and 75% (**p<0.001**) for the UC group as compared to the healthy group, as shown in **Figure 5.6 (C)**.

5.4.6 CML, protein, and disulfide bond content, and protein structure

The representative FTIR spectrum of the fingernail plate is shown in **Figure 5.10** for the healthy, DC, and UC groups. The shift in the position of protein bands (Amide I and Amide II) are observed and shown in **Table 5.2**. This shift in position indicates the altered secondary structure of proteins. The Amide I and Amide II band area are found decreased (**Table 5.2**), and the percentage decrease in the Amide I content for the DC group is 22.2% ($p=0.36$), and for the UC group is 46.7% ($p=0.002$) with respect to health, and Amide II content is 25% ($p=0.35$) for DC group, and UC group is 50% ($p=0.001$) with respect to healthy as shown in **Figure 5.6(C)**. These results indicate that the overall protein content gets decreased due to T2D.

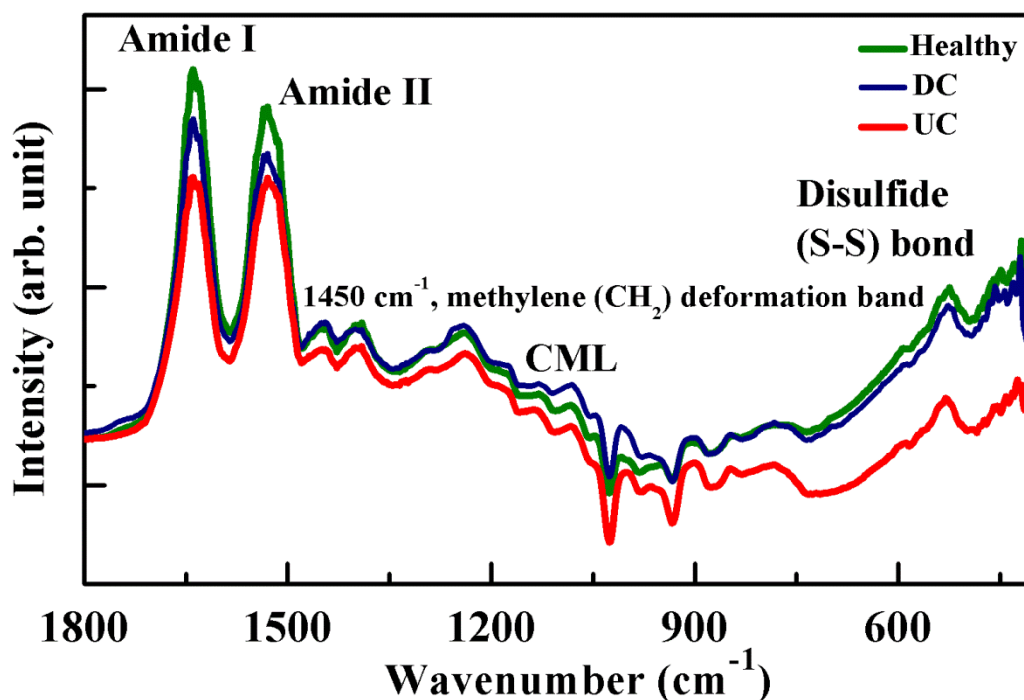


Figure 5.10 Representative FTIR spectrum of human fingernail plate showing the position of Amide I, Amide II and Disulfide (S-S) bond, CML and methylene (CH₂) deformation band vibrations for healthy, diabetic controlled (DC), and uncontrolled diabetic (UC) groups

The disulfide bond content is high in healthy, moderate in DC, and small in the UC group, as shown in **Table 5.2**. The percentage decrease in disulfide bond content for the DC group is 30.6% ($p=0.05$), and for the UC group is 66.3% ($p<0.001$) with respect to healthy as shown

in **Figure 5.6(C)**, which indicates that the overall disulfide bond content is decreased due to T2D.

The relative content of CML (AGE) was calculated for all three groups, as shown in **Figure 5.11**. The percentage increase in relative CML content for DC group is 34.7% ($p=0.02$) and UC group is 53.1% ($p<0.001$) with respect to healthy.

The above results are validated as per the published studies, which reported that the shift in peak position and/or increase in bandwidth is associated with altered protein's secondary structure [206], [237]. Also, the peak intensity and/or area under the curve implies the concentration of that particular protein which is associated with that peak [237].

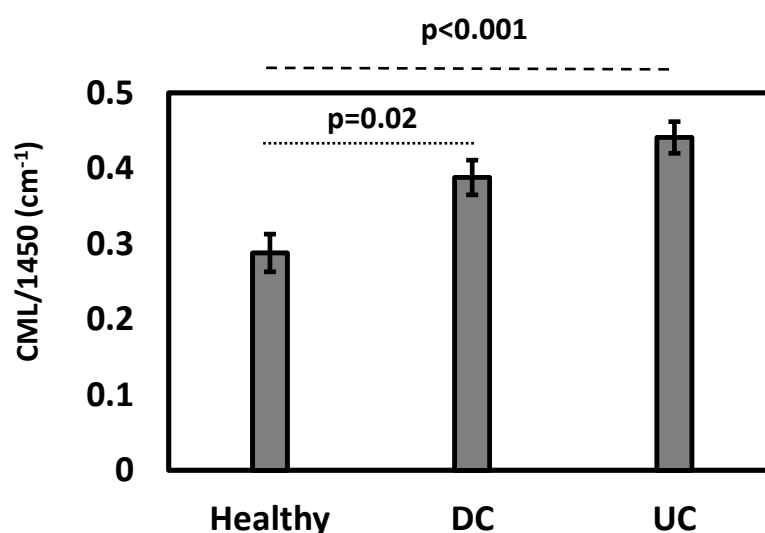


Figure 5.11 AGE measurement in the human fingernail plate through FTIR spectroscopy showed a higher level of relative carboxymethyl-lysine (CML) content in diabetic controlled (DC) and uncontrolled diabetic (UC) groups

5.5 Discussion

In the present study, we showed that the T2D is affecting the fingernail plate quality by changing its structural, material, and biochemical properties. We hypothesized that the main reason for degrading the nail plate quality is prolonged hyperglycemia which increases the accumulation of AGEs into the nail matrix. Later it is observed that the relative CML content is high in the DC group and higher in the UC group as compared to the healthy. The AGEs react irreversibly with amino acid residues of peptides or proteins of nail keratin and form protein adducts (protein – AGE) or protein crosslinks (AGE-protein-AGE) [20]. The continuous AGEs accumulation is further associated with prolonged Endoplasmic Reticulum

(ER) stress [238], [239]. Also, the stressed ER can increase the amount of misfolded proteins [238] in the nail matrix. Both this phenomenon ultimately leads to an alteration in ER homeostasis, which causes: 1) reduction of disulfide bonds 2) protein misfolding due to lack of chaperones 3) Ca^{+2} depletion [240].

To maintain the ER homeostasis, the unfolded protein response (UPR) pathway is get activated through IRE1 α , ATF6, and PERK stress sensors. This pathway aims to reduce the ER stress by 1) reducing the new protein synthesis to prevent the overloading of the organelle, 2) increase the number of ER chaperones to aid the protein folding, 3) to remove the misfolded proteins from the ER and degrade the misfolded proteins in the proteasome. In the case of continuous AGEs accumulation (prolonged ER stress), the above mechanism fails to restore the ER homeostasis and leads to cellular dysfunction and cellular apoptosis [240]. This cellular dysfunction and cellular apoptosis resulted in increased protein misfolding (altered secondary structure of proteins) and decreased overall protein synthesis (decreased Amide I, Amide II, and disulfide bond content), respectively.

These results are consistent in comparison to previous studies, which have also been reported that the accumulation of AGEs is responsible for the altered secondary structure of the protein and decreased total protein content in diabetic rat skeletal Soleus (SOL) muscles [206] and protein denaturation, abnormal collagen synthesis and altered collagen structure in bone [182]. The reduction in disulfide bond content has been reported for osteoporotic patients fingernails as compared to the healthy due to a reduction in total cystine content [209], and in the diabetic nail, the disulfide bond gets cleaved and forms the alkyl thiolated structure [220]. The reduction in cystine content and the reduction in disulfide bond content are one and the same because the cystine molecules are made only with the help of disulfide bonds between cysteine molecules. The nail keratin is rich in cystine content, and the altered cystine content (or disulfide content) is primarily responsible for the change in the structural integrity of the nail keratin. It results in microstructural deformation in the form of increased surface roughness and decreased material properties.

We have also observed that the calcium concentration is compromised in the UC group as compared to the other two groups. The reason for calcium depletion can be explained by ER stress-mediated apoptotic pathway [241]. As the ER plays a key role in maintaining the Ca^{+2} signaling by storing and secreting the Ca^{+2} (cytosol to intra-ER and vice versa), it controls several calcium-dependent cell processes such as organogenesis, stress responses, transcriptional activity, and apoptosis. The prolonged ER stress induces calcium depletion in the ER by activating the calcium release channel inositol 1,4,5-triphosphate receptor (IP₃),

which releases the Ca^{+2} into the cytoplasm. This increased calcium enters into mitochondria, which induces cytochrome *c*-mediated cell apoptosis, and the overall calcium content gets decreased in the tissue. It has been reported that the indirect effect of hyperglycemia is associated with calciuria, i.e., continuous removal of calcium from the bone, which leads to rapid bone loss [242]. Consequently, it was suggested that the nail mineral content might be a predictor of bone mineral metabolism [243]. We have also observed that the loss in calcium, increased porosity, and the decreased hardness are closely associated. Our result of depletion in calcium concentration is consistent with previous studies, which have been found the inferior calcium concentration in fingernail and toenail [243], and decreased modulus and hardness of fingernail in osteoporotic cases [244].

The nail plate quality is degrading due to T2D. Still, severe complications such as fracture or tearing are usually not observed in the diabetic nail. This is because the accumulation of AGE varies in the nail plate as it grows and gets replaced completely in 3-6 months' time [245], [246]. On the other hand, the continuous accumulation of AGE's plays a significant role in tissues with longer life spans such as bone, as it leads to fragile bone fractures [247]. In order to use the fingernail as a new avenue to assess bone health, we have investigated the relationship between bone (type I) collagen and nail keratin. Collagen and keratin are two fibrous structural proteins produced by osteoblasts and keratinocytes, respectively [225]. Both of these proteins undergo post-translational modifications in ER, and in that the important modification is the formation of a disulfide bond (S-S) between the cysteine molecules to get the structural stability of these proteins. In bone, the disulfide bonding is helpful for early bone formation as well as to provide strength during its matured phase, whereas in the nail, it provides structural integrity to the nail plate. The disulfide bonding is important for the stability of noncollagenous multifunctional bone proteins named Osteonectin and the family of transforming growth factor-B (TGF-B) proteins [248], [249]. Both collagen and keratin express the vibrations of Amide bands and disulfide bonds in the spectral region (Raman and FTIR) of $1200\text{-}1800\text{ cm}^{-1}$ and $500\text{-}550\text{ cm}^{-1}$, respectively [236]. Furthermore, the adverse effect of prolonged ER stress is also reflected on osteoblasts [239] and keratinocytes [250], which includes proteins misfolding, reduction in proteins, calcium, and disulfide bond content, cellular dysfunction, and cellular apoptosis.

Altogether, the authors proposed that the adverse effect of T2D is also reflected in the keratinized epithelial tissue, such as fingernail plate quality. T2D alters the secondary structure of the protein, total content of disulfide bond, calcium, and the protein itself. It also

causes the degradation in structural and mechanical properties of the fingernail plate. Comparing the results with the available literature on diabetic bone, it can be stated that T2D similarly affects nail and bone quality through AGEs accumulation and ER stress. Authors suggest that the fingernail seems to be a new avenue to assess diabetic bone quality.

CHAPTER 6

CAN FINGERNAIL PREDICT BONE DAMAGE IN TYPE 2 DIABETES?

A PILOT STUDY

Type 2 diabetes (T2D) adversely affects the normal functioning, intrinsic material properties, and structural integrity of many tissues, including bone. Therefore, there is a need to explore new diagnostic techniques that can better assist and improve the accuracy of the assessment of bone tissue quality. In the chapter, the link between material/compositional properties of bone and fingernail in T2D were investigated. For that, femoral head and fingernail samples were obtained from twenty-five adult female patients (with/without T2D) with fragility femoral neck fractures undergoing hemi/total hip arthroplasty. Cylindrical cores of trabecular bone were subjected to high-resolution μ -CT, and lower bone volume fraction was observed in the diabetic group than the non-diabetic group due to fewer and thinner trabeculae in individuals with T2D. Material and compositional properties of bone/fingernail were estimated using nanoindentation studies and Fourier Transform Infrared Spectroscopy, respectively. Both bone/fingernails in T2D had lower reduced modulus (E_r), hardness (H), lower Amide I and II area ratio (protein content), and higher sugar-to-matrix ratio compared with non-diabetic patients. The sugar-to-matrix ratio was strongly and positively correlated with HbA1c for both bone/fingernails. There was a positive correlation between bone and fingernail material/compositional properties. Our findings provide evidence that the degradation pattern of bone and fingernail properties go hand-in-hand in individuals with T2D. Hence, the fingernail compositional/material properties can serve as a non-invasive surrogate marker of bone quality in T2D.

6.1 Introduction

Type 2 diabetes (T2D) affects bone homeostasis and quality, leading up to a three-fold increased fracture risk depending on the skeletal site and glycemic load [6]–[10]. Nearly 60% of the world's diabetics live in Asia, and being with the fastest population growth rate, this burden is expected to increase further in the coming years [5]. Therefore, the early prediction and prevention of fracture risk is an important concern for the physician to reduce substantial socioeconomic burden and mortality caused by bone fractures.

Currently, the investigation of areal bone mineral density (aBMD) is the standard method to diagnose bone health, but it underestimates fracture risk in T2D, as aBMD is often

normal/slightly elevated compared to age-matched controls [214], [251]. Thus, many researchers/practitioners agreed that only mineral quantification alone is not sufficient to predict fracture risk, and beyond that, the study of collagen quality is also important to predict future fracture risk precisely [7], [12], [15]–[18], [38]. Further, bone histomorphometry is the gold standard to assess the bone quantity and quality [73], [109], but a trans-iliac bone biopsy is an invasive procedure, requires expertise, and may not always be feasible to perform. Additionally, bone biopsy involves the risk of infection or delayed healing, particularly in individuals with diabetes. Therefore, there is a need to develop new techniques that can better assist and improve the accuracy of assessment of bone tissue diagnosis.

Based on our previous study [208] that microstructural and macromolecular characteristics of a fingernail are degraded in patients with T2D, here we hypothesized that the fingernail plate has the potential to become a new surrogate marker to better predict diabetic bone damage because of the following reason: (i) The major constituent of fingernail plate (Keratins, present in $\pm 85\%$) is also prone to glycation [208], [219], [222], [223]. (ii) The growth of the nail plate is relatively slow; hence the long-term effects of hyperglycemia can reflect on the fingernail material and compositional properties [208], [224]. (iii) The rate of fingernail growth and the bone cycle is 90-120 days, which further makes it an ideal tissue to study. (iv) Study on fingernail is painless, non-invasive, and economical because neither it required specific storage nor consume expensive reagents [208], [219], [222], [223]. Thus, the present study aims to investigate the link between material/compositional properties of bone and fingernails in patients with T2D. Here we measured the bone microstructural properties (high-resolution μ -CT), material properties (reduced modulus and hardness), and compositional properties (relative content of glycation, normalized area of Amide I and Amide II) for both bone and fingernail.

6.2 Research design and methods

Study participants

Consecutive adult female patients with and without T2D admitted with fragility femoral neck fractures and undergoing either hemi- or total hip arthroplasty at our institution over six months were selected. Patients with a prior history of fracture, having onychomycosis, on anti-osteoporotic medications, glucocorticoid, thiazides, or calcium/vitamin D supplements (over the last six months) were excluded. All patients underwent assessment of aBMD of the

contralateral femoral neck using dual-energy X-ray absorptiometry (HOLOGIC Discovery A QDR 4500; Hologic, Inc., Bedford, MA, USA). The study was approved by the Institutional Ethics Committee (Approval Number PGI/IEC/2015/171) of the Postgraduate Institute of Medical Education and Research, Chandigarh. Prior written informed consent was obtained from all participants.

Sample procurement and storage

Excised femoral heads were collected from patients undergoing replacement surgery. From each femoral head, the cylindrical trabecular bone cores were extracted along the direction of the principal trabeculae using a drilling machine attached with a diamond core bit. The bone cores were cleaned with a water jet, wrapped in saline-soaked gauze (PBS 7.4 pH), transferred into sample bags, labeled, and subsequently stored at -20°C [38], [130]. Along with the femoral head, the fingernail plate samples were also collected with the same patients from a distal part of the right-hand middle finger using a nail clipper [208]. Collected nail samples were sectioned into 2-3 small pieces so that they can be utilized for different characterization techniques. All experiments were conducted within two months of the sample collection.

6.2.1 Microstructural parameters by μ -CT

One bone core of each patient was air-dried and scanned along the cylindrical axis on a high-resolution μ -CT system (GE Sensing & Inspection Technologies GmbH-phoenix|x-ray) using ten μm voxel size, 45 keV tube voltage, 250 μA beam current, 250 sec integration time, and ten frames. Reconstruction of scanned images was performed using Phoenix software (phoenix/x-ray, GE Measurement & Control; Germany), and reconstructed images were imported in Scan-IP (Simpleware Ltd, UK) for the analysis of structural parameters: bone volume fraction (BV/TV), trabecular thickness (Tb.Th), and trabecular number (Tb.N) were calculated as per published protocol [38], [130].

6.2.2 Fingernail and Bone material properties by nanoindentation

Nanoindentation tests were performed on both bone and fingernail samples using a TI-950 Tribo Indenter (Hysitron Inc., Minneapolis, MN, USA) with Berkovich pyramidal tip, having a tip radius of ~ 150 nm. Before testing, the samples were embedded in epoxy and polished with the previously published protocol [38], [208]. Locations for indents were identified using an in-situ scanning probe microscope imaging integrated with a nanoindentation system, and all tests were performed at room temperature in a moist condition.

Eight indents with a peak load of 1000 μN were applied to the surface of the samples. A load function consisting of a ten-second ramp to peak force segment, followed by a thirty-second hold and a ten-second unloading segment, was adopted[208]. The load-displacement curves obtained in these indentation tests were analyzed to determine the reduced modulus (E_r) and hardness (H) using Oliver and Pharr method in Triboscan (Hysitron) [146], [147].

6.2.3 Collagen and Keratin properties by Fourier Transform Infrared Spectroscopy (FTIR)

The trabecular bone was demineralized using a 9.5% ethylene diamine tetra-acetic acid (EDTA) solution in phosphate-buffered saline. The tissue was submerged in the EDTA solution for five days at 4°C, with a solution change every 24 hours. After five days, the demineralized tissue was rinsed twice with acetone for 10 minutes and then rinsed twice with deionized water for ten minutes [53]. Then, FTIR spectra were recorded from the freeze-dried fingernail and demineralized bone section using FTIR Spectrometer in Attenuated Total Reflectance (ATR) mode (Nicolet iS50, Thermo Scientific, Inc. Waltham, MA, USA) under the constant pressure, in the spectral region of 4000 to 400 cm^{-1} . One sample of both bone and fingernail is tested of each donor with four μm resolution, and 60 scans were averaged. The representative FTIR spectra of bone and fingernail with the appropriate label of various bands are shown in **Figure 1A**. The following parameters were calculated: the mean integrated area ratio (relative content) of Amide I (protein C = O stretching, 1600–1700 cm^{-1}) and Amide II (protein N–H bending, C–N stretching, 1500–1600 cm^{-1}) bands with respect to methylene (CH_2) deformation band at 1450 cm^{-1} [38], [206]–[208].

The mean integrated area ratio (relative content) of sugar-to-matrix ratio [area of the sugar peak [(ν CO and ν CC peaks) (900–1100 cm^{-1}) to Amide I peak (1596–1712 cm^{-1})] was calculated as per previous published protocol [53].

6.2.4 Statistical analysis

The distribution of the data was tested for normality by the Kolmogorov-Smirnov test. The homogeneity of variances was analyzed using Levene's test. Between-group differences of calculated parameters were analyzed for statistical significance using Student's t-tests after testing for normality and homogeneity of variances. Data are expressed in mean and standard deviation until otherwise specified. Pearson correlation and linear regression tests were used to determine relationships between structural, material, and compositional parameters. A confidence level of $p < 0.05$ implies a statistical significance between the groups where $p < 0.05$, $p < 0.01$, and $p < 0.001$ denote the level of significance. Statistical analysis was

performed using SPSS (v.21, SPSS Inc., Chicago, IL, USA) and Microsoft Office Excel (2007).

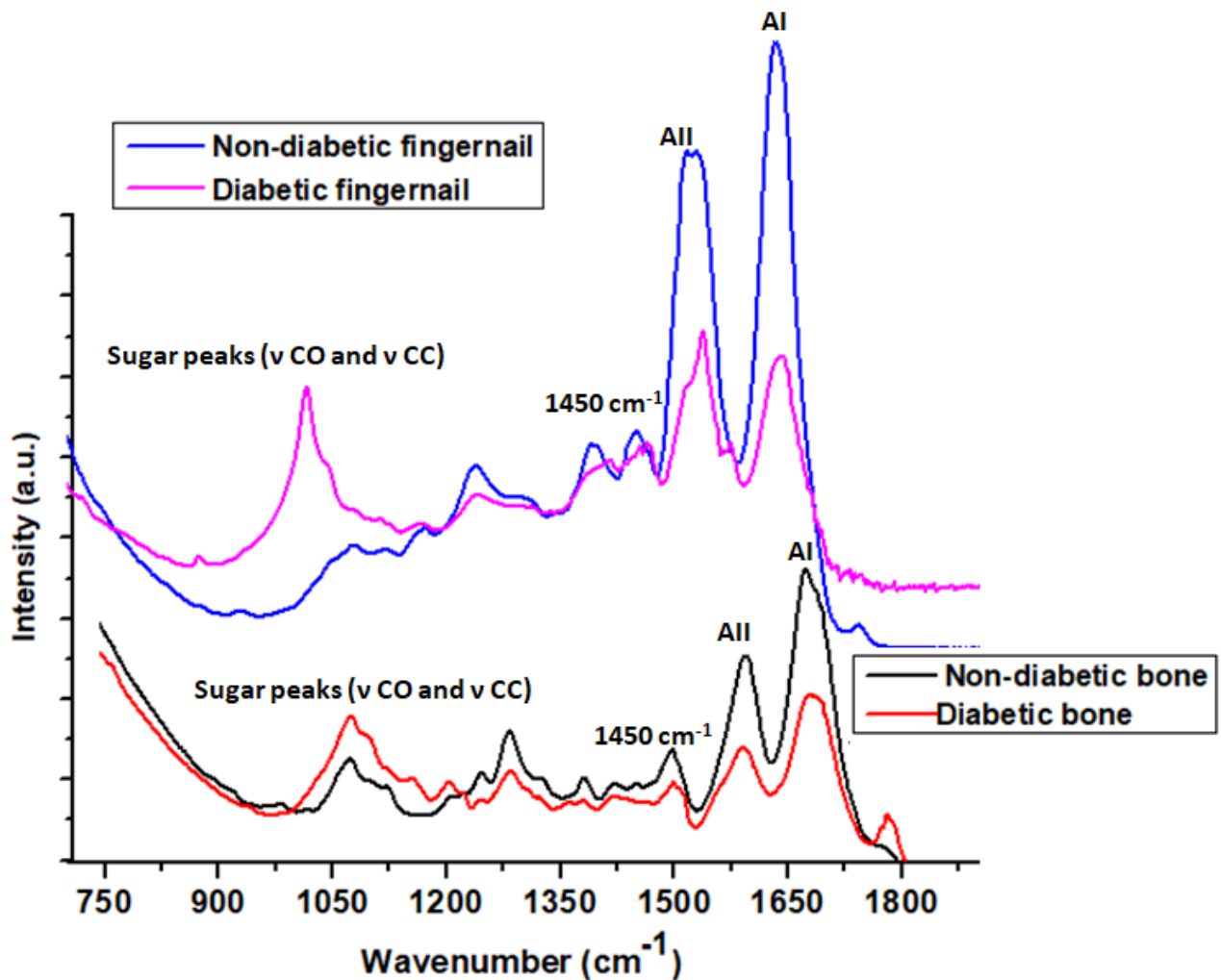


Figure 6.1 Representative FTIR spectra of the human fingernail and trabecular bone (demineralized) showing the position of Amide I, Amide II, sugar, and methylene (CH₂) deformation band vibrations for the non-diabetic and diabetic groups

6.3 Results

6.3.1 Patient's characteristics

Twenty-five patients each with (mean age 74.1 ± 7.8 years) and without T2D (mean age 72.2 ± 8.7 years) were analyzed. The mean duration of T2D was 7.0 ± 2.2 years; the mean HbA1c was $7.8 \pm 1.3\%$. There was no significant difference in age ($p=0.701$) or contralateral femoral neck BMD ($p=0.353$) between the two groups **Table 6.1**.

Table 6.1 Baseline demographic and radiographic parameters of diabetic and non-diabetic women suffered from fragility fracture of the hip

Parameters	Non-diabetic group (N=25)	Diabetic group (N=25)	p-value
Age (years)	74.1 ± 7.8	72.2 ± 8.7	0.701
HbA1c (%)	5.5 ± 0.6	7.8 ± 1.3	0.001
Duration of diabetes (years)	na	7.0 ± 2.2	na
Femoral Neck aBMD (gm/cm ²)	0.549 ± 0.079	0.487 ± 0.119	0.353
Femoral Neck T score	-2.8 ± 0.87	-2.9 ± 0.83	0.749

All data are expressed as mean ± SD, na: not applicable; HbA1c: glycosylated hemoglobin A1c; FN: Femoral neck; aBMD: areal bone mineral density

6.3.2 Structural parameters (μ -CT)

Representative μ -CT images and mean values of microstructural parameters of diabetic and non-diabetic groups are shown in **Figure 6.2**. The diabetic bone had significantly lower (mean) values of BV/TV (17.0±4.4 to 22.1±6.1, **p=0.009**), Tb.Th (0.146±0.03 to 0.166±0.03, **p=0.028**) and Tb.N (1.15±0.13 to 1.26±0.25, **p=0.032**) than the non-diabetic group. Here the diabetic group had significantly lower BV/TV (23.07%), Tb.Th (12.0%), and Tb.N (8.73%) compared to the non-diabetic group.

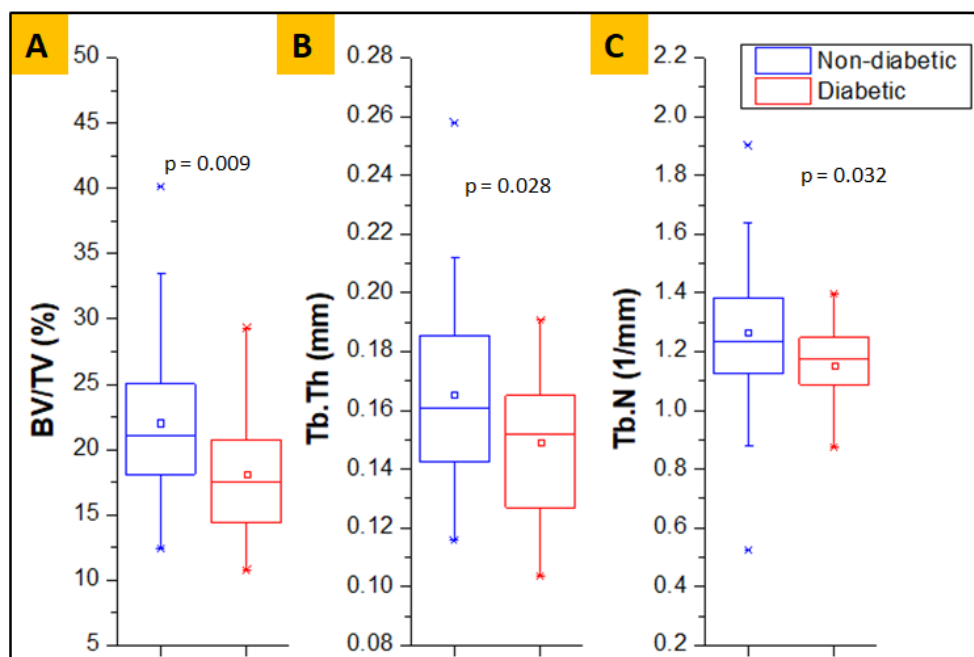


Figure 6.2 Measures of bone microstructural parameters for diabetic and non-diabetic trabecular bone, showing lower BV/TV (%) (A), Tb.Th (mm) (B) and Tb.N (1/mm) (C) in diabetic group

6.3.3 Collagen and keratin properties and measurement of glycation

The bone of diabetic individuals had a significantly higher sugar-to-matrix ratio 0.33 ± 0.07 to 0.25 ± 0.04 [by 27.9%, ($p < 0.001$)] compared to the non-diabetic individuals bone (**Figure 6.3A**). Likewise, the diabetic fingernail had significantly higher sugar-to-matrix ratio 0.30 ± 0.10 to 0.18 ± 0.07 [by 75.2%, ($p < 0.001$)] compared to the non-diabetic group (**Figure 6.3B**).

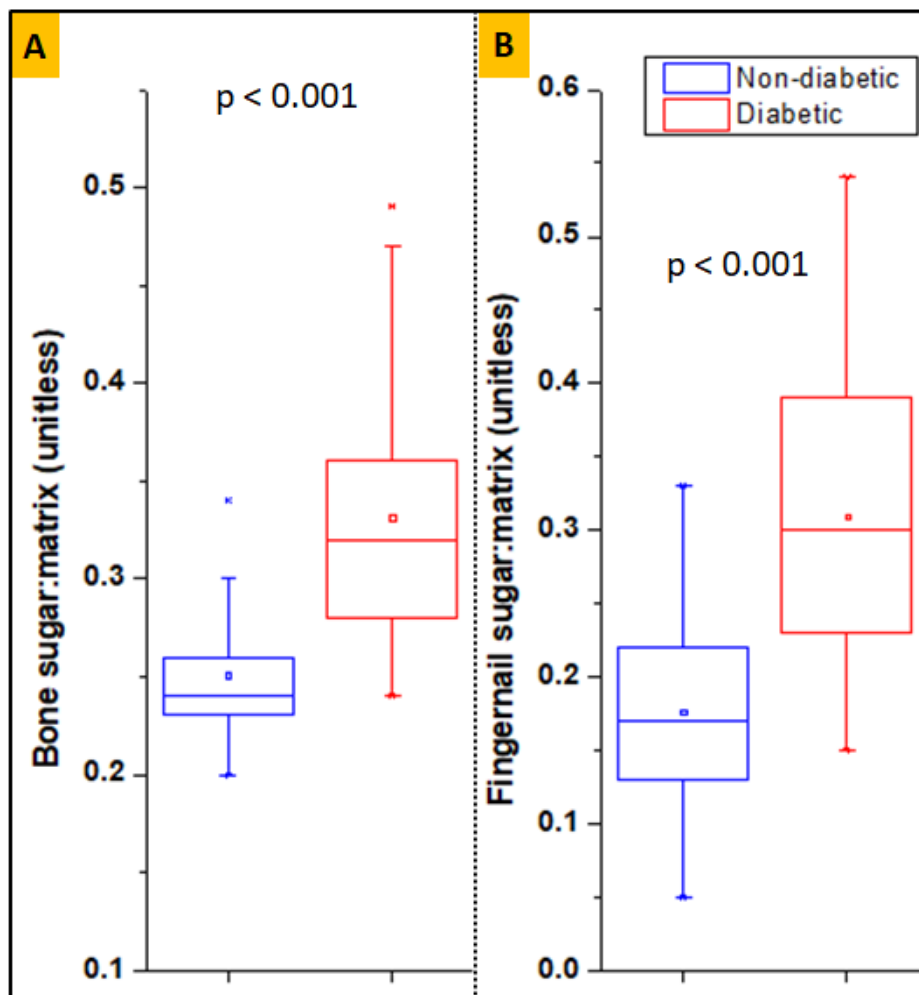


Figure 6.3 Sugar-to-matrix ratio obtained from FTIR, showing higher mean values in the diabetic group for both bone (A) and fingernail (B), respectively

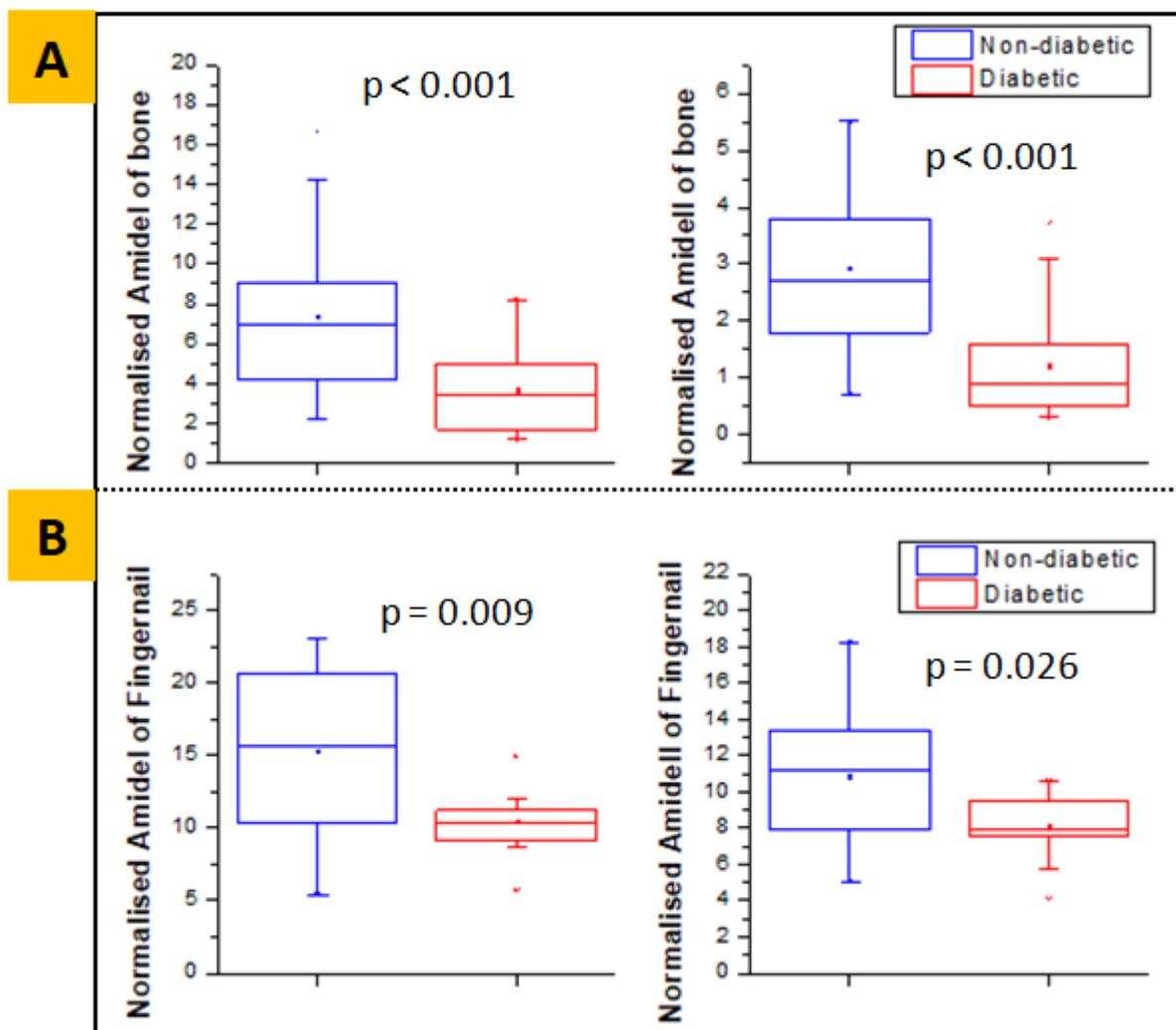


Figure 6.4 Normalized Amide I and Amide II area obtained from FTIR, showing lower mean values in the diabetic group for both bone (**A**) and fingernail (**B**), respectively

Also, the diabetic bone had a lower value of area under the normalized peak of Amide I and Amide II bands 3.67 ± 2.08 to 7.36 ± 3.93 [by 50.1% ($p < 0.001$)] and 1.22 ± 0.91 to 2.93 ± 1.49 [58.4% ($p < 0.001$)] respectively, compared to the non-diabetic group (**Figure 6.4A**). These results indicate that the quantity of these proteins is lower in the diabetic bone. Similarly, (**Figure 6.4B**) shows that the diabetic fingernail also had a lower value of area under the normalized peak of Amide I and Amide II bands 10.50 ± 2.39 to 15.33 ± 5.88 [by 31.5% ($p = 0.009$)] and 8.09 ± 1.76 to 10.90 ± 3.06 [25.8% ($p = 0.026$)], respectively, compared to the non-diabetic group. These results indicate that the quantity of these proteins is lower in the diabetic fingernail.

6.3.4 Material properties

Nanoindentation tests for both the groups revealed that under the same load of 1000 μN , the diabetic bone had significantly lower (mean) values of reduced modulus (7.38 ± 2.96 GPa to 9.13 ± 2.58 GPa, $p=0.022$) and hardness (0.268 ± 0.16 GPa to 0.441 ± 0.25 GPa, $p=0.004$) than the non-diabetic group (**Figure 6.5A**). The modulus and hardness were found to be lower by 19.17% and 39.23%, respectively, in the diabetic group as compared to the non-diabetic group.

With the same loading condition, the diabetic fingernail also had significantly lower (mean) values of reduced modulus (4.00 ± 0.56 GPa to 4.60 ± 0.98 GPa, $p=0.026$) and hardness (0.152 ± 0.04 GPa to 0.212 ± 0.06 GPa, $p=0.003$) than the non-diabetic group (**Figure 6.5B**). The reduced modulus and hardness were found to be lower by 13.04% and 28.3%, respectively, in the diabetic fingernails as compared to the non-diabetics.

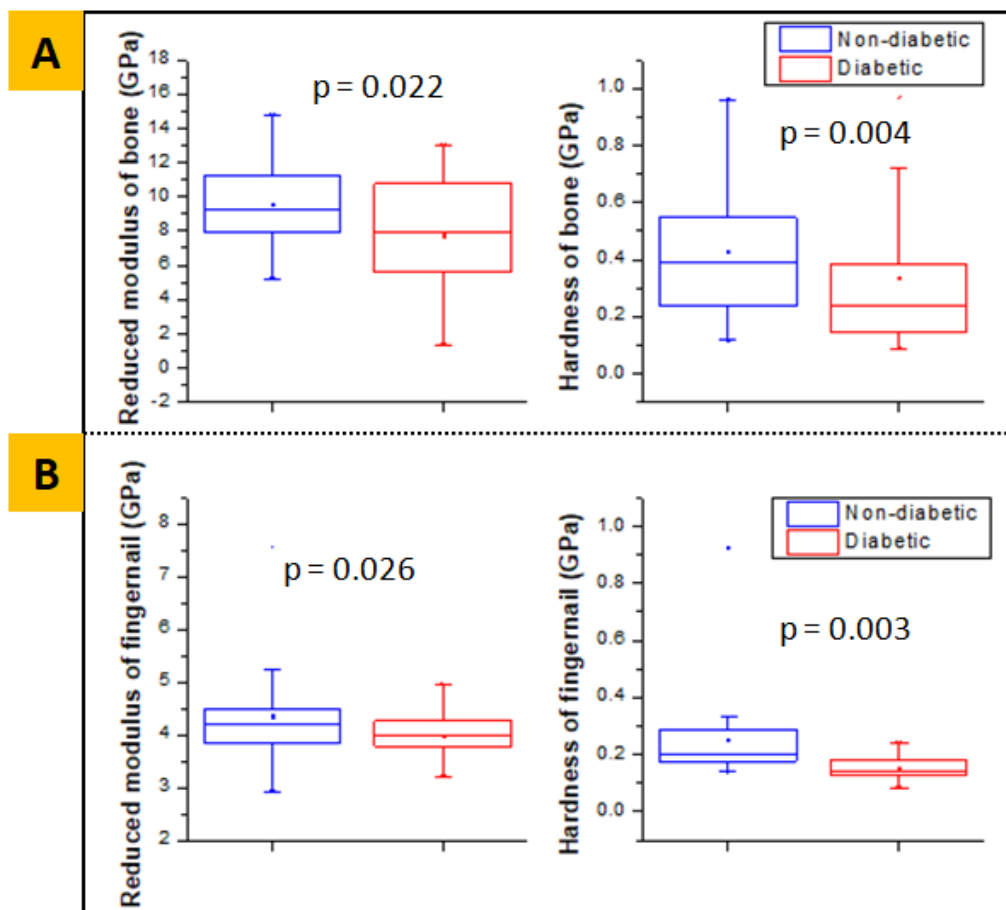


Figure 6.5 Reduced modulus and hardness obtained from nanoindentation, showing lower mean values in the diabetic group for both bone (A) and fingernail (B), respectively

6.3.5 Interrelationships between variables

In the diabetic group, the pre-operative HbA1c is positively correlated with the sugar-to-matrix ratio in bone ($r=0.654$, $p<0.001$) and fingernail ($r=0.527$, $p=0.007$) respectively, as shown in **Figure 6.6(A and B)** respectively. Linear regression tests to predict bone glycation as a dependent variable using fingernail glycation as an independent variable shows that in the diabetic group, the fingernail sugar-to-matrix ratio can explain up to 20% ($r=0.45$, $p=0.025$, $\beta=0.291$) of variance in the sugar-to-matrix ratio in bone (**Figure 6.7A**). Also, the variance in reduced modulus of bone and microstructural parameter BV/TV can be explained up to 23% ($r=0.48$, $p=0.015$, $\beta=2.937$) and 21% ($r=0.46$, $p=0.020$, $\beta=5.477$) (**Figure 6.7B and 6.7C**) respectively by the reduced modulus of a fingernail in the diabetic group. In the non-diabetic group, no parameter is found significant.

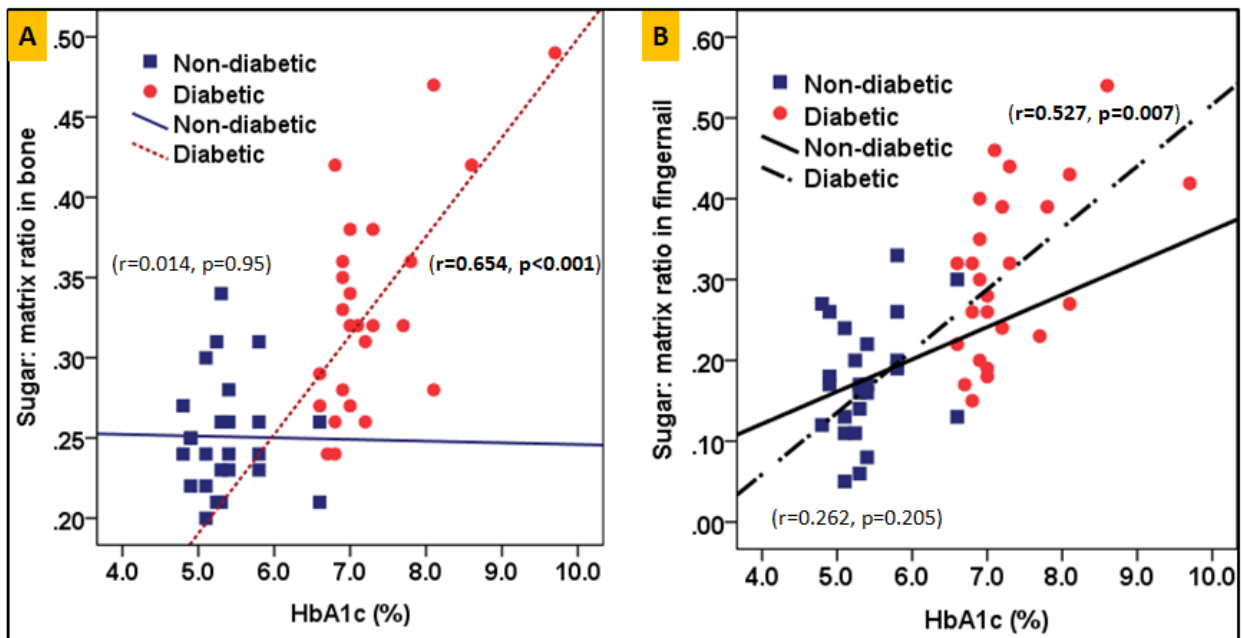


Figure 6.6 Correlation between HbA1c and the sugar-to-matrix ratio for both bone and fingernail is shown in 6(A) and 6(B), respectively, for diabetic and non-diabetics groups

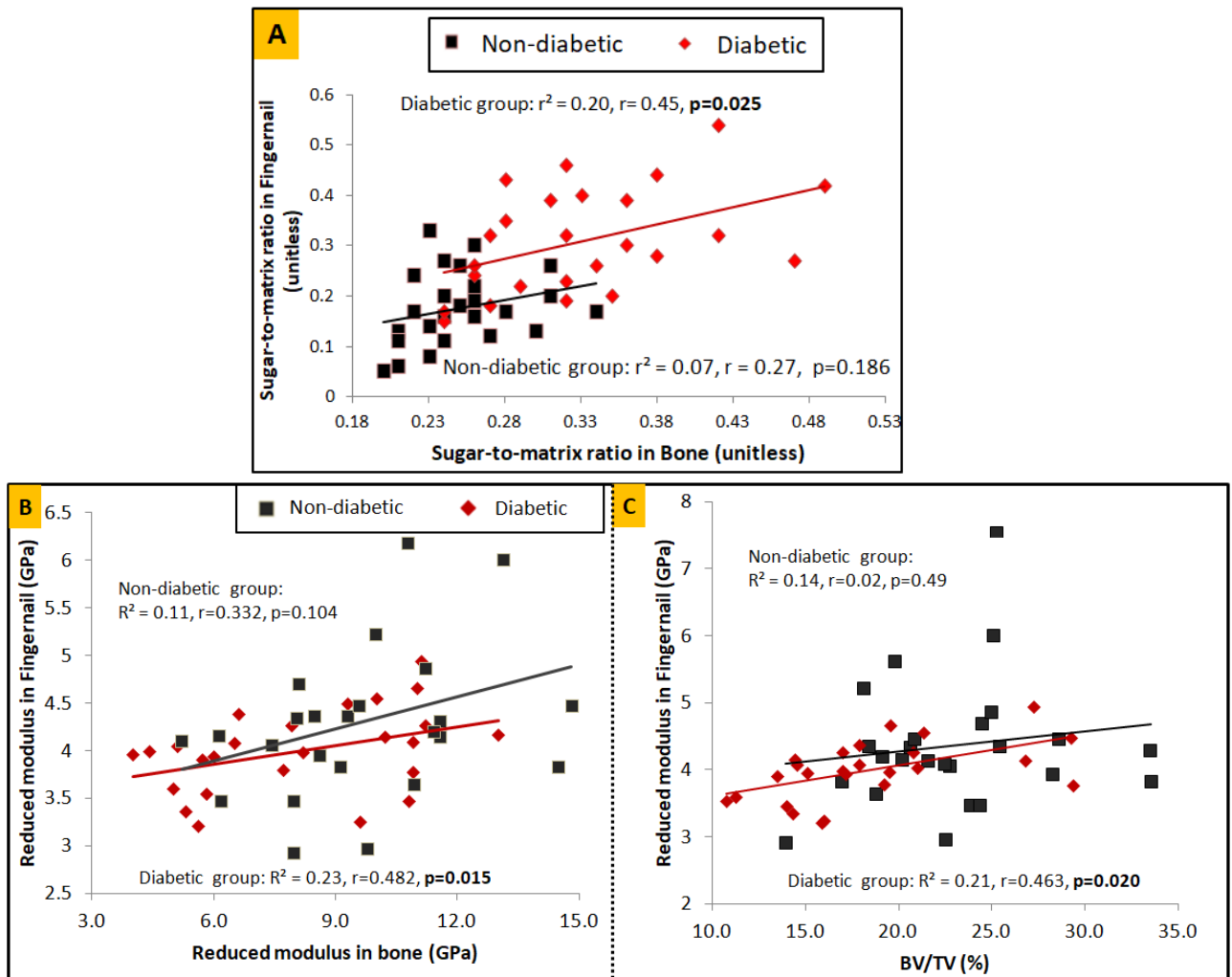


Figure 6.7 Correlation between fingernail and bone for diabetic patients and non-diabetics (A) for sugar-to-matrix ratio, (B) for nanoindentation determined reduced modulus, (C) BV/TV of trabecular bone and fingernail reduced modulus

6.4 Discussion

Study shows that in diabetic bone, microstructural and material properties altered which go hand in hand with fingernail plate properties. We found significant correlations between the two body tissues suggesting that material properties of a fingernail in patients with T2D can be used as a potential surrogate marker of underlying bone quality.

In our previous study on an animal model, it is reported that T2D alters the cortical bone quality, makes the bone weaker and tends to easily fracture through concurrent assessment of mechanical, microstructural, and compositional properties of bone. The diabetic bone reduces whole bone strength, compromises structural properties (μ -CT), and increases AGEs in the T2D group [130]. Our study on individuals with diabetes and known fragility fracture status

provides evidence that diabetes affects the trabecular bone quality at multiple organization levels. The accumulation of AGEs is one of the processes that favor deterioration of bone quality in diabetes leading to altered structural, material, and compositional properties and these changes in the bone lead to the lower energy absorption and toughness-indicative of increased propensity to bone fragility [38]. On the other hand, T2D also has an adverse effect on the human fingernail plate quality. T2D alters the surface roughness, density, suggest that T2D adversely affects both bone and fingernail, and hence there could be an association in the degradation pattern of both the tissues. Indeed, the fingernail is composed predominantly of keratin which is prone to glycation just as collagen in bone. In addition, the growth of the fingernail is slow, allowing time for hyperglycemia to exert its detrimental effect [208]. Carrying forward this hypothesis, in the present study, we found marked differences in compositional/material properties of bone and fingernail in patients with and without T2D.

Here, the assessment of bone microstructure after μ -CT showed lower BV/TV (%) in those with the diabetic group compared to the non-diabetic group. The bone microstructure was noticeably altered, evidenced by the thinning of trabeculae and by fewer trabecular numbers. However, few recent studies [49], [51]–[53] obtained the same or increased BV/TV in those with diabetes compared to non-diabetics. Notably, in these studies, [49], [51]–[53] bone tissue was obtained from individuals with obesity and/or severe arthritis, which possibly could explain the difference in findings of BV/TV from this study. Whereas the study published from our lab reported the lower BV/TV in individuals with diabetes and known fragility fracture status [38]. It is also possible that our study finding of lower BV/TV in diabetes is related to the distinct phenotypes of Asians [130], [188]–[192].

At the material level, the lower value of reduced modulus and hardness is observed in those with diabetes compared to the non-diabetic group. Thus, this finding describes that long-standing T2D alters bone microstructure and material properties and makes the bone weaker and fracture prone. These results also revealed that the above alteration in the properties locally, either at micro-scale or nano-scale, can affect the properties of the hierarchical organization of bone at higher scales [24], [25].

In the compositional analysis, we observed that the FTIR signatures and spectral changes of bone collagen and nail keratin are comparable and also have the capability to discriminate the samples of the diabetic and non-diabetic groups. We found significantly increased glycation content (relative CML content and sugar-to-matrix ratio) in the diabetic group of both bone

and fingernail as compared to the non-diabetic group. Along with the increased glycation content, the decreased relative protein content (Amide I/1450 cm^{-1} and Amide II/1450 cm^{-1}) is observed in the diabetic groups for both bone and fingernail compared to the non-diabetic group. These results are consistent in comparison to the previous studies, which have also been reported the decreased total protein content in diabetic rat skeletal Soleus (SOL) muscles [206], and decreased Amide content in diabetic fingernails [208].

Furthermore, the HbA1c is significantly and positively correlated with the sugar-to-matrix ratio for both bone and fingernail. This finding evidence that the main reason for degradation of bone and fingernail quality in the diabetic group is prolonged hyperglycemia which increases the accumulation of AGEs in the bone and nail matrix and induces tissue damage through structural modification of proteins and abnormal collagen fibril organization in the diabetic group [20]. Also, glycation decreases the osteogenic differentiation and activity [225], [252], which results in decreased overall protein synthesis (decreased Amide I, Amide II content) and decreased material properties of both bone and fingernail at nano-scale, and lower bone formation (BV/TV) at micro-scale.

Usually, severe complications such as fracture or tearing are not observed in the diabetic nail. This is because the accumulation of AGE varies in the fingernail as it grows and gets replaced completely within a few months, whereas the complete removal of accumulated AGE's from diabetic bone is not possible, and thus it causes severe damage and leads to bone fracture [208]. To predict the bone fracture risk, the present study revealed that the material and compositional properties of the fingernail are degrading as similar to the bone in individuals with diabetes. The marked correlation observed for measures of glycation between fingernail and bone in the diabetic group confirms the role of a fingernail in the prediction of bone glycation. Also, the reduced modulus of the fingernail is found correlated with the reduced modulus of bone and BV/TV, respectively, in the diabetic group, revealed that degraded fingernail material property is associated with lower bone material property and altered bone microstructure. Therefore, the investigation of diabetic fingernail properties at a small-scale can be an important solution to get the idea about the damage of diabetic bone properties and the prediction of fracture risk.

Altogether, the authors proposed that both bone and fingernail in T2D had significantly higher glycation content (sugar-to-matrix ratio) and reduced relative protein content (Amide I and Amide II) compared with non-diabetic women. We also found a significant positive

correlation between bone and fingernail parameters, implying that hyperglycemia-induced alterations in bone and fingernail go hand-in-hand. Although the effect size of variance was relatively small, fingernail properties could predict bone quality, thereby making it a potentially non-invasive modality to assess bone health in T2D.

Despite a well-designed study, we acknowledge a few limitations, such as small sample size and the collection of bone samples from the femoral head rather than conventional trans-iliac bone biopsy. However, there exists a weak association between the histomorphometric parameters of the iliac crest and proximal femur. Hence, femoral head samples may be clinically more relevant in femoral neck fractures [253].

In conclusion, we found that fingernail compositional/material properties are adversely affected in patients with T2D and propose that fingernail can serve as a non-invasive surrogate marker to study bone quality.

CHAPTER 7

SUMMARY, CONTRIBUTIONS, AND FUTURE SCOPE

7.1 Summary of key results

This thesis's primary objectives were: 1) To develop an animal model (rodent) that can better simulate type 2 diabetic patients' metabolic characteristics and investigate the effects of T2D on bone quality parameters at various organization levels of bone. 2) To explore the mechanical, material, and compositional determinants of human trabecular bone quality in individuals with and without T2D with known diabetic status and known fragility fracture status. 3) To investigate a new surrogate marker that can assist and improve the current diagnose of diabetic bone health. Therefore, in previous Chapters 3-6, the bone quality parameters from a rodent model and clinical populations of T2D were evaluated, and also the link between bone and fingernail quality were established; also, the main findings of these chapters are summarized below.

In Chapter 1, the prevalence of increased fracture risk in individuals with T2D and the limitations of current diagnostic tools to identify fracture risk in patients with T2D is presented. The hypothesis about how prolonged hyperglycemia and AGEs alter bone quality is briefly described. Also, the hierarchical structure of bone is discussed in detail, and a summary of the current state of relevant literature is provided. In Chapter 2, bone quality assessment techniques are presented to evaluate bone tissue's microstructural, mechanical, material, and compositional properties and the primary outcome of each method. Its utility in diabetic bone research is also summarized. Many of the techniques discussed in Chapter 2 are used to evaluate bone quality in Chapters 3-6.

In Chapter 3, a combination of high-fat diet and low dose STZ (35 mg/kg, i.p.) treated T2D female Sprague Dawley (SD) rat model is developed, and bone quality parameters at multiscale organization level of bone were analyzed. Here we found that NE-xLR in the T2D group is strongly and negatively correlated with post-yield-displacement, suggesting the possibility of bone fragility due to lack of glycaemic control. This model also simulates the metabolic characteristics of late-stage type 2 diabetes (insulin resistance and, as the disease progresses, develops hypoinsulinemia) for non-obese young T2D patients and provides potential evidence of diabetic bone fragility at various organizational levels.

In Chapter 4, the femoral head bone tissue specimens were collected from patients who underwent hemi/total hip arthroplasty for fragility hip fracture, and trabecular bone quality parameters were compared for diabetic and non-diabetic groups. Here we reported that aBMD and T-score obtained with DXA were similar among diabetic and non-diabetic groups. However, due to the increased accumulation of NE-xLR and total fAGE content in bone collagen, the apparent level of bone tissue toughness and post-yield energy were significantly lower in the diabetic group. Thus, in contrast to BMD, modifications of an organic matrix are the primary cause of enhanced fracture risk in the diabetic group. In other words, the energy absorption capacity is compromised in the diabetic group due to glycation in collagen, which is a significant cause of enhanced fracture risk in patients with T2D rather than BMD.

In Chapter 5, the microstructural, material, and macromolecular (disulfide bond content, protein content, and its secondary structure) properties of fingernail plate is investigated with the severity of disease: healthy, diabetic controlled (DC), and uncontrolled diabetic (UC). Here we found that the fingernail quality was changing in a pattern among all the three groups, and the degradation was higher in the UC group compared to the healthy and DC groups (Healthy<DC<UC). The extension of this study Chapter 6 described the link between material/compositional properties of bone and fingernail in T2D. For that, both femoral head and fingernail samples were obtained from twenty-five adult female patients (with/without T2D) with fragility femoral hip fractures undergoing hemi/total hip arthroplasty. Material and compositional properties of bone/fingernail were estimated using nanoindentation and FTIR, respectively. The sugar-to-matrix ratio was strongly and positively correlated with HbA1c for both bone/fingernails. Our findings provide evidence that bone and fingernail properties' degradation patterns go hand-in-hand in individuals with T2D. Hence, the fingernail compositional/material properties can serve as a non-invasive surrogate marker of bone quality in T2D.

7.2 Contribution of thesis

Many aspects of the research discussed in this thesis are essential to understand how T2D affects bone tissue quality. This thesis's major strength is the ability to relate the results of laboratory experiments to clinical practice: to diagnose diabetic patients who are fracture prone. In Chapter 3, an HFD-fed/low dose STZ treated T2D non-obese rat model is developed, which can simulate the natural history and metabolic characteristics of the non-

obese young Asian T2D patients. Also, this study showed that 8-week persistent hyperglycemia affects the femoral bone quality at various organization levels. Remarkably, the increased non-enzymatic cross-links result in compromised mechanical performance and diminished bone strength in T2D [130].

The finding of Chapter 4 provides evidence that detrimental effects of hyperglycemia and AGEs on trabecular bone quality at multiple scales leading to lower energy absorption and toughness-indicative of increased bone fragility. This human study is novel in examining multi-scale characterization of trabecular bone in humans with known diabetic status and known fragility fracture status [38].

Chapter 5 provides evidence that the adverse effect of T2D is also reflected in the keratinized epithelial tissue, such as fingernail plate quality. Prolonged hyperglycemia alters the protein's secondary structure and causes degradation in the fingernail plate's structural and mechanical properties. Also, this degradation follows a pattern, and the degradation is higher in the severity of T2D [208]. An extension of this study, Chapter 6, showed that bone and fingernail properties' degradation patterns go hand-in-hand in individuals with T2D. Therefore, fingernails can serve as a non-invasive surrogate marker to study bone quality.

Altogether, this thesis provides a foundation for studying the effects of T2D on bone quality. Moreover, it also offers several opportunities for further research, such as investigating cortical bone quality and quantifying AGEs in the fingernail, using available valuable clinical specimens.

7.3 Limitations of this thesis

Despite well-designed studies, we acknowledge a few limitations, such as this thesis was limited to *ex vivo* assessments of bone quality in animals (Chapter 3) as well as in human studies (Chapters 4 and 6). The main limitations in Chapter 3 were that the use of (low dose) chemical treatment (STZ), which causes partial loss of pancreatic beta cells by direct cytotoxic action on it, unlike in human T2D. It is unique and different from other combination rat models since the dose of STZ selected causes diabetes only in HFD-fed insulin-resistant rats, whereas it fails to induce the same in normal control rats resembling the situation in humans with risk factors of insulin resistance to be more prone to develop T2D than others without them. Another limitation was that we could not analyze the effect of hyperinsulinemia alone on bone quality. Limitations of Chapter 4 were that the non-fracture controls with and without diabetes were not studied; however, it was not feasible to obtain a

femoral head specimen from healthy controls. Second, the study focuses exclusively on trabecular bone in Chapters 4 and 6 and does not include properties of cortical bone. Also, in Chapter 4, the analysis of the effect of diabetes treatment type (insulin, metformin, and other anti-diabetic treatment) on the bone properties was not included in the thesis because the sample sizes within each subgroup were small, and a large randomized clinical trial was necessary to draw any conclusion on the effect of diabetes treatment on bone properties. Lastly, we used femoral head specimens instead of the femoral neck (typical fracture site) because, in most cases of fracture, femoral necks were extensively and variably damaged either due to fracture or during surgery. Thus, it was difficult to obtain uniform specimens from all the patients. Hence to avoid site-specific differences, we took samples from the femoral head.

7.4 Future scope of this study

Bone quality assessment techniques discussed in this dissertation were the preliminary steps to understand how T2D affects bone tissue properties. Based on this foundational work, many clinical problems related to bone research can be resolved, which is outlined below:

In this thesis, we have investigated bone quality parameters for patients suffering from T2D. Likewise, the same analysis of bone quality can be done for patients who have long-standing type-1 diabetes.

The HFD fed/low dose STZ treated T2D rat model can be utilized to conduct a randomized drug trial (insulin, metformin, and other anti-diabetic treatment) to understand the effect of diabetes treatment on bone quality.

Despite evidence for increased fracture risk in T2D, little is known about the effect of anti-osteoporotic treatment on bone quality, particularly in patients suffering from osteoporosis and T2D. Therefore, randomized controlled trials on the impact of anti-osteoporotic drugs on bone material properties in patients with osteoporosis and T2D can be conducted.

Finally, based on this *ex vivo* studies on diabetic bone, we would like to give some suggestion to predict the diabetic bone fracture risk better clinically:

This thesis demonstrates that the trabecular compartment (reduced BV/TV, Tb.Th, and Tb.N) is compromised in T2D. Therefore, in addition to aBMD evaluation, an assessment of the trabecular compartment (similar to trabecular bone score [12], [119]) should be included to improve the accuracy in evaluating diabetic bone fracture risk.

High resolution *in vivo* imaging of the trabecular compartment is needed, particularly at clinically relevant (fracture prone) sites. In available imaging techniques: the limitation of HRpQCT is that it is not approved for clinical use at this time; additionally, it is limited to peripheral skeletal sites. In contrast, the multi-detector CT can scan clinically relevant sites and is standard in clinical use. However, the radiation exposure required to achieve high spatial resolution and adequate image quality is substantial, which is expected to resolve as technological advances. Meanwhile, the advancement in high-resolution MRI imaging has made possible the trabecular structure analysis at the proximal femur [254], [255]. However, all these techniques are limited due to their expensive nature [16], [35], [110], [254], [255].

This thesis also reported that the trabecular bone material and compositional properties are compromised in diabetic bone compared to non-diabetic bone. Therefore, *in vivo* bone assessment techniques: Raman and Osteoprobe will provide an investigation of bone compositional properties and bone material strength [35], [48]–[50].

It is obvious that bone biopsy is not always feasible, which is required for *ex vivo* bone quality analysis. Therefore, the investigation of some surrogate tissue instead of bone will help to predict fracture risk of diabetic bone. For example, we have shown that fingernail tissue can be used as a surrogate marker to predict the bone quality of diabetic bone [208].

Finally, the advancements of *in vivo* bone quality assessments techniques will make possible to collect clinically relevant patient-specific diagnosis of diabetic bone fracture risk in the clinics.

7.5 Conclusive remarks

The findings of the current thesis are beneficial for clinicians to address the dilemma of bone fragility diagnosis in diabetes. The increased hyperglycemia, accumulation of NE-xLR, and total fAGE content in bone collagen are responsible for decreased apparent level bone tissue toughness and post-yield energy in the diabetic group. This reduction in energy required to fracture is the major cause of enhanced fracture risk in the diabetic group instead of aBMD. The message for clinicians from this study is that only diagnosing mineral content is insufficient to accurately diagnose diabetic bone fracture risk. Simultaneously, quantification of collagen quality and bone AGEs are also critical contributing parameters in bone fracture risk assessment. In conclusion, this thesis provides a foundation for studying the effects of T2D on bone quality.

References

- [1] M. C. Riddle *et al.*, “Introduction: Standards of Medical Care in Diabetes—2018,” *Diabetes Care*, vol. 41, no. Supplement 1, pp. S1–S2, 2018, doi: 10.2337/dc18-Sint01.
- [2] “International Diabetes Federation. IDF Diabetes Atlas, 8th edn. Brussels, Belgium: International Diabetes Federation, 2017. <http://www.diabetesatlas.org>,” Belgium, 2017.
- [3] M. Brownlee, M.D., “Advanced Protein Glycosylation in Diabetes and Aging,” *Annu. Rev. Med.*, vol. 46, no. 1, pp. 223–234, 1995, doi: 10.1146/annurev.med.46.1.223.
- [4] Diabetes Federation International, *IDF Diabetes Atlas Ninth edition 2019*. 2019.
- [5] P. Zhang *et al.*, “Global healthcare expenditure on diabetes for 2010 and 2030,” *Diabetes Res. Clin. Pract.*, vol. 87, no. 3, pp. 293–301, 2010, doi: 10.1016/j.diabres.2010.01.026.
- [6] D. E. Bonds *et al.*, “Risk of Fracture in Women with Type 2 Diabetes: the Women’s Health Initiative Observational Study,” *J. Clin. Endocrinol. Metab.*, vol. 91, no. 9, pp. 3404–3410, 2006, doi: 10.1210/jc.2006-0614.
- [7] P. Vestergaard, “Discrepancies in bone mineral density and fracture risk in patients with type 1 and type 2 diabetes - A meta-analysis,” *Osteoporos. Int.*, vol. 18, no. 4, pp. 427–444, 2007, doi: 10.1007/s00198-006-0253-4.
- [8] M. Janghorbani, R. M. Van Dam, W. C. Willett, and F. B. Hu, “Systematic review of type 1 and type 2 diabetes mellitus and risk of fracture,” *Am. J. Epidemiol.*, vol. 166, no. 5, pp. 495–505, 2007, doi: 10.1093/aje/kwm106.
- [9] A. C. Looker, M. S. Eberhardt, and S. H. Saydah, “Diabetes and fracture risk in older U.S. adults,” *Bone*, vol. 82, pp. 9–15, 2016, doi: 10.1016/j.bone.2014.12.008.
- [10] D. Martinez-Laguna *et al.*, “Incident type 2 diabetes and hip fracture risk: a population-based matched cohort study,” *Osteoporos. Int.*, vol. 26, no. 2, pp. 827–833, 2014, doi: 10.1007/s00198-014-2986-9.
- [11] A. V. Schwartz *et al.*, “Association of BMD and FRAX score with risk of fracture in older adults with type 2 diabetes,” *JAMA - J. Am. Med. Assoc.*, vol. 305, no. 21, pp. 2184–2192, 2011, doi: 10.1001/jama.2011.715.
- [12] R. Dhaliwal, D. Cibula, C. Ghosh, R. S. Weinstock, and A. M. Moses, “Bone quality assessment in type 2 diabetes mellitus,” *Osteoporos. Int.*, vol. 25, no. 7, pp. 1969–1973, 2014, doi: 10.1007/s00198-014-2704-7.
- [13] N. Jiang and W. Xia, “Assessment of bone quality in patients with diabetes mellitus,” *Osteoporos. Int.*, vol. 29, no. 8, pp. 1721–1736, 2018, doi: 10.1007/s00198-018-4532-7.
- [14] L. Karim, T. Rezaee, and R. Vaidya, “The Effect of Type 2 Diabetes on Bone Biomechanics,” *Curr. Osteoporos. Rep.*, 2019, doi: 10.1007/s11914-019-00526-w.
- [15] J. M. Patsch *et al.*, “Increased cortical porosity in type 2 diabetic postmenopausal women with fragility fractures,” *J. Bone Miner. Res.*, vol. 28, no. 2, pp. 313–324, 2013, doi: 10.1002/jbmr.1763.

- [16] A. J. Burghardt *et al.*, “High-resolution peripheral quantitative computed tomographic imaging of cortical and trabecular bone microarchitecture in patients with type 2 diabetes mellitus,” *J. Clin. Endocrinol. Metab.*, vol. 95, no. 11, pp. 5045–5055, 2010, doi: 10.1210/jc.2010-0226.
- [17] J. N. Farr and S. Khosla, “Determinants of bone strength and quality in diabetes mellitus in humans,” *Bone*, vol. 82, pp. 28–34, 2016, doi: 10.1016/j.bone.2015.07.027.
- [18] J. S. Linde, K. Hygum, and B. L. Langdahl, “Skeletal Fragility in Type 2 Diabetes Mellitus,” *Endocrinol. Metab.*, vol. 33, no. 3, pp. 339–351, 2018, doi: 10.3803/EnM.2018.33.3.339.
- [19] C. J. Thomas, T. P. Cleland, G. E. Sroga, and D. Vashishth, “Accumulation of carboxymethyl-lysine (CML) in human cortical bone,” *Bone*, no. Cml, 2018, doi: 10.1016/j.bone.2018.01.028.
- [20] P. Gkogkolou, M. Bohm, and M. Böhm, “Advanced glycation end products: key players in skin ageing?,” *Gkogkolou, Paraskevi Bohm, Markus*, vol. 4, no. 3, pp. 259–270, 2012, doi: 10.4161/derm.22028.
- [21] F. N. Schmidt *et al.*, “Assessment of collagen quality associated with non-enzymatic cross-links in human bone using Fourier-transform infrared imaging,” *Bone*, vol. 97, pp. 243–251, 2017, doi: 10.1016/j.bone.2017.01.015.
- [22] D. B. Burr, “Full Length Article: Changes in bone matrix properties with aging,” *Bone*, vol. 120, no. September 2018, pp. 85–93, 2019, doi: 10.1016/j.bone.2018.10.010.
- [23] M. R. Rubin *et al.*, “Advanced Glycation Endproducts and Bone Material Properties in Type 1 Diabetic Mice,” *PLoS One*, vol. 11, no. 5, p. e0154700, May 2016, doi: 10.1371/journal.pone.0154700.
- [24] R. K. Rai and N. Sinha, “Dehydration-induced structural changes in the collagen-hydroxyapatite interface in bone by high-resolution solid-state NMR spectroscopy,” *J. Phys. Chem. C*, vol. 115, no. 29, pp. 14219–14227, 2011, doi: 10.1021/jp2025768.
- [25] F. A. Sabet, A. R. Najafi, E. Hamed, and I. Jasiuk, “Modelling of bone fracture and strength at different length scales: A review,” *Interface Focus*, vol. 6, no. 1, pp. 20–30, 2016, doi: 10.1098/rsfs.2015.0055.
- [26] J.-Y. Rho, L. Kuhn-Spearing, and P. Zioupos, “Mechanical properties and the hierarchical structure of bone,” *Med. Eng. Phys.*, vol. 20, no. 2, pp. 92–102, 1998, doi: 10.1016/S1350-4533(98)00007-1.
- [27] S. Vignat-Carrin, P. Garnero, and P. D. Delmas, “The role of collagen in bone strength,” *Osteoporos. Int.*, vol. 17, no. 3, pp. 319–336, Mar. 2006, doi: 10.1007/s00198-005-2035-9.
- [28] A. L. Boskey, “Bone composition: relationship to bone fragility and antiosteoporotic drug effects,” *Bonekey Rep.*, vol. 2, no. DECEMBER, pp. 1–11, 2013, doi: 10.1038/bonekey.2013.181.
- [29] A. K. Nair, A. Gautieri, S.-W. Chang, and M. J. Buehler, “Molecular mechanics of mineralized collagen fibrils in bone,” *Nat. Commun.*, vol. 4, p. 1724, Apr. 2013, doi: 10.1038/ncomms2720.

- [30] F. W. Wehrli and M. A. Fernández-Seara, “Nuclear magnetic resonance studies of bone water,” *Ann. Biomed. Eng.*, vol. 33, no. 1, pp. 79–86, 2005, doi: 10.1007/s10439-005-8965-8.
- [31] R. K. Rai, C. Singh, and N. Sinha, “Predominant role of water in native collagen assembly inside the bone matrix,” *J. Phys. Chem. B*, vol. 119, no. 1, pp. 201–211, 2015, doi: 10.1021/jp511288g.
- [32] M. Granke, M. D. Does, and J. S. Nyman, “The Role of Water Compartments in the Material Properties of Cortical Bone,” *Calcif. Tissue Int.*, vol. 97, no. 3, pp. 292–307, 2015, doi: 10.1007/s00223-015-9977-5.
- [33] J. S. Nyman, Q. Ni, D. P. Nicoletta, and X. Wang, “Measurements of mobile and bound water by nuclear magnetic resonance correlate with mechanical properties of bone,” *Bone*, vol. 42, no. 1, pp. 193–199, 2008, doi: 10.1016/j.bone.2007.09.049.
- [34] A. K. Bembey, M. L. Oyen, A. J. Bushby, and A. Boyde, “Viscoelastic properties of bone as a function of hydration state determined by nanoindentation,” *Philos. Mag.*, vol. 86, no. 33-35 SPEC. ISSUE, pp. 5691–5703, 2006, doi: 10.1080/14786430600660864.
- [35] H. B. Hunt and E. Donnelly, “Bone quality assessment techniques: geometric, compositional, and mechanical characterization from macroscale to nanoscale,” *Clin Rev Bone Min. Metab.*, no. 14, pp. 133–149, 2016, doi: 10.1007/s12018-016-9222-4.
- [36] N. H. Hart, S. Nimphius, T. Rantalainen, A. Ireland, A. Sifarikas, and R. U. Newton, “Mechanical basis of bone strength: Influence of bone material, bone structure and muscle action,” *J. Musculoskelet. Neuronal Interact.*, vol. 17, no. 3, pp. 114–139, 2017.
- [37] C. A. M. Kulak and D. W. Dempster, “Bone histomorphometry: a concise review for endocrinologists and clinicians,” *Arq. Bras. Endocrinol. Metabol.*, vol. 54, no. 2, pp. 87–98, 2010, doi: 10.1590/s0004-27302010000200002.
- [38] P. Sihota *et al.*, “Investigation of mechanical, material and compositional determinants of human trabecular bone quality in type 2 diabetes,” *J. Clin. Endocrinol. Metab.*, 2021, doi: 10.1210/clinem/dgab027.
- [39] M. L. Bouxsein, “Bone quality: where do we go from here?,” *Osteoporos. Int.*, vol. 14, no. 0, pp. 118–127, 2003, doi: 10.1007/s00198-003-1489-x.
- [40] M. A. Gallant, D. M. Brown, J. M. Organ, M. R. Allen, and D. B. Burr, “Reference-point indentation correlates with bone toughness assessed using whole-bone traditional mechanical testing,” *Bone*, vol. 53, no. 1, pp. 301–305, 2013, doi: 10.1016/j.bone.2012.12.015.
- [41] C. Marin *et al.*, “Unraveling the compromised biomechanical performance of type 2 diabetes- and Roux-en-Y gastric bypass bone by linking mechanical-structural and physico-chemical properties,” *Sci. Rep.*, vol. 8, no. 1, pp. 1–12, 2018, doi: 10.1038/s41598-018-24229-x.
- [42] C. Acevedo *et al.*, “Contributions of Material Properties and Structure to Increased Bone Fragility for a Given Bone Mass in the UCD-T2DM Rat Model of Type 2 Diabetes,” *J. Bone Miner. Res.*, vol. 33, no. 6, pp. 1066–1075, 2018, doi: 10.1002/jbmr.3393.

- [43] D. A. Barrière *et al.*, “Combination of high-fat/high-fructose diet and low-dose streptozotocin to model long-term type-2 diabetes complications,” *Sci. Rep.*, vol. 8, no. 1, pp. 1–17, 2018, doi: 10.1038/s41598-017-18896-5.
- [44] D. Vashishth, G. J. Gibson, J. I. Khoury, M. B. Schaffler, J. Kimura, and D. P. Fyhrie, “Influence of nonenzymatic glycation on biomechanical properties of cortical bone,” *Bone*, vol. 28, no. 2, pp. 195–201, 2001, doi: 10.1016/S8756-3282(00)00434-8.
- [45] S. Y. Tang, U. Zeenath, and D. Vashishth, “Effects of non-enzymatic glycation on cancellous bone fragility,” *Bone*, vol. 40, no. 4, pp. 1144–1151, 2007, doi: 10.1016/j.bone.2006.12.056.
- [46] G. E. Sroga, A. Siddula, and D. Vashishth, “Glycation of human cortical and cancellous bone captures differences in the formation of maillard reaction products between glucose and ribose,” *PLoS One*, vol. 10, no. 2, pp. 1–19, 2015, doi: 10.1371/journal.pone.0117240.
- [47] L. Karim, S. Y. Tang, G. E. Sroga, and D. Vashishth, “Differences in non-enzymatic glycation and collagen cross-links between human cortical and cancellous bone,” *Osteoporos. Int.*, vol. 24, no. 9, pp. 2441–2447, 2013, doi: 10.1007/s00198-013-2319-4.
- [48] J. N. Farr, M. T. Drake, S. Amin, L. J. Melton, L. K. McCready, and S. Khosla, “In vivo assessment of bone quality in postmenopausal women with type 2 diabetes.,” *J. Bone Miner. Res.*, vol. 29, no. 4, pp. 787–95, 2014, doi: 10.1002/jbmr.2106.
- [49] A. G. Nilsson *et al.*, “Type 2 Diabetes Mellitus Is Associated With Better Bone Microarchitecture But Lower Bone Material Strength and Poorer Physical Function in Elderly Women: A Population-Based Study,” *J. Bone Miner. Res.*, vol. 32, no. 5, pp. 1062–1071, 2017, doi: 10.1002/jbmr.3057.
- [50] J. R. Furst *et al.*, “Advanced glycation endproducts and bone material strength in type 2 diabetes,” *J. Clin. Endocrinol. Metab.*, vol. 101, no. 6, pp. 2502–2510, 2016, doi: 10.1210/jc.2016-1437.
- [51] L. Karim *et al.*, “Bone microarchitecture, biomechanical properties, and advanced glycation end-products in the proximal femur of adults with type 2 diabetes,” *Bone*, 2018, doi: <https://doi.org/10.1016/j.bone.2018.05.030>.
- [52] A. Piccoli *et al.*, “Sclerostin Regulation, Microarchitecture, And Advanced Glycation End-Products In The Bone Of Elderly Women With Type 2 Diabetes,” *J. Bone Miner. Res.*, 2020, doi: 10.1002/jbmr.4153.
- [53] H. B. Hunt *et al.*, “Altered Tissue Composition, Microarchitecture, and Mechanical Performance in Cancellous Bone From Men With Type 2 Diabetes Mellitus,” *J. Bone Miner. Res.*, vol. 34, no. 7, pp. 1191–1206, Jul. 2019, doi: 10.1002/jbmr.3711.
- [54] L. Zhang *et al.*, “Bone biomechanical and histomorphometrical investment in type 2 diabetic Goto-Kakizaki rats,” *Acta Diabetol.*, vol. 46, no. 2, pp. 119–126, 2009, doi: 10.1007/s00592-008-0068-1.
- [55] Rhonda D Prisky, J. M. Swift, S. A. Bloomfiel, H. A. Hogan, and M. D. Delp, “Altered bone

- mass, geometry and mechanical properties during the development and progression of type 2 diabetes in the Zucker diabetic fatty rat,” *J. Endocrinol.*, vol. 199, no. 3, pp. 379–388, 2008, doi: 10.1677/JOE-08-0046.
- [56] J. S. Nyman *et al.*, “Increasing duration of type 1 diabetes perturbs the strength-structure relationship and increases brittleness of bone,” *Bone*, vol. 48, no. 4, pp. 733–740, 2011, doi: 10.1016/j.bone.2010.12.016.
- [57] A. Creecy *et al.*, “Changes in the Fracture Resistance of Bone with the Progression of Type 2 Diabetes in the ZDSD Rat,” *Calcif. Tissue Int.*, vol. 99, no. 3, pp. 289–301, 2016, doi: 10.1007/s00223-016-0149-z.
- [58] S. Reinwald, R. G. Peterson, M. R. Allen, and D. B. Burr, “Skeletal changes associated with the onset of type 2 diabetes in the ZDF and ZDSD rodent models,” *Am. J. Physiol. - Endocrinol. Metab.*, vol. 5120, pp. 765–774, 2009, doi: 10.1152/ajpendo.90937.2008.
- [59] M. J. Devlin *et al.*, “Early-onset type 2 diabetes impairs skeletal acquisition in the male TALLYHO/JngJ mouse,” *Endocrinology*, vol. 155, no. 10, pp. 3806–3816, 2014, doi: 10.1210/en.2014-1041.
- [60] A. J. Fields *et al.*, “Alterations in intervertebral disc composition, matrix homeostasis and biomechanical behavior in the UCD-T2DM rat model of type 2 diabetes,” *J Orthop Res. Author*, vol. 33, no. 5, pp. 738–746, 2015, doi: 10.1002/jor.22807.Alterations.
- [61] G. Kerckhofs *et al.*, “Changes in bone macro- and microstructure in diabetic obese mice revealed by high resolution microfocus X-ray computed tomography,” *Sci. Rep.*, vol. 6, no. September, pp. 1–13, 2016, doi: 10.1038/srep35517.
- [62] M. Saito, K. Fujii, Y. Mori, and K. Marumo, “Role of collagen enzymatic and glycation induced cross-links as a determinant of bone quality in spontaneously diabetic WBN/Kob rats,” *Osteoporos. Int.*, vol. 17, no. 10, pp. 1514–1523, 2006, doi: 10.1007/s00198-006-0155-5.
- [63] B. Wang, P. Chandrasekera, and J. Pippin, “Leptin- and Leptin Receptor-Deficient Rodent Models: Relevance for Human Type 2 Diabetes,” *Curr. Diabetes Rev.*, vol. 10, no. 2, pp. 131–145, 2014, doi: 10.2174/1573399810666140508121012.
- [64] R. J. Fajardo, L. Karim, V. I. Calley, and M. L. Bouxsein, “A review of rodent models of type 2 diabetic skeletal fragility,” *J. Bone Miner. Res.*, vol. 29, no. 5, pp. 1025–1040, 2014, doi: 10.1002/jbmr.2210.
- [65] K. Srinivasan, B. Viswanad, L. Asrat, C. L. Kaul, and P. Ramarao, “Combination of high-fat diet-fed and low-dose streptozotocin-treated rat: A model for type 2 diabetes and pharmacological screening,” *Pharmacol. Res.*, vol. 52, no. 4, pp. 313–320, 2005, doi: 10.1016/j.phrs.2005.05.004.
- [66] N. Erdal, S. Gürgül, S. Kavak, A. Yildiz, and M. Emre, “Deterioration of bone quality by streptozotocin (STZ)-induced type 2 diabetes mellitus in rats,” *Biol. Trace Elem. Res.*, vol. 140, no. 3, pp. 342–353, 2011, doi: 10.1007/s12011-010-8703-4.

- [67] K. Srinivasan and P. Ramarao, “Animal models in type 2 diabetes research: An overview,” *Indian J. Med. Res.*, vol. 136, no. 1, pp. 451–472, 2012.
- [68] S. Kimura, T. Sasase, T. Ohta, E. Sato, and M. Matsushita, “Characteristics of bone turnover, bone mass and bone strength in Spontaneously Diabetic Torii-Lepr fa rats,” *J. Bone Miner. Metab.*, vol. 30, no. 3, pp. 312–320, 2012, doi: 10.1007/s00774-011-0324-2.
- [69] G. K. Reddy, L. Stehno-Bittel, S. Hamade, and C. S. Enwemeka, “The biomechanical integrity of bone in experimental diabetes.,” *Diabetes Res. Clin. Pract.*, vol. 54, no. 1, pp. 1–8, 2001, doi: 10.1016/S0168-8227(01)00273-X.
- [70] A. Creecy, S. Uppuganti, M. Unal, R. Clay Bunn, P. Voziyan, and J. S. Nyman, “Low bone toughness in the TallyHO model of juvenile type 2 diabetes does not worsen with age,” *Bone*, vol. 110, pp. 204–214, 2018, doi: 10.1016/j.bone.2018.02.005.
- [71] S. S. Ionova-Martin *et al.*, “Changes in cortical bone response to high-fat diet from adolescence to adulthood in mice,” *Osteoporos. Int.*, vol. 22, no. 8, pp. 2283–2293, 2011, doi: 10.1007/s00198-010-1432-x.
- [72] M. J. Silva *et al.*, “Type 1 diabetes in young rats leads to progressive trabecular bone loss, cessation of cortical bone growth, and diminished whole bone strength and fatigue life,” *J. Bone Miner. Res.*, vol. 24, no. 9, pp. 1618–1627, 2009, doi: 10.1359/jbmr.090316.
- [73] D. Farlay, L. A. G. Armas, E. Gineyts, M. P. Akhter, R. R. Recker, and G. Boivin, “Nonenzymatic Glycation and Degree of Mineralization Are Higher in Bone from Fractured Patients with Type 1 Diabetes Mellitus,” *J. Bone Miner. Res.*, vol. 31, no. 1, pp. 190–195, 2016, doi: 10.1002/jbmr.2607.
- [74] H. B. Hunt, J. C. Pearl, D. R. Diaz, K. B. King, and E. Donnelly, “Bone Tissue Collagen Maturity and Mineral Content Increase With Sustained Hyperglycemia in the KK-Ay Murine Model of Type 2 Diabetes,” *J. Bone Miner. Res.*, vol. 33, no. 5, pp. 921–929, 2018, doi: 10.1002/jbmr.3365.
- [75] S. A. Mansur *et al.*, “Stable Incretin Mimetics Counter Rapid Deterioration of Bone Quality in Type 1 Diabetes Mellitus,” *J. Cell. Physiol.*, vol. 230, no. 12, pp. 3009–3018, 2015, doi: 10.1002/jcp.25033.
- [76] M. A. Hammond, M. A. Gallant, D. B. Burr, and J. M. Wallace, “Nanoscale changes in collagen are reflected in physical and mechanical properties of bone at the microscale in diabetic rats,” *Bone*, vol. 60, pp. 26–32, 2013, doi: 10.1016/j.bone.2013.11.015.
- [77] M. Zhang, X. Y. Lv, J. Li, Z. G. Xu, and L. Chen, “The characterization of high-fat diet and multiple low-dose streptozotocin induced type 2 diabetes rat model.,” *Exp. Diabetes Res.*, vol. 2008, p. 704045, 2008, doi: 10.1155/2008/704045.
- [78] F. Sassi *et al.*, “Type 2 diabetes affects bone cells precursors and bone turnover,” *BMC Endocr. Disord.*, vol. 18, no. 1, pp. 1–8, 2018, doi: 10.1186/s12902-018-0283-x.
- [79] D. Purnamasari, M. D. Puspitasari, B. Setiyohadi, P. Nugroho, and H. Isbagio, “Low bone

- turnover in premenopausal women with type 2 diabetes mellitus as an early process of diabetes-associated bone alterations: A cross-sectional study,” *BMC Endocr. Disord.*, vol. 17, no. 1, pp. 1–8, 2017, doi: 10.1186/s12902-017-0224-0.
- [80] N. Napoli *et al.*, “Bone Turnover Markers Do Not Predict Fracture Risk in Type 2 Diabetes,” *J. Bone Miner. Res.*, vol. 35, no. 12, pp. 2363–2371, 2020, doi: 10.1002/jbmr.4140.
- [81] J. Starup-Linde, “Diabetes, biochemical markers of bone turnover, diabetes control, and bone,” *Front. Endocrinol. (Lausanne)*, vol. 4, no. MAR, pp. 1–17, 2013, doi: 10.3389/fendo.2013.00021.
- [82] Y. Katayama, T. Akatsu, M. Yamamoto, N. Kugai, and N. Nagata, “Role of nonenzymatic glycosylation of type I collagen in diabetic osteopenia,” *J. Bone Miner. Res.*, vol. 11, no. 7, pp. 931–937, 1996, doi: 10.1002/jbmr.5650110709.
- [83] A. D. McCarthy, S. B. Etcheverry, L. Bruzzone, G. Lettieri, D. A. Barrio, and A. M. Cortizo, “Non-enzymatic glycosylation of a type 1 collagen matrix: Effects on osteoblastic development and oxidative stress,” *BMC Cell Biol.*, vol. 2, 2001, doi: 10.1186/1471-2121-2-16.
- [84] U. Valcourt, B. Merle, E. Gineyts, S. Viguier-Carrin, P. D. Delmas, and P. Garnero, “Non-enzymatic glycation of bone collagen modifies osteoclastic activity and differentiation,” *J. Biol. Chem.*, vol. 282, no. 8, pp. 5691–5703, 2007, doi: 10.1074/jbc.M610536200.
- [85] M. A. Petit *et al.*, “Bone mass and strength in older men with type 2 diabetes: The osteoporotic fractures in men study,” *J. Bone Miner. Res.*, vol. 25, no. 2, pp. 285–291, 2010, doi: 10.1359/jbmr.090725.
- [86] A. Shu *et al.*, “Bone structure and turnover in type 2 diabetes mellitus,” *Osteoporos. Int.*, vol. 23, no. 2, pp. 635–41, 2012, doi: 10.1007/s00198-011-1595-0.
- [87] J. Paccou, K. A. Ward, K. A. Jameson, E. M. Dennison, C. Cooper, and M. H. Edwards, “Bone Microarchitecture in Men and Women with Diabetes: The Importance of Cortical Porosity,” *Calcif. Tissue Int.*, vol. 98, no. 5, pp. 465–473, 2016, doi: 10.1007/s00223-015-0100-8.
- [88] S. D. Elizabeth J. Samelson *et al.*, “Diabetes and deficits in cortical bone density, microarchitecture, and bone size: Framingham HR-pQCT Study,” *J Bone Min. Res.*, 2018, doi: 10.1002/jbmr.3240.
- [89] J. M. Pritchard *et al.*, “Bone mineralization is elevated and less heterogeneous in adults with type 2 diabetes and osteoarthritis compared to controls with osteoarthritis alone,” *Bone*, vol. 54, no. 1, pp. 76–82, 2013, doi: 10.1016/j.bone.2013.01.032.
- [90] E. M. Wölfel; *et al.*, “Individuals with type 2 diabetes mellitus show dimorphic and heterogeneous patterns of loss in femoral bone quality,” *Bone*, p. 125871, 2020, doi: 10.1016/j.bone.2020.115556.
- [91] Y. Chen *et al.*, “Abnormal subchondral bone remodeling and its association with articular

- cartilage degradation in knees of type 2 diabetes patients,” *Bone Res.*, vol. 5, no. December 2016, p. 17034, 2017, doi: 10.1038/boneres.2017.34.
- [92] N. Napoli *et al.*, “Vertebral Fracture Risk in Diabetic Elderly Men: The MrOS Study,” *J. Bone Miner. Res.*, vol. 33, no. 1, pp. 63–69, 2018, doi: 10.1002/jbmr.3287.
- [93] L. J. Melton *et al.*, “A bone structural basis for fracture risk in diabetes,” *J. Clin. Endocrinol. Metab.*, vol. 93, no. 12, pp. 4804–4809, 2008, doi: 10.1210/jc.2008-0639.
- [94] C. Hamann *et al.*, “Sclerostin antibody treatment improves bone mass, bone strength, and bone defect regeneration in rats with type 2 diabetes mellitus,” *J. Bone Miner. Res.*, vol. 28, no. 3, pp. 627–638, 2013, doi: 10.1002/jbmr.1803.
- [95] S. S. Ionova-Martina *et al.*, “Reduced size-independent mechanical properties of cortical bone in high-fat diet-induced obesity,” vol. 46, no. 1, pp. 217–225, 2009, doi: 10.1016/j.bone.2009.10.015.Reduced.
- [96] K. N. Ealey, D. Fonseca, M. C. Archer, and W. E. Ward, “Bone abnormalities in adolescent leptin-deficient mice,” *Regul. Pept.*, vol. 136, no. 1–3, pp. 9–13, 2006, doi: 10.1016/j.regpep.2006.04.013.
- [97] V. V. Shanbhogue *et al.*, “Bone Geometry, Volumetric Density, Microarchitecture, and Estimated Bone Strength Assessed by HR-pQCT in Adult Patients with Type 1 Diabetes Mellitus,” *J. Bone Miner. Res.*, vol. 30, no. 12, pp. 2188–2199, 2015, doi: 10.1002/jbmr.2573.
- [98] M. Yamamoto, T. Yamaguchi, M. Yamauchi, S. Yano, and T. Sugimoto, “Serum pentosidine levels are positively associated with the presence of vertebral fractures in postmenopausal women with type 2 diabetes,” *J. Clin. Endocrinol. Metab.*, vol. 93, no. 3, pp. 1013–1019, 2008, doi: 10.1210/jc.2007-1270.
- [99] A. Schwartz *et al.*, “Older women with diabetes have an increased risk of fracture: a prospective study,” *J Clin Endocrinol Metab.*, vol. 86, no. 1, pp. 32–38, 2001.
- [100] A. V. Schwartz *et al.*, “Pentosidine and increased fracture risk in older adults with type 2 diabetes,” *J. Clin. Endocrinol. Metab.*, vol. 94, no. 7, pp. 2380–2386, 2009, doi: 10.1210/jc.2008-2498.
- [101] F. Xu *et al.*, “Decreased osteoclastogenesis, osteoblastogenesis and low bone mass in a mouse model of type 2 diabetes,” *Mol. Med. Rep.*, vol. 10, no. 4, pp. 1935–1941, 2014, doi: 10.3892/mmr.2014.2430.
- [102] G. Kerckhofs *et al.*, “Changes in bone macro-and microstructure in diabetic obese mice revealed by high resolution microfocus X-ray computed tomography,” *Sci. Rep.*, vol. 6, no. September, pp. 1–13, 2016, doi: 10.1038/srep35517.
- [103] L. Huang *et al.*, “Validity of leptin receptor-deficiency (db/db) type 2 diabetes mellitus mice as a model of secondary osteoporosis,” *Sci. Rep.*, vol. 6, no. December 2015, pp. 1–7, 2016, doi: 10.1038/srep27745.
- [104] S. Sekar, A. Chandrasekaran, U. Rao, and T. P. Sastry, “Comparison of some of the

- physicochemical characteristics of type 2 diabetic and normal human bones: A sample study,” *J. Diabetes Complications*, vol. 25, no. 3, pp. 187–192, 2011, doi: 10.1016/j.jdiacomp.2010.07.003.
- [105] S. F. Bozkurt O, Bilgin MD, Evis Z, Pleshko N, “Early Alterations in Bone Characteristics of Type i Diabetic Rat Femur: A Fourier Transform Infrared (FT-IR) Imaging Study,” *Appl. Spectrosc.*, vol. 70, no. 12, pp. 2005–2015, 2016, doi: doi:10.1177/0003702816671059.
- [106] H. Boyar, B. Turan, and F. Severcan, “FTIR spectroscopic investigation of mineral structure of streptozotocin induced diabetic rat femur and tibia,” *Spectroscopy*, vol. 17, no. 2–3, pp. 627–633, 2003, doi: 10.1155/2003/826545.
- [107] A. Mieczkowska, S. A. Mansur, N. Irwin, P. R. Flatt, D. Chappard, and G. Mabileau, “Alteration of the bone tissue material properties in type 1 diabetes mellitus: A Fourier transform infrared microspectroscopy study,” *Bone*, vol. 76, pp. 31–39, 2015, doi: 10.1016/j.bone.2015.03.010.
- [108] T. W. Oren, S. Botolin, A. Williams, A. Bucknell, and K. B. King, “Arthroplasty in veterans: Analysis of cartilage, bone, serum, and synovial fluid reveals differences and similarities in osteoarthritis with and without comorbid diabetes,” *J. Rehabil. Res. Dev.*, vol. 48, no. 10, pp. 1195–1210, 2011, doi: 10.1682/JRRD.2010.09.0186.
- [109] J. C. Krakauer, M. J. McKenna, N. F. Buderer, D. Sudhaker Rao, F. W. Whitehouse, and A. Michael Parfitt, “Bone loss and bone turnover in diabetes,” *Diabetes*, vol. 44, no. 7, pp. 775–782, 1995, doi: 10.2337/diab.44.7.775.
- [110] T. M. Link and G. Kazakia, “Update on Imaging-Based Measurement of Bone Mineral Density and Quality,” *Curr. Rheumatol. Rep.*, vol. 22, no. 5, 2020, doi: 10.1007/s11926-020-00892-w.
- [111] J. Damilakis, J. E. Adams, G. Guglielmi, and T. M. Link, “Radiation exposure in X-ray-based imaging techniques used in osteoporosis,” *Eur. Radiol.*, vol. 20, no. 11, pp. 2707–2714, 2010, doi: 10.1007/s00330-010-1845-0.
- [112] K. Engelke *et al.*, “Quantitative computed tomography (QCT) of the forearm using general purpose spiral whole-body CT scanners: Accuracy, precision and comparison with dual-energy X-ray absorptiometry (DXA),” *Bone*, vol. 45, no. 1, pp. 110–118, 2009, doi: 10.1016/j.bone.2009.03.669.
- [113] C. Schmidt *et al.*, “Precision and accuracy of peripheral quantitative computed tomography (pQCT) in the mouse skeleton compared with histology and microcomputed tomography (μ CT),” *J. Bone Miner. Res.*, vol. 18, no. 8, pp. 1486–1496, 2003, doi: 10.1359/jbmr.2003.18.8.1486.
- [114] K. Chiba *et al.*, “Precision of Second-Generation High-Resolution Peripheral Quantitative Computed Tomography: Intra- and Intertester Reproducibilities and Factors Involved in the Reproducibility of Cortical Porosity,” *J. Clin. Densitom.*, vol. 21, no. 2, pp. 295–302, 2018,

- doi: 10.1016/j.jocd.2017.01.006.
- [115] A. Kroker, R. Plett, K. K. Nishiyama, D. D. McErlain, C. Sandino, and S. K. Boyd, “Distal skeletal tibia assessed by HR-pQCT is highly correlated with femoral and lumbar vertebra failure loads,” *J. Biomech.*, vol. 59, no. 2017, pp. 43–49, 2017, doi: 10.1016/j.jbiomech.2017.05.011.
- [116] G. Iori *et al.*, “Large cortical bone pores in the tibia are associated with proximal femur strength,” *PLoS One*, vol. 14, no. 4, pp. 1–18, 2019, doi: 10.1371/journal.pone.0215405.
- [117] P. Tothill and W. J. Hannan, “Precision and accuracy of measuring changes in bone mineral density by dual-energy X-ray absorptiometry,” *Osteoporos. Int.*, vol. 18, no. 11, pp. 1515–1523, Nov. 2007, doi: 10.1007/s00198-007-0382-4.
- [118] S. L. Ferrari *et al.*, “Diagnosis and management of bone fragility in diabetes: an emerging challenge,” *Osteoporos. Int.*, vol. 29, no. 12, pp. 2585–2596, 2018, doi: 10.1007/s00198-018-4650-2.
- [119] W. D. Leslie, B. Aubry-Rozier, O. Lamy, and D. Hans, “TBS (trabecular bone score) and diabetes-related fracture risk,” *J. Clin. Endocrinol. Metab.*, vol. 98, no. 2, pp. 602–609, 2013, doi: 10.1210/jc.2012-3118.
- [120] E. V. McCloskey *et al.*, “A Meta-Analysis of Trabecular Bone Score in Fracture Risk Prediction and Its Relationship to FRAX,” *J. Bone Miner. Res.*, vol. 31, no. 5, pp. 940–948, 2016, doi: 10.1002/jbmr.2734.
- [121] J. P. Bilezikian *et al.*, “Abaloparatide-SC improves trabecular microarchitecture as assessed by trabecular bone score (TBS): a 24-week randomized clinical trial,” *Osteoporos. Int.*, vol. 29, no. 2, pp. 323–328, 2018, doi: 10.1007/s00198-017-4304-9.
- [122] L. Imbert, J. C. Auregan, K. Pernelle, and T. Hoc, “Microstructure and compressive mechanical properties of cortical bone in children with osteogenesis imperfecta treated with bisphosphonates compared with healthy children,” *J. Mech. Behav. Biomed. Mater.*, vol. 46, pp. 261–270, 2015, doi: 10.1016/j.jmbbm.2014.12.020.
- [123] M. L. Bouxsein, S. K. Boyd, B. A. Christiansen, R. E. Guldberg, K. J. Jepsen, and R. Müller, “Guidelines for assessment of bone microstructure in rodents using micro-computed tomography,” *J. Bone Miner. Res.*, vol. 25, no. 7, pp. 1468–1486, 2010, doi: 10.1002/jbmr.141.
- [124] H. Hemmatian *et al.*, “Accuracy and reproducibility of mouse cortical bone microporosity as quantified by desktop microcomputed tomography,” *PLoS One*, vol. 12, no. 8, pp. 1–16, 2017, doi: 10.1371/journal.pone.0182996.
- [125] A. M. Parfitt *et al.*, “Bone histomorphometry: Standardization of nomenclature, symbols, and units: Report of the asbmr histomorphometry nomenclature committee,” *J. Bone Miner. Res.*, vol. 2, no. 6, pp. 595–610, 1987, doi: 10.1002/jbmr.5650020617.
- [126] J. S. Manavalan *et al.*, “Circulating osteogenic precursor cells in type 2 diabetes mellitus,” *J.*

- Clin. Endocrinol. Metab.*, vol. 97, no. 9, pp. 3240–3250, 2012, doi: 10.1210/jc.2012-1546.
- [127] Y. H. An and R. A. Draughn, “Mechanical testing of bone and the bone implant interface,” p. 624, 2000, doi: 10.1088/1751-8113/44/8/085201.
- [128] K. A. Belill, T. L. Settle, C. R. Angel, S. Kim, and S. W. Rothwell, “Femoral strength after induced lesions in rats,” *Comp. Med.*, vol. 64, no. 3, pp. 186–92, 2014.
- [129] K. J. Jepsen, M. J. Silva, D. Vashishth, X. E. Guo, and M. C. H. Van Der Meulen, “Establishing biomechanical mechanisms in mouse models: Practical guidelines for systematically evaluating phenotypic changes in the diaphyses of long bones,” *J. Bone Miner. Res.*, vol. 30, no. 6, pp. 951–966, 2015, doi: 10.1002/jbmr.2539.
- [130] P. Sihota *et al.*, “Development of HFD -fed/low dose STZ treated female Sprague Dawley rat model to investigate diabetic bone fragility at different organization levels ,” *JBMR Plus*, 2020, doi: 10.1002/jbm4.10379.
- [131] M. J. Silva, M. D. Brodt, Z. Fan, and J. Y. Rho, “Nanoindentation and whole-bone bending estimates of material properties in bones from the senescence accelerated mouse SAMP6,” *J. Biomech.*, vol. 37, no. 11, pp. 1639–1646, 2004, doi: 10.1016/j.jbiomech.2004.02.018.
- [132] J. Wang *et al.*, “Trabecular plates and rods determine elastic modulus and yield strength of human trabecular bone,” *Bone*, vol. 72, pp. 71–80, Mar. 2015, doi: 10.1016/J.BONE.2014.11.006.
- [133] L. Karim and D. Vashishth, “Heterogeneous glycation of cancellous bone and its association with bone quality and fragility,” *PLoS One*, vol. 7, no. 4, 2012, doi: 10.1371/journal.pone.0035047.
- [134] L. Karim, M. Van Vliet, and M. L. Bouxsein, “Comparison of cyclic and impact-based reference point indentation measurements in human cadaveric tibia,” *Bone*, vol. 106, pp. 90–95, 2018, doi: 10.1016/j.bone.2015.03.021.
- [135] A. Setters and I. Jasiuk, “Towards a standardized reference point indentation testing procedure,” *J. Mech. Behav. Biomed. Mater.*, vol. 34, pp. 57–65, 2014, doi: 10.1016/j.jmbbm.2014.01.012.
- [136] P. Hansma *et al.*, “The bone diagnostic instrument II: Indentation distance increase,” *Rev. Sci. Instrum.*, vol. 79, no. 6, pp. 1–8, 2008, doi: 10.1063/1.2937199.
- [137] M. R. Allen, C. L. Newman, E. Smith, D. M. Brown, and J. M. Organ, “Variability of in vivo reference point indentation in skeletally mature inbred rats,” *J Biomech*, vol. 47, no. 10, pp. 2504–2507, 2014, doi: 10.1016/j.jbiomech.2014.04.035.
- [138] A. Diez-Perez *et al.*, “Technical note: Recommendations for a standard procedure to assess cortical bone at the tissue-level in vivo using impact microindentation,” *Bone Reports*, vol. 5, pp. 181–185, 2016, doi: 10.1016/j.bonr.2016.07.004.
- [139] D. Bridges, C. Randall, and P. K. Hansma, “A new device for performing reference point indentation without a reference probe,” *Rev. Sci. Instrum.*, vol. 83, no. 4, 2012, doi:

- 10.1063/1.3693085.
- [140] C. Randall *et al.*, “Applications of a New Handheld Reference Point Indentation Instrument Measuring Bone Material Strength,” *J Med Device*, vol. 7, no. 4, pp. 410051–410056, 2013, doi: 10.1115/1.4024829.
- [141] D. Sundh *et al.*, “High-Impact Mechanical Loading Increases Bone Material Strength in Postmenopausal Women—A 3-Month Intervention Study,” *J. Bone Miner. Res.*, vol. 33, no. 7, pp. 1242–1251, 2018, doi: 10.1002/jbmr.3431.
- [142] M. R. Allen, E. M. B. McNerny, J. M. Organ, and J. M. Wallace, “True gold or pyrite: A review of reference point indentation for assessing bone mechanical properties in vivo,” *J. Bone Miner. Res.*, vol. 30, no. 9, pp. 1539–1550, 2015, doi: 10.1002/jbmr.2603.
- [143] C. Edward Hoffer, X. Edward Guo, P. K. Zysset, and S. A. Goldstein, “An application of nanoindentation technique to measure bone tissue lamellae properties,” *J. Biomech. Eng.*, vol. 127, no. 7, pp. 1046–1053, 2005, doi: 10.1115/1.2073671.
- [144] B. Bhushan, “Depth-sensing nanoindentation measurement techniques and applications,” *Microsyst. Technol.*, vol. 23, no. 5, pp. 1595–1649, 2017, doi: 10.1007/s00542-017-3372-2.
- [145] K. Saini, D. Discher, and N. Kumar, “Static and time-dependent mechanical response of organic matrix of bone,” *J. Mech. Behav. Biomed. Mater.*, vol. 91, no. December 2018, pp. 315–325, 2019, doi: 10.1016/j.jmbbm.2018.12.031.
- [146] W. C. Oliver and G. M. Pharr, “An improved technique for determining hardness and elastic modulus using load and displacement sensing indentation experiments,” *J. Mater. Res.*, vol. 7, no. 06, pp. 1564–1583, Jun. 1992, doi: 10.1557/JMR.1992.1564.
- [147] R. Das, A. Kumar, A. Patel, S. Vijay, S. Saurabh, and N. Kumar, “Biomechanical characterization of spider webs,” *J. Mech. Behav. Biomed. Mater.*, vol. 67, no. September 2016, pp. 101–109, 2017, doi: 10.1016/j.jmbbm.2016.12.008.
- [148] H. Isaksson, S. Nagao, M. Małkiewicz, P. Julkunen, R. Nowak, and J. S. Jurvelin, “Precision of nanoindentation protocols for measurement of viscoelasticity in cortical and trabecular bone,” *J. Biomech.*, vol. 43, no. 12, pp. 2410–2417, 2010, doi: 10.1016/j.jbiomech.2010.04.017.
- [149] E. Donnelly, S. P. Baker, A. L. Boskey, and M. C. H. Van Der Meulen, “Effects of surface roughness and maximum load on the mechanical properties of cancellous bone measured by nanoindentation,” *Mater. Res. Soc. Symp. - Proc.*, vol. 823, no. 2, pp. 103–108, 2004, doi: 10.1557/proc-823-w8.5.
- [150] N. Rodriguez-Florez *et al.*, “An investigation of the mineral in ductile and brittle cortical mouse bone,” *J. Bone Miner. Res.*, vol. 30, no. 5, pp. 786–795, 2015, doi: 10.1002/jbmr.2414.
- [151] L. D. Mkukuma, C. T. Imrie, J. M. S. Skakle, D. W. L. Hukins, and R. M. Aspden, “Thermal stability and structure of cancellous bone mineral from the femoral head of patients with osteoarthritis or osteoporosis,” *Ann. Rheum. Dis.*, vol. 64, no. 2, pp. 222–225, 2005, doi:

- 10.1136/ard.2004.021329.
- [152] M. Suryanarayana, C., Grant Norton, *X-Ray Diffraction A practical Approach*, vol. 53. 1998.
- [153] D. Farlay, G. Panczer, C. Rey, P. D. Delmas, and G. Boivin, “Mineral maturity and crystallinity index are distinct characteristics of bone mineral,” *J. Bone Miner. Metab.*, vol. 28, no. 4, pp. 433–445, 2010, doi: 10.1007/s00774-009-0146-7.
- [154] M. J. Turunen *et al.*, “Bone mineral crystal size and organization vary across mature rat bone cortex,” *J. Struct. Biol.*, vol. 195, no. 3, pp. 337–344, Sep. 2016, doi: 10.1016/j.jsb.2016.07.005.
- [155] U. Vetter, E. D. Eanes, J. B. Kopp, J. D. Termine, and P. G. Robey, “Changes in apatite crystal size in bones of patients with osteogenesis imperfecta,” *Calcif. Tissue Int.*, vol. 49, no. 4, pp. 248–250, 1991, doi: 10.1007/BF02556213.
- [156] B. Foley, M. Greiner, G. McGlynn, and W. W. Schmahl, “Anatomical variation of human bone bioapatite crystallography,” *Crystals*, vol. 10, no. 10, pp. 1–25, 2020, doi: 10.3390/cryst10100859.
- [157] Maximilien Vanleene, A. Porter, P.-V. Guillot, A. Boyde, M. Oyen, and S. Shefelbine, “Ultrastructural defects cause low bone matrix stiffness despite high mineralization in osteogenesis imperfecta mice,” *Bone*, vol. 50, no. 6, pp. 1317–1323, 2012, doi: 10.1016/j.bone.2012.03.007.
- [158] P. Fratzl *et al.*, “Mineral crystals in calcified tissues: A comparative study by SAXS,” *J. Bone Miner. Res.*, vol. 7, no. 3, pp. 329–334, Dec. 2009, doi: 10.1002/jbmr.5650070313.
- [159] C. Giannini *et al.*, “Scanning SAXS-WAXS microscopy on osteoarthritis-affected bone - An age-related study,” *J. Appl. Crystallogr.*, vol. 47, no. 1, pp. 110–117, 2014, doi: 10.1107/S1600576713030215.
- [160] A. A. Poundarik, A. Boskey, C. Gundberg, and D. Vashishth, “Biomolecular regulation, composition and nanoarchitecture of bone mineral,” *Sci. Rep.*, vol. 8, no. 1, p. 1191, 2018, doi: 10.1038/s41598-018-19253-w.
- [161] P. Fratzl, P. Roschger, J. Eschberger, B. Abendroth, and K. Klaushofer, “Abnormal bone mineralization after fluoride treatment in osteoporosis: A small-angle x-ray-scattering study,” *J. Bone Miner. Res.*, vol. 9, no. 10, pp. 1541–1549, 1994, doi: 10.1002/jbmr.5650091006.
- [162] S. Rinnerthaler, P. Roschger, H. F. Jakob, A. Nader, K. Klaushofer, and P. Fratzl, “Scanning small angle X-ray scattering analysis of human bone sections,” *Calcif. Tissue Int.*, vol. 64, no. 5, pp. 422–429, 1999, doi: 10.1007/PL00005824.
- [163] R. Naresh *et al.*, “Prediction of mechanical properties of trabecular bone in patients with type 2 diabetes using damage based finite element method,” *J. Biomech.*, vol. 123, p. 110495, 2021, doi: 10.1016/j.jbiomech.2021.110495.
- [164] B. Hofko, M. Z. Alavi, H. Grothe, D. Jones, and J. Harvey, “Repeatability and sensitivity of FTIR ATR spectral analysis methods for bituminous binders,” *Mater. Struct. Constr.*, vol. 50, no. 3, pp. 1–15, 2017, doi: 10.1617/s11527-017-1059-x.

- [165] A. Boskey and R. Mendelsohn, "Infrared analysis of bone in health and disease," *J. Biomed. Opt.*, vol. 10, no. 3, p. 31102, 2005, doi: 10.1117/1.1922927.
- [166] L. Spevak, C. R. Flach, T. Hunter, R. Mendelsohn, and A. L. Boskey, "FTIRI Parameters describing Acid Phosphate Substitution in Biologic Hydroxyapatite," *Calcif. Tissue Int.*, vol. 92, no. 5, pp. 418–428, 2013, doi: 10.1007/s00223-013-9695-9.
- [167] E. P. Paschalis, S. Gamsjaeger, D. N. Tatakis, N. Hassler, S. P. Robins, and K. Klaushofer, "Fourier transform infrared spectroscopic characterization of mineralizing type I collagen enzymatic trivalent cross-links," *Calcif. Tissue Int.*, vol. 96, no. 1, pp. 18–29, 2014, doi: 10.1007/s00223-014-9933-9.
- [168] D. Farlay *et al.*, "The ratio 1660/1690 cm⁻¹ measured by infrared microspectroscopy is not specific of enzymatic collagen cross-links in bone tissue," *PLoS One*, vol. 6, no. 12, 2011, doi: 10.1371/journal.pone.0028736.
- [169] A. L. Boskey and R. Mendelsohn, "Infrared spectroscopic characterization of mineralized tissues," *Vib. Spectrosc.*, vol. 38, no. 1–2, pp. 107–114, 2005, doi: 10.1016/j.vibspec.2005.02.015.
- [170] M. D. Morris and G. S. Mandair, "Raman Assessment of Bone Quality," 2010, doi: 10.1007/s11999-010-1692-y.
- [171] E. A. Taylor and E. Donnelly, "Raman and Fourier transform infrared imaging for characterization of bone material properties," *Bone*, vol. 139, no. May, p. 115490, 2020, doi: 10.1016/j.bone.2020.115490.
- [172] P. Roschger, P. Fratzl, J. Eschberger, and K. Klaushofer, "Validation of quantitative backscattered electron imaging for the measurement of mineral density distribution in human bone biopsies," *Bone*, vol. 23, no. 4, pp. 319–326, 1998, doi: 10.1016/S8756-3282(98)00112-4.
- [173] N. Kourkoumelis, I. Balatsoukas, and M. Tzaphlidou, "Ca/P concentration ratio at different sites of normal and osteoporotic rabbit bones evaluated by Auger and energy dispersive X-ray spectroscopy," *J. Biol. Phys.*, vol. 38, no. 2, pp. 279–291, 2012, doi: 10.1007/s10867-011-9247-3.
- [174] C. Perdikouri, M. Tägil, and H. Isaksson, "Characterizing the composition of bone formed during fracture healing using scanning electron microscopy techniques," *Calcif. Tissue Int.*, vol. 96, no. 1, pp. 11–17, 2015, doi: 10.1007/s00223-014-9930-z.
- [175] S. J. Eppell, W. Tong, J. L. Katz, L. Kuhn, and M. J. Glimcher, "Shape and size of isolated bone mineralites measured using atomic force microscopy," *J. Orthop. Res.*, vol. 19, no. 6, pp. 1027–34, 2001, doi: 10.1016/S0736-0266(01)00034-1.
- [176] P. J. Thurner, E. Oroudjev, R. Jungmann, C. Kreutz, J. H. Kindt, and G. Schitter, "Imaging of Bone Ultrastructure using Atomic Force Microscopy," *Mod. Res. Educ. Top. Microsc.*, pp. 37–48, 2007.

- [177] T. Hassenkam, G. E. Fantner, J. A. Cutroni, J. C. Weaver, D. E. Morse, and P. K. Hansma, “High-resolution AFM imaging of intact and fractured trabecular bone,” *Bone*, vol. 35, no. 1, pp. 4–10, 2004, doi: 10.1016/j.bone.2004.02.024.
- [178] T. Hassenkam, H. L. Jørgensen, M. B. Pedersen, A. H. Kourakis, L. Simonsen, and J. B. Lauritzen, “Atomic force microscopy on human trabecular bone from an old woman with osteoporotic fractures,” *Micron*, vol. 36, no. 7–8, pp. 681–687, 2005, doi: 10.1016/j.micron.2005.06.007.
- [179] A. A. Poundarik *et al.*, “A direct role of collagen glycation in bone fracture,” *J. Mech. Behav. Biomed. Mater.*, vol. 52, pp. 120–130, 2015, doi: 10.1016/j.jmbbm.2015.08.012.
- [180] J. F. Woessner, “The determination of hydroxyproline in tissue and protein samples containing small proportions of this imino acid,” *Arch. Biochem. Biophys.*, vol. 93, no. 2, pp. 440–447, 1961, doi: 10.1016/0003-9861(61)90291-0.
- [181] J. E. Eastoe, “The amino acid composition of mammalian collagen and gelatin,” *Biochem. J.*, vol. 61, no. 4, pp. 589–600, 1955, doi: 10.1042/bj0610589.
- [182] K. Wongdee and N. Charoenphandhu, “Update on type 2 diabetes-related osteoporosis,” *World J. Diabetes*, vol. 6, no. 5, pp. 673–8, 2015, doi: 10.4239/wjd.v6.i5.673.
- [183] K. H. Mroue, A. Viswan, N. Sinha, and A. Ramamoorthy, *Solid-State NMR Spectroscopy: The Magic Wand to View Bone at Nanoscopic Resolution*, 1st ed., vol. 92. Elsevier Ltd., 2017.
- [184] G. E. Sroga and D. Vashishth, “UPLC methodology for identification and quantitation of naturally fluorescent crosslinks in proteins: A study of bone collagen,” *J. Chromatogr. B Anal. Technol. Biomed. Life Sci.*, vol. 879, no. 5–6, pp. 379–385, 2011, doi: 10.1016/j.jchromb.2010.12.024.
- [185] M. Saito, K. Marumo, K. Fujii, and N. Ishioka, “Single-column high-performance liquid chromatographic-fluorescence detection of immature, mature, and senescent cross-links of collagen,” *Anal. Biochem.*, vol. 253, no. 1, pp. 26–32, 1997, doi: 10.1006/abio.1997.2350.
- [186] M. Saito, Y. Kida, S. Kato, and K. Marumo, “Diabetes, collagen, and bone quality,” *Curr. Osteoporos. Rep.*, vol. 12, no. 2, pp. 181–188, 2014, doi: 10.1007/s11914-014-0202-7.
- [187] M. Saito and K. Marumo, “Collagen cross-links as a determinant of bone quality: A possible explanation for bone fragility in aging, osteoporosis, and diabetes mellitus,” *Osteoporos. Int.*, vol. 21, no. 2, pp. 195–214, 2010, doi: 10.1007/s00198-009-1066-z.
- [188] J. S. Walsh and T. Vilaca, “Obesity, Type 2 Diabetes and Bone in Adults,” *Calcif. Tissue Int.*, vol. 100, no. 5, pp. 528–535, 2017, doi: 10.1007/s00223-016-0229-0.
- [189] Y. M. Cho, “Characteristics of the pathophysiology of type 2 diabetes in Asians,” *Ann. Laparosc. Endosc. Surg.*, vol. 2, pp. 14–14, 2017, doi: 10.21037/ales.2017.01.03.
- [190] J. C. N. Chan, R. Yeung, and A. Luk, “The Asian diabetes phenotypes: Challenges and opportunities,” *Diabetes Res. Clin. Pract.*, vol. 105, no. 1, pp. 135–139, 2014, doi: 10.1016/j.diabres.2014.05.011.

- [191] M. Fukushima *et al.*, “Insulin secretion and insulin sensitivity at different stages of glucose tolerance: A cross-sectional study of Japanese type 2 diabetes,” *Metabolism.*, vol. 53, no. 7, pp. 831–835, 2004, doi: 10.1016/j.metabol.2004.02.012.
- [192] K. Matsumoto *et al.*, “Glucose tolerance, insulin secretion, and insulin sensitivity in nonobese and obese Japanese subjects,” *Diabetes Care*, vol. 20, no. 10, pp. 1562–1568, 1997, doi: 10.2337/diacare.20.10.1562.
- [193] M. Doube *et al.*, “BoneJ: Free and extensible bone image analysis in ImageJ,” *Bone*, vol. 47, no. 6, pp. 1076–1079, 2010, doi: 10.1016/j.bone.2010.08.023.
- [194] A. Diez-Perez *et al.*, “Microindentation for in vivo measurement of bone tissue mechanical properties in humans,” *J. Bone Miner. Res.*, vol. 25, no. 8, pp. 1877–1885, 2010, doi: 10.1002/jbmr.73.
- [195] A. Boskey, “Bone mineral crystal size,” *Osteoporos Int.*, vol. 14, 2003, doi: 10.1007/s00198-003-1468-2.
- [196] G. Molino *et al.*, “Osteoporosis-related variations of trabecular bone properties of proximal human humeral heads at different scale lengths,” *J. Mech. Behav. Biomed. Mater.*, vol. 100, no. January, p. 103373, 2019, doi: 10.1016/j.jmbbm.2019.103373.
- [197] O. L. Katsamenis, T. Jenkins, and P. J. Thurner, “Toughness and damage susceptibility in human cortical bone is proportional to mechanical inhomogeneity at the osteonal-level,” *Bone*, vol. 76, pp. 158–168, 2015, doi: 10.1016/j.bone.2015.03.020.
- [198] M. Saito and K. Marumo, “Bone quality in diabetes,” *Front. Endocrinol. (Lausanne).*, vol. 4, no. JUN, pp. 1–9, 2013, doi: 10.3389/fendo.2013.00072.
- [199] M. J. Reed *et al.*, “A new rat model of type 2 diabetes: The fat-fed, streptozotocin-treated rat,” *Metabolism.*, vol. 49, no. 11, pp. 1390–1394, 2000, doi: 10.1053/meta.2000.17721.
- [200] A. Vaag and S. S. Lund, “Non-obese patients with type 2 diabetes and prediabetic subjects: Distinct phenotypes requiring special diabetes treatment and (or) prevention?,” *Appl. Physiol. Nutr. Metab.*, vol. 32, no. 5, pp. 912–920, 2007, doi: 10.1139/H07-100.
- [201] A. Palermo, L. D’Onofrio, R. Eastell, A. V. Schwartz, P. Pozzilli, and N. Napoli, “Oral anti-diabetic drugs and fracture risk, cut to the bone: safe or dangerous? A narrative review,” *Osteoporos. Int.*, vol. 26, no. 8, pp. 2073–2089, 2015, doi: 10.1007/s00198-015-3123-0.
- [202] E. M. Wölfel *et al.*, “Individuals with type 2 diabetes mellitus show dimorphic and heterogeneous patterns of loss in femoral bone quality,” *Bone*, vol. 140, no. July, p. 115556, 2020, doi: 10.1016/j.bone.2020.115556.
- [203] American Diabetes Association (ADA), “Standard of medical care in diabetes - 2017,” *Diabetes Care*, vol. 40 (sup 1), no. January, pp. s4–s128, 2017, doi: 10.2337/dc17-S001.
- [204] R. Zdero, *Experimental methods in orthopaedic biomechanics*. 2017.
- [205] N. Rodriguez-florez, M. L. Oyen, S. J. Shefelbine, and O. Pharr, “Insight into differences in nanoindentation properties of bone,” *J. Mech. Behav. Biomed. Mater.*, vol. 18, pp. 90–99,

- 2013, doi: 10.1016/j.jmbbm.2012.11.005.
- [206] O. Bozkurt, M. Severcan, and F. Severcan, "Diabetes induces compositional, structural and functional alterations on rat skeletal soleus muscle revealed by FTIR spectroscopy: a comparative study with EDL muscle," *Analyst*, vol. 135, no. 12, p. 3110, 2010, doi: 10.1039/c0an00542h.
- [207] C. Gu, D. R. Katti, and K. S. Katti, "Microstructural and Photoacoustic Infrared Spectroscopic Studies of Human Cortical Bone with Osteogenesis Imperfecta," *Jom*, vol. 68, no. 4, pp. 1116–1127, 2016, doi: 10.1007/s11837-016-1838-9.
- [208] P. Sihota, R. N. Yadav, V. Dhiman, S. K. Bhadada, V. Mehandia, and N. Kumar, "Investigation of diabetic patient's fingernail quality to monitor type 2 diabetes induced tissue damage," *Sci. Rep.*, vol. 9, no. 1, p. 3193, 2019, doi: 10.1038/s41598-019-39951-3.
- [209] M. R. Towler, A. Wren, N. Rushe, J. Saunders, N. M. Cummins, and P. M. Jakeman, "Raman spectroscopy of the human nail: A potential tool for evaluating bone health?," *J. Mater. Sci. Mater. Med.*, vol. 18, no. 5, pp. 759–763, May 2007, doi: 10.1007/s10856-006-0018-9.
- [210] H. Lv *et al.*, "Comparison of microstructural and mechanical properties of trabeculae in femoral head from osteoporosis patients with and without cartilage lesions: A case-control study Pathophysiology of musculoskeletal disorders," *BMC Musculoskelet. Disord.*, vol. 16, no. 1, pp. 1–10, 2015, doi: 10.1186/s12891-015-0530-5.
- [211] I. Aleixo *et al.*, "A method for the evaluation of femoral head trabecular bone compressive properties," *Mater. Sci. Forum*, vol. 730–732, no. January, pp. 3–8, 2013, doi: 10.4028/www.scientific.net/MSF.730-732.3.
- [212] U. Wolfram, H. J. Wilke, and P. K. Zysset, "Damage accumulation in vertebral trabecular bone depends on loading mode and direction," *J. Biomech.*, vol. 44, no. 6, pp. 1164–1169, 2011, doi: 10.1016/j.jbiomech.2011.01.018.
- [213] R. Hambli, "Micro-CT finite element model and experimental validation of trabecular bone damage and fracture," *Bone*, vol. 56, no. 2, pp. 363–374, 2013, doi: 10.1016/j.bone.2013.06.028.
- [214] N. Napoli, M. Chandran, D. D. Pierroz, B. Abrahamsen, A. V. Schwartz, and S. L. Ferrari, "Mechanisms of diabetes mellitus-induced bone fragility," *Nat. Rev. Endocrinol.*, vol. 13, no. 4, pp. 208–219, 2017, doi: 10.1038/nrendo.2016.153.
- [215] M. X. Fu, J. R. Requena, A. J. Jenkins, T. J. Lyons, J. W. Baynes, and S. R. Thorpe, "The advanced glycation end product, N ϵ -(carboxymethyl)lysine, is a product of both lipid peroxidation and glycoxidation reactions," *J. Biol. Chem.*, vol. 271, no. 17, pp. 9982–9986, 1996, doi: 10.1074/jbc.271.17.9982.
- [216] S. Y. Tang and D. Vashishth, "The relative contributions of non-enzymatic glycation and cortical porosity on the fracture toughness of aging bone," *J. Biomech.*, vol. 44, no. 2, pp. 330–336, 2011, doi: 10.1016/j.jbiomech.2010.10.016.

- [217] G. Leanza *et al.*, “Risk factors for fragility fractures in type 1 diabetes,” *Bone*, vol. 125, no. December 2018, pp. 194–199, 2019, doi: 10.1016/j.bone.2019.04.017.
- [218] H. Sueki, S. Nozaki, S. Numazawa, K. Aoki, Y. Kuroiwa, and R. Fujisawa, “Effect of Non-Enzymatic Glycosylation and Heating on Browning of Human Stratum corneum and Nail,” *Dermatology*, vol. 183, no. 3, pp. 197–202, 1991, doi: 10.1159/000247669.
- [219] A. S. Kishabongo *et al.*, “Glycation of nail proteins: From basic biochemical findings to a representative marker for diabetic glycation-associated target organ damage,” *PLoS One*, vol. 10, no. 3, pp. 1–13, 2015, doi: 10.1371/journal.pone.0120112.
- [220] K. M. Farhan, T. P. Sastry, and A. B. Mandal, “Comparative study on secondary structural changes in diabetic and non-diabetic human finger nail specimen by using FTIR spectra,” *Clin. Chim. Acta*, vol. 412, no. 3–4, pp. 386–389, 2011, doi: 10.1016/j.cca.2010.11.016.
- [221] B. Behm, S. Schreml, M. Landthaler, and P. Babilas, “Skin signs in diabetes mellitus,” *J. Eur. Acad. Dermatology Venereol.*, vol. 26, no. 10, pp. 1203–1211, 2012, doi: 10.1111/j.1468-3083.2012.04475.x.
- [222] R. Coopman *et al.*, “Glycation in human fingernail clippings using ATR-FTIR spectrometry, a new marker for the diagnosis and monitoring of diabetes mellitus,” 2017, doi: 10.1016/j.clinbiochem.2016.09.001.
- [223] A. S. Kishabongo *et al.*, “Glycated nail proteins: A new approach for detecting diabetes in developing countries,” *Trop. Med. Int. Heal.*, vol. 19, no. 1, pp. 58–64, 2014, doi: 10.1111/tmi.12218.
- [224] A. Jabłęcka, J. Olszewski, and E. Marzec, “Dielectric properties of keratin-water system in diabetic and healthy human fingernails,” *J. Non. Cryst. Solids*, vol. 355, no. 50–51, pp. 2456–2460, 2009, doi: 10.1016/j.jnoncrsol.2009.08.024.
- [225] P. Saedi, “Nail Properties and Bone Health : A Review,” *J. Funct. Biomater.*, vol. 9, no. 31, 2018, doi: 10.3390/jfb9020031.
- [226] B. Lecka-Czernik and J. L. Fowlkes, *Basic and Translational Research and Clinical Applications Diabetic Bone Disease*. Springer International Publishing Switzerland 2016.
- [227] X. LIAO, W. XU, Y. WANG, B. JIA, and G. ZHOU, “Effect of porous structure on mechanical properties of C/PLA/nano-HA composites scaffold,” *Trans. Nonferrous Met. Soc. China*, vol. 19, no. 30870609, pp. s748–s751, 2009, doi: 10.1016/S1003-6326(10)60144-6.
- [228] P. Fleckman and E. F. Omura, “Histopathology of the nail.,” *Adv. Dermatol.*, vol. 17, pp. 385–406, 2001.
- [229] R. Caputo, G. Gasparini, and D. Contini, “A freeze-fracture study of the human nail plate,” *Arch. Dermatol. Res.*, vol. 272, no. 1–2, pp. 117–125, 1981, doi: 10.1007/BF00510401.
- [230] J. C. Garson, F. Baltenneck, F. Leroy, C. Riekel, and M. Müller, “Histological structure of human nail as studied by synchrotron X-ray microdiffraction.,” *Cell. Mol. Biol. (Noisy-le-grand)*, vol. 46, no. 6, pp. 1025–34, Sep. 2000.

- [231] L. Farren, S. Shayler, and A. R. Ennos, "The fracture properties and mechanical design of human fingernails," *J. Exp. Biol.*, vol. 207, no. Pt 5, pp. 735–41, Feb. 2004, doi: 10.1242/JEB.00814.
- [232] P. Wei, L. Qian, J. Zheng, and Z. Zhou, "Effect of water on the mechanical and frictional behaviors of human fingernails," *Tribol. Lett.*, vol. 38, no. 3, pp. 367–375, 2010, doi: 10.1007/s11249-010-9616-2.
- [233] "The Role of Saprophytic Fungi in the Production of Eczematous Dermatitis: I. The Location of Fungi Within Human Nails," *J. Invest. Dermatol.*, vol. 28, no. 2, pp. 137–146, Feb. 1957, doi: 10.1038/JID.1957.14.
- [234] Y. Kobayashi, M. Miyamoto, K. Sugibayashi, and Y. Morimoto, "Drug Permeation through the Three Layers of the Human Nail Plate," *J. Pharmaceuticals Pharmacol.*, vol. 51, pp. 271–278, 1999, doi: 10.1211/0022357991772448.
- [235] J. L. Koenig and P. L. Suttun, "Raman Spectra of Poly-L-Lysines," *Appl. Polym. Spectrosc.*, vol. 3, no. c, pp. 121–133, 1978, doi: 10.1016/B978-0-12-125450-6.50014-4.
- [236] M. C. Caraher *et al.*, "Raman spectroscopy predicts the link between claw keratin and bone collagen structure in a rodent model of oestrogen deficiency," *Biochim. Biophys. Acta - Mol. Basis Dis.*, vol. 1864, no. 2, pp. 398–406, 2018, doi: 10.1016/j.bbadis.2017.10.020.
- [237] O. Bozkurt, M. D. Bilgin, and F. Severcan, "The effect of diabetes mellitus on rat skeletal extensor digitorum longus muscle tissue: An FTIR study," *Spectroscopy*, vol. 21, pp. 151–160, 2007, doi: 10.1155/2007/390908.
- [238] C. Adamopoulos *et al.*, "Systemic effects of AGEs in ER stress induction in vivo," *Glycoconj. J.*, vol. 33, no. 4, pp. 537–544, 2016, doi: 10.1007/s10719-016-9680-4.
- [239] K. ichiro Tanaka, T. Yamaguchi, H. Kaji, I. Kanazawa, and T. Sugimoto, "Advanced glycation end products suppress osteoblastic differentiation of stromal cells by activating endoplasmic reticulum stress," *Biochem. Biophys. Res. Commun.*, vol. 438, no. 3, pp. 463–467, 2013, doi: 10.1016/j.bbrc.2013.07.126.
- [240] D. L. Eizirik, A. K. Cardozo, and M. Cnop, "The role for endoplasmic reticulum stress in diabetes mellitus," *Endocr. Rev.*, vol. 29, no. 1, pp. 42–61, 2008, doi: 10.1210/er.2007-0015.
- [241] D. Mekahli, G. Bultynck, J. B. Parys, H. de Smedt, and L. Missiaen, "Endoplasmic-reticulum calcium depletion and disease," *Cold Spring Harb. Perspect. Biol.*, vol. 3, no. 6, pp. 1–30, 2011, doi: 10.1101/cshperspect.a004317.
- [242] F. Gregorio, S. Cristallini, F. Santeusano, P. Filippini, and P. Fumelli, "Osteopenia associated with non-insulin-dependent diabetes mellitus: what are the causes?," *Diabetes Res. Clin. Pract.*, vol. 23, no. 1, pp. 43–54, 1994, doi: 10.1016/0168-8227(94)90126-0.
- [243] S. Ohgitani, T. Fujita, Y. Fujii, C. Hayashi, and H. Nishio, "Nail calcium and magnesium content in relation to age and bone mineral density," *J. Bone Miner. Metab.*, vol. 23, no. 4, pp. 318–322, 2005, doi: 10.1007/s00774-005-0606-7.

- [244] I. Pillay *et al.*, “The Use of Fingernails as a Means of Assessing Bone Health: A Pilot Study,” *J. Women’s Heal.*, vol. 14, no. 4, pp. 339–344, May 2005, doi: 10.1089/jwh.2005.14.339.
- [245] G. Rani Gupta, V. Dhruw, B. Athawal, P. Siddiqui, H. K. Agrawal, and L. Heeresh Chandra, “Human nail growth pattern and medicolegal aspect,” *J. Indian Acad. Forensic Med.*, vol. 27, no. 2, pp. 87–91, 2005.
- [246] C. Grover and A. Khurana, “An update on treatment of onychomycosis,” *Mycoses*, vol. 55, no. 6, pp. 541–551, 2012, doi: 10.1111/j.1439-0507.2012.02199.x.
- [247] D. Vashishth, “Advanced glycation end-products and bone fractures,” *IBMS Bonekey*, vol. 6, no. 8, pp. 268–278, 2009, doi: 10.1138/20090390.
- [248] M. E. Bolander, M. F. Young, L. W. Fisher, Y. Yamada, and J. D. Termine, “Osteonectin cDNA sequencing reveals potential binding regions for calcium and hydroxapatite, and shows homologies with both a basement membrane protein (SPARC) and a serum proteinase inhibitor (Ovomucoid),” *Proc Natl Acad Sci*, vol. 85, no. May, pp. 2919–2923, 1988.
- [249] J. R. Beattie *et al.*, “Raman spectroscopic analysis of fingernail clippings can help differentiate between postmenopausal women who have and have not suffered a fracture,” *Clin. Med. Insights Arthritis Musculoskelet. Disord.*, vol. 9, pp. 109–116, 2016, doi: 10.4137/CMAMD.S38493.
- [250] M. Tohyama, X. Dai, K. Shiraishi, M. Murakami, and K. Sayama, “Endoplasmic reticulum stress-induced keratinocyte necrosis is a new mechanism of epidermal cell death in SJS/TEN,” *J. Dermatol. Sci.*, vol. 84, no. 1, p. e20, 2016, doi: 10.1016/j.jdermsci.2016.08.071.
- [251] T. Vilaca *et al.*, “The risk of hip and non-vertebral fractures in type 1 and type 2 diabetes: A systematic review and meta-analysis update,” *Bone*, vol. 137, p. 115457, 2020, doi: 10.1016/j.bone.2020.115457.
- [252] N. Mercer, H. Ahmed, S. B. Etcheverry, G. R. Vasta, and A. M. Cortizo, “Regulation of advanced glycation end product (AGE) receptors and apoptosis by AGEs in osteoblast-like cells,” *Mol. Cell. Biochem.*, vol. 306, no. 1–2, pp. 87–94, 2007, doi: 10.1007/s11010-007-9557-8.
- [253] N. L. Fazzalari, R. J. Moore, B. A. Manthey, and B. Vernon-Roberts, “Comparative study of iliac crest and proximal femur histomorphometry in normal patients,” *J. Clin. Pathol.*, vol. 42, no. 7, pp. 745–748, 1989, doi: 10.1136/jcp.42.7.745.
- [254] M. Han, K. Chiba, S. Banerjee, J. Carballido-Gamio, and R. Krug, “Variable flip angle three-dimensional fast spin-echo sequence combined with outer volume suppression for imaging trabecular bone structure of the proximal femur,” *J. Magn. Reson. Imaging*, vol. 41, no. 5, pp. 1300–1310, May 2015, doi: 10.1002/jmri.24673.
- [255] G. J. Kazakia *et al.*, “Trabecular bone microstructure is impaired in the proximal femur of human immunodeficiency virus-infected men with normal bone mineral density,” *Quant. Imaging Med. Surg.*, vol. 8, no. 1, pp. 5–13, 2018, doi: 10.21037/qims.2017.10.10.

Complete list of publications

Published Papers

1. **Sihota P**, Yadav RN, Dhaliwal R, Bose JC, Dhiman V, Neradi D, Karn S, Sharma S, Aggarwal S, Goni VG, Mehandia V, Vashishth D, Bhadada SK, Kumar N. Investigation of mechanical, material and compositional determinants of human trabecular bone quality in type 2 diabetes. *J. Clin. Endocrinol. Metab.* 2021. (doi:10.1210/clinem/dgab027)
2. **Sihota P**, Yadav RN, Poleboina S, Mehandia V, Bhadada SK, Tikoo K, Kumar N. Development of HFD-fed/low-dose stz-treated female sprague-dawley rat model to investigate diabetic bone fragility at different organization levels. *JBMR Plus* 2020. (doi:10.1002/jbm4.10379)
3. **Sihota P**, Yadav RN, Dhiman V, Bhadada SK, Mehandia V, Kumar N. Investigation of diabetic patient's fingernail quality to monitor type 2 diabetes induced tissue damage. *Sci. Rep.* 2019. (doi:10.1038/s41598-019-39951-3)
4. Yadav RN, **Sihota P**, Neradi D, Bose JC, Dhiman V, Karn S, Sharma S, Aggarwal S, Goni VG, Kumar S, Bhadada SK, Kumar N., "Prediction of mechanical properties of trabecular bone in patients with type 2 diabetes using damage based finite element method," *J. Biomech.*, vol. 123, p. 110495, 2021, (doi: 10.1016/j.jbiomech.2021.110495)
5. Yadav RN, Uniyal P, **Sihota P**, Kumar S, Kumar N, Sahni D, Bhadada SK, Effect of ageing on microstructure and fracture behavior of cortical bone using experiment and Extended Finite Element Method (XFEM), *Medical Engineering and Physics* (2021) (Accepted).
6. Kumar R, Tiwari AK, Tripathi D, Main RP, Kumar N, **Sihota P**, Ambwani S, Sharma NN. Anatomical variations in cortical bone surface permeability: tibia versus femur. *J Mech Behav Biomed Mater.* 2020. (doi:10.1016/j.jmbbm.2020.104122)
7. Yadav JP, Yadav RN, **Sihota P**, Chen H, Wang C, Sun CC, Kumar N, Bansal A, Jain S. Single-crystal plasticity defies bulk-phase mechanics in isoniazid cocrystals with analogous cofomers. *Cryst. Growth Des.* 2019. (doi:10.1021/acs.cgd.9b00247)
8. Das R, Yadav RN, **Sihota P**, Uniyal P, Kumar N, Bhushan B. Biomechanical evaluation of wasp and honey bee stingers. *Sci Rep.* 2018. (doi:10.1038/s41598-018-33386-y)

Publication under peer review process

1. **Sihota P**, Pal R, Yadav RN, Neradi D, Karn S, Goni VG, Sharma S, Mehandia V, Bhadada SK, Kumar N, Rao SD, Can Fingernail quality predict the bone damage in type 2 diabetes mellitus: A pilot study, *PLOS ONE* (2021) PONE-D-21-04313 (Under Review)
2. **Sihota P**, Poleboina S, Bhadada SK, Tikoo K, Mehandia V, Kumar N, Investigation of a new non-invasive surrogate marker to predict diabetic bone fragility, (2021) (Under Submission)
3. **Sihota P**, Bhadada SK, Kumar N, Assessment of bone fragility in type 2 diabetes beyond bone mineral density, Review article (Under preparation)

4. Uniyal P, **Sihota P**, Tikoo K, Kumar N, Anatomical variation in intracortical canal network microarchitecture and its influence on bone fracture risk, *JMBBM* (2021) JMBBM-D-21-00160 (Under Review)
5. Yadav RN, **Sihota P**, Neradi D, Bose JC, Dhiman V, Karn S, Sharma S, Aggarwal S, Goni VG, Bhadada SK, Kumar N, Effects of type 2 diabetes on the viscoelastic behaviour of human trabecular bone, *Calcified Tissue International* (2021) CTIN-D-21-00252 (Under Review)
6. Neradi D, Sharma S, Kanojia R, Dhillon M, Yadav RN, **Sihota P**, Kumar N, Bhadada SK, Association of hip geometry with femoral head microarchitecture and strength: an *ex vivo* study on patients undergoing arthroplasty for hip fracture, *HIP International* (2021) HIPINT-21-0089 (Under Review)

Publications without peer review process

1. **Sihota P**, Yadav RN, Dhaliwal R, Bose JC, Dhiman V, Neradi D, Karn S, Sharma S, Aggarwal S, Goni VG, Mehandia V, Vashishth D, Bhadada SK, Kumar N. Investigation of human trabecular bone quality in osteoporosis with and without type 2 diabetes. ASBMR 2020 Annual Meeting Virtual Event. September 11-15, 2020. ID: A20022270 (e-Poster P-040)
2. Dhaliwal R, Bose JC, Kumar N, **Sihota P**, Yadav RN, Goni VG, Aggarwal S, Rao SD, Bhadada SK. Bone mechanical properties (nanoindentation) and microarchitecture (micro-CT) in type 2 diabetes. ASBMR 2018, Annual Meeting Canada. September 28 - October 1, 2018. (Abstract #SUN0081)
3. Sharma S, Khing J, Sudesh P, Dhillon M, **Sihota P**, Yadav RN, Kumar N. Can intermittent teriparatide facilitate supraphysiological-rate distraction osteogenesis? A feasibility study in the rabbit tibial lengthening model. Virtual EFORT Congress (VEC), 28 October - 30 October 2020. Abstract #1832
4. Kumar R, Tiwari AK, **Sihota P**, Tripathi D, Kumar N, Ahmad AH, Ambwani S. Investigation on viscoelastic properties of cortical surfaces using dynamic mechanical analysis. International conference on Advances in Thermal Systems, Materials and Design Engineering (ATSMDE2017)

Patents

1. **Sihota P**, Yadav RN, Kumar N, Mehandia V, Bhadada SK, Dhiman V, Method for analyzing a health status on a health measurement scale, Indian patent (application no: 202011006130, application date 11.02.2021)
2. Das R, Yadav RN, **Sihota P**, Uniyal P, Kumar N, Bhushan B. Painless micro syringe needle system. Indian patent (application no: 201911012456, application date 29.03.2019)

RESUME

Personal Information

Praveer Sihota
Senior Research Fellow (SRF)
Biomedical Engineering Lab, TC1, IIT Ropar
Mobile number: +91-8289094945
Email: praveer.sihota@iitrpr.ac.in, praveersihota@gmail.com
Date of Birth: October 10th 1989
Permanent Address: #C12/4, Sant Kripa, Vasant Vihar, Ujjain,
M.P., Bharat - 456010



Educational Qualifications

Degree	Institution	Department	Year	Percentage/CGPA
BE	Rajiv Gandhi Technical University, Bhopal, India	Biomedical Engineering	2006-2010	73.5%
MTech	Manipal University, Karnataka, India	Biomedical Engineering	2011-2013	8.14 (CGPA)
PhD	Indian Institute of Technology Ropar, Punjab, India	Mechanical Engineering	27.07.2015-18.03.2021	7.25 (In course work)

Research Exposure/Training

Duration	Institution	Particulars
10.07.2012 - 30.06.2013	CSIR-CSIO Chandigarh	MTech Trainee (Bioinstrumentation)
05.07.2013 - 30.12.2014	IIT Mandi	Senior Research Fellow (Biostatistics)
05.01.2015 - 26.07.2015	PGIMER Chandigarh	Senior Research Fellow (Endocrinology)

Field of Research and Contributions

Multiscale characterization of bone with a special interest in exploring the area of prolonged hyperglycemia, effects of glycation on bone mineralization, collagen quality, and skeletal fragility. My interest lies in the exploration of non-invasive diagnostic techniques to assess bone quality. Using multiscale bone quality assessment, I will continue to study the underlying mechanisms due to pathological changes in the bone, which will give us an idea about how these disease aspects contribute to increased fracture risk. These findings will be essential to explore new clinically relevant information for the diagnosis and treatment options to prevent fragility fractures.

Achivements and Awards

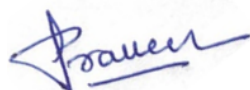
1. Best oral presentation award, Indian Society of Bone and Mineral Research (ISBMR 2017), 10th-12th November, 2017
2. Second place in the poster presentation, Indian Society of Bone and Mineral Research (ISBMR) and Karnataka Endocrine Society. 19th and 20th October 2019, Bengaluru, Karnataka
3. Sponsorship provided by ISBMR to present a poster in American Society of Bone and Mineral Research (ASBMR) in 2020 and a gifted 1-year membership in ASBMR
4. The manuscript, “Investigation of mechanical, material and compositional determinants of human trabecular bone quality in type 2 diabetes,” is accepted for Editorial in JCEM.

Rreferees

1. Dr. Navin Kumar, Associate Professor, Department of Mechanical Engineering, IIT Ropar, Email nkumar@iitrpr.ac.in, Mobile no. +91-9501212380
2. Dr. Sanjay Kumar Bhadada, Professor, Department of Endocrinology, PGIMER Chandigarh, Email bhadadask@rediffmail.com, Phone no. +91-9876602448
3. Dr. Vishwajeet Mehandia, Assistant Professor, Department of Chemical Engineering, IIT Ropar, Email vishwajeet@iitrpr.ac.in, Mobile no. +91-8146789450

Declaration

I hereby declare that the information mentioned above is correct up to my knowledge, and I bear the responsibility for the correctness of the particulars as mentioned above.



Praveer Sihota

01/06/2021

IIT Ropar, Punjab, India